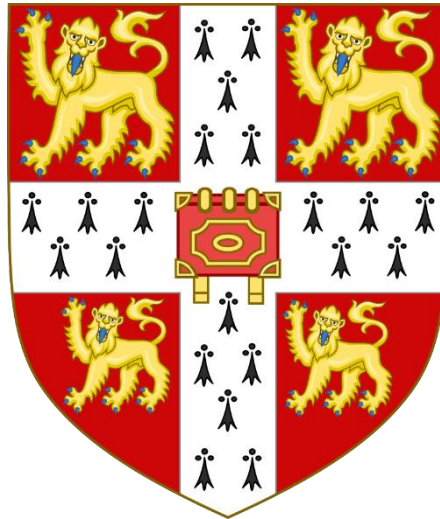


# Angiotensin II signalling in sensory neurons



A dissertation submitted for the Degree of Doctor of Philosophy

**James Higham**

Department of Pharmacology

University of Cambridge

August 2022

## **I. Preface**

This thesis is the result of my own work carried out in the Department of Pharmacology, University of Cambridge, between September 2018 and August 2022, and includes nothing which is the outcome of work done in collaboration except as declared in the preface and specified in the text. It is not substantially the same as any work that has already been submitted before for any degree or other qualification at the University of Cambridge or other institution except as declared in the preface and specified in the text. It does not exceed the prescribed word limit of 60,000 excluding references.

## **II. Acknowledgments**

I must first acknowledge my supervisor, Dr David Bulmer, for his enduring enthusiasm, sense of humour and endless ideas which have helped to form the substance of this Thesis. I am grateful for all of his advice, on matters both inside and outside the lab. I'm also indebted to Professor Ewan St John Smith for being so generous with his time, ideas and scientific criticism.

All members of the Bulmer/Smith lab have made my time in Cambridge so enjoyable and have made the lab a brilliant place to work. Special thanks must go to Katie, Luke and Becky for their lasting friendship and all the memories over the past four years.

As ever, I am thankful for the love and unerring support given to me by my mum and sisters, Steph and Lynsey. I owe all that I have to you – for raising me, being there for me, and putting up with me.

And lastly, to Sarah. While waiting for you on a bench by the Cam before our first date, I couldn't have imagined how much my life would change – and now can't imagine it without you. Thank you for making me so happy and for always being by my side.

### III. Summary

Angiotensin II (Ang II) is a peptide associated with the regulation of blood pressure, though the elevated presence of Ang II in the inflamed bowel – and other inflamed tissues – and the presence of receptors for Ang II on sensory neurons may point to additional roles in nociception in inflammatory disease. Work in this Thesis sought to examine the identity of sensory neurons with which Ang II interacts, the mechanisms underpinning these interactions, and the consequences on neuronal properties and function.

Ca<sup>2+</sup> imaging revealed that Ang II stimulated a rise in cytosolic Ca<sup>2+</sup> in small-diameter sensory neurons which expressed the nociceptive markers TRPV1 and Nav1.8. This population of Ang II-sensitive neurons could be divided in two, with one subpopulation expressing Tmem45b and binding the non-peptidergic marker isolectin-B4 (IB4), while the other subpopulation lacked both Tmem45b and IB4 binding. The response of IB4-binding sensory neurons to Ang II was mediated by the Type I Ang II receptor (AT1R). Conversely, the response of IB4-negative neurons to Ang II did not require AT1R but did require the presence of non-neuronal satellite cells.

Ang II-evoked Ca<sup>2+</sup> signals downstream of AT1R were mediated by Ca<sup>2+</sup> release from intracellular stores via the activation of IP<sub>3</sub> receptors, followed by store-operated Ca<sup>2+</sup> entry (SOCE). SOCE downstream of Ang II application was found to be mediated by the non-selective cation channel, TRPC3, activated by the endoplasmic reticulum Ca<sup>2+</sup> sensor, STIM.

Incubation of sensory neurons with Ang II induced to nuclear translocation of the transcription factor, nuclear factor of activated T-cells 5 (NFAT5). This translocation was dependent on Ca<sup>2+</sup> influx through TRPC3 and the Ca<sup>2+</sup>-sensitive phosphatase, calcineurin. Translocation of NFAT5 may indicate prolonged changes in nociceptor properties induced by Ang II, as evidenced by an increase in electrical excitability of IB4-binding neurons following overnight Ang II incubation.

In summary, experiments detailed in this Thesis have revealed that Ang II stimulated nociceptive sensory neurons *in vitro*. Ang II-evoked Ca<sup>2+</sup> signals were mediated by store depletion and subsequent SOCE through TRPC3. These Ca<sup>2+</sup> signals drove translocation of NFAT5 to the nucleus in a manner dependent on calcineurin. Finally, non-peptidergic neurons exposed to Ang II displayed elevated excitability. These data

highlight a mechanism through which Ang II may drive prolonged changes in nociceptor function.

## IV. Contents

1.1. Inflammatory bowel disease .....	- 11 -
1.1.1. Epidemiology and burden of disease .....	- 11 -
1.1.2. Symptoms and disease sequelae .....	- 14 -
1.1.3. Pathophysiology of IBD .....	- 15 -
1.1.3.1. Intestinal barrier dysfunction.....	- 17 -
1.1.3.1.1. Intestinal mucus .....	- 17 -
1.1.3.1.2. Intestinal epithelium and cell-cell adhesion.....	- 19 -
1.1.3.2. Microbial dysbiosis .....	- 21 -
1.1.3.3. Immune response .....	- 22 -
1.2. Mechanisms driving (visceral) pain.....	- 27 -
1.3. Angiotensin II, inflammation and IBD.....	- 30 -
1.3.1. Ang II beyond blood pressure .....	- 30 -
1.3.2. Ang II in the pathophysiology of IBD .....	- 31 -
1.4. Investigating nociception in vitro.....	- 37 -
1.4.1. Fluorescent Ca <sup>2+</sup> imaging.....	- 37 -
1.4.2. Patch-clamp electrophysiology .....	- 38 -
1.4.3. Protein expression .....	- 38 -
1.5. Principle aims .....	- 39 -
2.1. Methods and materials .....	- 41 -
2.1.1. Animals .....	- 41 -
2.1.2. Ca <sup>2+</sup> imaging of cultured sensory neurons.....	- 44 -
2.1.2.1. Culture of sensory neurons from dorsal root ganglia .....	- 44 -
2.1.2.2. Ca <sup>2+</sup> imaging .....	- 44 -
2.1.2.3. Image analysis .....	- 46 -
2.1.2.3.1. Response to a drug.....	- 46 -
2.1.2.3.2. Estimating Ca <sup>2+</sup> store content and store-operated Ca <sup>2+</sup> entry .....	- 47 -
2.1.2.3.3. Ca <sup>2+</sup> signals in non-neuronal cells .....	- 47 -
2.1.3. Magnetic activated cell sorting .....	- 49 -
2.1.4. Immunocytochemistry for MACS validation .....	- 52 -
2.1.4.1. Cell preparation and imaging.....	- 52 -
2.1.4.2. Analysis.....	- 52 -
2.1.5. Immunocytochemistry for NFAT translocation .....	- 53 -
2.1.5.1. Cell preparation and imaging.....	- 53 -
2.1.5.2. Analysis.....	- 54 -
2.1.6. Patch-clamp electrophysiology .....	- 54 -

2.1.6.1. Acute application of Ang II.....	- 54 -
2.1.6.2. Incubation with Ang II.....	- 55 -
2.1.7. Ca <sup>2+</sup> imaging of bone marrow-derived macrophages.....	- 55 -
2.1.7.1. Culture of bone marrow-derived macrophages (BMDMs).....	- 55 -
2.1.7.2. Ca <sup>2+</sup> imaging .....	- 56 -
2.1.7.3. Image analysis .....	- 56 -
2.1.8. Reagents.....	- 57 -
2.1.9. Data analysis .....	- 57 -
2.1.9.1. Curve fitting.....	- 57 -
2.1.9.2. Statistics.....	- 57 -
3.1. Introduction .....	- 61 -
3.1.1. Diversity and classification of sensory neurons .....	- 61 -
3.1.2. Non-neuronal cells in the DRG.....	- 62 -
3.1.3. Experimental outline.....	- 63 -
3.2. Results.....	- 64 -
3.2.1. Ang II stimulates nociceptive neurons in culture .....	- 64 -
3.2.1.1. Ang II-sensitive neurons are small-sized .....	- 64 -
3.2.1.2. Most Ang II-sensitive neurons are co-sensitive the capsaicin .....	- 66 -
3.2.1.3. Na <sub>v</sub> 1.8 is expressed in Ang II-sensitive neurons.....	- 70 -
3.2.1.3.1. Ang II stimulates Na <sub>v</sub> 1.8-positive neurons identified using tdTomato .....	- 70 -
3.2.1.3.2. Ablation of Na <sub>v</sub> 1.8-expressing neurons abolished the response to Ang II .....	- 74 -
3.2.2. Ang II stimulates both IB4-positive and IB4-negative neurons.....	- 78 -
3.2.2.1. IB4 labelling revealed a population of IB4-negative Ang II-sensitive neurons .....	- 78 -
3.2.2.2. The response of IB4-negative neurons to Ang II is not dependent on IB4-positive neurons.....	- 82 -
3.2.2.2.1. There was no time delay between Ang II-evoked Ca <sup>2+</sup> signals in IB4-positive and -negative neurons .....	- 82 -
3.2.2.2.2. Ablation of IB4-positive neurons did not affect the response of IB4-negative neurons.....	- 84 -
3.2.2.3. Non-neuronal satellite cells are required for the response of IB4-negative neurons to Ang II .....	- 87 -
3.2.2.3.1. Magnetic cell sorting of dissociated sensory neuron cultures .....	- 90 -
3.2.2.3.2. Removal of satellite cells attenuated the neuronal response to Ang II .....	- 95 -
3.2.3. The pharmacology of the response to Ang II is altered by neuronal culture conditions. -	98 -
3.2.4. Non-neuronal satellite cells respond to Ang II .....	- 100 -
3.2.5. Alamandine stimulates sensory neurons independently of AT1R .....	- 102 -
3.3. Discussion.....	- 104 -
3.3.1.1. Ang II-sensitive neurons are small-sized .....	- 104 -

3.3.1.2. Ang II stimulates a TRPV1-positive neuronal population .....	105 -
3.3.1.3. Expression of Na <sub>v</sub> 1.8 in Ang II-sensitive neurons .....	106 -
3.3.2. Unexpected sensitivity of a subpopulation of IB4-negative neurons to Ang II .....	108 -
3.3.2.1. Stimulation of IB4-negative neurons is not dependent on IB4-positive neurons .....	109 -
3.3.2.2. Non-neuronal satellite cells are required for the response of IB4-negative neurons to Ang II application .....	110 -
3.3.2.3. Stimulation of NNSCs in vitro .....	111 -
3.3.2.4. How do NNSCs communicate with IB4-negative neurons? .....	113 -
3.3.3. What's the (patho)physiological relevance? .....	115 -
3.4. Key points .....	117 -
4.1. Introduction .....	119 -
4.1.1. Intracellular Ca <sup>2+</sup> stores.....	119 -
4.1.2. Store-operated Ca <sup>2+</sup> entry .....	120 -
4.1.3. Store-independent Ca <sup>2+</sup> entry.....	122 -
4.1.4. Experimental outline.....	122 -
4.2. Results.....	123 -
4.2.1. Ang II signals through AT1R to release Ca <sup>2+</sup> from intracellular stores .....	123 -
4.2.2. Ang II depletes intracellular Ca <sup>2+</sup> stores in small-sized sensory neurons .....	127 -
4.2.3. Neither activation of AT2R nor action potential firing underlies Ang II-evoked Ca <sup>2+</sup> signals .....	129 -
4.2.4. Ang II also stimulates Ca <sup>2+</sup> influx through TRPC3 channels .....	132 -
4.2.5. Agonist-induced desensitisation of TRPC3 attenuates the neuronal response to Ang II	134 -
4.2.6. TRPC3 functions in TRPV1-expressing neurons.....	137 -
4.2.7. Ca <sup>2+</sup> influx through TRPC3 drives prolongation of Ang II-evoked Ca <sup>2+</sup> signals .....	139 -
4.2.8. TRPC3 is activated by store depletion in mouse sensory neurons .....	141 -
4.2.9. TRPC3 contributes to SOCE in small-sized sensory neurons.....	144 -
4.2.10. Ang II activates TRPC3 via store depletion .....	146 -
4.2.11. Regulation of SOCE and TRPC3 by protein kinases C and G .....	148 -
4.2.12. Stimulation of TRPC3 by store-independent pathways.....	150 -
4.2.12.1. Diacylglycerol activates TRPC3 in sensory neurons.....	150 -
4.2.12.2. Ang II-evoked Ca <sup>2+</sup> signals do not require PKC .....	152 -
4.2.13. Pre-incubation with vehicles does not affect the response to Ang II .....	154 -
4.3. Discussion.....	156 -
4.3.1. Signalling downstream of AT1R .....	156 -
4.3.2. Mechanisms underpinning the activation of TRPC3 .....	158 -
4.3.3. Regulation of TRPC3 channels by PKC .....	165 -
4.4. Key points .....	170 -

5.1. Introduction .....	- 172 -
5.1.1. Nuclear Factor of Activated T-cells.....	- 172 -
5.1.2. Experimental outline.....	- 174 -
5.2. Results.....	- 175 -
5.2.1. Neuronal staining for NFAT5 .....	- 175 -
5.2.2. Nuclear translocation of NFAT5 depends on AT1R and TRPC3.....	- 177 -
5.2.3. Calcineurin mediates nuclear translocation of NFAT5 .....	- 181 -
5.2.4. Incubation with Ang II causes increased excitability of IB4-positive neurons .....	- 183 -
5.3. Discussion.....	- 185 -
5.3.1. Ang II-mediated nuclear translocation of NFAT5 .....	- 185 -
5.3.2. Sensitisation of IB4-positive sensory neurons .....	- 187 -
5.4. Key points .....	- 190 -
6.1. A potential role for Ang II in nociception .....	- 192 -
6.2. Conclusion .....	- 194 -
Appendix 1: Additional data.....	- 196 -
A1.1. Preliminary data implicating TNF $\alpha$ in Ang II signalling.....	- 196 -
A1.2. Examining the kinetics of KCl-evoked Ca <sup>2+</sup> transients.....	- 199 -
A1.3. Measuring absolute [Ca <sup>2+</sup> ] using Fluo4 .....	- 202 -
A1.4. Response of cultured sensory neurons to cold.....	- 206 -
8.1. References.....	- 211 -

All abbreviations are defined at their first use in the text.

# **Chapter 1**

## **General introduction**

## 1.1. Inflammatory bowel disease

### 1.1.1. Epidemiology and burden of disease

Inflammatory bowel disease (IBD) is an umbrella term encompassing Crohn's Disease (CD) and Ulcerative Colitis (UC), in addition to other rarer colitides. IBD is clinically associated with abdominal pain, bloody diarrhoea, weight loss and fatigue. These symptoms arise from chronic sterile inflammation of the gastrointestinal (GI) tract. CD can affect any part of the GI tract – most commonly the terminal ileum – while UC is restricted to the colon and frequently affects the rectum.

The cause of IBD remains incompletely understood, though many risk factors have been identified. Evidence supporting a role for genetics in the development of IBD arose from reports of familial clustering of IBD and disease concordance between monozygotic twins. For CD and UC, 2-14% and 8-14% of patients report a family history of the disease (Ananthkrishnan, 2015), though if both parents are affected by IBD, the risk of the offspring developing IBD can be as high as ~30% (Bennett, Rubin and Present, 1991; Laharie *et al.*, 2001). A heritable component of IBD has also been inferred from twin concordance studies. Monozygotic twins showed a 20-50% concordance of CD compared to only 10% for dizygotic twins (Orholm *et al.*, 2000). Concordance between twins was lower for UC, estimated at 16% and 4% for monozygotic and dizygotic twins, respectively, suggesting less dependence of UC on heritable factors (Orholm *et al.*, 2000).

Genome-wide association studies have identified a wealth of loci associated with IBD, the majority of which contribute to both CD and UC (Jostins *et al.*, 2012). Many of these loci are also shared with autoimmune diseases, such as psoriasis (Ellinghaus *et al.*, 2012; Jostins *et al.*, 2012), suggesting at least partly overlapping aetiologies. Consistently, within IBD-associated loci, are genes expressed by various immune cell types, particularly dendritic cells, and implicated in immune cell activation (Mokry *et al.*, 2014; De Lange *et al.*, 2017). Geographic stratification demonstrated that many loci are common to multiple ancestral groups with some notable exceptions; for example, variants in *IL23R* are found more commonly in those with IBD in Europe but not east Asia (Jostins *et al.*, 2012; Jairath and Feagan, 2020). The use of neutralising anti-IL23 antibodies and *IL23* knock-out mice has further clarified the role of this cytokine and its receptor in bringing about inflammation, from IL23 release from

dendritic cells to the activation of neutrophils and macrophages via IL23R (McGovern and Powrie, 2007).

While most identified IBD risk loci contribute to elevated risk in both CD and UC, mutations in *NOD2*, a gene encoding a pattern recognition receptor in immune and epithelial cells, have been associated with higher risk of CD only (Ananthakrishnan, 2015). More than this, CD risk alleles of *NOD2* show protective effects against UC (Jostins *et al.*, 2012). Subtle differences between CD and UC such as this may offer an explanation into their overlapping, but distinct, aetiology, symptomology and sequelae.

Genetic studies in IBD have revealed novel risk variants and highlighted the roles of various cell types and signalling pathways, though they have not yet been useful in the diagnosis of IBD, predicting the efficacy of treatment or predicting disease progression (Jairath and Feagan, 2020).

Genetic susceptibility encompasses only one component of disease risk; there is a convoluted interplay between genetic and environmental factors which determines the risk of developing IBD. As alluded to above, some genetic variants associated with IBD risk in Western populations are not replicated in Eastern populations (Sood and Midha, 2007; Jostins *et al.*, 2012). What's more, the incidence of IBD has been rising in Eastern countries – including Japan, South Korea, Hong Kong and Saudi Arabia – concomitant with a perceived “Westernisation” of these countries (Thia *et al.*, 2008; Al-Mofarreh and Al-Mofleh, 2013; Ananthakrishnan, 2015). Alongside socio-political changes, Westernisation also leads to changes in lifestyle and behaviour, thereby affecting diet, sleep and the use of medication – all of which may influence IBD risk.

Dietary factors have long been linked IBD, with reduced fibre being the most consistent dietary association with IBD. One study reported that, in a cohort of 170776 women followed up for 26 years, those in the highest quintile of daily fibre intake exhibited a 40% reduction in the risk of CD compared to those in the lowest quintile (Ananthakrishnan *et al.*, 2013). The reduction in the risk of CD was greatest for soluble fibre from fruits and vegetables, though there was no effect of daily fibre intake on the risk of UC. This reduction in the risk of CD is paralleled by the attenuation of inflammatory mediator release and histological changes in experimental models of

colitis in which dietary fibre is supplemented (Rodríguez-Cabezas *et al.*, 2002; Galvez, Rodríguez-Cabezas and Zarzuelo, 2005; Koleva *et al.*, 2012).

The use of numerous medications has been implicated in the development of IBD. A modest association between the use of non-steroidal anti-inflammatories has been identified, but this small risk is likely not relevant in light of the clinical benefits of these drugs (Ananthakrishnan *et al.*, 2012). In contrast, there is a more robust association between the use of oral contraception and CD, though the association with UC was limited to only women with a history of smoking (Khalili *et al.*, 2013). The use of antibiotics – particularly in the first year of life (Kronman *et al.*, 2012) – is linked with the development of IBD. Children receiving one or more antibiotic course(s) in their first year of life were 2.9 times more likely to develop IBD (Shaw, Blanchard and Bernstein, 2010).

The part played by environmental factors in determining IBD risk is further highlighted by studies investigating the risk of IBD in immigrants to Western countries. Although the incidence of IBD is rising in Eastern populations, it is still considerably lower than in Western populations. Early migration studies examined the incidence of IBD in first- and second- generation Indian immigrants in the UK. The incidence of UC amongst these immigrants was higher than in their country of origin and similar to that of the native UK population (Probert *et al.*, 1992). Parsing data from first- and second-generation immigrants revealed that the increase in risk was most evident in second-generation immigrants (Li *et al.*, 2011). First-generation immigrants continued to show lower risk than the native population of the country to which they immigrated (Li *et al.*, 2011). Younger age at immigration was associated with a higher risk of developing IBD (Benchimol *et al.*, 2015), which – along with the elevated risk in second-generation immigrants – implies an importance of early-life exposures in determining IBD risk.

Evidently, the cause of IBD still remains unknown. It is clear, however, that the incidence, and therefore burden, of IBD is increasing. The burden of IBD varies greatly between countries, though the global prevalence of IBD increased from 79.5 to 84.3 per 100000 people between 1990-2017, with a total of 6.8 million IBD cases in 2017 (Alatab *et al.*, 2020). The USA, UK and Northern Europe had the highest age-standardised prevalence rate (ASPR) in 2017 at circa 400 cases per 100000 people, though some countries in Northern Europe had seen a decrease in ASP since 1990

(Alatab *et al.*, 2020). In general, ASPR positively correlates with socio-demographic index, showing that more economically developed countries have a greater prevalence of IBD (Alatab *et al.*, 2020).

Between 1990-2017, the total number of years lived with disability for those with IBD increased almost two-fold, while the standardised disease-adjusted life years (DALYs) – which takes into account the years of ‘healthy’ life lost due to premature death or disability – decreased from 26.5-23.2 per 100000 (Alatab *et al.*, 2020). IBD-related deaths also increased by 67%, though the age-standardised death rate (ASDR) was diminished over the study period (Alatab *et al.*, 2020). The reduction in DALYs and ASDR likely reflects improvements in disease treatment, from disease-modifying drugs, surgical techniques and cancer screening. Although those with CD are not at an increased risk of colorectal cancer, those with UC have a risk twice that of the general population (M. Zhao *et al.*, 2021). However, both CD and UC confer an elevated risk of extra-intestinal cancers, such as haematological, skin and lung (M. Zhao *et al.*, 2021).

Beyond the personal burden of IBD, there is a significant economic burden associated with IBD, too. The costs associated with IBD have shifted from hospitalisation and surgery to outpatient care and pharmacological therapies. For European IBD patients, the mean direct cost per patient per year is €3542 for CD and €2088 for UC (M. Zhao *et al.*, 2021). Given that there is an estimated 1.3 million IBD cases in Europe (M. Zhao *et al.*, 2021), this puts the total annual cost at around €2.7-4.6 billion.

### **1.1.2. Symptoms and disease sequelae**

Although IBD can develop at any age, people are more frequently diagnosed between the ages of 15-35 years. While the symptoms of CD and UC are overlapping, their relative frequencies do differ between diseases. In a study of symptoms present at diagnosis, fatigue and abdominal pain were the most common symptoms for those with CD, with 80.6% and 80.4% reporting these symptoms, respectively (Perler *et al.*, 2019). In contrast, the passage of blood with bowel movements (86.6%) and loose bowel movements (86.5%) were the most commonly reported symptoms upon diagnosis of UC, while abdominal pain was reported by 68.1% of those diagnosed with UC (Perler *et al.*, 2019). Another study found that 87.9% of those with IBD reported abdominal pain (Schirbel *et al.*, 2010). The severity of IBD can be broadly categorised

using the Colitis Activity Index (CAI), which records symptoms such as passage of blood with bowel movements and frequency of bowel movements (Walmsley *et al.*, 1998). CAI positively correlates with patient-reported pain intensity and negatively correlates with health-related quality of life (Schirbel *et al.*, 2010). However, many patients still report abdominal pain during IBD remission (Norton *et al.*, 2017), suggesting persistent changes to the sensory innervation of the gut, rather than inflammation *per se*, can drive abdominal pain.

The above symptoms pertain largely to intestinal disease, but IBD is also linked to numerous extra-intestinal disease manifestations. The reported prevalence of extra-intestinal manifestations in IBD varies substantially, from 6-38% (Rankin *et al.*, 1979; Bernstein *et al.*, 2001; Lakatos *et al.*, 2003; M. Zhao *et al.*, 2021). The risk of extra-intestinal manifestations in CD is associated with disease activity, female gender and advancing age; in UC, the major predictor is extensive colitis (Vavricka *et al.*, 2011).

The most commonly reported extra-intestinal manifestations are those affecting the musculoskeletal system. Peripheral arthropathies, such as rheumatoid arthritis, are more prevalent manifestations than axial arthropathies, such as ankylosing spondylitis (Veloso, Carvalho and Magro, 1996; Lakatos *et al.*, 2003). Reports of arthropathies varies between gender, with females reporting peripheral arthropathies – particularly of the knee – more frequently than males, while the reverse is true for axial arthropathies (Schirbel *et al.*, 2010). Other extra-intestinal manifestations are less common: skin manifestations affect 5-15% of IBD patients, 3-6% have ocular manifestations and 0.7-4% have primary sclerosing cholangitis, an inflammatory condition affecting the bile ducts which can lead to liver damage (M. Zhao *et al.*, 2021).

### **1.1.3. Pathophysiology of IBD**

The pathophysiology of IBD is multifaceted, involving multiple intestinal components and myriad cell types and inflammatory mediators. Primarily, much of what is currently understood about IBD pathophysiology pertains to the dysfunction of the intestinal barrier, microbial dysbiosis in the gut and the immune response in the gut wall (Figure 1.1) (Kobayashi *et al.*, 2020; Roda *et al.*, 2020).

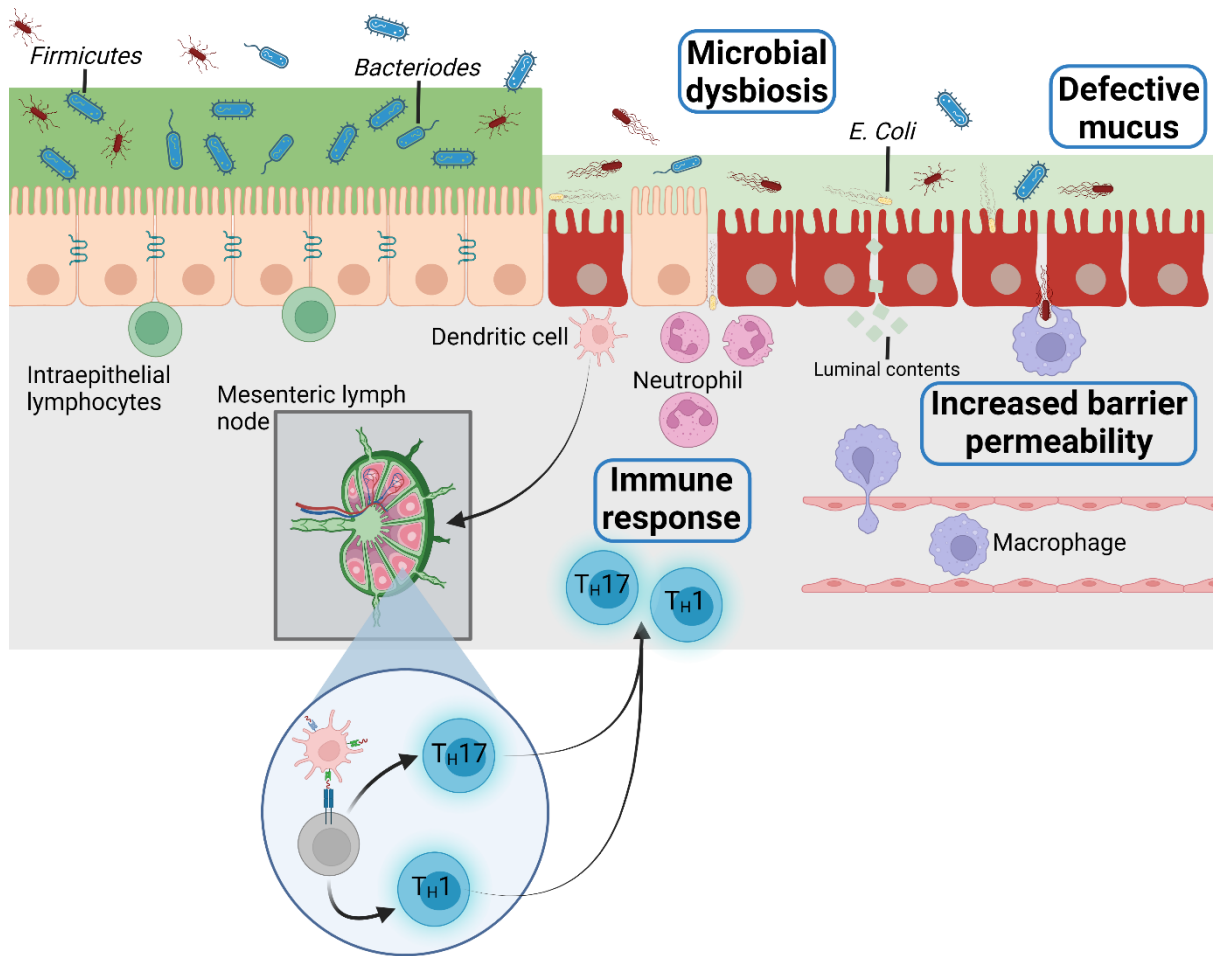


**Figure 1.1 Pathophysiology of IBD**

Summary of the key components of IBD pathophysiology. Microbial dysbiosis and defects in the mucosal lining occur in tandem with changes in the gut barrier – including increased permeability – leading to increased antigen load in the lamina propria (grey shaded area). Resident immune cells drive a local inflammatory response through cytokine release, while antigen-presenting dendritic cells migrate to nearby lymph nodes, where they drive the differentiation and proliferation of effector T-cells. Expression of gut-specific chemokine receptors and integrins enables gut-homing of activated T-cells. In the lamina propria, T-cells carry out further pro-inflammatory functions, such as the release of interferon- $\gamma$  ( $T_H1$ ) or IL-17 and IL-22 ( $T_H2$ ), and the recruitment of further immune cells, leading to persistent inflammation. See text for discussion. Image created in Biorender.

### **1.1.3.1. Intestinal barrier dysfunction**

An intact intestinal barrier minimises luminal antigens crossing into the lamina propria. Immunological tolerance seeks to avoid an inflammatory response from resident immune cells directed against any luminal contents which do cross the barrier. However, if this barrier breaks down and becomes dysfunctional, the increased load of antigens crossing into the lamina propria can overcome immunological tolerance and precipitate a local inflammatory response. The subsequent release of chemokines and cytokines attracts circulating immune cells to the site and activates them, exacerbating the inflammation. This is thought to be a key driver of intestinal inflammation in IBD (Kobayashi *et al.*, 2020; Roda *et al.*, 2020).

#### **1.1.3.1.1. Intestinal mucus**

The intestinal barrier comprises multiple components, all of which can become dysfunctional in IBD. A layer of luminal mucus on the intestinal epithelium is the first part of this barrier encountered by luminal contents. Intestinal mucus is mostly made up of proteins from the heavily glycosylated mucin family, with MUC2 being the most intensely studied member. Production of mucins is a demanding and tightly-controlled task carried out by Goblet cells. Mucins are large proteins (circa 5200 amino acids) produced in a compact form requiring high  $[Ca^{2+}]$  and low pH; upon secretion into the lumen – where  $[Ca^{2+}]$  is lower and pH is higher – mucins expand and form a gel-like layer (Ambort *et al.*, 2012).

In the small intestine, mucus, in addition to a variety of structural proteins, is also laced with antimicrobial peptides secreted by Paneth cells residing within crypts at the base of the villi. The primary function of mucus is to limit the exposure of the intestinal epithelium to luminal antigens. However, the small intestinal mucus remains porous to allow for the absorption of nutrients from the lumen, while Paneth cell-derived antimicrobial products keep the microbiota at bay. There is some evidence that Goblet cells take up luminal antigens, as do M cells, and present these to the underlying dendritic cells (Shan *et al.*, 2013; Johansson, 2014). This is thought to be a tolerogenic signal under healthy conditions (Pelaseyed *et al.*, 2014).

In the colon, there is less need for the mucus layer to remain porous and there is reduced microbe defence due to a lack of Paneth cells. The colonic epithelium is covered by two distinct layers of mucus (Pelaseyed *et al.*, 2014). The outermost is similar in character to that in the small intestine: gel-like, expanded and colonised by

microbes. The inner layer is compact and stratified, behaving as a sub-micron filter. This layer is largely devoid of microbes and serves to more comprehensively limit epithelial exposure to antigens in the absence of antimicrobial secretions (Johansson *et al.*, 2008).

Intestinal mucus undergoes substantial changes in IBD, and these changes differ between CD and UC. The role played by intestinal mucus in the pathophysiology of CD is not clear. It has been reported that the mucus layer is thickened in CD (Pullan *et al.*, 1994). As CD causes a focal, discontinuous inflammation of the GI tract, dysfunction of the mucus barrier in general may not be expected. That being said, some CD-associated polymorphisms lie within genes important for autophagy and mucin production: two such examples are *Xbp1* and *ATG16L1*. *Xbp1* has recently been shown to regulate mucus secretion in the airway (Xu *et al.*, 2021). *ATG16L1* encodes a protein which functions in autophagy, wherein intracellular organelles are trafficked to lysosomes for degradation. Autophagy is important for a broad range of processes, including mucin granule accumulation in Goblet cells (Patel *et al.*, 2013). Paneth cell function may also be impaired in CD (Wehkamp and Stange, 2020). For example, *ATG16L1* is required for normal Paneth cell granule secretion, demonstrated using *ATG16L1* knock-out mice (Bel *et al.*, 2017). Consistently, patients with CD-related ileal inflammation exhibit reduced expression of  $\alpha$ -defensins, the primary antimicrobial peptide family secreted by Paneth cells (Wehkamp *et al.*, 2004, 2005). While the contribution of intestinal mucus to CD pathophysiology is yet to be fully elucidated, there is emerging evidence of dysfunction of this structure in CD.

Contrary to CD, there is a more well-defined role for intestinal mucus in the pathophysiology of UC. The thickness and continuity of the colonic mucosal layer is reduced in UC (Pullan *et al.*, 1994; Strugala, Dettmar and Pearson, 2008). More than this, the composition of the mucus appears to be significantly altered. Important structural components, such as MUC2, are diminished in UC (Van Der Post *et al.*, 2019). Consistently, a reduction in the number of Goblet cells in the colon, as well as abrogated mucus secretion, is observed in colonic biopsies from UC patients (Van Der Post *et al.*, 2019). Abnormal penetrability of the inner layer of the colonic mucus is also present in both animal models of colitis and patients with UC (Johansson *et al.*, 2014; Van Der Post *et al.*, 2019). Mucus penetrability in human colonic biopsies was ascertained using fluorescent beads of differing diameters: in biopsies from UC

patients, the beads were in much closer proximity to the epithelium compared to biopsies from non-inflamed controls (Johansson *et al.*, 2014). In multiple mouse models of colitis, bacteria were observed in the inner mucosal layer of the colon which is sterile under non-inflamed conditions (Johansson *et al.*, 2014). Of particular interest is the finding that colonic sections from mice lacking MUC2 show substantial bacterial penetration and inflammation, demonstrating a key role for this protein in maintaining mucosal integrity (Johansson *et al.*, 2014).

#### **1.1.3.1.2. Intestinal epithelium and cell-cell adhesion**

Beneath the mucus layer, the intestinal epithelium forms an effective physical barrier between the lumen and the lamina propria. Although the major cell type within this layer is the absorptive enterocyte, tasked with absorbing dietary nutrients from the lumen, there are numerous other cell types present, too. Accompanying the previously mentioned Goblet and Paneth cells, enteroendocrine cells secrete hormones in response to luminal stimuli.

While it is vital for nutrients to be absorbed through the epithelial barrier, it must be impenetrable to other luminal contents, microbes and toxins. This is achieved by maintaining neighbouring epithelial cells in very close apposition, requiring cell-cell junctions comprised of large protein complexes. Such complexes can be broadly parsed into three groups based on structure, function and position: desmosomes, adherens junctions and tight junctions.

Of the three groups, desmosomes lie closest to the basolateral aspect of the epithelium. These complexes are made up of desmoplakins and desmogleins, large transmembrane proteins whose extracellular domains interact with congruent complexes on neighbouring cells while the intracellular domain is anchored by keratin filaments (Garrod and Chidgey, 2008). Desmosomes are the most mechanically robust of the junctional complexes and support the structural integrity of the epithelium during mechanical stress (Wallez and Huber, 2008; Brunner, Ragupathy and Borchard, 2021).

Adherens junctions are dynamic cell-cell anchors in which the intracellular face is linking with the actin cytoskeleton. These complexes, made up of extracellular E-cadherins and intracellular catenins, are not only vital for maintaining a structured epithelial layer, but also regulate pericellular passage of leukocytes and the formation

of tight junctions (Hartsock and Nelson, 2008; Brunner, Ragupathy and Borchard, 2021).

Finally, the most apical cell-cell junction – the tight junction – limits the size of the pericellular space at less than 50 Angstroms, allowing only water, electrolytes and small molecules to pass (van Itallie *et al.*, 2008). As such, these complexes are less important for the mechanical and structural integrity of the epithelial layer, but vital for the restriction of pericellular movement (Salama, Eddington and Fasano, 2006). They contain multiple interacting proteins, including members of the claudin family and occludin – important for barrier function – and membrane-associated guanylate kinase, which forms anchors between the transmembrane proteins and the cytoskeleton (Díaz-Coránguez, Liu and Antonetti, 2019).

Both CD and UC are associated with increased permeability of the epithelial barrier. Permeability can be ascertained by monitoring the urinary excretion of a small, neutral, water-soluble compound which is neither metabolised nor stored (Teshima, Dieleman and Meddings, 2012). In CD, a substantial proportion of patients show elevated intestinal permeability across both inflamed and non-inflamed regions of the GI tract (Adenis *et al.*, 1993; Wyatt *et al.*, 1997; Teshima, Dieleman and Meddings, 2012). Furthermore, in a mouse model of spontaneous CD-like ileitis, increased intestinal permeability precedes colitis, and colitis is attenuated if changes in permeability are pharmacologically blocked (Teshima, Dieleman and Meddings, 2012). Similarly, bowel sections from patients with UC are more electrically conductive than non-inflamed controls, suggesting a disruption of the epithelial barrier (Schmitz *et al.*, 1999; Gitter *et al.*, 2001).

Increased epithelial barrier permeability in IBD is associated with enhanced enterocyte apoptosis and changes in the expression of genes required for cell adhesion. The expression of multiple members of the claudin family is suppressed in bowel biopsies from IBD patients: claudins 3, 4 and 7 are decreased in UC (Oshima, Miwa and Joh, 2008), whereas 3, 5 and 8 are decreased in CD (Zeissig *et al.*, 2007). In keeping with this, tight junction strands – micrographic signatures of functional tight junctions are reduced in the inflamed colon (Schmitz *et al.*, 1999). In both colitides, the pore-forming claudin 2 – usually associated with ‘leaky’ epithelium in the proximal tubule of the

nephron – is elevated, offering another explanation for increased permeability (Zeissig *et al.*, 2007; Oshima, Miwa and Joh, 2008; Landy *et al.*, 2016).

### **1.1.3.2. Microbial dysbiosis**

The potential role of the gut microbiome in numerous pathologies has garnered great interest over the last two decades. Intestinal microbial dysbiosis – that is, a change in the microbial composition of the gut – has been repeatedly observed in patients with IBD, though any causative link is still lacking. Environmental factors, such as diet, have a significant influence the microbial composition of the gut. Of particular interest is the observation that a low-fibre diet reduces the diversity of the gut microbiota and raises the risk of developing IBD, especially CD, as discussed above (Pituch-Zdanowska, Banaszkiwicz and Albrecht, 2015; Yao and Staudacher, 2019; Roda *et al.*, 2020). Gut dysbiosis is a major feature of CD and provides a potential mechanistic link between reduced dietary fibre intake and the development of CD.

Differences in the abundance of many specific bacterial species have been observed between those with IBD and healthy control subjects. Generally, the pattern of dysbiosis in IBD is one of increased load and decreased diversity. A decrease in commensal bacteria, namely *Firmicutes*, *Lactobacillus* and *Bacteroides*, concomitant with an increase in *Escherichia* and *Streptococcus* is strongly associated with an inflammatory phenotype (De Hertogh *et al.*, 2008; Joossens *et al.*, 2011; Palmela *et al.*, 2018).

How does a change in the composition of the gut microbiota precipitate inflammation? Commensal bacteria are vital for the integrity of the intestinal barrier and for preventing inflammation through the secretion of various compounds. For example, *F. prausnitzii* is an important commensal whose abundance is suppressed in IBD (Quévrain *et al.*, 2016). This commensal induces a tolerogenic cytokine profile – reducing the risk of local inflammation in the gut – in addition to secreting butyrate and microbial anti-inflammatory molecule which suppresses inflammation by blocking NF-κB and the production of IL-8 and 17 (Sokol *et al.*, 2008; M. Zhang *et al.*, 2016; Quévrain *et al.*, 2016). Many commensals secrete other short-chain fatty acids, like butyrate, which contribute to the anti-inflammatory environment of the healthy gut.

In parallel with a decrease of anti-inflammatory commensals, IBD is also characterised by an increase pro-inflammatory bacterial species. Many strains of *E. coli* colonise the

gut and are not associated with disease. However, the prevalence of some pathogenic strains is elevated in IBD. Adherent invasive *E. coli* (AIEC) has been identified in 90% of CD patients with ileal and ileocolic inflammation, and in 47% of UC patients (Elliott *et al.*, 2013). The pathogenicity of this strain arises from its ability to invade host enterocytes and cross the intestinal barrier into the lamina propria, where it is observed both in the extracellular space and within macrophages (Kleessen *et al.*, 2002). Invasive bacteria are normally disposed of by autophagy, but AIEC may be able to avoid this due to the increased prevalence in CD of genetic variants in genes required for the normal functioning of autophagy, such as *NOD2* (Stevens *et al.*, 2013). Upon arrival into the lamina propria, AIEC are engulfed by macrophages but can survive and replicate within the acidic, proteolytic phagosome and prevent the death of the macrophage leading to secretion of substantial levels of TNF $\alpha$  (Glasser *et al.*, 2001). This will drive further inflammatory signalling and the recruitment and activation of other immune cells.

In mice, the reduction of the gut microbiota by antibiotic treatment blunted the visceral pain response following intracolonic capsaicin administration (Aguilera, Cerdà-Cuéllar and Martínez, 2015). A ten-day antibiotic treatment in male neonatal rats potentiated colonic afferent sensitivity in adulthood (O'Mahony *et al.*, 2014). Moreover, the transfer of antibiotic-perturbed microbiota into mouse pups worsened subsequent colitis induced by dextran sodium sulphate (DSS) treatment. While this study may suggest that the gut microbiota have some role in determining the course of colitis, it does not provide evidence that perturbed gut microbiota predisposes an individual to colitis *per se* (Ozkul *et al.*, 2020). Whether changes in the microbiota is a causative factor in IBD and visceral hypersensitivity, or if it represents a downstream effect of another initiating event is not yet clear.

### **1.1.3.3. Immune response**

Changes in the gut microbiota and the intestinal barrier led to an increase in pathogens and antigens crossing into the lamina propria, where they are able to stimulate resident immune cells, overcome normal immunological tolerance and promote a pro-inflammatory state. Both the innate and adaptive arms of the immune system in the gut have a clear role in precipitating and maintaining inflammation, with myriad cell types and chemical mediators implicated.

The innate immune system in the gut is made up of the mucus and epithelial barriers, alongside innate immune cells resident in the underlying lamina propria. In the healthy gut, dendritic cells play a vital role in antigen capture and the maintenance of intestinal immunological tolerance. Dendritic cells capture antigens through multiple mechanisms. Antigens can be shuttled into the lamina propria by Goblet cells and M-cells scattered within the epithelial barrier; these antigens are then phagocytosed by dendritic cells (Ng *et al.*, 2010). What's more, if the epithelial barrier breaks down, luminal antigens may gain direct access to the lamina propria without the need of a shuttling mechanism. Dendritic cells don't only have to rely on antigens arriving in the lamina propria; they can project dendrites through the epithelial barrier into the lumen to directly capture antigens (Rescigno *et al.*, 2001). This continued observation of antigens passing through the gut appears to be vital for the induction of immune tolerance and pro-inflammatory responses.

Upon capturing a luminal antigen, dendritic cells migrate to the mesenteric lymph nodes which drain the gut, where these antigens are presented to naïve T cells. The conditions which favour the induction of tolerance versus an inflammatory response are not entirely clear. With that being said, it does appear that the conditioning of dendritic cells by factors released by the intestinal epithelium is important for the generation of tolerance (Iliev *et al.*, 2009). Thymic stromal lymphopoietin and retinoic acid – both released by intestinal epithelial cells – drive the differentiation of tolerogenic dendritic cells which go on to promote the development of regulatory T cells (Stagg, 2018). Particular subsets of dendritic cells may favour the generation of a particular response. For instance, CD103<sup>+</sup>, but not CD103<sup>-</sup>/CD11b<sup>+</sup>, dendritic cells induce the expansion of regulatory T cells which secrete anti-inflammatory mediators such as TGFβ and IL-10 (Stagg, 2018), as opposed to effector T cells which drive inflammatory responses.

Tolerogenic mechanisms seem to fail during intestinal inflammation. The process by which immune tolerance is suppressed and a protective immune response is engaged remains a fundamental question in immunology. Dendritic cells have been identified as gatekeepers regulating this process. It has been shown that p38α activity in CD103<sup>+</sup> dendritic cells programs their tolerogenic actions on T cells (Huang, Wang and Chi, 2013). Loss of p38α in only this subset of dendritic cells ameliorated the generation of regulatory T cells and promoted the generation of type 1 helper T cells (Th1) which

produces an inflammatory response. What's more, the number of CD103<sup>+</sup> dendritic cells is depleted in both experimental colitis in mice and in UC (Collins *et al.*, 2011; Matsuno *et al.*, 2017). The importance of dendritic cells in intestinal inflammation has been highlighted by the observation that adoptive transfer of bone marrow-derived dendritic cells worsened experimental colitis in mice, while the selective ablation of CD11b<sup>+</sup> dendritic cells ameliorated colitis (Berndt *et al.*, 2007).

In inflamed tissue from IBD patients, a greater cohort of dendritic cells express the pathogen-associated molecular pattern receptors TLR2 and 4 – activation of which promotes the release of pro-inflammatory cytokines (Hart *et al.*, 2005). Consistently, dendritic cells from inflamed tissue show enhanced microbial antigen recognition and activation (Stagg, 2018). Production of the inflammatory cytokines IL-12, 23 and 6 by dendritic cells in the lamina propria is elevated in CD; production of these cytokines correlates well with disease activity (Ng *et al.*, 2011).

The release of inflammatory cytokines will promote the activation of other immune cell types within the lamina propria. Lymphocytes infiltrate the gut from nearby lymphoid tissue due to gut homing: dendritic cells migrating from the lamina propria to mesenteric lymph nodes induce the expression of the  $\alpha 4\beta 7$  integrin and the chemokine receptor CCR9 in the lymphocytes with which they interact. The ligands for  $\alpha 4\beta 7$  and CCR9 – MAdCAM-1 and CCL25, respectively – are selectively expressed in the gut, resulting in the clustering of these cells here (Mora and von Andrian, 2006). If tolerogenic mechanisms fail, the antigen-presenting dendritic cells drive the maturation of naïve T cells into effector T cells. Of particular importance in IBD are the helper T (Th) cells which release myriad cytokines to orchestrate the immune response. Th1-, Th2- and Th17-associated cytokine profiles can be observed in CD and UC, despite early work suggesting the CD was driven by Th1 cells and UC by Th2 cells (Kobayashi *et al.*, 2020). Many key cytokines play important roles in the intestinal inflammation seen in both diseases, and so such a division is now not usually drawn.

Exemplar mediators with a clear role in intestinal inflammation include:

#### *Tumour necrosis factor alpha (TNF $\alpha$ )*

TNF $\alpha$  is released from immune cells by proteolytic cleavage of its membrane-bound form by ADAM17 (TNF-converting enzyme). The pro-inflammatory activity of TNF $\alpha$  is

mediated by its interaction with its receptors, TNFR1 and TNFR2, which are activated by the soluble and membrane-bound form of TNF $\alpha$ , respectively. Macrophages and T cells from mucosal biopsies of the inflamed bowel – due to IBD or infectious colitis – exhibit markedly elevated production of TNF $\alpha$  (Strober, Fuss and Blumberg, 2002; Neurath, 2014). Animal models of colitis provide further evidence for a causative role of TNF $\alpha$  in inflammation. Mice engineered to persistently over-produce TNF $\alpha$  – either systemically, only from the intestinal epithelium, or only from T cells – develop ileitis, as well as inflammation in other areas, such as the joints (Kontoyiannis *et al.*, 1999). Antibody-mediated neutralisation of membrane-bound TNF $\alpha$  ameliorated colitis in immune-deficient mice, while the activation of TNFR2 exacerbated colitis (Holtmann *et al.*, 2002; Perrier *et al.*, 2013). The potential importance of TNF $\alpha$ -TNFR2 signalling in IBD is highlighted by the observation that TNFR2 expression is elevated in T cells from CD patients (Holtmann *et al.*, 2002). TNF $\alpha$  drives numerous pro-inflammatory changes in the gut, including angiogenesis, further impairment of the epithelial barrier, and the activation of macrophages and effector T cells. These effects perpetuate the inflammatory response by increasing immune cell infiltration and activation.

Anti-TNF $\alpha$  antibodies, such as infliximab, bind to and neutralise the soluble and membrane-bound forms of TNF $\alpha$ . Paediatric patients given infliximab as a first-line therapy were more likely to exhibit clinical remission of disease and to maintain this remission at one year compared to patients given standard corticosteroid therapy (Jongsma *et al.*, 2022). Maintenance of infliximab treatment (administered every 8 weeks) is also associated with an increased likelihood of remission and discontinuation of steroid treatment (Hanauer *et al.*, 2002). However, anti-TNF $\alpha$  therapies are not a silver bullet: around one-third of patients given anti-TNF $\alpha$  therapies show no clinical response and many continue to report significant abdominal pain (Gisbert and Chaparro, 2021). As such, it is important to identify other mediators of inflammation and pain in IBD to shed new light on potential targets for treatment.

#### *Interleukin-12 (IL-12) family cytokines*

The family of IL-12-like cytokines are unique as they comprise the only heterodimeric cytokines, including IL-12, -23, -27 and -35. Of particular importance in IBD are IL-12 and -23, which share a p40 subunit coupled to either a p35 (IL-12) or p19 (IL-23) subunit. Studies utilising p40-lacking mice and p40-neutralising antibodies identified

this subunit and, hence, IL-12 as a key regulator of immune cell function and inflammation in multiple models of colitis (Neurath *et al.*, 1995; Liu *et al.*, 2001). The observation that p40 can dimerise with other subunits called into question these conclusions and the importance of IL-12 (Oppmann *et al.*, 2000), and substantial focus was shifted to examining the role of IL-23. The subsequent use of p19-deficient mice and p19-neutralising antibodies demonstrated a dominant role for IL-23 in driving inflammation in experimental colitis (Hue *et al.*, 2006; Yen *et al.*, 2006). A phase II clinical trial of adults with moderate-to-severe CD in whom TNF $\alpha$ -neutralising therapy was ineffective showed improvements in disease activity after administration of a p19 antibody (Sands *et al.*, 2017). The role of IL-12 remained unclear until recently, Eftychi *et al.* (2019) clarified the temporally distinct roles of IL-12 and -23 (Eftychi *et al.*, 2019). Using a primary epithelial barrier defect to precipitate colitis, the authors showed that interferon- $\gamma$  (IFN $\gamma$ ), along with IL-12 and -23, drove inflammation. Interestingly, in young mice, the initiation of colitis was critically dependent on IL-12 signalling. However, as the mice aged, the chronic inflammatory phenotype was dependent on IL-23, but no longer on IL-12. These observations resolve many other contradictory reports and define a clear rationale for the targeting of IL-12 and -23 in the early and later stages of IBD, respectively.

#### *Interleukin-6 (IL-6)*

The implication of IL-6 in the pathophysiology of IBD is longstanding, with studies in the 1990s finding elevated levels of IL-6 in both the serum and intestinal mucosa of those with CD (Gross *et al.*, 1992). The source of IL-6 was shown to be primarily macrophages and T-cells infiltrating the lamina propria, as well as resident colonic epithelial cells (Kusugami *et al.*, 1995). Endoscopically graded colonic inflammation is positively correlated with levels of serum IL-6, and disease relapse is more likely if IL-6 remains persistently raised during remission (Reinisch, 1999; Van Kemseke, Belaiche and Louis, 2000). In addition to IL-6, the soluble IL-6 receptor (sIL-6R) was reported to be raised in the serum of patients with CD and UC (Mitsuyama *et al.*, 1995). A small clinical trial (n = 36) evaluating the efficacy of an anti-sIL-6R antibody found a clinical response – that is, a reduction in disease activity – in 80% of patients given the antibody, compared to 31% of those receiving placebo (Ito, 2005). A later trial with a greater sample of patients (n = 247) – all of whom were refractory to conventional treatments – also reported a reduction in disease activity and a reduced risk of relapse

in those receiving an anti-sIL-6R antibody (Danese *et al.*, 2019). Despite this, it was noted that in the treatment group, there was a greater risk of abscess formation and bowel perforation, which will require meticulous characterisation before the further development of this potential treatment.

The pathophysiology of IBD is clearly multifactorial and incompletely understood, involving a complex interplay between a multitude of factors.

## **1.2. Mechanisms driving (visceral) pain during inflammation**

The sensory nervous system provides information about internal and external stimuli. Nociception is the process by which the sensory nervous system encodes damaging, or potentially damaging, stimuli, and is carried out by nociceptors, a subset of primary sensory neurons which respond to noxious stimuli. These specialised neurons project peripheral axons which innervate peripheral structures, such as the skin or viscera, and central axons which innervate second order sensory neurons in the spinal dorsal horn projecting to the brain. Their cell bodies reside in the dorsal root ganglia (DRG) or trigeminal ganglia (TG), depending on whether they innervate the body or head, respectively.

Under normal conditions, nociceptors are activated by noxious stimuli, such as extreme temperatures or high pressures. However, during inflammation, nociceptors can become sensitised, leading to their activation by previously innocuous stimuli, known as allodynia, and augmented activity in response to mildly noxious stimuli, known as hyperalgesia (Figure 1.2). Inflammatory mediators and cytokines released by damaged cells and immune cells can drive processes leading to the sensitisation of nociceptors, which may outlast the inflammatory insult and result in persistent pain. Gut-innervating nociceptors respond to high pressure, as may be experienced during constipation or bowel obstruction. However, sensitisation during IBD leads to their activation by previously innocuous pressures, such as those resulting from normal gut transit, leading to persistent abdominal pain. Pain is frequently present in patients exhibiting clinical remission of inflammation, indicating that the inflammatory insult drives prolonged changes in sensory neuron function and, hence, chronic pain (Bakshi *et al.*, 2021).

Purine and pyrimidine nucleotides – ATP and UTP – are released from both damaged epithelial cells and immune cells during colitis (Shinoda, Feng and Gebhart, 2009).

Both of these mediators stimulate visceral nociceptors via P2X and P2Y receptors, leading to action potential firing dependent on the voltage-gated Na<sup>+</sup> channel, Nav1.9 (Hockley *et al.*, 2016). Enhanced nocifensive responses to colorectal distention due to experimental colitis could be attenuated by inhibition of P2X receptors (Xu *et al.*, 2008). Many other inflammatory mediators released by immune cells act on nociceptive neurons, changing their properties and leading to pain. TNF $\alpha$  induces thermal and mechanical hyperalgesia by elevating the excitability of nociceptive neurons. This sensitising effect is the result of a hyperpolarising shift in the voltage dependence of activation of a persistent Na<sup>+</sup> current, likely conveyed by Nav1.9 (Gudes *et al.*, 2015). TNF $\alpha$ -mediated changes in the properties of Na<sup>+</sup> currents are dependent on p38 mitogen-activated protein kinase (MAPK), indicating that Na<sup>+</sup> channel phosphorylation may underpin the effect of TNF $\alpha$  (Gudes *et al.*, 2015). Additionally, mechanical hypersensitivity of colonic afferents induced by serum samples from patients with irritable bowel syndrome was attenuated by infliximab, while no hypersensitivity was observed with samples from healthy volunteers (Hughes *et al.*, 2013).

Numerous proteases, which act via protease-activated receptors (PARs), are released by immune cells. Activation of PAR2 expressed on sensory neurons *in vitro* resulted in a marked increase in excitability due to the suppression of a sustained K<sup>+</sup> current (Kayssi *et al.*, 2007), likely to be M-current carried by members of the K<sub>v</sub>7 family (Linley *et al.*, 2008). PAR2 activation also contributes to hypersensitivity to colorectal distension. In this study, it was found that PAR2 acts by enhancing currents through the V4 member of the transient receptor potential family of ion channels (TRPV4), leading to elevated action potential discharge in colonic afferent nerves in response to colon distention (Sipe *et al.*, 2008). These reports highlight the interaction between inflammatory mediators and sensory neurons, demonstrating that these mediators can exert profound changes in sensory neuronal function. The development of novel analgesics for pain in inflammatory diseases will require a more complete understanding of the mediators which interact with sensory neurons, and the mechanisms by which they drive changes in neuronal function.

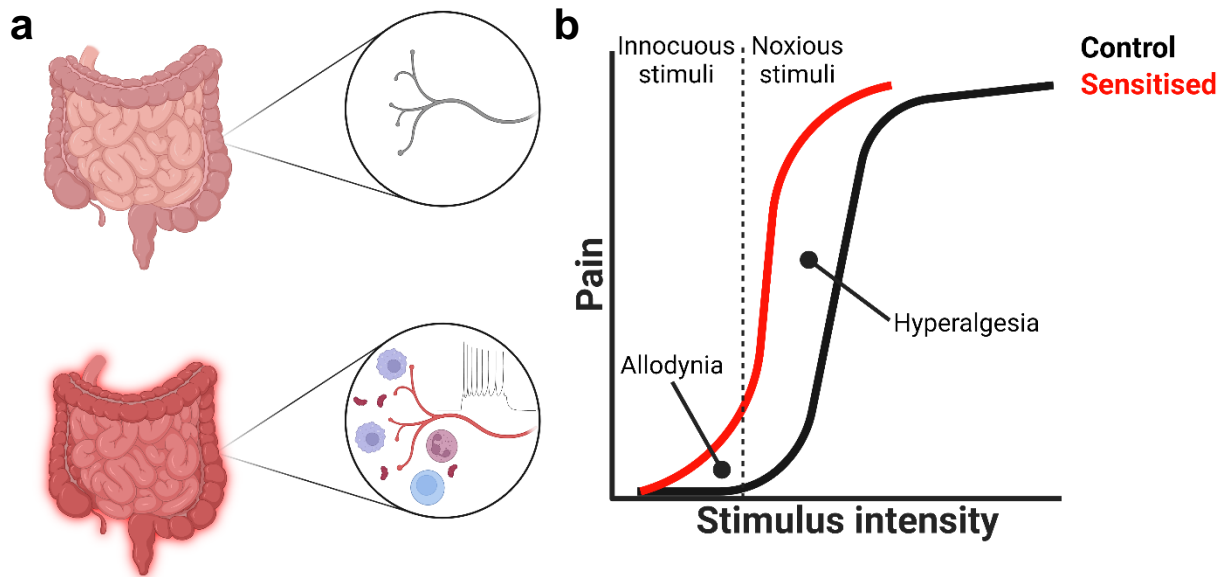


**Figure 1.2 Sensitisation of nociceptive sensory neurons**

- (a) In the healthy gut (*top*), high-threshold nociceptors only respond to noxious stimuli, such as high pressure and distention of the gut. However, in the inflamed gut (*bottom*), infiltrating immune cells, as well as damaged epithelia, secrete inflammatory mediators and cytokines which drive electrical activity of nociceptors directly, or result in nociceptor sensitisation, resulting in activity in response to ordinarily innocuous stimuli.
- (b) Graph depicting sensitisation. The black curve shows the normal response to stimuli – say, colon distension – of increasing intensity. Stimuli to the left of the dashed line are innocuous and do not elicit pain, whereas those to the right of the dashed line are noxious and elicit increasing pain intensity. The curve shows the sensitised state. Under these conditions, innocuous stimuli elicit pain – referred to as allodynia – and noxious stimuli elicit greater pain intensity – known as hyperalgesia. Image created using Biorender.

### **1.3. Angiotensin II, inflammation and IBD**

Angiotensin II (Ang II) is an octapeptide known to play a key role in the regulation of circulating volume and blood pressure (for review, see (Hall, 1991)). Its precursor, Angiotensinogen (Agt) is produced by the liver and is a substrate for the enzyme renin, which produces Ang I. The secretion of renin by pericytes in the kidney is promoted by reduced blood pressure, detected by baroreceptors, or by a decrease in Na<sup>+</sup> delivered to the macula densa, an area of specialised cells lining the distal tubule of the nephron. As such, serum levels of Ang I are elevated when blood pressure is lowered. In turn, Ang II is produced from Ang I by the action of angiotensin converting enzyme (ACE). Ang II exerts myriad effects on the cardiovascular system to raise blood pressure, from acting directly to constrict blood vessels, prompting the release of aldosterone to promote water reabsorption in the kidney, inducing catecholamine release to increase heart rate and contractility, to promoting thirst. Ang II acts through two G-protein-coupled receptors (GPCRs), AT1R and AT2R, which have a broad expression pattern. AT1R is expressed in the heart, vasculature, discrete components of the nervous system and the kidney: this receptor mediates the effects of Ang II on blood pressure. AT2R is expressed more highly in the foetus and neonate, with its roles including the development of the vascular system, cellular differentiation and certain immune functions. AT2R is not widespread in the adult, and its function remains controversial, though its expression is elevated in disease states such as myocardial infarction.

#### **1.3.1. Ang II beyond blood pressure**

More recently, Ang II has been implicated in inflammatory processes. The first evidence for this came from studies on the mechanisms underlying atherosclerosis. Inhibition of ACE or AT1R was found to reduce the formation and progression of atherosclerotic lesions. Ang II was found to promote proliferation of vascular smooth muscle cells, endothelial cell apoptosis and the induction of cell adhesion molecules and pro-inflammatory cytokines (Schmidt-Ott, Kagiya and Phillips, 2000). Beyond atherosclerosis, Ang II is now known to promote inflammation through various mechanisms, largely acting through AT1R, which could be of significance in inflammatory diseases. This includes inducing T-cell proliferation and release of cytokines, and increasing dendritic cell migration (Benigni, Cassis and Remuzzi, 2010).

Rheumatoid arthritis (RA) is a chronic, progressive inflammatory disease, predominantly affecting the joints – leading to joint damage, pain and impaired function – with numerous possible extra-articular manifestations (Conforti *et al.*, 2021). Comparable with IBD, immune cell infiltration and pro-inflammatory cytokine release is a key feature of joints affected by RA (Epstein and Harris, 1990). Studies in patients and animal models have indicated a potential role for Ang II in RA pathophysiology. AT1R blockade is effective in reducing markers of inflammation, such as TNF $\alpha$  production and immune cell infiltration (Chang and Wei, 2015). Raised expression of ACE in the joint synovium in RA may contribute to locally raised Ang II (Walsh, Catravas and Wharton, 2000). Therefore, it is becoming clear that Ang II signalling is of importance outside of the cardiovascular system, and it may represent a key pro-inflammatory mediator.

### **1.3.2. Ang II in the pathophysiology of IBD**

There is now growing evidence that Ang II and AT1R function in the pathophysiology of IBD. Compelling evidence has been garnered from animal models of colitis. DSS-induced colitis in mice results in weight loss, histopathological changes in the colon and the release of pro-inflammatory cytokines, such as TNF $\alpha$ . Concomitant administration of enalaprilat, an ACE inhibitor, attenuated weight loss and the expression of TNF $\alpha$  mRNA during DSS colitis (Spencer *et al.*, 2007). The occurrence of ulcerative lesions and apoptotic epithelial cells in the colon was also reduced by ACE inhibition (Spencer *et al.*, 2007). In rats, blockade of AT1R with valsartan attenuated gross inflammation in two models of chemically-induced colitis. This included a reduction in immune cell infiltration in the colonic mucosa, reduced pro-inflammatory cytokines, namely TNF $\alpha$  and IL-18, and the reduced occurrence of diarrhoea (Santiago *et al.*, 2008; Shi *et al.*, 2016). Valsartan also increased the level of IL-10, known to be anti-inflammatory, in DSS colitis (Santiago *et al.*, 2008). The severity of DSS-induced colitis was also reduced in mice lacking AT1R expression (Katada *et al.*, 2008). This study also revealed elevated Ang II in the colonic mucosa after the induction of colitis (Katada *et al.*, 2008). Importantly, stimulation of Ang II production through the overexpression of renin, or chronic Ang II administration, precipitated colitis in mice, leading to elevated mucosal expression of TNF $\alpha$ , IL-1 $\beta$ , IL-6 and IL-17 (Shi *et al.*, 2016). Finally, those with IBD are at greater risk of developing colorectal cancer, though AT1R antagonists also abrogated colitis-induced

tumorigenesis (Hachiya *et al.*, 2021). Taken together, these studies indicate that Ang II is elevated in experimental colitis and that it exerts a pro-inflammatory effect, potentially by promoting the synthesis and/or secretion of cytokines which drive an aberrant immune response.

While animal models are useful in untangling the mechanisms of disease, it is important to validate the role of Ang II in IBD in humans. In the colonic mucosa of patients with IBD, levels of Ang I and Ang II were elevated compared to non-inflamed controls (Jaszewski *et al.*, 1990). Ang II was greater in CD compared to UC, and it correlated with endoscopically graded inflammation (Jaszewski *et al.*, 1990). A later study corroborated this initial finding by showing elevated levels of Agt mRNA in the inflamed bowel (Garg *et al.*, 2020). Colonic biopsies have revealed elevated Agt mRNA in the mucosa of paediatric patients who are treatment naïve, as well as those treated with infliximab, suggesting the Ang II-producing pathway is not targeted by anti-TNF $\alpha$  treatments (Figure 1.3a-d; Prof. Nick Croft, unpublished observation). While an increase in renin mRNA was also observed, levels of ACE were no different between those with IBD and non-inflamed controls (Garg *et al.*, 2020). These findings, and those in animal models, prompted investigations into the effects of ACE inhibitors and AT1R antagonists on the severity and progression of IBD. No randomised control trial data pertaining to the use of ACE inhibitors and AT1R antagonists yet exists, though retrospective observational studies have been performed. Coincidental prescription of either ACE inhibitors and AT1R antagonists has been associated with a milder disease course and reduced need for immunomodulators, such as corticosteroids (Jacobs *et al.*, 2019; Mantaka *et al.*, 2021). This may be due to the reduced mucosal expression of TNF $\alpha$ , IL-1 $\beta$  and IL-6 in IBD patients prescribed AT1R antagonists (Shi *et al.*, 2016). IBD patients in whom Ang II signalling was suppressed also had a reduced risk of hospitalisation and surgery (Jacobs *et al.*, 2019; Fairbrass *et al.*, 2021). Retrospectively comparing disease outcomes before and during the use of ACE inhibitors and AT1R antagonists revealed an increase in hospitalisations in those with UC, though the authors urge caution when interpreting these results due to the low sample size and variable follow-up time (Jacobs *et al.*, 2019). The utility of these studies is limited as they are observational; prospective, interventional studies will be required to properly ascertain the efficacy of ACE inhibitors and AT1R antagonists in IBD treatment.

Serum Ang II is not elevated in patients with IBD (Garg *et al.*, 2015), indicating that local production underpins Ang II elevation in the inflamed bowel. As stated above, Agt is raised in the inflamed bowel, and expression is correlated with markers of macrophages (e.g., CD14 and CD68) indicating these immune cells as a potential source of Agt (Figure 1.3e; Prof Nick Croft, unpublished observation) (Kitazono *et al.*, 1995), but how is Ang II produced? The pro-renin receptor, which binds renin and stimulates the conversion of Agt to Ang I is highly expressed on sensory neurons, including those innervating the colon (Usoskin *et al.*, 2015; Hockley *et al.*, 2019). Cathepsin G, a serine protease secreted by neutrophils and upregulated in IBD, can produce Ang II from either Agt or Ang I (Figure 1.4) (Owen and Campbell, 1998; Dabek *et al.*, 2009; Jablaoui *et al.*, 2020). This pathway provides a local source of Ang II during inflammation.

Current data strongly suggests that Ang II is an important mediator of inflammation in IBD, and other inflammatory diseases, but what about pain? If Ang II drives inflammation, it will undoubtedly also drive pain, but it is not yet known if Ang II *itself* is pro-nociceptive. A significant proportion of IBD patients whose inflammation is in remission still experience significant visceral pain (Takahashi *et al.*, 2021). In those who are treated with infliximab, an anti-TNF $\alpha$  antibody, Agt – and presumably Ang II – remains elevated in the bowel wall (Prof. Nick Croft, unpublished observation). If Ang II is able to interact with nociceptive sensory neurons, it may be partly responsible for driving pain, even in patients whose inflammation is in remission. Ang II has been implicated in neuropathic – but not inflammatory – pain, and it has been posited that it acts through AT2R expressed on macrophages, which subsequently release reactive oxygen species to drive pain (Shepherd *et al.*, 2018). AT2R antagonists showed promise in pre-clinical studies of neuropathic pain (Smith *et al.*, 2013), and displayed superior efficacy compared to placebo in the relief of postherpetic neuralgia (Rice *et al.*, 2014). The proposed mechanism of action is suppression of aberrant neurite outgrowth and inhibition of the V1 member of the transient receptor potential family of ion channels (TRPV1) (Anand *et al.*, 2015). However, this is at odds with the lack of expression of AT2R on sensory neurons (Usoskin *et al.*, 2015; Zeisel *et al.*, 2018), so perhaps a non-neuronal site of action should be considered (Shepherd *et al.*, 2018). The role of AT1R in nociception and pain is not known, though AT1R is highly expressed on sensory neurons (Usoskin *et al.*, 2015). Co-expression of AT1R with the

voltage-gated Na<sup>+</sup> channel, Nav1.8, indicates that the AT1R-expressing sensory neuron population may be nociceptive (Usoskin *et al.*, 2015). In colon-innervating neurons, AT1R is highly expressed in a MrgD-expressing neuronal population (Hockley *et al.*, 2019). MrgD is a receptor for  $\beta$ -alanine and 5-oxo-ete, a pro-nociceptive lipid elevated in irritable bowel syndrome, and this MrgD-positive population of neurons is known to transmit noxious signals from the colon (Bautzova *et al.*, 2018; Castro *et al.*, 2019). A greater understanding of the interaction between Ang II and sensory neurons will shed new light on the role of this peptide in nociception.

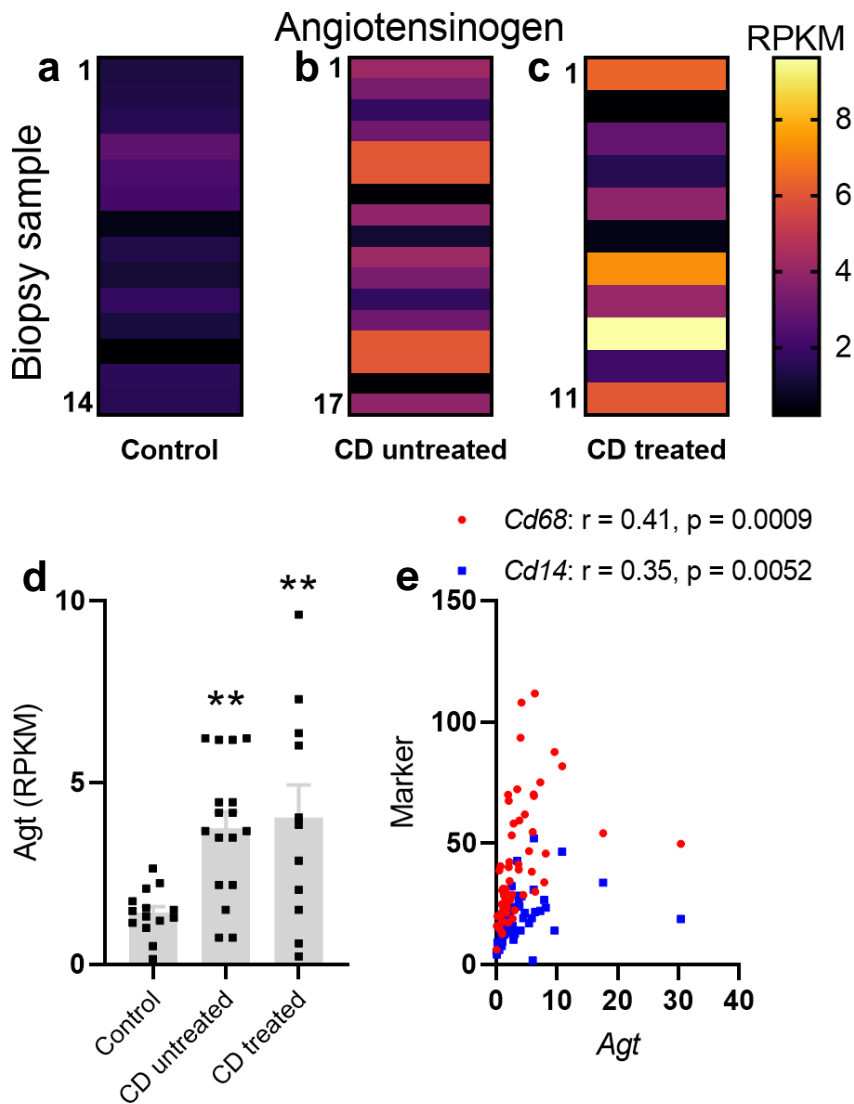


**Figure 1.3 Angiotensinogen mRNA is raised in paediatric CD patients**

- (a) Heatmap showing the presence of *Agt* transcripts (expressed as reads per kilobase per million, RPKM) in colonic biopsies from non-inflamed control patients (n = 14).
- (b) Heatmap showing the presence of *Agt* transcripts in colonic biopsies from treatment naïve patients with CD (n = 17).
- (c) Heatmap showing the presence of *Agt* transcripts in colonic biopsies from patients with CD currently being treated with infliximab (n = 11).
- (d) Grouped data showing *Agt* RPKM in colonic biopsies in each patient group. Data analysed using a one-way ANOVA with Bonferroni's post-tests.
- (e) Correlation between the expression (given as RPKM) of *Agt* and markers of macrophages, *Cd14* and *Cd64*, in biopsy samples from patients with CD and UC. Data analysed using Pearson's correlation.

Data collected and donated by Prof. Nick Croft, Queen Mary University of London; graphed and analysed by the author.

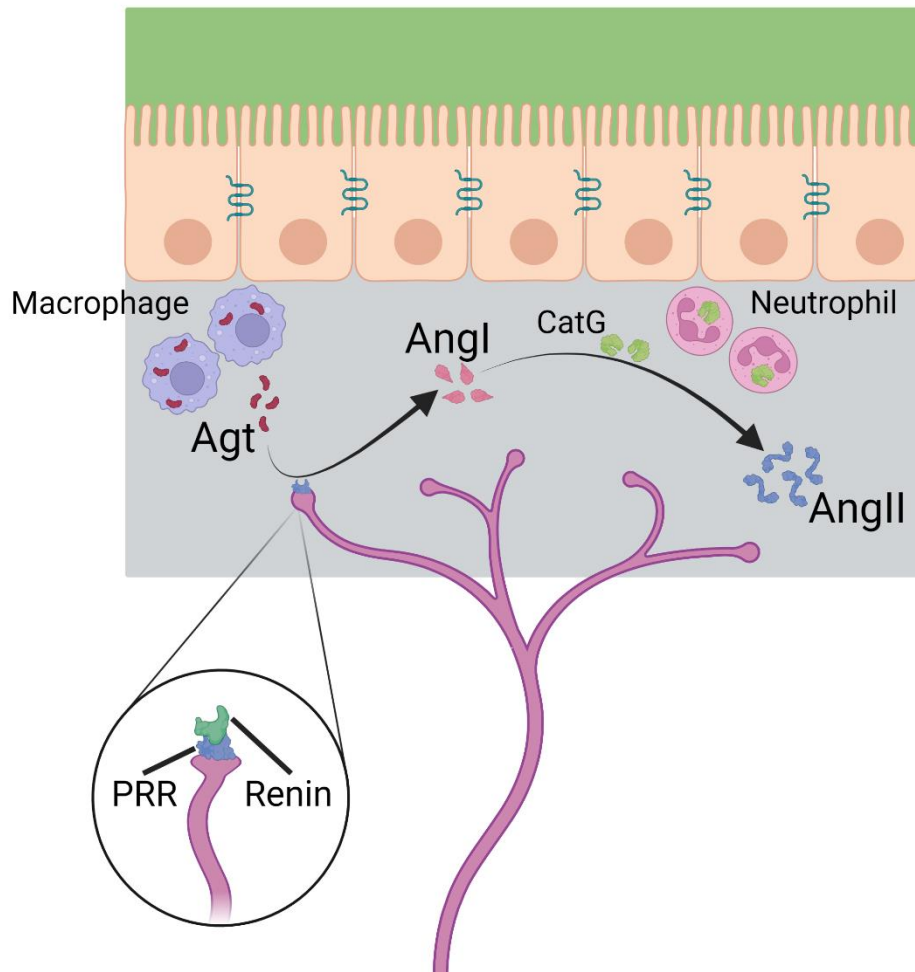


**Figure 1.4 Local production of Ang II during inflammation**

Agt, released by macrophages, can be broken down to Ang I by renin bound to its receptor (PRR) expressed on colon-innervating sensory neurons. Ang I conversion to Ang II can be catalysed by Cathepsin G (CatG), secreted by infiltrating neutrophils, yielding locally elevated Ang II levels. Image created using Biorender.

## 1.4. Investigating nociception *in vitro*

*In vitro* assays can be used prospectively to provide important information regarding the pro-nociceptive potential of a given mediator, before moving into *in vivo* studies. Insights into the mechanisms which drive pain *in vivo* can also be gained by examining sensory neuronal function *in vitro*. Myriad assays for investigating neuronal function *in vitro* are now available, each of which can be used to answer distinct questions.

### 1.4.1. Fluorescent Ca<sup>2+</sup> imaging

The development of Ca<sup>2+</sup>-sensitive indicators, largely attributed to work by Roger Tsien (Tsien, 1980; Zhou, Belavek and Miller, 2021), made it possible to non-invasively track the stimulation of large numbers of neurons simultaneously. The utility of these indicators relies on a change in their spectral properties upon Ca<sup>2+</sup> binding. Single wavelength indicators – such as Fluo4 – are excited by a single wavelength and undergo an increase in fluorescence at a given emission wavelength upon Ca<sup>2+</sup> binding. Dual wavelength indicators – such as Fura2 – emit at a single wavelength but can be excited by two wavelengths; the ratio of their emission at each excitation wavelength provides a metric of Ca<sup>2+</sup> concentration. The ratiometric nature of Fura2 provides an accurate measure of Ca<sup>2+</sup> concentration, and avoids problems associated with single wavelength indicators, such as differential loading, photobleaching and differing illumination intensity. Fluo4 is more applicable for the measurement of changes in Ca<sup>2+</sup> concentration, though measurement of absolute Ca<sup>2+</sup> concentration is possible (Maravall *et al.*, 2000; see Appendix A1.3.). The affinity of Fluo4 for Ca<sup>2+</sup> is also lower than Fura2 (~325 vs ~225 nM). While small increases in Ca<sup>2+</sup> may be missed, Fluo4 is useful for examining bulk changes in Ca<sup>2+</sup> in a broad range of cell types (i.e., average across a whole cell, rather than small changes associated with subcellular domains). Moreover, the relatively low affinity for Ca<sup>2+</sup> means saturation of Fluo4 is less of a concern, and Fluo4 has a much greater fluorescence and greater dynamic range than its predecessors (Gee *et al.*, 2000).

Ca<sup>2+</sup> imaging is used extensively in the study of sensory neurons *in vitro*. This approach permitted the functional profiling of sensory neurons, highlighting differential effects of algogens and K<sup>+</sup> channel blockers (Teichert *et al.*, 2012). These pharmacological differences indicated heterogeneous expression of multiple receptors and ion channels across sensory neurons, an observation later confirmed using transcriptomics and electrophysiology (Usoskin *et al.*, 2015; Zheng *et al.*, 2019). Ca<sup>2+</sup>

imaging of DRG neurons also provided insights into the mechanism underlying neuronal stimulation by biopsy supernatants from patients with irritable bowel syndrome (Desormeaux *et al.*, 2018).

While  $\text{Ca}^{2+}$  imaging is of great value for investigating intracellular signalling, changes in intracellular  $\text{Ca}^{2+}$  should not necessarily be conflated with electrical activity of a neuron. A rise in cytosolic  $\text{Ca}^{2+}$  may provide an indirect measure of action potential discharge, but  $\text{Ca}^{2+}$  may also arise from voltage-independent sources, such as TRP channels, ligand-gated ion channels and intracellular stores. Probing neuronal electrical activity requires a direct measure of membrane potential.

#### **1.4.2. Patch-clamp electrophysiology**

Patch-clamp electrophysiology, whereby a glass pipette is used to form a high-resistance electrical seal with the cell membrane to measure transmembrane voltage or current, has yielded unprecedented insights into neuronal physiology. Patch-clamp was developed by Neher and Sakmann, building upon work by Cole, Hodgkin and Huxley using the voltage-clamp (Neher and Sakmann, 1976). The voltage-clamp circuit measures the current required to hold the membrane potential at a given value set by the experimenter, thereby providing a measure of the current across the neuronal membrane. Measurements of membrane voltage are also possible in current-clamp mode, in which a known current is applied to the cell and changes in membrane potential are monitored. While this technique can provide exquisitely detailed information on neuronal physiology and ion channel function, it is time-consuming and low-throughput. Beyond this, the technique is invasive, requiring the rupture of the cell membrane and dialysis of the intracellular milieu. The electrical properties of the recording equipment can also interfere with the signal, and so care is required to ensure recordings are of sufficient quality and artefacts do not affect the interpretation of the data obtained.

#### **1.4.3. Protein expression**

Neuronal function is largely dependent on the complement of proteins they express, and, while gene expression studies provide important information, gene expression does not always indicate protein expression, nor whether the protein is functional. Identification of proteins present in sensory neurons complements functional studies and can provide greater mechanistic understanding. Immunofluorescent staining of

sensory neurons provides a semi-quantitative method of probing protein expression *in vitro* (Cregger, Berger and Rimm, 2006), under the same conditions as  $\text{Ca}^{2+}$  imaging and patch-clamp electrophysiology. Immunofluorescence requires the fixing of neurons and the subsequent labelling of expressed proteins using antibodies raised against specific epitopes on the protein of interest. This antibody may be conjugated to a fluorophore, or bound with a secondary conjugated antibody, to reveal protein localisation, whether within individual cells (e.g., plasma membrane vs cytosol) or within populations of cells (e.g., small vs large neurons).

### **1.5. Principle aims**

Given the apparent importance of Ang II and AT1R in IBD, and other painful inflammatory diseases, and the expression of AT1R on sensory neurons, it was hypothesised that Ang II may exert pro-nociceptive effects through an interaction with a sub-population of sensory neurons. In order to test this hypothesis, the following questions were asked:

- i. Does Ang II stimulate cultured sensory neurons, indicated by a rise in cytosolic  $\text{Ca}^{2+}$ ?
  - a. Do these neurons display key characteristics of nociceptors, e.g., small soma size, expression of TRPV1, and expression of  $\text{Nav}1.8$ ?
- ii. What are the mechanisms that underpin the interaction between Ang II and sensory neurons?
  - a. Are neurons stimulated directly, or is there a requirement for other cell types?
  - b. What mechanisms drive cytosolic  $\text{Ca}^{2+}$  signals?
- iii. Does Ang II induce prolonged changes in neuronal function?

## **Chapter 2**

### **Methods and materials**

## 2.1. Methods and materials

### 2.1.1. Animals

All animal work was carried out in accordance with the Animals (Scientific Procedures) Act 1986. Male wild-type C57Bl/6 mice (Charles River, MA, USA) were housed in groups of up to six littermates with nesting material and shelter at 21°C under a 12h/12h light/dark cycle with *ad libitum* access to food and water. Mice aged 8-16 weeks were culled by procedures outlined in Schedule 1 of the Animals (Scientific Procedures) Act 1986, specifically by exposure to a rising concentration of CO<sub>2</sub> and cervical dislocation.

All genetically-engineered mice used in the main body of this Thesis were generated, housed, genotyped and kindly donated by the laboratories of Prof James Cox and Prof John Wood of the Molecular Nociception Group, University College London.

Labelling of Nav1.8-positive neurons was achieved by neuron-specific expression of the red fluorescent reporter, tdTomato (tdTom). Mice heterozygous for Nav1.8-Cre were crossed with mice heterozygous for ROAS26-CAG-floxstop-tdTom, generating mice in which Nav1.8-expressing neurons express tdTom due to the Cre-mediated excision of the floxed stop sequence (Figure 2.1a) (J. Zhao *et al.*, 2021). A CAG promoter was used to ensure robust expression of tdTom.

Ablation of Nav1.8-positive neurons was achieved by neuron-specific expression of the A Chain of Diphtheria Toxin (DTA). Mice heterozygous for Nav1.8-Cre were crossed with mice homozygous for ROSA26-floxstop-DTA, generating mice in which Nav1.8-expressing neurons were ablated (Figure 2.1b) (Ivanova *et al.*, 2005; Abrahamsen *et al.*, 2008). For the purposes of Ca<sup>2+</sup> imaging, the response of neurons from Nav1.8-Cre-DTA mice was compared to that of wild type mice because of the presence of GFP within the floxed stop sequence which would have masked Fluo4 fluorescence. In future experiments, ROSA26-floxstop-DTA-negative, Cre-positive mice will be used as a control genotype, but these were not available at the time of the experiments detailed here.

Ablation of non-peptidergic, Tmem45b-expressing neurons was again achieved by neuron-specific expression of DTA (Usoskin *et al.*, 2015; J. Zhao *et al.*, 2021). Mice heterozygous for Tmem45b-Cre were crossed with mice homozygous for Advil-floxstop-DTA, generating mice in which Tmem45b-expressing neurons were ablated

(Figure 2.1c). Offspring which were positive for Advil-floxstop-DTA but negative for Tmem45b-Cre were used as a control genotype. See Section 3.3 for discussion of mouse lines used.

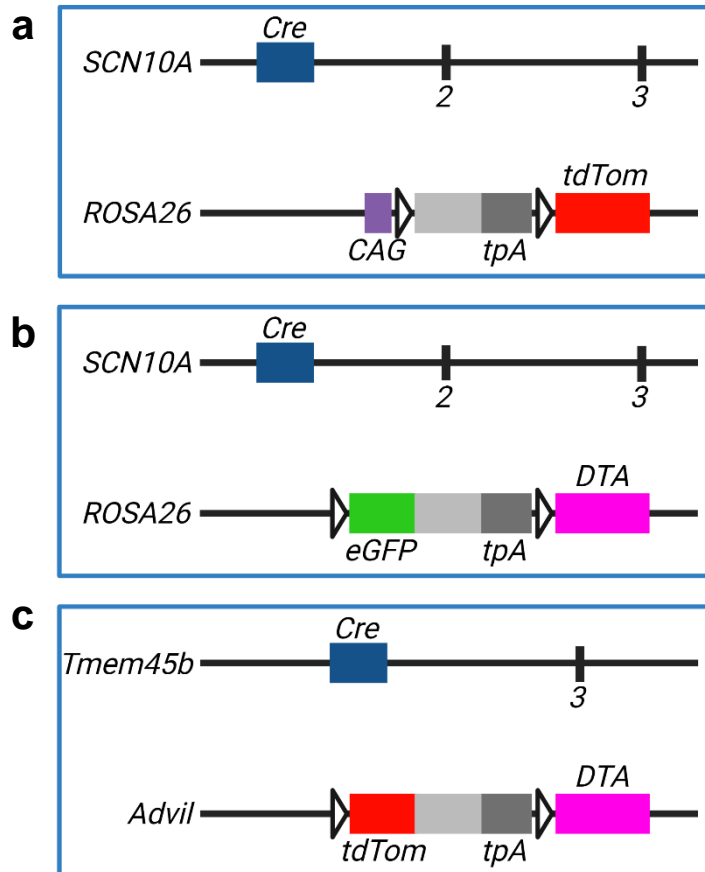


**Figure 2.1 Generation of mouse genotypes for the selective labelling or ablation of sensory neuron populations**

- (a) Generation of Na<sub>v</sub>1.8-Cre-tdTom mice. Cre recombinase was inserted in exon 1 of the *SCN10A* gene. TdTom was inserted downstream of a floxed (triangles) stop sequence (*tpA*), such that excision of the floxed site yields tdTom expression in only Cre-positive neurons.
- (b) Generation of Na<sub>v</sub>1.8-Cre-DTA mice.
- (c) Generation of *Tmem45b*-Cre-DTA mice. Cre recombinase was inserted in exon 2 of the *Tmem45b* gene. Image created using Biorender.

## **2.1.2. Ca<sup>2+</sup> imaging of cultured sensory neurons**

### **2.1.2.1. Culture of sensory neurons from dorsal root ganglia**

Following euthanasia, the spinal column was removed, divided in two along its mid-sagittal plane and the spinal cord excised to expose the dorsal root ganglia (DRG) within the intervertebral foramina. DRG from spinal levels T12-L5 were dissected out of their foramina, trimmed of connective tissue and nerve roots, and placed immediately into ice cold L-15 culture medium (Gibco, supplemented with 24 mM NaHCO<sub>3</sub>). DRG were then incubated at 37 °C with collagenase (Sigma-Aldrich; 1 mg/mL with 6 mg/mL bovine serum albumin [BSA]) for 15 minutes, followed by washing and subsequent incubation with trypsin (Sigma-Aldrich; 1 mg/mL with 6 mg/mL BSA) for 30 minutes. After enzymatic incubation, DRG were transferred into L-15 culture media warmed to 37 °C and supplemented with 10% foetal bovine serum (FBS), 24 mM NaHCO<sub>3</sub>, 38 mM glucose and 2% penicillin/streptomycin. DRG were gently triturated (P1000 tip) to mechanically disperse neurons. Five rounds of trituration were performed. After each round, the DRG were centrifuged at 1100 rpm for 30 s; the supernatant was collected, and the pellet resuspended in supplemented L-15 media. The collected supernatant (final volume 10 mL) was centrifuged at 1000 rpm for 5 minutes to pellet the neurons, which were resuspended in 250 µL supplemented L-15. 50 µL of this neuronal suspension was added to 35 mm glass-bottomed culture dishes (MatTek, MA, USA; coated with poly-D-lysine and laminin) and incubated at 37 °C with 95% air/5% CO<sub>2</sub> for three hours to allow the neurons to adhere to the plate. Finally, dishes were flooded with 2 mL supplemented L-15 and used for experiments after 16-24 hours.

### **2.1.2.2. Ca<sup>2+</sup> imaging**

Culture media was removed from dishes and cells were loaded with Fluo-4 by incubation with 100 µL of 10 µM Fluo-4-AM (Thermofisher Scientific; diluted in bath solution below) for 30-45 minutes at room temperature shielded from light. After incubation with Fluo-4-AM, cells were washed with bath solution to rinse extracellular dye and dishes were filled with 200 µL bath solution. For experiments in which neurons were pre-incubated with drug, 200 µL of drug-containing solution was added after Fluo-4-AM rather than bath solution. Drug incubations were 10 minutes unless stated otherwise, after which the neurons were imaged. To identify non-peptidergic neurons in culture, neurons were incubated with isolectin-B4 (IB4) conjugated to Alexa Fluor

568 (ThermoFisher Scientific; 10 µg/mL) for 30-45 min at room temperature (in parallel with Fluo-4-AM incubation).

Dishes were mounted on the stage of an inverted microscope (Nikon Eclipse TE-2000S) and cells were visualised by brightfield illumination with a 10X air objective. The tip of a flexible perfusion inflow tube (AutoMate Scientific, CA, USA) was placed beside a region of appropriate cell density to ensure rapid exchange of solution over the cells. A six-channel, gravity-fed perfusion system fed the tip and was controlled by electronic clasp valves (Warner Instruments, CT, USA). Cells were superfused with room temperature bath solution (~0.5 mL/min) containing (in mM): 140 NaCl, 4 KCl, 2 CaCl<sub>2</sub>, 1 MgCl<sub>2</sub>, 4 glucose, 10 HEPES adjusted to pH 7.35-7.45 (with NaOH) with a final osmolality of 290-310 mOsm (all reagents listed purchased from Sigma). For experiments in which calcium was omitted from the bathing solution, the composition of the solution was changed to (in mM): 140 NaCl, 4 KCl, 2 MgCl<sub>2</sub>, 4 glucose, 10 HEPES, 1 EGTA (pH 7.35-7.45 with NaOH; 290-310 mOsm). The MgCl<sub>2</sub> concentration was raised to partially compensate for the loss of extracellular divalent cations and EGTA was added to chelate any residual Ca<sup>2+</sup>, ensuring the solution was nominally Ca<sup>2+</sup>-free.

Fluorescent images were acquired at 2.5 fps with 100 ms exposure using a CCD camera (Retiga Electro, QImaging, BC, Canada). Fluo-4 was excited by a 470 nm light source (Cairn Research, Faversham, UK) and emission at 520 nm was recorded using µManager (Edelstein et al., 2014). IB4 was excited by a 580 nm light source, and emission was recorded at 620 nm. To assess the response to a drug, a 10 s bath solution baseline preceded drug superfusion and, if multiple drugs were added to the same dish, at least 4 min wash out with bath solution elapsed between additions. At the end of each experiment, a 10 s pulse of 50 mM KCl was washed over the cells to identify viable neurons, exclude satellite cells (which may respond to some mediators but not to KCl) and permit normalisation of fluorescence. Only one recording was made per dish/cover slip of neurons. A previous report showed that application of 55 mM KCl to cultured hippocampal neurons raised intracellular calcium to circa 320 nM (De et al., 2003). Calcium binds to Fluo-4 with a  $K_d$  of 320-340 nM, indicating that in experiments carried out here the indicator was unlikely to have been saturated by 50 mM KCl (see Appendix A1.3).

### 2.1.2.3. Image analysis

Regions of interest were manually traced around individual cells and the pixel intensity per frame was measured using ImageJ. Pixel intensities were processed using custom-written scripts (adapted from L. Pattison and S. Chakrabarty) in RStudio (RStudio, MA, USA). Background fluorescence (a region of interest in which there were no neurons) was subtracted from all values and fluorescence intensity ( $F$ ) was baseline-corrected (to account for varying baselines between neurons, likely to be due in part to differential loading of Fluo-4-AM) and normalised to the maximum fluorescence value during the 50 mM KCl positive control ( $F_{\text{pos}}$ ). Consequently, 0  $F/F_{\text{pos}}$  corresponds to baseline fluorescence and 1  $F/F_{\text{pos}}$  to maximum fluorescence in KCl. Cells were excluded from analysis if their fluorescence did not increase by >5% over baseline following KCl perfusion. Unless otherwise stated, the average change in fluorescence evoked by KCl application was not different between experimental groups.

Neurons positively stained with IB4 or expressing tdTomato were identified using the same method as in Thakur *et al.* (2014). After the subtraction of background fluorescence, the top ten brightest neuronal profiles were identified. Neurons exhibiting a fluorescence >30% of the mean of these ten neurons were classified as positive for the marker of interest (see Figure 3.9a for example).

#### 2.1.2.3.1. Response to a drug

A cell was counted as a 'responder' to a drug (e.g., capsaicin, Ang II) if fluorescence reached 0.1  $F/F_{\text{pos}}$  within 30 s of the termination of drug superfusion. For each experiment, the proportion of responsive neurons was measured, as well as the magnitude of this response. The proportion of responding neurons was taken from each experiment, rather than pooling all neurons across experiments, as this better reflects differences between experimental replicates. The peak response magnitude per experiment was taken by averaging the fluorescence values for all responding neurons at each time point and taking the peak from this average trace, a similar approach to that which was taken by Hoge *et al.* (2021) (Figure 2.2). Fluo4 fluorescence traces for neurons are either plotted as  $F/F_{\text{pos}}$  or  $\Delta F$ , which gives the change in fluorescence from that of baseline.

### **2.1.2.3.2. Estimating Ca<sup>2+</sup> store content and store-operated Ca<sup>2+</sup> entry**

To estimate the content of intracellular Ca<sup>2+</sup> stores, ionomycin (5 μM) was applied to neurons in Ca<sup>2+</sup>-free external buffer. All neurons exhibit a rise in cytosolic Ca<sup>2+</sup> in response to this challenge, albeit of differing magnitudes, as all neurons possess Ca<sup>2+</sup> stores. As such, it seems unreasonable to draw an arbitrary cut off demarcating responding neurons from those which do not respond, as was done for the response to a given drug above. Similarly, all neurons exhibit store-operated Ca<sup>2+</sup> entry after the depletion of intracellular Ca<sup>2+</sup> stores by pre-incubation with thapsigargin (1 μM). In these experiments, no fluorescence cut off was used to determine whether a neuron was a responder. Rather, data from all neurons – instead of an average of all responsive neurons – which exhibited a stable baseline, and which responded to KCl application were included in analysis.

### **2.1.2.3.3. Ca<sup>2+</sup> signals in non-neuronal cells**

DRG cultures contain many non-neuronal cells, including glia and immune cells (Thakur *et al.*, 2014; this study). To determine if these cells were stimulated by Ang II application, they were first identified by their insensitivity to 50 mM KCl (<5% increase in fluorescence over baseline). Non-neuronal cells were counted as Ang II-sensitive if their fluorescence increased by >5% over baseline during Ang II application. Fluo4 fluorescence traces for non-neuronal cells are plotted as

$$\frac{\Delta F}{F_0} = \frac{F - F_0}{F_0}$$

where F is the fluorescence at a given point in time and F<sub>0</sub> is baseline fluorescence given by the mean fluorescence during the first 10 s of the recording. This gives the fold change in Fluo4 fluorescence over baseline.

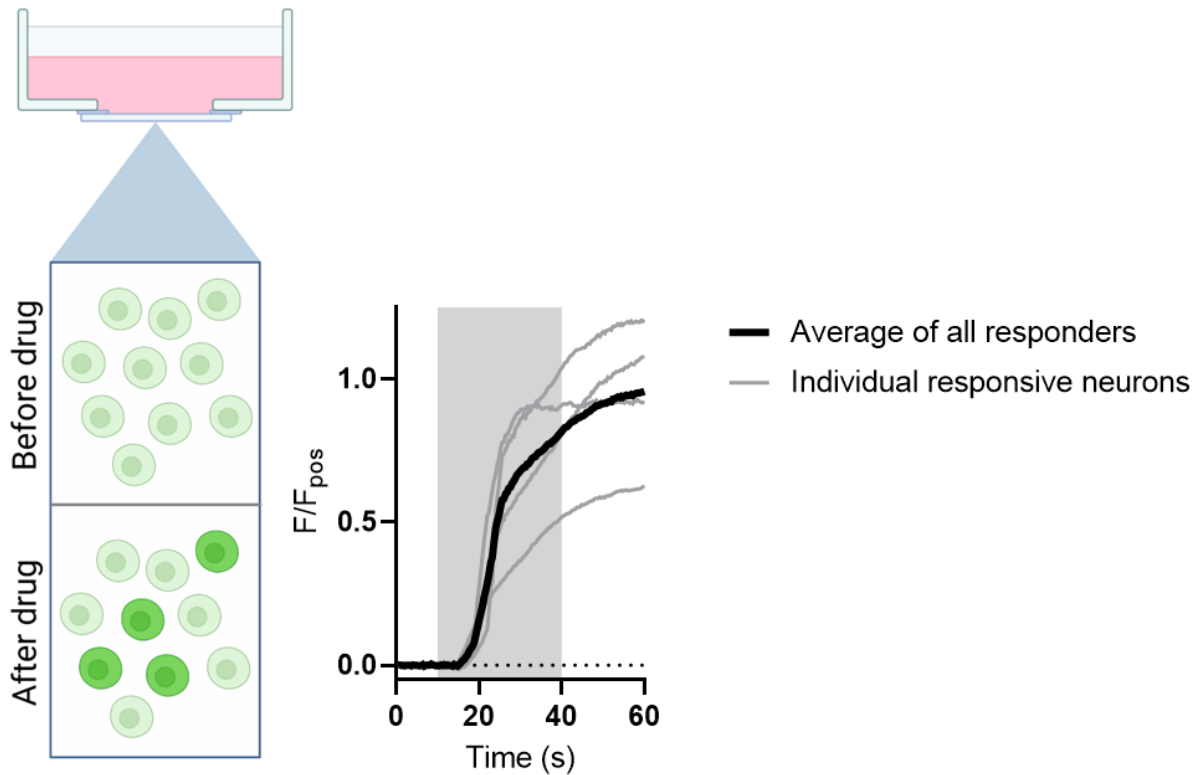


**Figure 2.2 Neuronal response to drug application**

In an individual experiment, a given proportion of neurons will respond to the application of a drug – here, 4 of 10 neurons responded (darker green cells). From each experiment, the proportion of responsive neurons and the peak magnitude of this response is taken. To find the peak magnitude, the Fluo-4 fluorescence traces of all responsive neurons (grey traces) are averaged at each time point. The peak of this average trace is used as the peak magnitude of the response to the drug for this experiment (black trace). Image created using Biorender.

### **2.1.3. Magnetic activated cell sorting**

To ascertain whether satellite cells (glia, immune cells, etc) in DRG cultures were important for the response to a mediator, satellite cells were removed from DRG cultures using magnetic-activated cell sorting (MACS). MACS was performed using equipment purchased from Miltenyi Biotec using protocols optimised by Thakur *et al.* (2014).

DRG from 2-3 mice were harvested (to account for loss of neurons during sorting) and neurons were cultured as above, except only collagenase was used to enzymatically disperse neurons (45 min incubation, 1 mg/mL with 6 mg/mL BSA), as a trypsin digest prohibits the adherence of neurons in the absence of non-neuronal cells (Dr D Tewari, personal communication). Following the final centrifugation to pellet the neurons after mechanical dispersion, they were resuspended in 2 mL Dulbecco's phosphate-buffered saline (DPBS, containing 0.9 mM CaCl<sub>2</sub> and 0.5 mM MgCl<sub>2</sub>). The suspension was centrifuged for 7 minutes at 1000 rpm, after which the pellet was dried and suspended in 120 µL MACS rinsing solution (Miltenyi Biotec) supplemented with 0.5% w/v BSA (solution sterile filtered at 0.2 µm). 30 µL biotin-conjugated non-neuronal antibody cocktail (Miltenyi Biotec, cat. no. 130-115-389) was added and the suspension incubated for 5 minutes at 4°C. Following incubation, the suspension was topped-up to 2 mL with DPBS and centrifuged for 7 minutes at 1000 rpm. After drying, the pellet was again resuspended in 120 µL MACS rinsing solution and 30 µL biotin-binding magnetic beads (Miltenyi Biotec) were added and the suspension was incubated for 10 minutes at 4°C. After incubation, the cell suspension was topped-up to 500 µL with MACS buffer.

To separate antibody-bound from -unbound cells, the suspension was filtered by gravity through a magnetic column (filter size ~35 µm) mounted on a QuadroMACS magnetic stand (Miltenyi Biotec) (Figure 2.3). The column was first primed with 2.5 mL MACS rinsing solution. After adding 500 µL cell suspension, 1 mL MACS rinsing solution was used to wash the tube which had contained the suspension, and a final 1 mL was run through the column to ensure all unbound cells were eluted. A total of 5 mL was eluted from the column, which was centrifuged for 7 minutes at 1000 rpm. The final pellet (antibody-bound or -unbound) was resuspended in 100 µL supplemented L-15 and divided between two MatTek dishes coated with poly-D-lysine and Matrigel (Corning; diluted 1:10 in L-15 media). Cells were incubated for three hours at 37°C to

allow adherence to the plate, after which dishes were flooded with 2 mL supplemented L-15 media. MACS cultures were incubated for 48 hours at 37°C with 5% CO<sub>2</sub> (rather than ~24 hours for ordinary unsorted cultures) prior to imaging, with the media being changed after 24 hours.

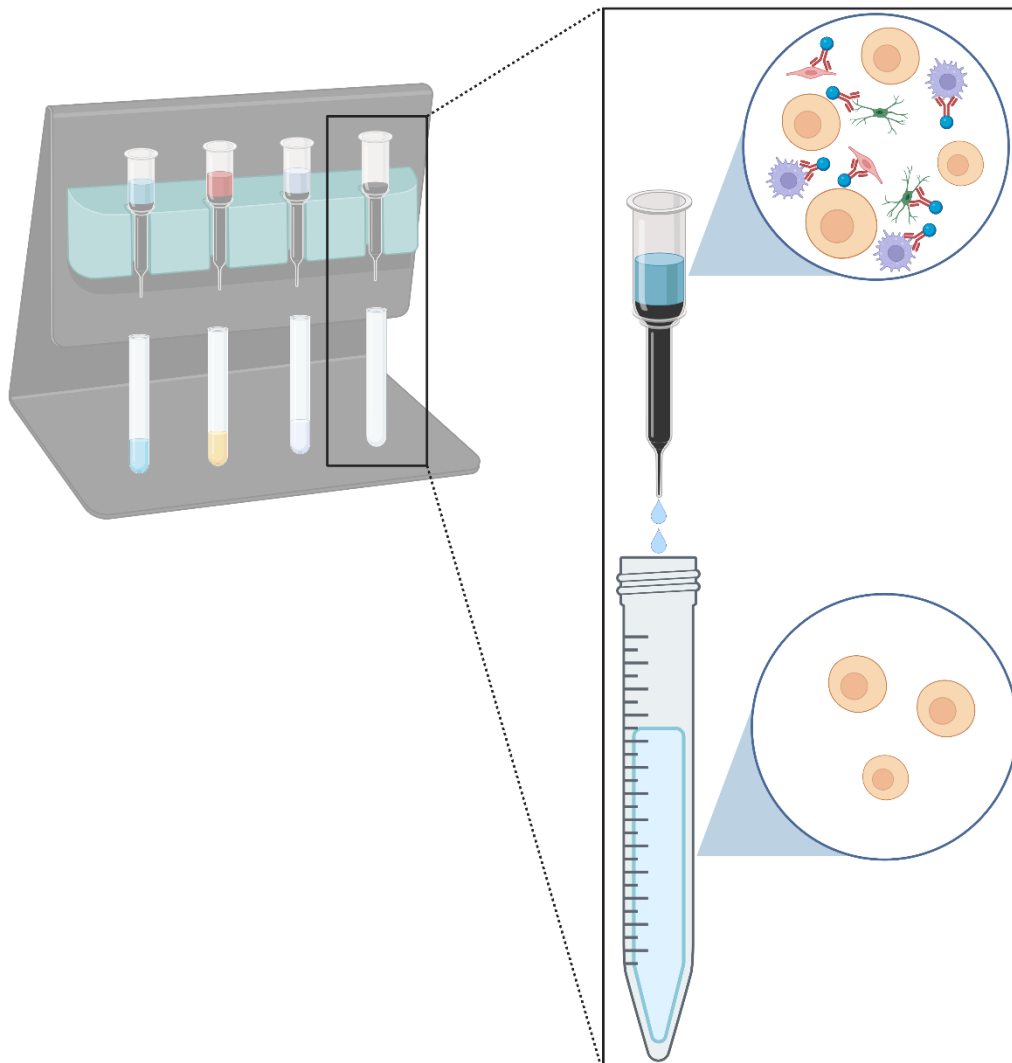


**Figure 2.3 Magnetic cell sorting of DRG cultures**

LD columns are loaded into the QuadroMACS magnetic stand (*left*) and the dispersed neuronal suspension, previously incubated with biotin-conjugated antibodies against non-neuronal cells and biotin-binding magnetic beads, is filtered through by gravity (*right*). Magnetic beads – and, hence, the cells bound by the antibodies – are sequestered in the column, allowing a pure neuronal suspension to be eluted. Image created using Biorender.

## **2.1.4. Immunocytochemistry for MACS validation**

### **2.1.4.1. Cell preparation and imaging**

DRG were cultured as above and neurons were seeded onto 12 mm coverslips coated in poly-L-lysine and laminin. After 24-48 hours in culture, cells were fixed in 4% paraformaldehyde for 10 min at room temperature. A subsequent 10 min wash in PBS was followed by permeabilization in 0.05% Triton-X100 for 5 min at room temperature. Cells were washed again in PBS and then blocked with goat serum in 0.2% Triton-X100. After blocking, cells were incubated with rabbit anti- $\beta$ III tubulin primary antibodies (1:1000, Abcam: ab18207) at room temperature for 3 hours.

Following primary antibody incubation, cells were washed in PBS and incubated with Alexafluor-568 goat anti-rabbit secondary antibodies diluted in PBS (1:1000, Invitrogen: A11008) plus 4'-6-diamidino-2-phenylindole (DAPI, 1:1000, Abcam: ab228549) for 1 hour at room temperature. After a final 10 min washing step, excess fluid was drawn off coverslips to allow mounting cell side down on 25x75x1 mm glass slides using Mowoil 4-88 mounting medium (Sigma-Aldrich: 81381). Mounting medium was set at 4°C and slides were imaged within 1 hour.

Slides were imaged using an Olympus BX51 microscope. Fluorophores were excited with 568 nm (Alexafluor-568) or 350 nm (DAPI) light sources. Images were captured on a Qicam CCD camera (QImaging) with a 100 ms exposure and false coloured ( $\beta$ III tubulin, green; DAPI, blue). No  $\beta$ III tubulin staining was observed after the omission of the primary antibody (see Figure 3.12).

### **2.1.4.2. Analysis**

Images were analysed using ImageJ. 8-bit images of either  $\beta$ III tubulin or DAPI staining underwent thresholding to exclude artefacts (e.g., objects with low staining intensity) and enable further processing. An automatic 'minimum error' threshold algorithm was used to set the initial threshold and generate a binary image. The binary image histogram, and comparison with the raw image, was then used to manually adjust the threshold to ensure that regions of interest were appropriately captured. Generally, the threshold was placed at the first minimum after the first (major) peak of the image histogram to distinguish objects of interest from the background (see section 3.2.2.3.). The binary image then underwent watershed segmentation to separate distinct objects in close apposition (see section 3.2.2.3.). Identified objects were

automatically counted using an ImageJ plugin (“Analyse Particles”), and the proportion of neurons within the culture calculated (ratio of the number of  $\beta$ III-tubulin-positive cells to the total number of DAPI-positive cells).

## **2.1.5. Immunocytochemistry for NFAT translocation**

### **2.1.5.1. Cell preparation and imaging**

DRG were cultured as above and neurons were seeded onto 12 mm coverslips coated in poly-L-lysine and laminin. After 16-24 hours in culture, cells were stimulated with vehicle (0.02% ddH<sub>2</sub>O), Ang II (2  $\mu$ M), Ang II + valsartan (1  $\mu$ M), Ang II + Pyr3 (10  $\mu$ M) or Ang II + Cyclosporine A (CsA, 1  $\mu$ M) for 60 min. Subsequently, cells were fixed with 4% paraformaldehyde for 10 min at room temperature. A subsequent 10 min wash in PBS was followed by permeabilization in 0.05% Triton-X100 for 5 min at room temperature. Cells were washed again in PBS and then blocked with goat serum in 0.2% Triton-X100. After blocking, cells were incubated with rabbit anti-NFAT5 antibodies (1:1000, Invitrogen, PA1-023) at room temperature for 3 hours.

Following primary antibody incubation, cells were washed in PBS and incubated with Alexafluor-568 goat anti-rabbit secondary antibodies diluted in PBS (1:1000, Invitrogen: A11008) plus 4'-6-diamidino-2-phenylindole (DAPI, 1:1000, Abcam: ab228549) for 1 hour at room temperature. After a final 10 min washing step, excess fluid was drawn off coverslips to allow mounting cell side down on 25x75x1 mm glass slides using Mowiol 4-88 mounting medium (Sigma-Aldrich: 81381). Mounting medium was set at 4°C and slides were imaged within 1 hour.

Slides were imaged using an Olympus BX51 microscope. Fluorophores were excited with 568 nm (Alexafluor-568) or 350 nm (DAPI) light sources. Images were captured on a Qicam CCD camera (QImaging) with a 100 or 200 ms exposure for DAPI and NFAT5, respectively, and false coloured (NFAT5, red; DAPI, white). Attenuated NFAT5 staining was observed after the omission of the primary antibody (see Figure 5.1).

### **2.1.5.2. Analysis**

Images were analysed using ImageJ. Neurons were identified from brightfield images and nuclei were identified by DAPI staining, with regions of interest manually traced around individual neurons and nuclei. Images were corrected for background fluorescence and cytoplasmic NFAT5 staining intensity was subtracted from nuclear staining intensity. For all experiments, nuclear staining intensity was greater than that of the cytoplasm, suggesting preferential nuclear localisation of NFAT5. A neuron which exhibited nuclear NFAT5 staining intensity greater than three standard deviations above the mean of the unstimulated (vehicle) group was counted as 'translocated'. The proportion of neurons exhibiting NFAT5 nuclear translocation was compared between experimental conditions.

### **2.1.6. Patch-clamp electrophysiology**

DRG neurons were cultured as above but were seeded onto culture dishes at a lower density to ensure individual cells could be clamped. Neurons were bathed in a solution containing (in mM): 140 NaCl, 4 KCl, 2 CaCl<sub>2</sub>, 1 MgCl<sub>2</sub>, 4 glucose, 10 HEPES adjusted to pH 7.35-7.45 (with NaOH) with a final osmolality of 290-310 mOsm. Patch pipettes were fabricated from borosilicate glass capillaries pulled to a tip resistance of 3-7 MΩ using a P-97 filament puller (Sutter Instruments). Pipettes were filled with an internal solution containing (in mM): 110 KCl, 10 NaCl, 1 MgCl<sub>2</sub>, 1 EGTA, 10 HEPES, 2 Na<sub>2</sub>ATP, 0.5 Na<sub>2</sub>GTP adjusted to pH 7.35-7.45 (with KOH) with a final osmolality of 310-315 mOsm.

Current-clamp data were obtained using an EPC-10 amplifier (HEKA Electronics, Lambrecht, Germany) in bridge-balance mode, filtered at 10 kHz (-3 dB cut off; 4-pole low-pass Bessel filter), digitised at 20 kHz and recorded for analysis using Patch Master (HEKA Electronics). Whole-cell capacitance and series resistance were measured, and only neurons with an uncorrected series resistance less than 25 MΩ were included. Series resistance compensation was at least 65%.

#### **2.1.6.1. Acute application of Ang II**

Neurons used for these experiments were incubated with IB4-568 (10 µg/mL in bath solution) for 10 min prior to recording. Individual neurons – not in contact with other cells – were whole-cell voltage-clamped at -60 mV. After the whole-cell patch-clamp configuration had been obtained, membrane potential was recorded in 'free-clamp'

mode, i.e., with no injected current. A 30 s baseline determined the resting membrane potential, after which Ang II (2  $\mu$ M) was applied for 60 s via a gravity-fed perfusion tip placed in close proximity to the cell from which the recording was made. Membrane potential was measured for a further 60 s after the cessation of Ang II application. At the end of each experiment, a 1 nA depolarising current was applied to the neuron: only neurons which discharged at least one action potential were included in analysis.

### **2.1.6.2. Incubation with Ang II**

Control neurons were incubated overnight (~16 hours) with vehicle (0.1% ddH<sub>2</sub>O in culture medium as above) and experimental neurons with 10  $\mu$ M Ang II. A greater concentration of Ang II was used for overnight incubations than for acute application to account for any degradation of the peptide over time. Prior to recording, cultures were incubated with IB4 (10 minutes at 37°C) such that only IB4-positive neurons could be selected for analysis. Each dish of neurons was used for at most one hour after IB4 incubation to ensure no loss of neuronal viability.

Individual neurons – not in contact with other cells – were whole-cell voltage-clamped at -60 mV. Whole-cell capacitance and series resistance were measured, and only neurons with series resistance less than 25 M $\Omega$  were included. The configuration was then switched to bridge-balanced current-clamp mode to assess neuronal excitability.

Rheobase, the minimum current required to evoke action potential firing, was measured by applying depolarising current steps of 80 ms duration from 0-1050 pA in 50 pA increments. Only neurons which fired well-resolved action potentials were included in analysis.

### **2.1.7. Ca<sup>2+</sup> imaging of bone marrow-derived macrophages**

#### **2.1.7.1. Culture of bone marrow-derived macrophages (BMDMs)**

The hind leg was pinned straight from the iliopubic eminence to the foot and the quadriceps and hamstring muscles were removed, exposing the femur. The bone was cleaned of all muscle and connective tissue. The shaft of the femur was removed by cutting – using rongeurs soaked in 70% ethanol – below the lesser trochanter (proximally) and above the medial and lateral epicondyles (distally). A 2G needle was inserted into one end of the femoral shaft bone marrow cavity and bone marrow was flushed out with 10 mL ice cold PBS (0 mM Ca<sup>2+</sup>/Mg<sup>2+</sup>). The cell suspension was centrifuged at 2000 rpm for 8 minutes and the resulting pellet resuspending in 5 mL

Dulbecco's modified eagle's medium (DMEM) supplemented with 10% FBS, 2% penicillin/streptomycin and 25 ng/mL monocyte colony-stimulating factor (MCSF). To remove debris, the suspension was filtered through a 40 µm strainer. The strained suspension was divided between poly-D-lysine-coated glass-bottomed culture dishes for imaging after 48 hours, and a T25 culture flask in which macrophages were maintained for imaging at different time points.

To remove macrophages from T25 flasks, culture medium was discarded, and cells were washed twice with warmed PBS and subsequently incubated with 3 mL Versene (1:5000; Gibco) – a non-enzymatic, EDTA-based dissociation solution – for 10 minutes. Cells were gently scraped to encourage dislodging from the substrate and the base of the flask was washed five times with 7 mL supplemented DMEM (without MCSF). The 10 mL suspension was centrifuged at 2000 rpm for 8 minutes and the pellet was resuspended in 100-200 µL supplemented DMEM (with MCSF). The macrophage suspension was divided between 2-4 culture dishes coated in poly-D-lysine and incubated for 2-3 hours to adhere. Dishes were then flooded with 3 mL supplemented DMEM (with MCSF) and incubated for a further 48 hours before imaging. Media was changed after 24 hours.

#### **2.1.7.2. Ca<sup>2+</sup> imaging**

Culture medium was removed, and macrophages were covered with 100 µL of 10 µM Fluo-4-AM for 30-45 minutes at room temperature. Cells were then washed with bath solution and then filled with 200 µL bath solution. Imaging was carried out as for neuronal cultures (above).

Macrophages were stimulated with 2 µM Ang II for 30 s. Ionomycin (5 µM in 10 mM Ca<sup>2+</sup> bath solution) was used as a positive control and as a calibration against which the response to Ang II was normalised.

#### **2.1.7.3. Image analysis**

Analysis was carried out as for neuronal cultures, except normalisation of the response to Ang II was against 5 µM ionomycin rather than 50 mM KCl.

### **2.1.8. Reagents**

Drug solutions were made up in external bath solution on the day of the experiment for which they were used. See Table 2.1 for details of drugs used in the main body of this Thesis.

### **2.1.9. Data analysis**

#### **2.1.9.1. Curve fitting**

To compare neuronal soma sizes between conditions (e.g., genotype or responder/non-responder), the distribution of soma areas was fit with a single Gaussian curve, or the sum of two curves, according to the equation:

$$y = A_1 e^{-0.5\left(\frac{X-\mu_1}{\sigma_1}\right)^2} + A_2 e^{-0.5\left(\frac{X-\mu_2}{\sigma_2}\right)^2}$$

Where  $A$  is the amplitude of the distribution at the mean,  $\mu$ , and  $\sigma$  is the standard deviation of the distribution. Whether a single or double component Gaussian curve was required to best fit the data was determined using a sum-of-squares F-test which ascertains if the simpler (single component) model can adequately account for the variability in the data.

#### **2.1.9.2. Statistics**

All data were scrutinised to verify that they met the assumptions of parametric analyses. Normality was assessed using the Shapiro-Wilk test, and homogeneity of variances with F-tests; heterogeneity of variances corrected using Welch's correction where appropriate. Where the assumptions required for parametric analyses were not met, rank-based, non-parametric alternatives were used. Nested analyses were used where appropriate to take into account experimental replicates that were drawn from the same biological replicate, i.e., different coverslips seeded with neurons from the same DRG culture.

Sample sizes were not prespecified before data acquisition, but inter-group comparisons were decided before data was obtained, and all statistical tests carried out are reported. Data are presented as mean  $\pm$  standard error (SEM). "N" represents the number of independent DRG cultures from which neurons were derived and "n" the number of experimental replicates, i.e., different coverslips/culture dishes. Where data from individual neurons – rather than an average of a group of neurons – are used for analysis, the total number of neurons per experimental group is given. Details

of sample sizes and the statistical tests used for analysis are in figure legends. P-value cut offs are denoted in figures as \*  $p < 0.05$ , \*\*  $p < 0.01$ , \*\*\*  $p < 0.001$ .

<b>Drug</b>	<b>Source</b>	<b>Stock (mM)</b>	<b>Vehicle</b>
<b>Ang II</b>	Sigma	10	ddH <sub>2</sub> O
<b>Valsartan</b>	Tocris	10	DMSO
<b>EMD66684</b>	Tocris	10	Ethanol
<b>YM254890</b>	Sigma	100	DMSO
<b>U73122</b>	Tocris	10	DMSO
<b>Thapsigargin</b>	Tocris	1	DMSO
<b>Xestospongine C</b>	Tocris	1	DMSO
<b>Ionomycin</b>	Tocris	10	Ethanol
<b>PD123319</b>	Tocris	10	DMSO
<b>TTX</b>	Tocris	1	ddH <sub>2</sub> O (pH 5)
<b>Pyr3</b>	Tocris	10	DMSO
<b>GSK1702349A</b>	Tocris	10	Ethanol
<b>GdCl<sub>3</sub></b>	Tocris	100	ddH <sub>2</sub> O
<b>ML-9</b>	Tocris	10	DMSO
<b>PDBu</b>	Sigma	1	DMSO
<b>8-Br-cGMP</b>	Tocris	1	ddH <sub>2</sub> O
<b>RHC80267</b>	Tocris	25	DMSO
<b>Staurosporine</b>	Sigma	1	DMSO
<b>OAG</b>	Tocris	100	DMSO
<b>Capsaicin</b>	Sigma	1	Ethanol
<b>Alamandine</b>	Tocris	1	ddH <sub>2</sub> O
<b>Cyclosporine A</b>	Tocris	1	DMSO

**Table 2.1 Drugs used for experiments outlined in Chapters 3-5**

## **Chapter 3**

### **Molecular identity of Ang II-sensitive sensory neurons**

### 3.1. Introduction

Peripheral sensory neurons represent a diverse family of specialised cells which orchestrate an organism's interaction with the environment. To gain insight into the potential sensory function of Ang II, an understanding of the sensory neuronal subtypes with which it interacts is required.

#### 3.1.1. Diversity and classification of sensory neurons

Peripheral sensory neurons transduce environmental cues – whether internal, for example, from the viscera, or external – to guide an organism's behaviour. Given the myriad stimuli presented to the peripheral sensory system, it is unsurprising that sensory neurons exhibit diverse functional properties. Thermally-, mechanically- and chemically-gated ion channels residing on sensory neuron terminals transduce stimuli into generator potentials: localised depolarisation of the terminal. These potentials may be integrated over time and space and are subject to modulation by voltage-gated ion channels, such as  $Na_v1.9$ , which serves to amplify generator potentials (Priest *et al.*, 2005). If the generator potentials reaches the threshold of activation for  $Na_v$  channels at the axon initial segment, an action potential will be generated and transmitted to the central terminal of the sensory neuron.

Early classifications of sensory neurons focussed on neuronal size, extent of myelination and speed of conduction. These properties are co-variant; larger sensory neurons tend to exhibit greater myelination and conduction speed (Lawson, 1979; Lawson and Waddell, 1991). The sensory function of a given neuron is determined by the complement of transducing ion channels it expresses. Members of the TRP family of cation channels are important in the transduction of external stimuli, with TRPV1 gated by noxious heat ( $>42^\circ\text{C}$ ) (Caterina *et al.*, 1997), TRPM8 by cold ( $<26^\circ\text{C}$ ) (Bautista *et al.*, 2007), and Piezo2 by pressure (Ranade *et al.*, 2014). The discovery of genetic markers of sensory functions – i.e., expression of *Trpv1* indicates sensitivity to noxious heat, etc – led to the hypothesis that the functional identity of sensory neurons may be reflected in their gene expression profile (Wichterle, Gifford and Mazzoni, 2013). Substantial evidence supporting this hypothesis has been garnered from single-cell transcriptomic studies of sensory neurons, in which neurons were clustered by transcriptome similarity (Usoskin *et al.*, 2015; Zeisel *et al.*, 2018; Zheng *et al.*, 2019).

These studies enabled a more thorough classification of sensory neuron subtypes, identifying key genetic markers for each (Usoskin *et al.*, 2015). What's more, differences in ion channel expression – particularly K<sup>+</sup> channels – was found to underpin the distinct intrinsic physiological properties of different neuronal populations (Zheng *et al.*, 2019).

Most important for this study is the identification of nociceptive neurons *in vitro*. Like all sensory neurons, nociceptors are a heterogeneous population. On the whole, nociceptors have a smaller soma area compared to low-threshold neurons, like proprioceptors (Lawson, Fang and Djouhri, 2019). These small-sized neurons tend to express the voltage-gated Na<sup>+</sup> channel, Nav1.8, known to be involved in inflammatory pain signalling. Multiple algogens, including prostaglandin E<sub>2</sub>, serotonin and adenosine, potentiate currents carried by Nav1.8 and cause a hyperpolarising shift in its voltage-dependence of activation (Gold *et al.*, 1996). Nav1.8-expressing nociceptors can be split into two subpopulations – peptidergic and non-peptidergic neurons, neither of which is homogeneous (Usoskin *et al.*, 2015). Peptidergic neurons express neuropeptides such as Substance P and calcitonin gene-related peptide (CGRP) which mediate neurogenic inflammation (Helyes *et al.*, 1997). Non-peptidergic neurons, which selectively bind isolectin B4 (IB4) due to their expression of laminin β2 (Fullmer *et al.*, 2004), have been implicated in pain (Bautzova *et al.*, 2018) and itch (Ru *et al.*, 2017). *Agtr1a* and *Agtr1b* – the genes encoding AT1R in mouse – are selectively expressed in non-peptidergic neurons (Usoskin *et al.*, 2015; Ray *et al.*, 2018; Zeisel *et al.*, 2018). TRPV1, a non-selective cation channel sensitive to heat, acidosis and capsaicin, is expressed in a subset of both non-peptidergic and peptidergic nociceptors (Usoskin *et al.*, 2015). These characteristics – namely, small soma area, expression of Nav1.8, sensitivity to capsaicin, and IB4 binding – will prove useful for the identification of nociceptors *in vitro*.

### **3.1.2. Non-neuronal cells in the DRG**

The importance of non-neuronal cells in sensory neurophysiology was largely underappreciated for some time. Recent work has demonstrated that numerous non-neuronal cells are present in the DRG, as well as a dynamic cross-talk between neuronal and non-neuronal cells. Approximately 80% of the cells present in dissociated DRG are non-neuronal, with the majority being glial cells (Thakur *et al.*, 2014). Granulocyte-macrophage colony stimulating factor (GM-CSF) is a proinflammatory

cytokine which induces acute pain (Achuthan *et al.*, 2016) and functions in models of inflammatory pain (Cook *et al.*, 2013). It had been suggested that the pain-inducing effects of GMCSF were due to an interaction with peripheral sensory neurons, but transcriptome studies revealed poor expression of receptors for GMCSF (Thakur *et al.*, 2014; Zeisel *et al.*, 2018). Subsequently, GMCSF was shown to exert no direct effects on sensory neurons *in vitro* and the knock-out of receptors for GMCSF in Nav1.8-expressing neurons had no effect on pain behaviours elicited by intra-plantar injection of GMCSF (Tewari *et al.*, 2020). However, application of GMCSF to cultured sensory neurons resulted in transcriptional changes in genes known to function in nociception, such as CGRP (Tewari *et al.*, 2020). This effect of GMCSF was ablated if non-neuronal cells were removed from DRG cultures, and the effect was recapitulated by the application of conditioned media from macrophages stimulated with GMCSF (Tewari *et al.*, 2020). This report strongly suggests that GMCSF evokes macrophage-to-neuron crosstalk in the DRG, resulting in prolonged changes in nociceptor function through changes in gene expression. Glial cells may also modulate neuronal function. During inflammation, expression and release of tumour necrosis factor  $\alpha$  (TNF $\alpha$ ) by DRG glial cells contributes neuronal sensitisation and hyperalgesia (Song *et al.*, 2014). Consequently, when examining the effects of a potentially novel pro-nociceptive mediator, it is important to consider the array of non-neuronal cells resident in the DRG.

### **3.1.3. Experimental outline**

Based on the expression of *Agtr1a/b* in sensory neurons, it was hypothesised that Ang II would stimulate a population of neurons exhibiting a small soma area, sensitivity to the TRPV1 agonist capsaicin and expression of Nav1.8. Moreover, given the selective expression of *Agtr1a/b* in non-peptidergic neurons, IB4 was used to identify neurons within this population *in vitro* to ascertain if Ang II exerted a selective effect on IB4-binding neurons. Finally, the role of non-neuronal cells was investigated through the removal of non-neuronal cells from DRG cultures using magnetic sorting. It was anticipated that Ang II would exert its effects through a direct interaction with neurons, and, as such, would not require the presence of non-neuronal cells.

## 3.2. Results

### 3.2.1. Ang II stimulates nociceptive neurons in culture

To ascertain the identity of Ang II-sensitive neurons in culture, Ca<sup>2+</sup> imaging was employed to examine the features of the neuronal population responding to Ang II application. Three salient characteristics of nociceptive neurons were used to distinguish them from other neurons present in culture: (i) small soma size, (ii) expression of TRPV1, and (iii) expression of Nav1.8.

#### 3.2.1.1. Ang II-sensitive neurons are small-sized

The soma area of neurons which exhibited a rise in intracellular Ca<sup>2+</sup> following Ang II (2 µM) application was compared with those which showed no such response. Figure 3.1a shows a field of view under brightfield illumination containing exemplar small (blue arrow) and large (orange arrow) neurons. False colouring of the Fluo-4 fluorescence of these neurons shows a rise in intracellular Ca<sup>2+</sup> in only the highlighted small-sized neuron. The change in Fluo-4 fluorescence in this pair of neurons over time is shown in Figure 3.1b. The soma areas of all neurons imaged in this experiment were grouped and normalised to that of the mean of the Ang II-insensitive population. The distribution of soma areas of Ang II-insensitive neurons (311 neurons) was best fit by the sum of two Gaussian curves ( $R^2 = 0.99$ ) corresponding to a small- and large-sized population of neuronal soma (Figure 3.1c). The null hypothesis that a single curve could fit the distribution of soma areas for both Ang II-insensitive and Ang II-sensitive neurons was rejected ( $p < 0.0001$ ). For Ang II-sensitive neurons (208 neurons; 40.1% of total), the soma size distribution was best fit by a single Gaussian curve ( $R^2 = 0.95$ ) corresponding to only a small-sized population of neuronal soma (Figure 3.1c). This single Gaussian corresponds to the first, smaller component of the double Gaussian describing the soma area of Ang II-insensitive neurons, suggesting that Ang II stimulated a subset of small-sized neurons. The mean area of Ang II-sensitive neurons was  $54.3 \pm 2.3\%$  of that of the Ang II-insensitive population ( $p < 0.0001$ , Figure 3.1d).

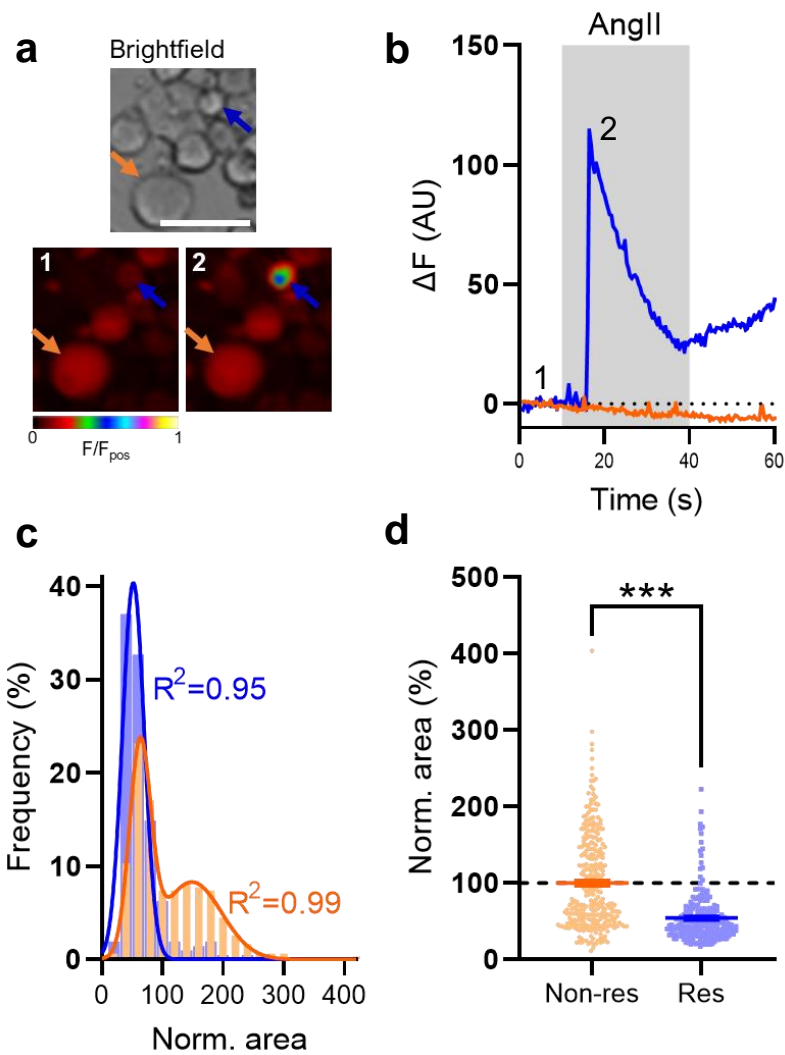


**Figure 3.1 Ang II raised intracellular  $\text{Ca}^{2+}$  in small-sized sensory neurons**

- (a) *Top*: brightfield image depicting sensory neurons in culture. Scale bar: 50  $\mu\text{m}$ . *Bottom left*: False-coloured Fluo-4 fluorescence image prior to Ang II application. Blue arrow highlights small-diameter neuron; orange arrow highlights large-diameter neuron. *Bottom right*: False-coloured Fluo-4 fluorescence image after to Ang II application.
- (b) Corresponding fluorescence traces ( $\Delta F$ : change in fluorescence over baseline) for the neurons highlighted in (a). Numbers 1 and 2 correspond to time points of the images in (a).
- (c) Histogram showing the distribution of normalised soma areas for the Ang II-sensitive (blue) and Ang II-insensitive (orange) populations.
- (d) Grouped data showing the normalised soma area for all neurons imaged in this experiment. Ang II-insensitive (non-res): 311 neurons,  $n = 7$ ,  $N = 3$ ; Ang II-sensitive (res): 208 neurons,  $n = 7$ ,  $N = 3$ . Data analysed using two-tailed Mann-Whitney U test.

### 3.2.1.2. Most Ang II-sensitive neurons are co-sensitive to the capsaicin

The non-selective cation channel TRPV1 – activated by extracellular acidosis, noxious heat (>42°C) and capsaicin – is a marker of nociceptive neurons. The functional expression of TRPV1 in Ang II-sensitive neurons was determined by sequential application of Ang II (2 µM, 30 s) and capsaicin (1 µM, 10 s). After the exclusion of neurons which responded to neither stimulus, three populations were identified. The first population, accounting for 6.9±1.5% of all neurons, was sensitive to Ang II but not capsaicin (Figure 3.2a *red trace* and 3.2b). A second population, making up 5.9±1.3% of all neurons, was insensitive to Ang II but sensitive to capsaicin (Figure 3.2a *blue trace* and 3.2b). The largest population identified in this experiment was sensitive to both Ang II and capsaicin (Figure 3.2a *purple trace*) and accounted for 35.0±4.4% of all neurons (Figure 3.2b). The total capsaicin-sensitive population accounted for 41.0±3.9% of all neurons (Figure 3.2b), in line with previous reports (Caterina *et al.*, 1997; Chakrabarti *et al.*, 2018). Within the Ang II-sensitive population, 82.8±3.8% were co-sensitive to capsaicin (Figure 3.2c), suggesting that they express the nociceptive neuronal marker TRPV1.

Some inflammatory mediators are known to sensitise TRPV1, thereby increasing the Ca<sup>2+</sup> conductance across the neuronal membrane in response to capsaicin due either to an increase in the expression of TRPV1 or a change in its single channel properties. Not only has this been shown to be important in nociception and pain, but it may also hinder the interpretation of the previous experiment. If Ang II sensitises TRPV1, its application prior to capsaicin may result in neurons being labelled as capsaicin-sensitive when, in their basal state, they are insensitive. To ascertain whether Ang II application can sensitise TRPV1, neurons were pre-incubated with Ang II (or vehicle: 0.02% water) for one hour, after which capsaicin (10 nM, 10 s) was applied; a lower concentration of capsaicin was used for this experiment to ensure the response was not saturated and any increase in the response could be observed. Figure 3.3a shows the response to capsaicin from a single exemplar experiment. While the magnitude of the response to capsaicin was increased from 0.36±0.05 to 0.51±0.05, this change was not labelled statistically significant ( $p = 0.11$ , Figure 3.3b). In this case, a more important metric of the response to capsaicin was the proportion neurons responding, because this could artificially elevate the size of the population co-sensitive to Ang II

and capsaicin. After vehicle incubation,  $16.4 \pm 6.2\%$  of neurons responded to capsaicin, compared to  $18.8 \pm 5.8\%$  after Ang II incubation ( $p = 0.89$ , Figure 3.3c).

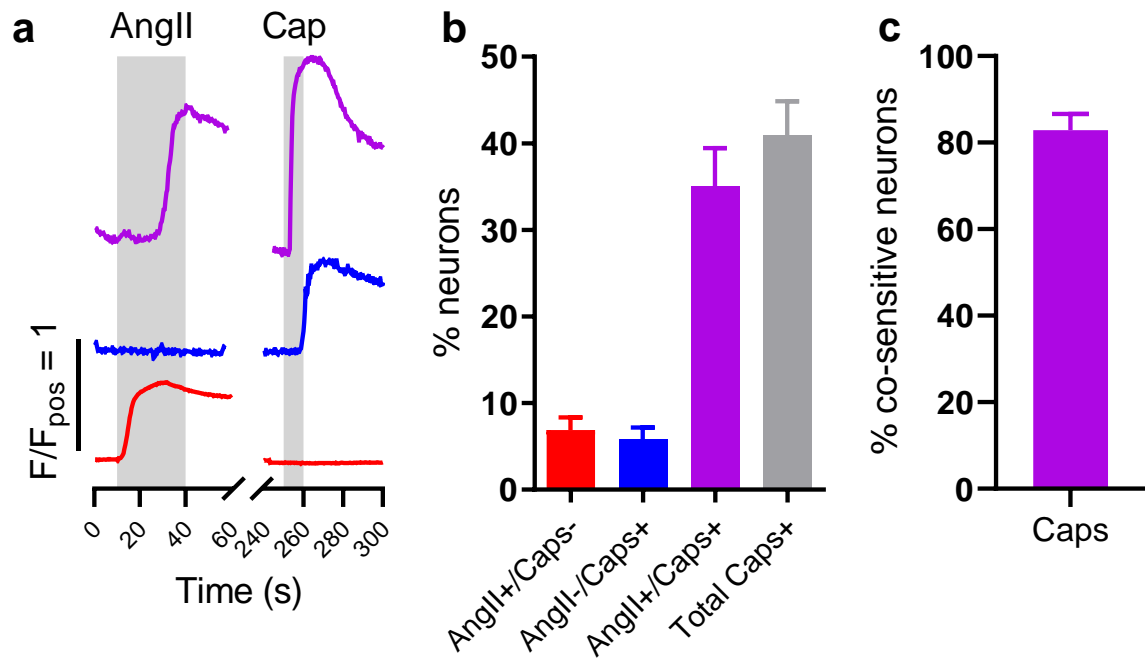


**Figure 3.2 Ang II-sensitive neurons are co-sensitive to capsaicin, a TRPV1 agonist**

- (a) Representative traces from single neurons within each of the populations identified based on sensitivity to Ang II and capsaicin. Neurons insensitive to both stimuli not shown.
- (b) Grouped data showing the size (proportion of neurons present in culture) of each of the identified populations.
- (c) Grouped data showing the proportion of Ang II-sensitive neurons which were also sensitive to capsaicin. 221 neurons, n = 6, N = 4.

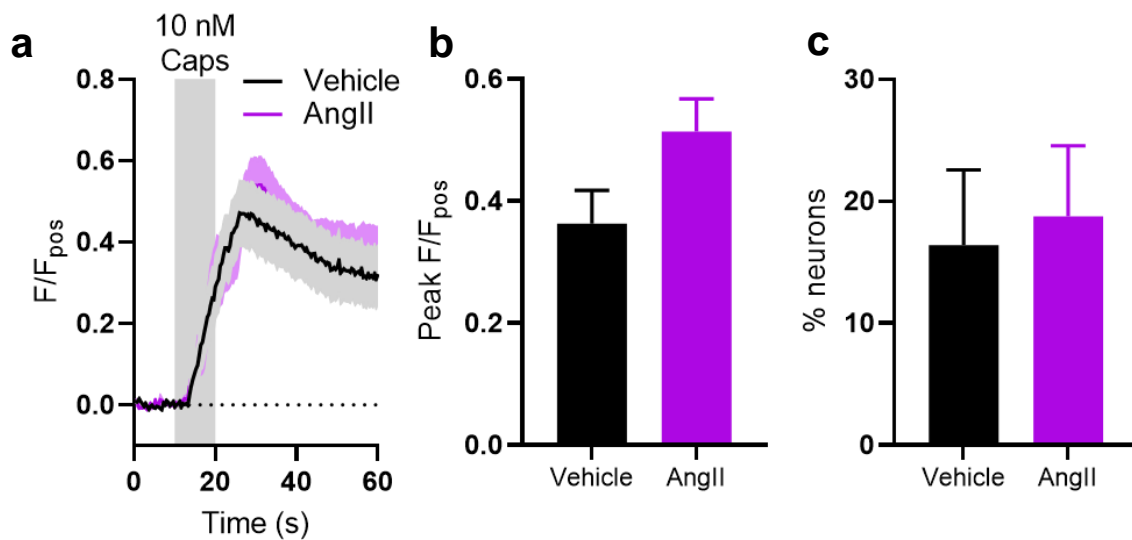


**Figure 3.3 Ang II application does not sensitise TRPV1**

- (a) Average responses to capsaicin from representative experiments. Vehicle: 23 neurons; Ang II: 13 neurons.
- (b) Average peak responses to capsaicin. Data analysed using two-tailed Mann-Whitney U test.
- (c) Proportion of neurons responding to capsaicin. Data analysed using two-tailed Mann-Whitney U test. Vehicle: n = 4, N = 3; Ang II: n = 4, N = 3.

### 3.2.1.3. Nav1.8 is expressed in Ang II-sensitive neurons

#### 3.2.1.3.1. Ang II stimulates Nav1.8-positive neurons identified using tdTomato

The voltage-gated sodium channel, Nav1.8, is widely expressed in sensory neurons and is particularly enriched in nociceptive populations. To further evaluate the identity of Ang II-sensitive neurons, Nav1.8-expressing neurons were labelled with the red fluorescent reporter tdTomato using a Nav1.8-Cre mouse line and a tdTomato reporter mouse line (breeding scheme shown in Figure 3.4a). Sensory neurons from mice heterozygous for both Nav1.8-Cre and tdTomato were loaded with Fluo-4 (Figure 3.4b) such that Ang II-evoked Ca<sup>2+</sup> transients could be tracked in Nav1.8-positive and Nav1.8-negative neurons. Of all neurons imaged in this experiment, 311 were tdTomato-positive, while 73 were tdTomato-negative (81% tdTomato-positive, Figure 3.4a *inset*), in agreement with previous reports. Exemplar tdTomato-positive and -negative neurons are shown in Figure 3.4c, with their respective Fluo-4 fluorescence profiles shown in Figure 3.4d. In these randomly chosen neurons, the small-sized tdTomato-positive neuron responded to Ang II, while the large-diameter tdTomato-negative neuron did not. A total of 86.6±4.4% of Ang II-sensitive neurons were tdTomato-positive (Figure 3.4e). This value is significantly less than a hypothetical value of 100% ( $p = 0.038$ ), suggesting the presence of a small – but distinct – population of Ang II-sensitive, tdTomato-negative neurons in these cultures (Figure 3.4f). However, as suggested by the above data, and as shown in Figure 3.4g, tdTomato-positive – and, therefore, Nav1.8-expressing – neurons made up most of the Ang II-sensitive population. Ang II-sensitive, tdTomato-negative neurons accounted for 14 of 106 Ang II-sensitive neurons identified and were of a similarly small cross-sectional area to tdTomato-positive, Ang II-sensitive neurons (Figure 3.4h).

Fluorescence from tdTomato was not observed in neuronal cultures from mice lacking Cre expression (Nav1.8-Cre<sup>-/-</sup>/floxedtdTomato<sup>+/-</sup>, Figure 3.5a and 3.5b). Incubation of these cultures with an adeno-like virus containing the Cre-recombinase gene (Ad-Cre, a gift from Dr Cathy Wilson, Department of Pharmacology, University of Cambridge) resulted in expression of tdTomato in a small subset of neurons (Figure 3.5b).

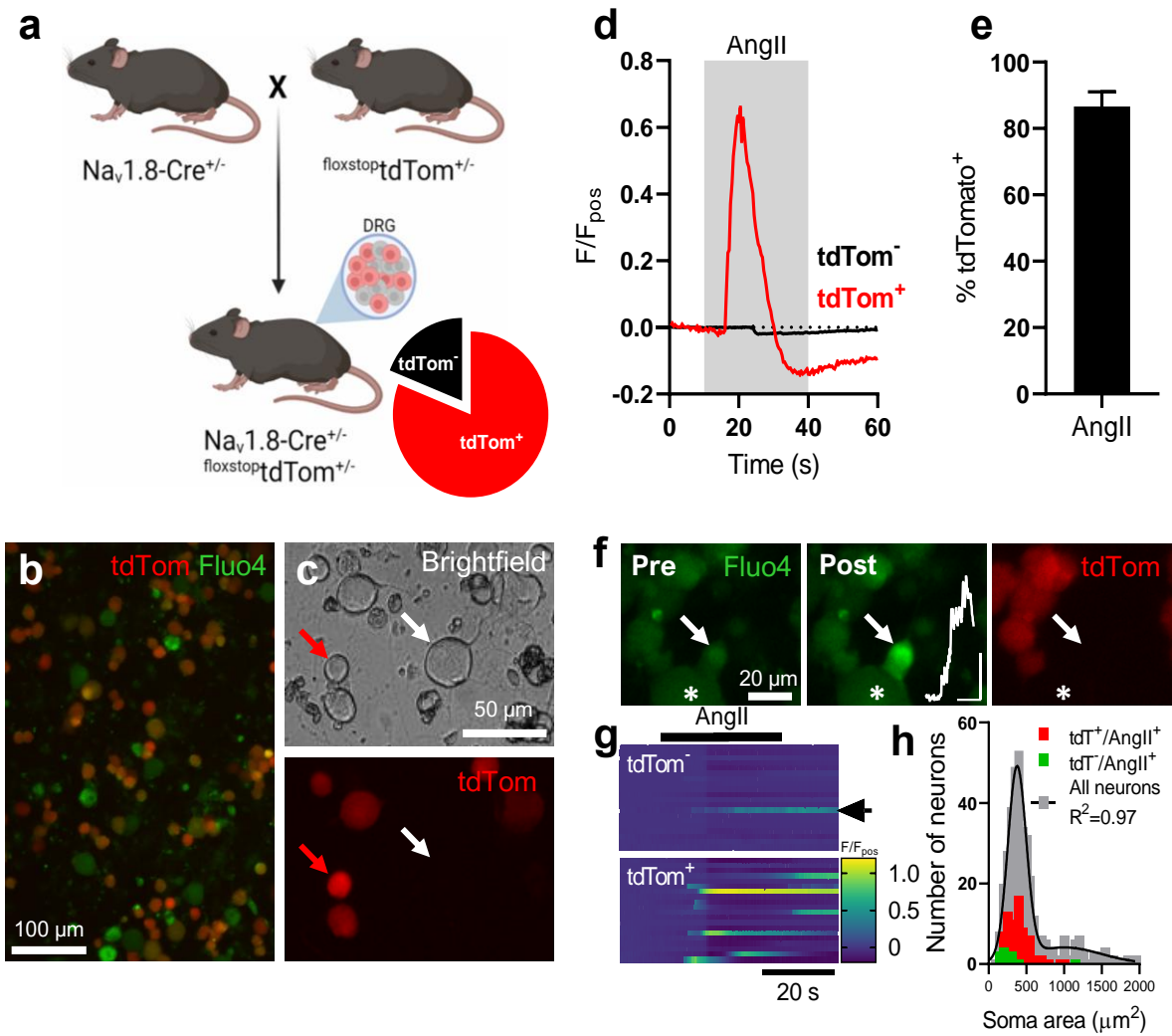
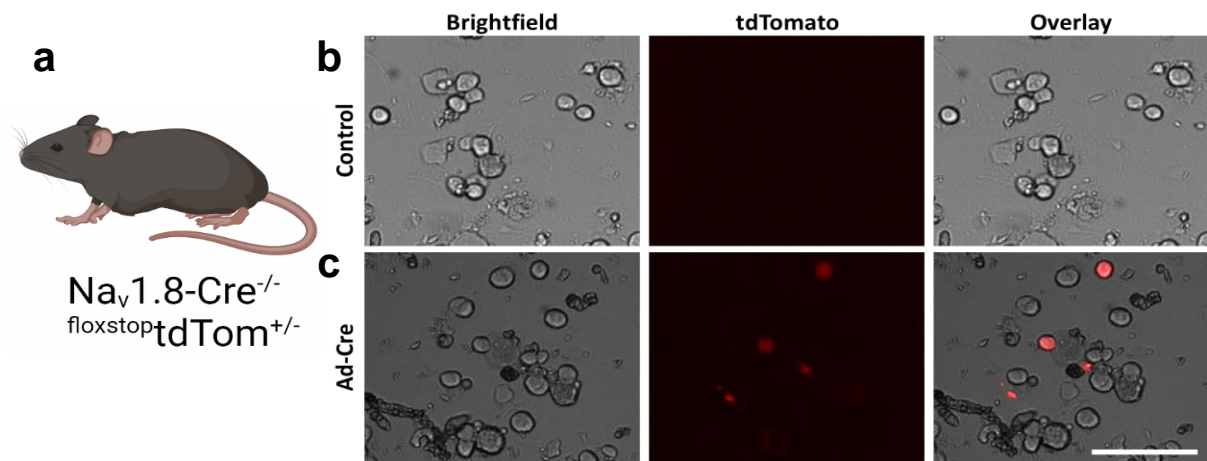


Figure 3.4 Legend on next page

### Figure 3.4 Ang II stimulated Na<sub>v</sub>1.8-expressing sensory neurons

- (a) Breeding scheme depicting the generation of mice heterozygous for both Na<sub>v</sub>1.8-Cre and flox<sup>stop</sup>tdTomato. *Inset*: pie chart showing the proportion of all neurons in culture expressing tdTomato.
- (b) Overlay image showing fluorescence derived from tdTomato expression (red) and the loading of Fluo-4 (green). Green neurons are negative for tdTomato expression.
- (c) *Top*: Brightfield image highlighting a small- (red arrow) and large-diameter (white arrow) neuron. *Bottom*: Corresponding tdTomato fluorescence image.
- (d) Fluo-4 fluorescence traces for the neurons highlighted by the red and white arrows in (c).
- (e) Grouped data showing the proportion of Ang II-sensitive neurons which expressed tdTomato. Data analysed using a one-sample t-test against a hypothetical value of 100%.
- (f) Fluorescence images (*left* and *centre*: Fluo-4; *right*: tdTomato) showing an exemplar tdTomato-negative neuron responding to Ang II application (white arrow). The inset trace in white is that of the neuron highlighted by the white arrow (scale: 30 s/0.2 F/F<sub>pos</sub>). A neighbouring tdTomato-negative neuron did not respond to Ang II application (asterisk).
- (g) Heatmaps showing the fluorescence of 40 randomly chosen neurons (20 each from the tdTomato-positive (*top*) and -negative (*bottom*) population) during Ang II application. The response highlighted by the black arrow is that of the neuron highlighted by the white arrow in (f).
- (h) Histogram showing the distribution of soma areas for neurons within the tdTomato-positive/Ang II-sensitive (red) and tdTomato-negative/Ang II-sensitive (green) populations. The size distribution for all neurons in this experiment is shown in grey and is fit by the sum of two Gaussian curves (black line).  
384 neurons, n = 5, N = 3.



**Figure 3.5 Expression of tdTomato by exogenously applied Cre**

- (a) Genotype of the mouse used for this experiment.
- (b) Sensory neurons cultured in the absence of Ad-Cre.
- (c) Sensory neurons cultured with Ad-Cre for 24 hours, showing expression of tdTomato (red). Scale bar: 100  $\mu$ m, applies to all panels.

### 3.2.1.3.2. Ablation of Nav1.8-expressing neurons abolished the response to Ang II

To validate the observations made using tdTomato reporter mice, the same Nav1.8-Cre was used to excise a floxed stop sequence upstream of a Diphtheria Toxin A (DTA) chain gene, leading to the selective destruction of Nav1.8-expressing neurons (Figure 3.6a and 3.6b; see Methods). Examining the soma size distributions of neurons from wild-type and Nav1.8-Cre-DTA mice shows a selective loss of small-sized neurons (Figure 3.6c). The size distribution of neurons from wild-type mice showed two components with mean soma areas of  $461 \pm 136 \mu\text{m}^2$  and  $979 \pm 291 \mu\text{m}^2$ , respectively (Figure 3.6d). In contrast, the size distribution of neurons from Nav1.8-Cre-DTA mice showed only a single component with a mean of  $1019 \pm 390 \mu\text{m}^2$  (Figure 3.6d). There was no difference between the larger of the two components from wild-type neurons and the single component from Nav1.8-Cre-DTA neurons ( $p = 0.69$ ). Labelling of neurons with IB4 was used to show whether non-peptidergic nociceptors – an important subset of the Nav1.8-expressing population – were lost following DTA expression. In wild-type mice, IB4-positive neurons made up  $40.4 \pm 2.3\%$  of all neurons in culture, compared to  $8.03 \pm 1.7\%$  of all neurons cultured from Nav1.8-Cre-DTA mice ( $p = 0.0003$ , Figure 3.6e).

The neuronal response to Ang II and capsaicin was substantially reduced in cultures from Nav1.8-Cre-DTA mice compared to those from wild-type mice (Figure 3.7a, b and c). In cultures from wild-type mice,  $37.1 \pm 3.9\%$  of neurons responded to Ang II, whereas only  $4.2 \pm 1.9\%$  of Nav1.8-Cre-DTA neurons responded ( $p < 0.0001$ , Figure 3.7d). To corroborate the loss of nociceptive neurons in cultures from Nav1.8-Cre-DTA mice, the response to capsaicin was also tested. In wild-type cultures,  $42.7 \pm 4.3\%$  of neurons responded to capsaicin application, compared to  $7.9 \pm 1.1\%$  of neurons in Nav1.8-Cre-DTA cultures ( $p = 0.0008$ , Figure 3.7e) (Abrahamsen *et al.*, 2008).

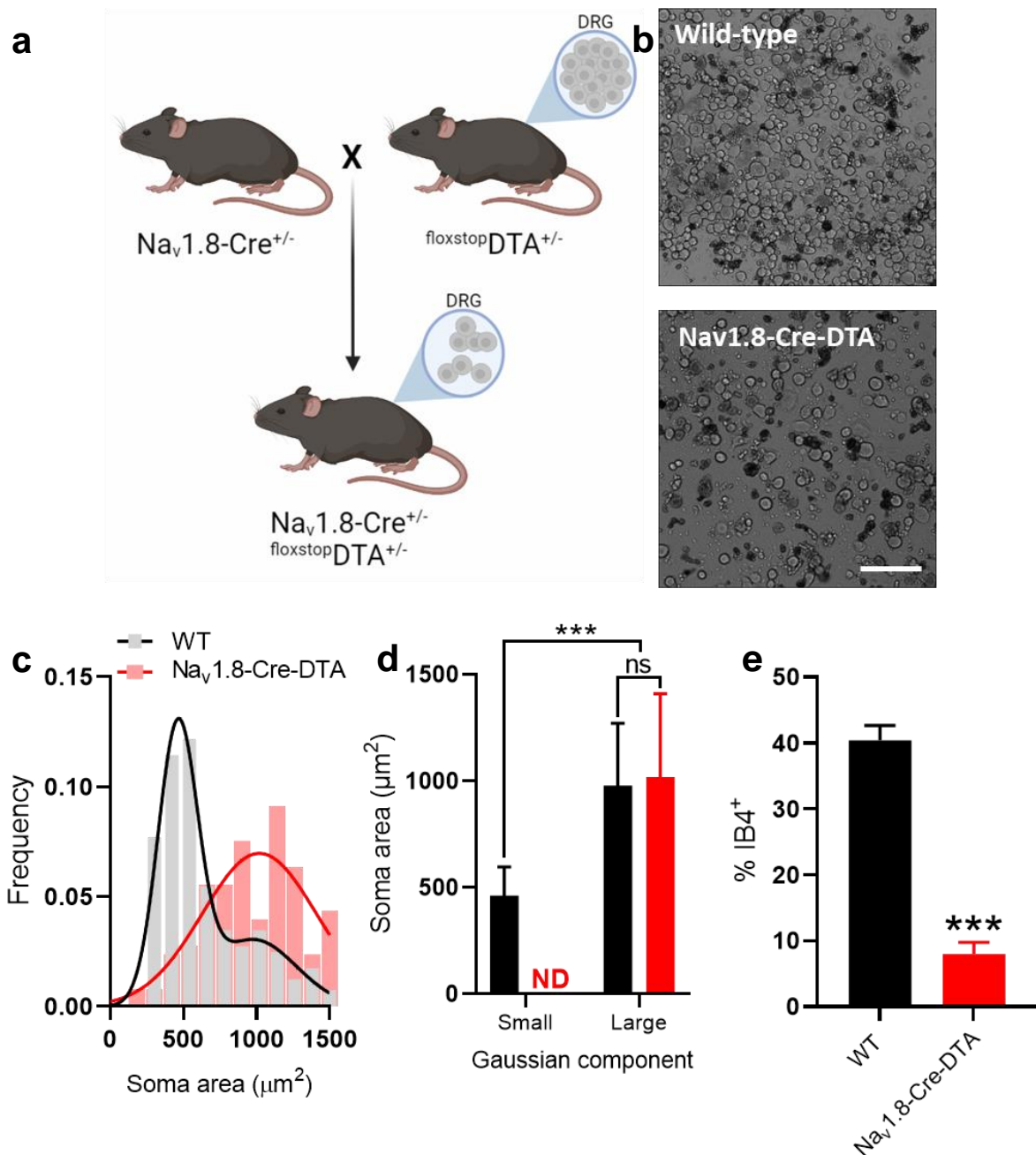


**Figure 3.6 Genetic ablation of Na<sub>v</sub>1.8-positive neurons by expression of DTA**

- (a) Breeding scheme showing the generation of mice heterozygous for Na<sub>v</sub>1.8-Cre and floxstopDTA.
- (b) Brightfield images of sensory neurons cultured from wild-type (*top*) and Na<sub>v</sub>1.8-Cre-DTA (*bottom*) mice. Scale bar 100 μm, applies to both panels.
- (c) Histogram showing the distribution of soma areas for wild-type (black, R<sup>2</sup> = 0.97) and Na<sub>v</sub>1.8-Cre-DTA (red, R<sup>2</sup> = 0.74) neurons.
- (d) Mean soma area of neurons making up the components of the single and double Gaussian curves fit to the data in (c). Mean and standard deviation is shown. ND, Gaussian component not detected. Data analysed using two-way ANOVA with Holm-Sidak post-tests.
- (e) The proportion of neurons labelled with IB4 in sensory neuron cultures from wild-type and Na<sub>v</sub>1.8-Cre-DTA mice. Data analysed using a two-tailed unpaired t-test.

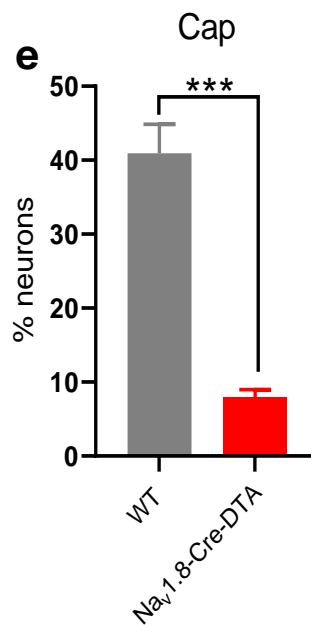
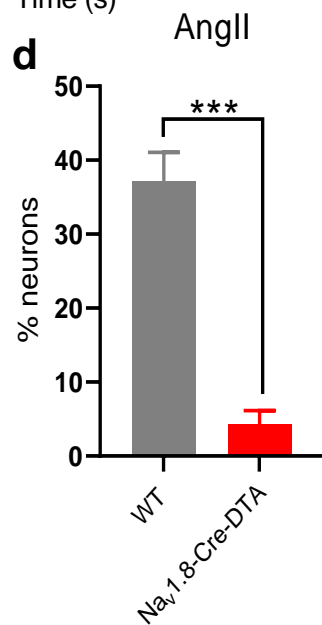
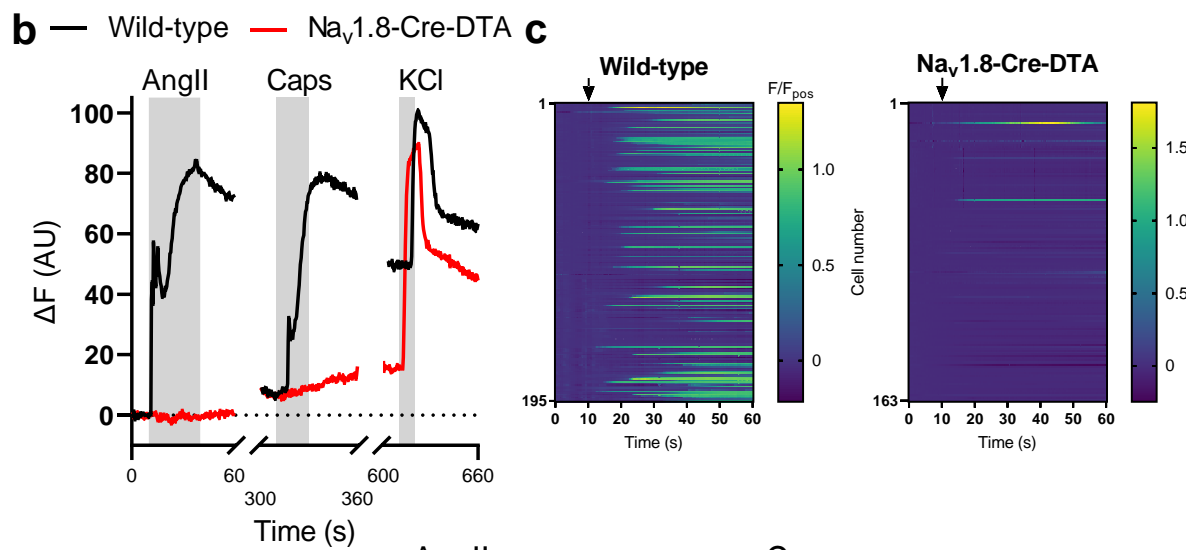
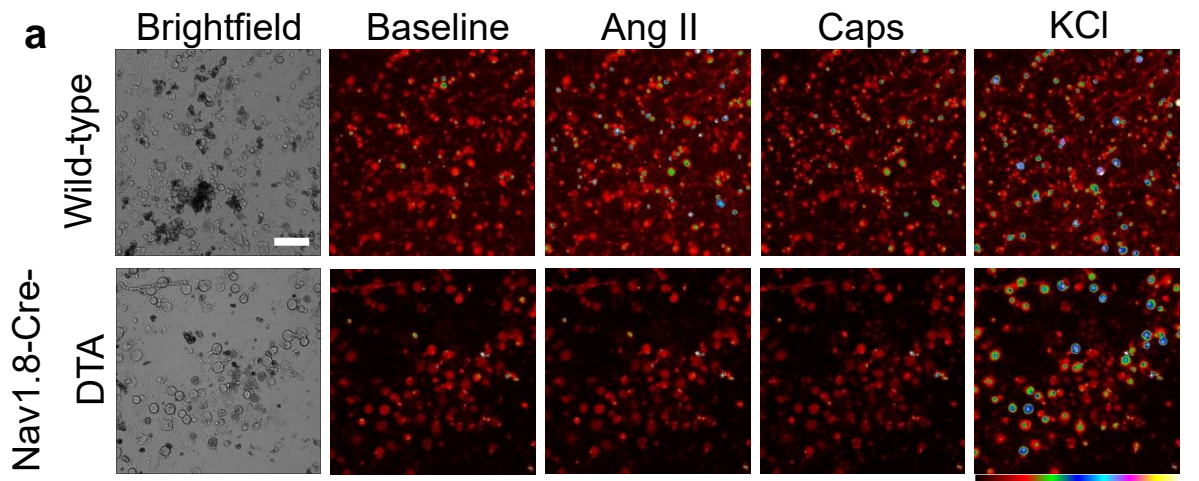


Figure 3.7 Legend on next page

**Figure 3.7 Ablation of Na<sub>v</sub>1.8-positive neurons abolished the response to Ang II and capsaicin**

- (a) False-coloured Fluo-4 fluorescence images depicting the response to Ang II, capsaicin and KCl in neurons from wild-type (*top*) and Na<sub>v</sub>1.8-Cre-DTA (*bottom*) mice. Scale bar (*top left* panel): 100 μm, applies to all panels.
- (b) Exemplar Fluo-4 fluorescence traces showing the application of Ang II, capsaicin and KCl in single neurons from wild-type (black) and Na<sub>v</sub>1.8-Cre-DTA (red) mice.
- (c) Heatmaps showing the response to Ang II application (arrow) in sensory neuron cultures from wild-type (*left*) and Na<sub>v</sub>1.8-Cre-DTA (*right*) mice.
- (d) Grouped data showing the proportion of neurons responding to Ang II. Data analysed using a two-tailed unpaired t-test.
- (e) Grouped data showing the proportion of neurons responding to capsaicin. Data analysed using a two-tailed unpaired t-test with Welch's correction.  
Wild-type: 312 neurons, n = 5, N = 4; Na<sub>v</sub>1.8-Cre-DTA: 183 neurons, n = 6, N = 2.

### 3.2.2. Ang II stimulates both IB4-positive and IB4-negative neurons

Single cell transcriptomics has revealed the selective expression of the genes encoding the Type 1 Ang II receptor (AT1R encoded by *Agtr1a* and *Agtr1b*) within the non-peptidergic population. This population of sensory neurons can be identified *in vitro* through its labelling with IB4. The hypothesis for this set of experiments was that – based on the expression of its receptor – Ang II would raise intracellular  $Ca^{2+}$  in only neurons which bind IB4. This was tested by pre-incubating neuronal cultures with IB4, in addition to Fluo-4-AM, and examining the co-localisation of Ang II-evoked  $Ca^{2+}$  signals with IB4 fluorescence.

#### 3.2.2.1. IB4 labelling revealed a population of IB4-negative Ang II-sensitive neurons

$Ca^{2+}$  imaging of IB4-labelled cultures revealed an unexpected result: a subset of IB4-negative neurons responded to Ang II application (Figure 3.8). This response was further analysed to gain a clearer understanding of the nature of this IB4-negative Ang II-sensitive population.

Neurons were parsed into IB4-positive and IB4-negative populations based on the intensity of IB4 binding (inferred through fluorescence intensity of AlexaFluor-568 conjugated to IB4, Figure 3.9a). IB4-binding non-peptidergic neurons also express P2X3, an ATP-activated non-selective cation channel (Usoskin *et al.*, 2015). Responses to  $\alpha$ - $\beta$ -meATP, a selective agonist for P2X3, were observed in culture, further demonstrating the presence of this neuronal population (Figure 3.9b). IB4 bound to the periphery of the neuronal soma (Figure 3.9c), in line with its interaction with  $\alpha$ - $\delta$ -galactose moieties on the extracellular leaf of the membrane. The IB4-positive population was substantially smaller than the IB4-negative: IB4-positive neurons accounted for  $28.4 \pm 3.2\%$  of neurons, with IB4-negative neurons accounting for the remaining  $71.6 \pm 3.2\%$  ( $p = 0.0002$ , Figure 3.9d). The proportion of each population which was Ang II-sensitive was also calculated. Ang II-sensitive neurons made up  $62.8 \pm 8.1\%$  of the IB4-positive population, and  $31.6 \pm 5.0\%$  of the IB4-negative population ( $p = 0.006$ , Figure 3.9e). Based on the expression of *Agtr1a* and *Agtr1b*, only 1.8% of IB4-negative sensory neurons in the DRG should be sensitive to Ang II, at odds with the observed sensitivity ( $p = 0.0006$ , one sample t-test). Conversely, the expected sensitivity of the IB4-positive population matches the observations made

here ( $p = 0.59$ , one sample t-test), indicating that the response of IB4-negative neurons to Ang II may be independent of AT1R.

The size of Ang II-insensitive IB4-positive neurons was indistinguishable from that of Ang II-sensitive IB4-positive neurons ( $p = 0.59$ , Figure 3.9f). However, while Ang II-sensitive IB4-negative neurons were also no different in size to those in the IB4-positive population, Ang II-insensitive IB4-negative neurons were of substantially larger soma size ( $p < 0.0001$ , Figure 3.9f). Finally, the magnitude of the response to Ang II in IB4-positive and -negative neurons was found to differ (Figure 3.9g). The response to Ang II in IB4-negative neurons was larger than that in IB4-positive neurons ( $0.70 \pm 0.02$  vs  $0.52 \pm 0.06$ ,  $p = 0.01$ , Figure 3.9h).

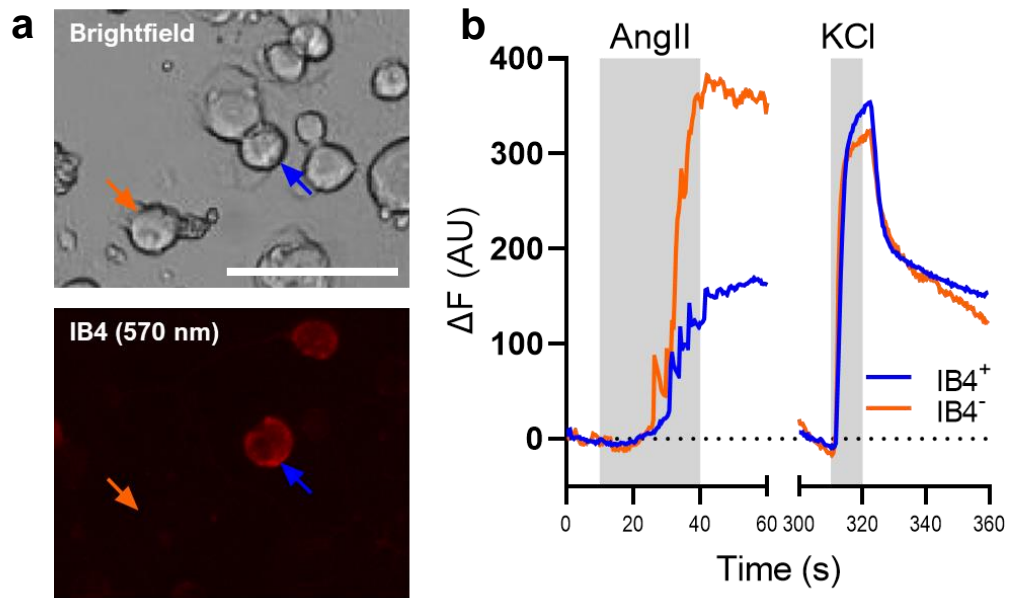


**Figure 3.8 Ang II stimulates both IB4-positive and IB4-negative sensory neurons**

- (a) *Top*: Brightfield image showing dissociated sensory neurons in culture. *Bottom*: IB4 fluorescence (arising from conjugated AlexaFluor-568, image illuminated at 570 nm) highlighting exemplar IB4-positive (blue arrow) and IB4-negative (orange arrow) neurons. Scale bar: 50  $\mu\text{m}$ .
- (b) Fluo-4 fluorescence traces for the neurons highlighted in (a) showing the application of Ang II and KCl.

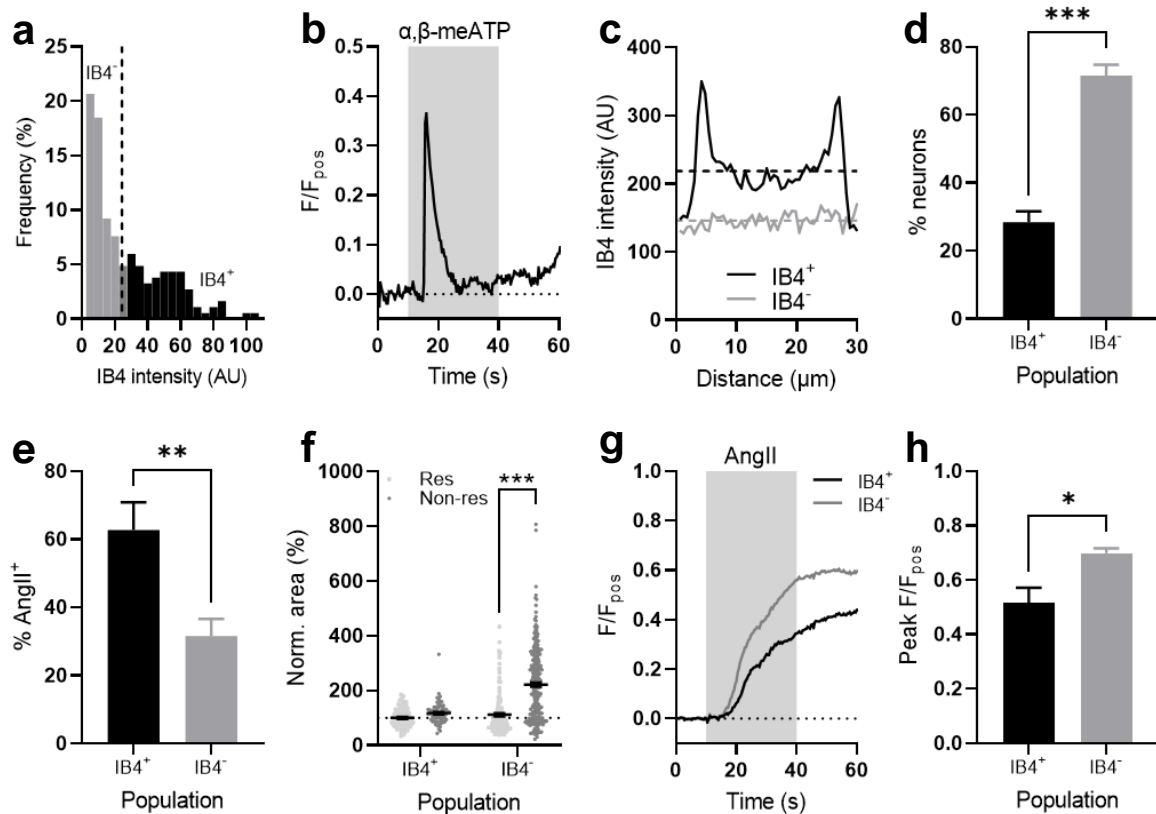


**Figure 3.9 Characterisation of the response of IB4-positive and -negative neurons to Ang II**

- Histogram showing the distribution of IB4 intensity for a single representative experiment. The vertical dashed line separates IB4-positive from -negative neurons.
- Example trace from a single neuron showing a rise in intracellular  $\text{Ca}^{2+}$  in response to application of  $\alpha,\beta\text{-meATP}$  ( $30\ \mu\text{M}$ ).
- IB4 intensity profiles from single IB4-positive and -negative neurons.
- Grouped data showing the size of the IB4-positive and -negative neuronal populations as a proportion of all neurons in culture. Data analysed using a two-tailed Mann-Whitney U test.
- The proportion of neurons within the IB4-positive and -negative populations which responded to Ang II application. Data analysed using a two-tailed unpaired t-test.
- Normalised soma areas (normalised to the mean of IB4-positive Ang II responder) of neurons within the IB4-positive and -negative populations which did or did not respond to Ang II application. Data analysed using two-way ANOVA with Holm-Sidak post-tests.
- Exemplar Fluo-4 fluorescence traces from single IB4-positive and negative neurons showing the application of Ang II.
- The peak Fluo-4 fluorescence evoked by Ang II for neurons within the IB4-positive and -negative populations. Data analysed using a two-tailed unpaired t-test with Welch's correction.

IB4-positive: Ang II-sensitive = 99, Ang II-insensitive = 71; IB4-negative: Ang II-sensitive = 136, Ang II-insensitive = 284;  $n = 8$ ,  $N = 4$ .

### **3.2.2.2. The response of IB4-negative neurons to Ang II is not dependent on IB4-positive neurons**

The stimulation of IB4-negative neurons raises interesting questions. Is the expression of *Agtr1a* and *Agtr1b* more widespread in sensory neurons than suggested by transcriptomic studies? Multiple single cell RNAseq studies of dissociated sensory neurons are now available – each with subtly different RNA extraction techniques and read depth – which all demonstrate the selective expression of the Ang II receptor in only non-peptidergic neurons. The expression of *Agtr2* has not been observed in sensory neurons. This implies another explanation for the sensitivity of an IB4-negative subpopulation to Ang II.

Perhaps IB4-positive neurons release a mediator in response to stimulation with Ang II; this unknown mediator(s) can then, in turn, go on to evoke a response in Ang II-insensitive IB4-negative neurons. If this were true, two observations would be expected: (i) there would be a time delay between the Ca<sup>2+</sup> rise in IB4-positive and -negative neurons, and (ii) the response of IB4-negative neurons to Ang II would be dependent on the presence of IB4-positive neurons.

#### **3.2.2.2.1. There was no time delay between Ang II-evoked Ca<sup>2+</sup> signals in IB4-positive and -negative neurons**

The time-to-peak of the Ang II-evoked Ca<sup>2+</sup> transients was no different between IB4-positive and -negative neurons (Figure 3.10a). For IB4-positive neurons, the time-to-peak was 55.2±2.2 s compared to 50.0±1.8 s for IB4-negative neurons, a difference of 5.2±2.8 s (p = 0.06, Figure 3.10b). These data do not suggest that there is any time delay in the response of IB4-negative neurons relative to IB4-positive neurons. That said, it may be possible that the Ca<sup>2+</sup> imaging protocols used here – e.g., washout of superfusate and the kinetics of Fluo-4 – may preclude such an observation.

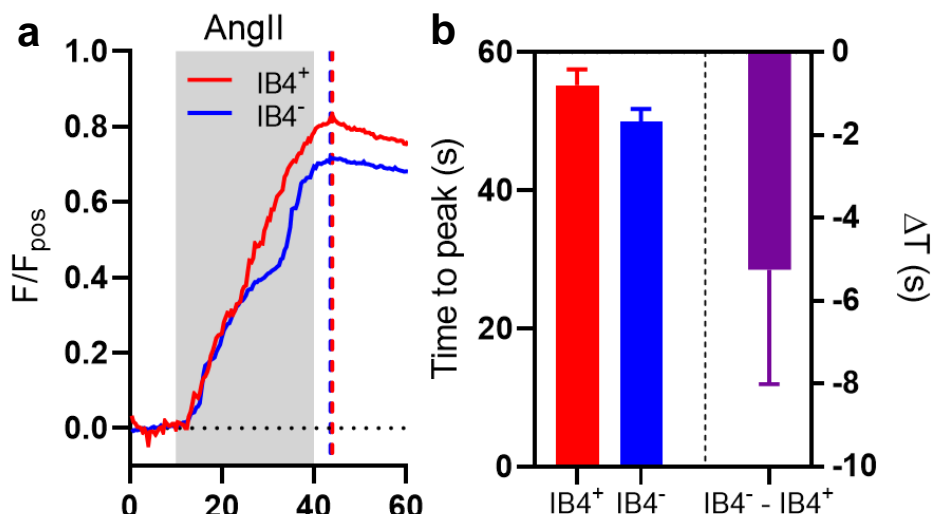


**Figure 3.10 No time delay between Ca<sup>2+</sup> signals in IB4-positive and -negative neurons**

- (a) Representative Fluo-4 fluorescence traces from neurons within the IB4-positive and -negative populations showing the response to Ang II. Vertical coloured dashed lines show the time corresponding to peak fluorescence.
- (b) Grouped data showing the time-to-peak response for neurons within the IB4-positive and -negative populations. The difference in time-to-peak response between IB4-positive and -negative neurons is shown on the right. Data analysed using a two-tailed Mann-Whitney U test.

590 neurons (IB4-positive = 170; IB4-negative = 420), n = 8, N = 4

### **3.2.2.2. Ablation of IB4-positive neurons did not affect the response of IB4-negative neurons**

To better understand whether the response of IB4-negative neurons to Ang II was dependent on IB4-positive neurons, the IB4-positive neurons were selectively ablated. This was achieved by driving Cre expression in Tmem45b-positive sensory neurons to excise a floxed stop sequence upstream of a DTA gene (Figure 3.11a, similar to above experiments with Nav1.8-Cre-DTA mice; see Methods). The use of Tmem45b-Cre-DTA mice has been validated previously (J. Zhao *et al.*, 2021). Staining of cultures with IB4 revealed a loss of IB4-positive neurons in cultures from Tmem45b-Cre<sup>+</sup>/DTA<sup>+</sup> mice (Figure 3.11b). To ensure no leaky expression of DTA in Cre-negative control mice, the proportion of Ang II-sensitive neurons within the IB4-positive and -negative populations was compared to that of C57Bl/6 wild-type mice. No difference in the proportion of Ang II-sensitive neurons was observed for either population (IB4-positive,  $p = 0.78$ ; IB4-negative,  $p = 0.78$ , Figure 3.11c).

Tmem45b is selectively expressed in non-peptidergic neurons, so one would expect to observe a loss of IB4 binding in cultures from Tmem45b-Cre<sup>+</sup>/DTA<sup>+</sup> mice. In control (Tmem45b-Cre<sup>-</sup>/DTA<sup>+</sup>) mice,  $49.6 \pm 3.7\%$  of neurons bound IB4, whereas only  $10.8 \pm 5.3\%$  bound IB4 in cultures from Tmem45b-Cre<sup>+</sup>/DTA<sup>+</sup> mice ( $p = 0.0003$ , Figure 3.11d). A corresponding decrease in the proportion of IB4-positive neurons making up the Ang II-sensitive population was also observed ( $p = 0.005$ , Figure 3.11e), in line with a loss of the non-peptidergic neuronal population. However, while the overall proportion of neurons responding to Ang II was modestly decreased, an Ang II-sensitive population remained in Tmem45b-Cre<sup>+</sup>/DTA<sup>+</sup> neuronal cultures. This Ang II-sensitive population was almost entirely made up of IB4-negative neurons ( $87.3 \pm 6.4\%$ , increased from  $47.7 \pm 7.9\%$  in control cultures,  $p = 0.005$ , Figure 3.11f). What's more, there was no change in the proportion of Ang II-sensitive neurons within the IB4-negative population ( $p = 0.45$ , Figure 3.11g), demonstrating a selective effect of DTA expression on IB4-positive neurons. These data indicate that Ang II-sensitive IB4-negative neurons respond to Ang II in a manner independent of IB4-positive neurons, suggesting no mediator release by IB4-positive neurons in response to Ang II.

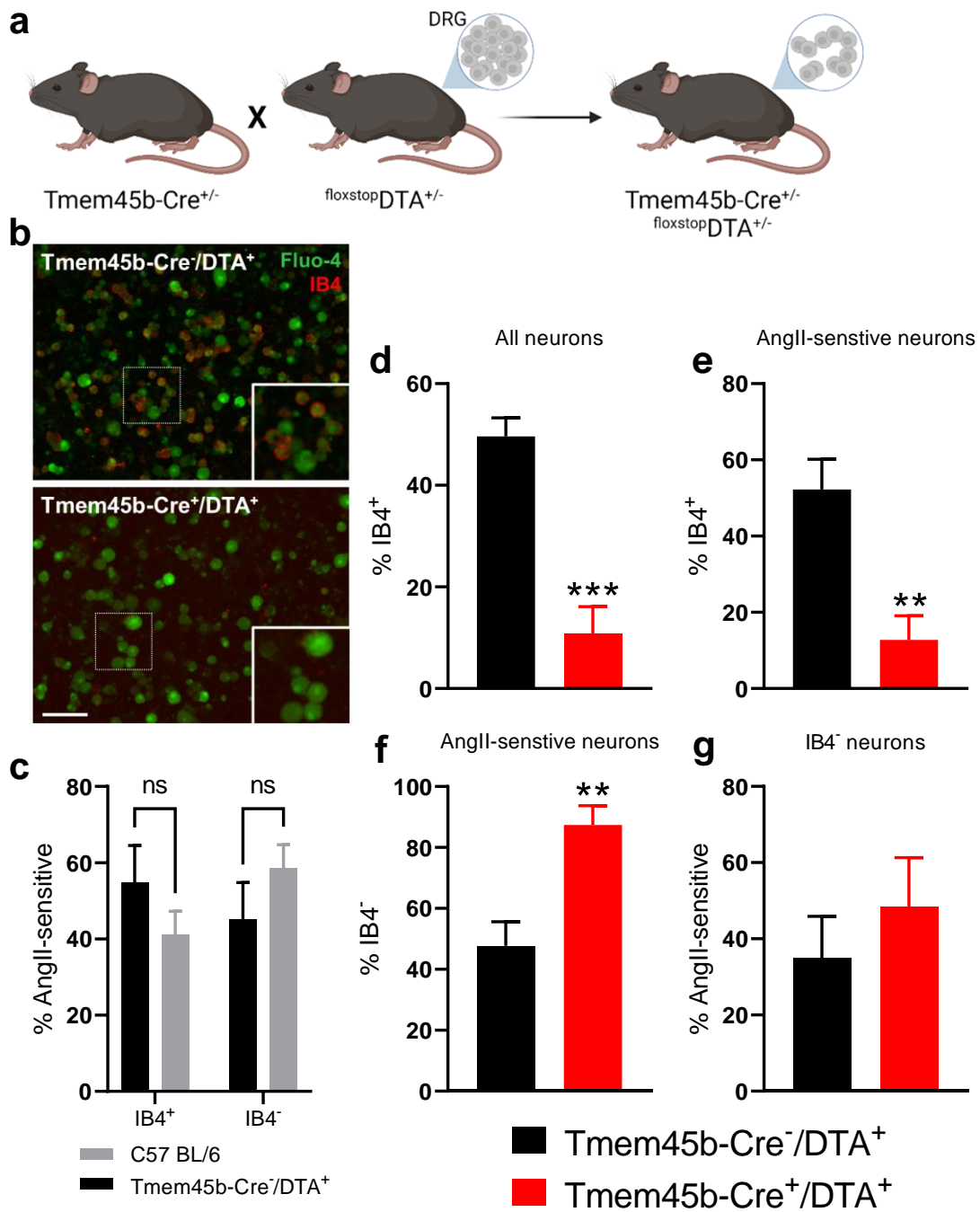


Figure 3.11 Legend on next page

**Figure 3.11 Ablation of Tmem45b-expressing neurons did not affect the Ang II response in IB4-negative neurons**

- (a) Breeding scheme showing the generation of mice heterozygous for Tmem45b-Cre and floxstopDTA.
- (b) Images showing Fluo-4 and IB4-568 fluorescence in cultures from Tmem45b-Cre<sup>-</sup>/DTA<sup>+</sup> and Tmem45b-Cre<sup>+</sup>/DTA<sup>+</sup> mice. Scale bar: 100 μm, applies to both panels.
- (c) Comparison of the proportion of Ang II-sensitive neurons within the IB4-positive and -negative neuronal populations between wild-type (C57Bl/6) and Tmem45b-Cre<sup>-</sup>/DTA<sup>+</sup> mice. Insets show higher magnification of highlighted region; 100x100 μm. Data analysed using two-way ANOVA with Holm-Sidak post-tests.
- (d) The proportion of all neurons in culture labelled IB4-positive. Data analysed using a two-tailed unpaired t-test.
- (e) The proportion of Ang II-sensitive neurons labelled IB4-positive. Data analysed using a two-tailed unpaired t-test.
- (f) The proportion of Ang II-sensitive neurons labelled IB4-negative. Data analysed using a two-tailed unpaired t-test.
- (g) The proportion of IB4-negative neurons which exhibited a response to Ang II. The proportion of Ang II-sensitive neurons labelled IB4-positive. Data analysed using a two-tailed unpaired t-test.  
Tmem45b-Cre<sup>-</sup>/DTA<sup>+</sup>: 477 neurons, n = 5, N = 5; Tmem45b-Cre<sup>+</sup>/DTA<sup>+</sup>: 238 neurons, n = 5, N = 5.

### **3.2.2.3. Non-neuronal satellite cells are required for the response of IB4-negative neurons to Ang II**

As IB4-positive neurons were not required for the response of IB4-negative neurons to Ang II, the mechanism underpinning this response remained unclear. Cultures made from dissociated DRG do not exclusively contain neurons, satellite cells – including glia and immune cells – have also been identified. To verify the presence of non-neuronal satellite cells, cultures were incubated with antibodies against  $\beta$ III-tubulin, a neuronal marker, and DAPI, a marker of nuclei. Many DAPI-positive,  $\beta$ III-tubulin-negative neurons were observed in culture, ratifying the presence of non-neuronal satellite cells (Figure 3.12a).

To quantify the numbers of neurons and non-neurons in culture, raw fluorescence images were converted into binary images to identify objects of interest (Figure 3.12b). The threshold distinguishing objects of interest from the background was set within the first minimum of the image histogram (Figure 3.12c). Closely apposed objects were separated by watershed segmentation to ensure multiple objects were not counted as one (Figure 3.12d) and objects were automatically counted. This process gave the number of neurons, and the total number of cells present in each culture. No staining was observed if the primary  $\beta$ III-tubulin antibody was omitted (Figure 3.12e).

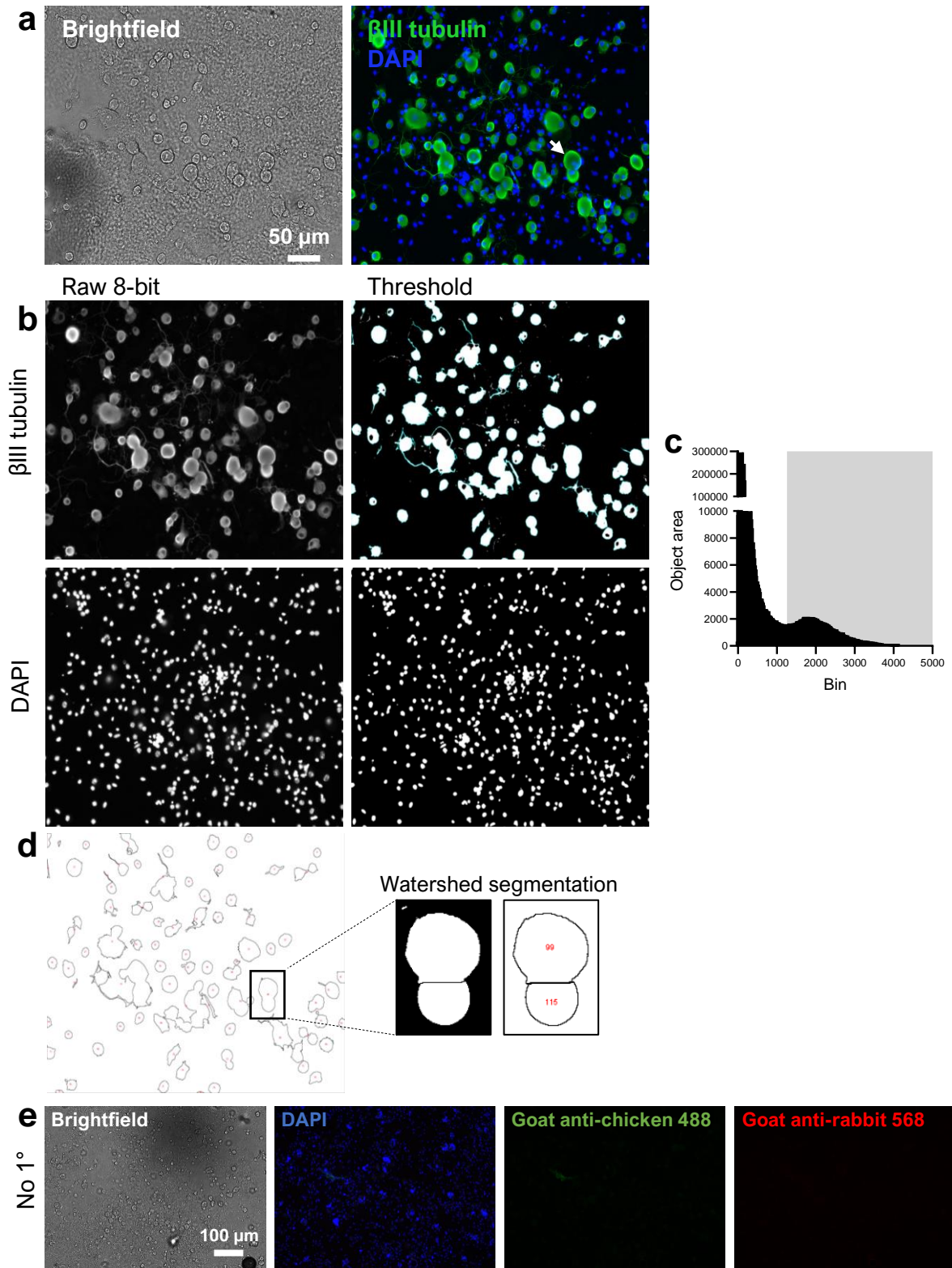


Figure 3.12 Legend on next page

### Figure 3.12 Non-neuronal satellite cells are present in dissociated DRG cultures

- (a) *Left*: brightfield image showing dissociated DRG culture. *Right*: Immunofluorescent labelling showing expressing of  $\beta$ III-tubulin (green) and nuclear labelling with DAPI (blue). Scale bar applies to all panels in (a) and (b).
- (b) Raw 8-bit images (*left*) showing staining for  $\beta$ III-tubulin (*top*) and DAPI (*bottom*), with corresponding threshold binary images (*right*).
- (c) Image histogram corresponding to the  $\beta$ III-tubulin image in (b). 'Bin' refers to the staining intensity of an object. The threshold for counting an object of interest (i.e., a neuron) is placed within the first minimum of the histogram; all objects within the grey box are labelled as neurons.
- (d) Watershed segmentation separates objects in close apposition. *Left*: outlines of the neurons identified from the  $\beta$ III-tubulin images in (b). *Right*: the separation of two neighbouring cells in contact, such that they are appropriately counted. These exemplar cells are highlighted by the white arrow in (a).
- (e) Omission of primary antibody incubation resulted in a lack of  $\beta$ III-tubulin staining with either secondary antibody used. DAPI staining was unaffected.

### **3.2.2.3.1. Magnetic cell sorting of dissociated sensory neuron cultures**

To determine the role of non-neuronal cells in the neuronal response to Ang II, it was necessary to remove them from the culture. This was achieved using magnetically-activated cell sorting (MACS). This process involved labelling non-neuronal cells with antibodies conjugated to biotin, incubating with magnetic biotin-binding beads, and passing the resulting suspension through a magnetic column. Non-neuronal cells would become trapped within the column, allowing neurons to be eluted. Following MACS, a loss of DAPI-positive,  $\beta$ III-tubulin-negative cells was observed (Figure 3.13a). The number of satellite cells per neuron was  $4.1 \pm 0.28$  in control (unsorted) cultures, and  $0.27 \pm 0.12$  in MACS cultures ( $p < 0.0001$ , Figure 3.13b). In unsorted cultures, neurons made up only  $20.2 \pm 1.3\%$  of all cells present, but this was increased to  $83.8 \pm 5.4\%$  after MACS ( $p < 0.0001$ , Figure 3.13c).

Upon closer inspection of the images in Figure 3.13a, it seems that – in addition to a loss of non-neuronal cells – there may also be a loss of large-diameter neurons, too. Indeed, the average size of neurons present in culture following MACS was significantly less than that in control cultures ( $p = 0.0005$ , Figure 3.14a). This difference in size was not observed if neurons were passed through the magnetic column in the absence of the non-neuronal antibodies and magnetic beads ( $p = 0.81$ , Figure 3.14a), suggesting a physical association between non-neuronal cells and large-diameter neurons. The distribution of soma areas showed a loss of large diameter neurons following MACS ( $p = 0.0017$ , Figure 3.14b). The size of Ang II-sensitive neurons was unchanged after MACS ( $p = 0.64$ ), but Ang II-insensitive neurons were significantly reduced in size ( $p < 0.0001$ , Figure 3.14c), indicating a loss of large-diameter, Ang II-insensitive neurons. MACS reduced the proportion of IB4-negative neurons in culture ( $71.6 \pm 3.2\%$  vs  $44.8 \pm 8.7\%$ ,  $p = 0.0073$ , Figure 3.14d), in agreement with the majority of large-diameter, Ang II-insensitive neurons being IB4-negative (see Figure 3.9f). Examining the IB4-negative population in isolation revealed a reduction in average soma size ( $p = 0.0005$ , Figure 3.14e) due to a loss of large-diameter neurons within this population ( $p = 0.0013$ , Figure 3.14f). The size distribution of IB4-negative neurons after MACS was indistinguishable from that of Ang II-sensitive, IB4-negative neurons in unsorted cultures ( $p = 0.99$ , Figure 3.14f). These data show that the IB4-negative neurons remaining in culture after MACS are small-diameter and more likely to be Ang

II-sensitive, i.e., there was no loss of Ang II-sensitive neurons. The size of IB4-positive neurons was unchanged after MACS ( $p = 0.25$ , Figure 3.14g) and there was no observed loss of these neurons due to MACS ( $p = 0.18$ , Figure 3.14h). The size distribution of neurons in unsorted and MACS cultures ratifies this loss of large-diameter neurons ( $>1000 \mu\text{m}^2$ ) and the consequent enrichment of small-diameter neurons after MACS (Figure 3.14i). The size distribution of AngII-sensitive neurons is closely matched to that of neurons in MACS cultures.

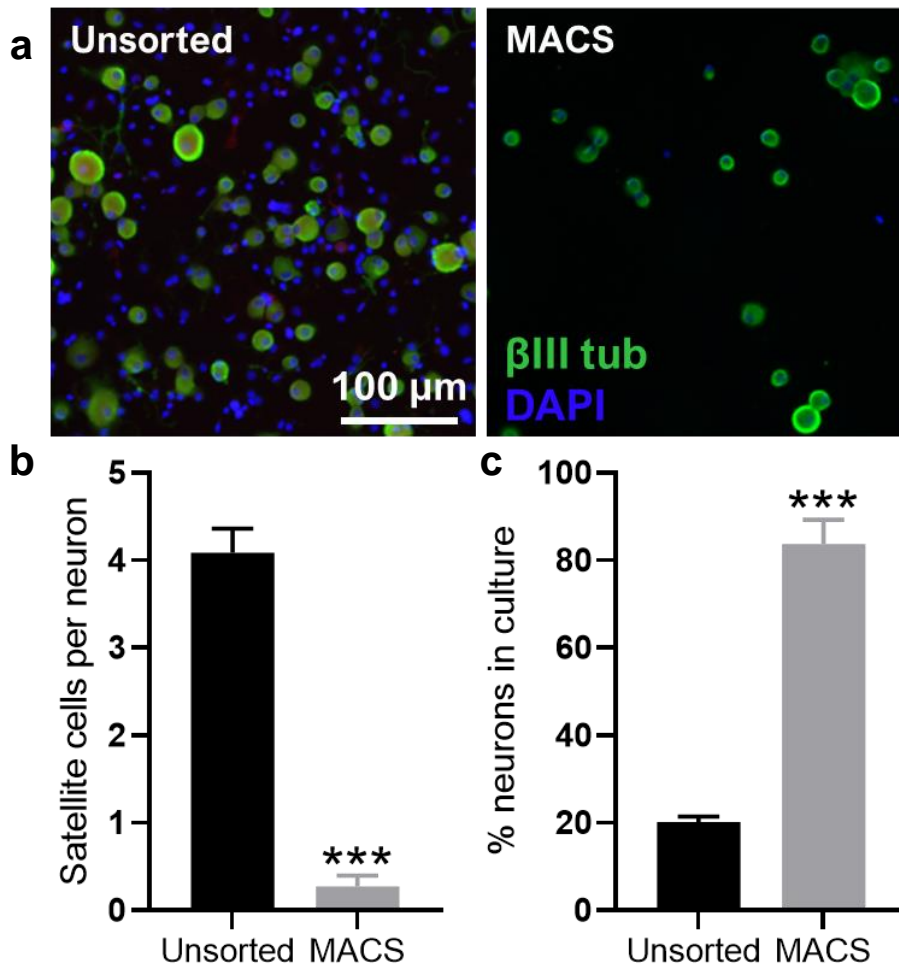


**Figure 3.13 Removal of satellite cells from DRG cultures using magnetic cell sorting**

- (a) *Left*: immunofluorescent staining showing  $\beta$ III-tubulin (green) and DAPI (blue) in an unsorted (control) culture. *Right*: equivalent immunofluorescent staining in a culture after magnetically-activated cell sorting (MACS).
- (b) Number of satellite cells per neuron for unsorted and MACS cultures. Data analysed using a two-tailed Mann-Whitney U test.
- (c) The proportion of all cells labelled as neurons for unsorted and MACS cultures. Data analysed using a two-tailed Mann-Whitney U test.  
Unsorted: n = 9, N = 3. MACS: n = 11, N = 4.

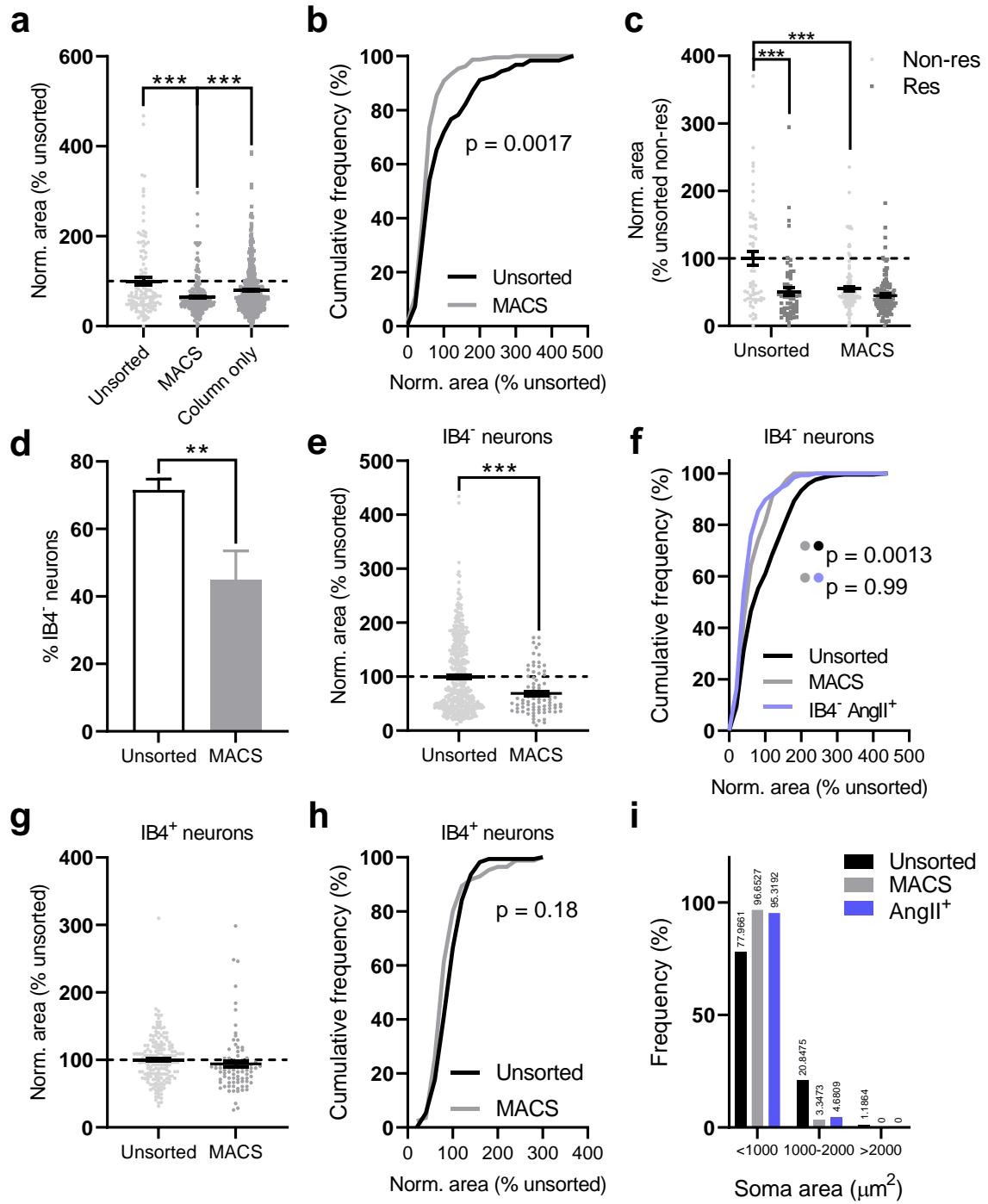


Figure 3.14 Legend on next page

### Figure 3.14 Magnetic cell sorting preserved small-sized neurons

- (a) Soma area (normalised to mean unsorted) of neurons in unsorted, MACS and MACS (antibody cocktail omitted) cultures. Unsorted: 124 neurons; MACS: 239 neurons; MACS (antibody cocktail omitted): 586 neurons. Data analysed using a Kruskal-Wallis test with Dunn's post-tests.
- (b) Cumulative frequency distribution of soma areas of neurons from unsorted and MACS cultures in (a). Data analysed using a Kolmogorov-Smirnov test.
- (c) Soma area (normalised to mean unsorted Ang II-insensitive) of Ang II-sensitive and -insensitive neurons from unsorted and MACS cultures. Unsorted: 124 neurons; MACS: 239 neurons. Data analysed using two-way ANOVA with Holm-Sidak post-tests.
- (d) The proportion of IB4-negative neurons in unsorted and MACS cultures. Unsorted:  $n = 8$ ,  $N = 6$ ; MACS:  $n = 6$ ,  $N = 6$ . Data analysed using a two-tailed unpaired t-test.
- (e) Soma area (normalised to mean unsorted) of IB4-negative neurons in unsorted and MACS cultures. Unsorted: 420 neurons; MACS: 81 neurons. Data analysed using a Mann-Whitney U test.
- (f) Cumulative frequency distribution of soma areas of data in (e), and of IB4-negative Ang II-sensitive neurons from unsorted cultures. Data analysed using a Kolmogorov-Smirnov test.
- (g) Soma area (normalised to mean unsorted) of IB4-positive neurons in unsorted and MACS cultures. Unsorted: 170 neurons; MACS: 85 neurons. Data analysed using a two-tailed unpaired t-test.
- (h) Cumulative frequency distribution of data in (g). Data analysed using a Kolmogorov-Smirnov test.
- (i) Size distribution of neurons from unsorted and MACS cultures, and of neurons responsive to AngII application.

### **3.2.2.3.2. Removal of satellite cells attenuated the neuronal response to Ang II**

A method for removing satellite cells from DRG cultures and an understanding of the characteristics of the remaining neurons permits an investigation into the role of satellite cells in the response to Ang II. After MACS, neurons required longer to adhere to the culture dish, so an additional unsorted control group with the same incubation time (48 hours, compared to 24 hours for standard unsorted cultures) was required. There was neither a difference between the proportion of neurons responding to Ang II ( $p = 0.99$ , Figure 3.15a), nor in the magnitude of this response ( $p = 0.11$ , Figure 3.15b) in neurons which had been cultured for 24 or 48 hours. After MACS, there was no change in the proportion of neurons responding to Ang II compared to the 48-hour unsorted control ( $p = 0.99$ , Figure 3.15a). However, due to the loss of IB4-negative, Ang II-insensitive neurons in MACS cultures, one would have expected the proportion of Ang II-sensitive neurons to increase if their response to stimulation was unaffected by the removal of satellite cells. That this was not observed suggests that the response of the remaining Ang II-sensitive neurons was inhibited by the loss of satellite cells. What's more, there was a reduction in the magnitude of the response to Ang II after MACS ( $p = 0.009$ , Figure 3.15b). The proportion of neurons responding to Ang II in MACS cultures was attenuated by pre-incubation with the AT1R antagonist valsartan ( $44.5 \pm 5.9\%$  vs  $8.5 \pm 3.5\%$ ,  $p = 0.0065$ , Figure 3.15a). These data indicated a reduction – but not abolition – of the response to Ang II after the removal of satellite cells, and that the response to Ang II in the absence of satellite cells was almost entirely dependent on AT1R.

After MACS, the contribution of IB4-positive and IB4-negative neurons to the Ang II-sensitive population was shifted. IB4-positive neurons made up  $72.6 \pm 10.8\%$  of the Ang II-sensitive population after MACS, an increase from  $41.3 \pm 6.0\%$  in unsorted cultures ( $p = 0.028$ , Figure 3.16a). A corresponding decrease in the contribution of IB4-negative neurons to the Ang II-sensitive population was also observed ( $p = 0.028$ , Figure 3.16b). Given the loss of large-diameter, Ang II-insensitive IB4-negative neurons after MACS, one would expect an increase in the proportion of Ang II-sensitive neurons within the IB4-negative population. This was not observed: Ang II-sensitive neurons accounted for  $32.9 \pm 5.7\%$  and  $17.3 \pm 7.5\%$  of the IB4-negative population in unsorted and MACS cultures, respectively ( $p = 0.13$ , Figure 3.16c).

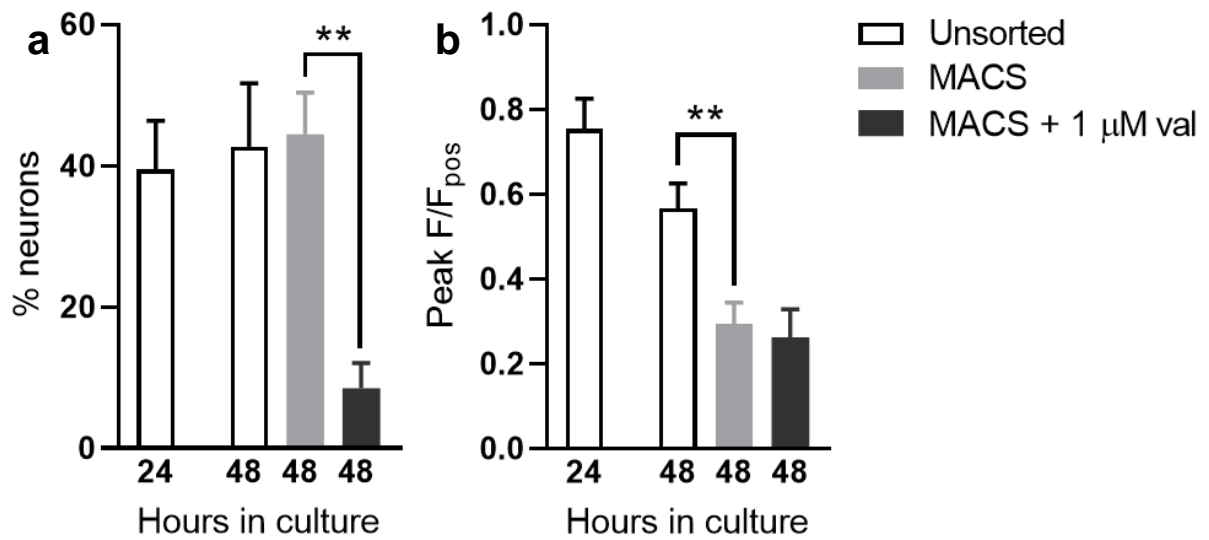


**Figure 3.15 Removal of satellite cells attenuated the neuronal response to Ang II**

- (a) The proportion of neurons responding to Ang II under different culture conditions. Data analysed using a one-way ANOVA with Holm-Sidak post-tests.
- (b) The peak magnitude of the neuronal response to Ang II under different culture conditions. Data analysed using a Kruskal-Wallis test with Dunn's post-tests.
- Unsorted (24 hours): n = 5, N = 4. Unsorted (48 hours): n = 6, N = 6. MACS: n = 10, N = 9. MACS + valsartan: n = 5, N = 5.

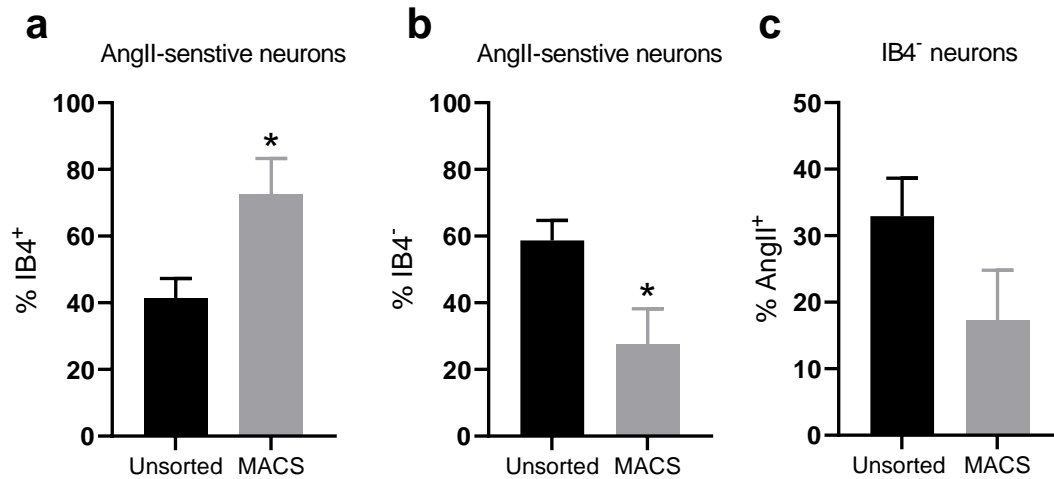


**Figure 3.16 Attenuation of the response of IB4-negative neurons to Ang II after MACS**

- (a) The proportion of Ang II-sensitive neurons which were labelled as IB4-positive in unsorted and MACS cultures. Unsorted: n = 8, N = 6. MACS: n = 4, N = 4. Data analysed using a two-tailed Mann-Whitney U test.
- (b) The proportion of Ang II-sensitive neurons which were labelled as IB4-negative in unsorted and MACS cultures. Unsorted: n = 8, N = 6. MACS: n = 4, N = 4. Data analysed using a two-tailed Mann-Whitney U test.
- (c) The proportion of IB4-negative neurons which responded to Ang II in unsorted and MACS cultures. Unsorted: n = 6, N = 4. MACS: n = 5, N = 5. Data analysed using a two-tailed unpaired t-test.

### **3.2.3. The pharmacology of the response to Ang II is altered by neuronal culture conditions**

The inhibitory effect of valsartan on the response to Ang II in different culture conditions (unsorted, MACS, *Tmem45b-Cre<sup>+</sup>/DTA<sup>+</sup>*) was investigated. A differential effect of this AT1R antagonist was observed across the different neuronal cultures (Figure 3.17a). In unsorted cultures, pre-incubation with valsartan attenuated the response to Ang II (the difference in the proportion of neurons responding between vehicle and valsartan incubation) by  $40.11 \pm 3.3\%$  (Figure 3.17b). Valsartan's inhibitory effect was elevated in MACS cultures, blocking  $80.8 \pm 7.9\%$  of the response to Ang II ( $p = 0.036$ , Figure 3.17b). Conversely, the inhibitory effect of valsartan was reduced in *Tmem45b-Cre<sup>+</sup>/DTA<sup>+</sup>* cultures to  $-19.0 \pm 16.3\%$  ( $p = 0.015$ , Figure 3.17b). A one-sample t-test revealed that the inhibitory effect of valsartan in *Tmem45b-Cre<sup>+</sup>/DTA<sup>+</sup>* cultures was no different to a hypothetical value of 0% ( $p = 0.33$ ), indicating a loss of valsartan's inhibitory effect in these cultures.

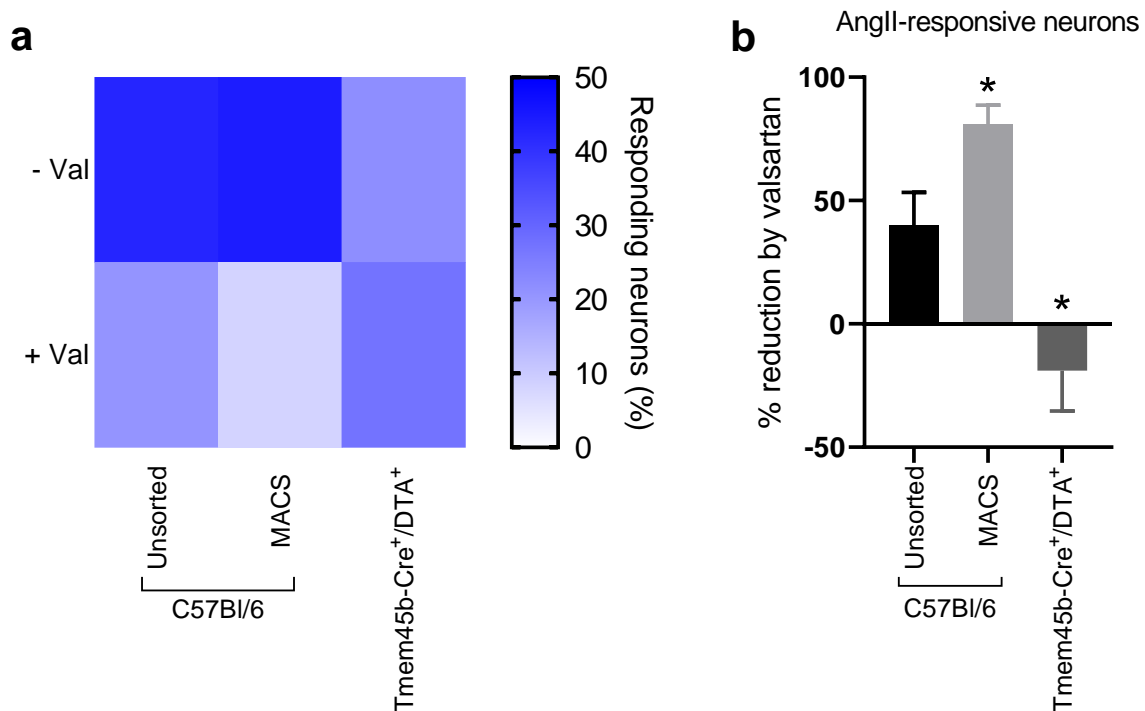


**Figure 3.17 Culture conditions alter the inhibitory effect of valsartan on the neuronal response to Ang II**

- (a) Heatmap summarising the effect of valsartan; top row is the proportion of Ang II-responsive neurons in the absence of valsartan, while the bottom row is following pre-incubation with valsartan. Darker blue represents a greater proportion of Ang II-responsive neurons (the mean for each condition is represented). This schematic highlights the differential effect of valsartan in different culture conditions.
- (b) Grouped data showing the reduction in Ang II-responsive neurons by pre-incubation with valsartan. Unsorted: n = 5, N = 5. MACS: n = 5, n = 5. Tmem45b-Cre<sup>+</sup>/DTA<sup>+</sup>: n = 4, N = 4. Data analysed using a one-way ANOVA with Holm-Sidak post-tests.

### **3.2.4. Non-neuronal satellite cells respond to Ang II**

Given the apparent dependence of the response to Ang II by IB4-negative neurons on satellite cells, it was hypothesised that these non-neuronal cells must also respond to Ang II. Non-neuronal cells were identified in culture by their lack of  $\text{Ca}^{2+}$  response to 50 mM  $\text{K}^+$  application. A rise in intracellular  $\text{Ca}^{2+}$  following Ang II application was observed in  $\text{K}^+$ -insensitive neurons in 11 of 12 (91.7%) control cultures examined (Figure 3.18a and 3.18c). The same observation was made in 5 of 5 (100%) cultures from  $\text{Nav}1.8\text{-Cre-DTA}$  mice ( $p > 0.99$ , Figure 3.18b and 3.18c), indicating that Ang II-sensitive neurons were not required for Ang II-evoked responses in non-neuronal cells. Application of Ang II in extracellular buffer lacking  $\text{Ca}^{2+}$  did not reduce the proportion of cultures in which stimulation of non-neuronal cells was observed (Figure 3.18d). Pre-incubation of cultures with thapsigargin – which depletes intracellular  $\text{Ca}^{2+}$  stores – resulted in Ang II-stimulated non-neuronal cells being observed in only 2 of 8 (25%) cultures ( $p = 0.083$ , Figure 3.18d).

While the identity of these Ang II-sensitive non-neuronal cells remains unclear, they are not likely macrophages. Of 65 macrophages to which Ang II was applied, 0 exhibited a rise in intracellular  $\text{Ca}^{2+}$  (Figure 3.18e shows representative traces), indicating that macrophages are not the elusive Ang II-sensitive non-neuronal cells in the DRG.

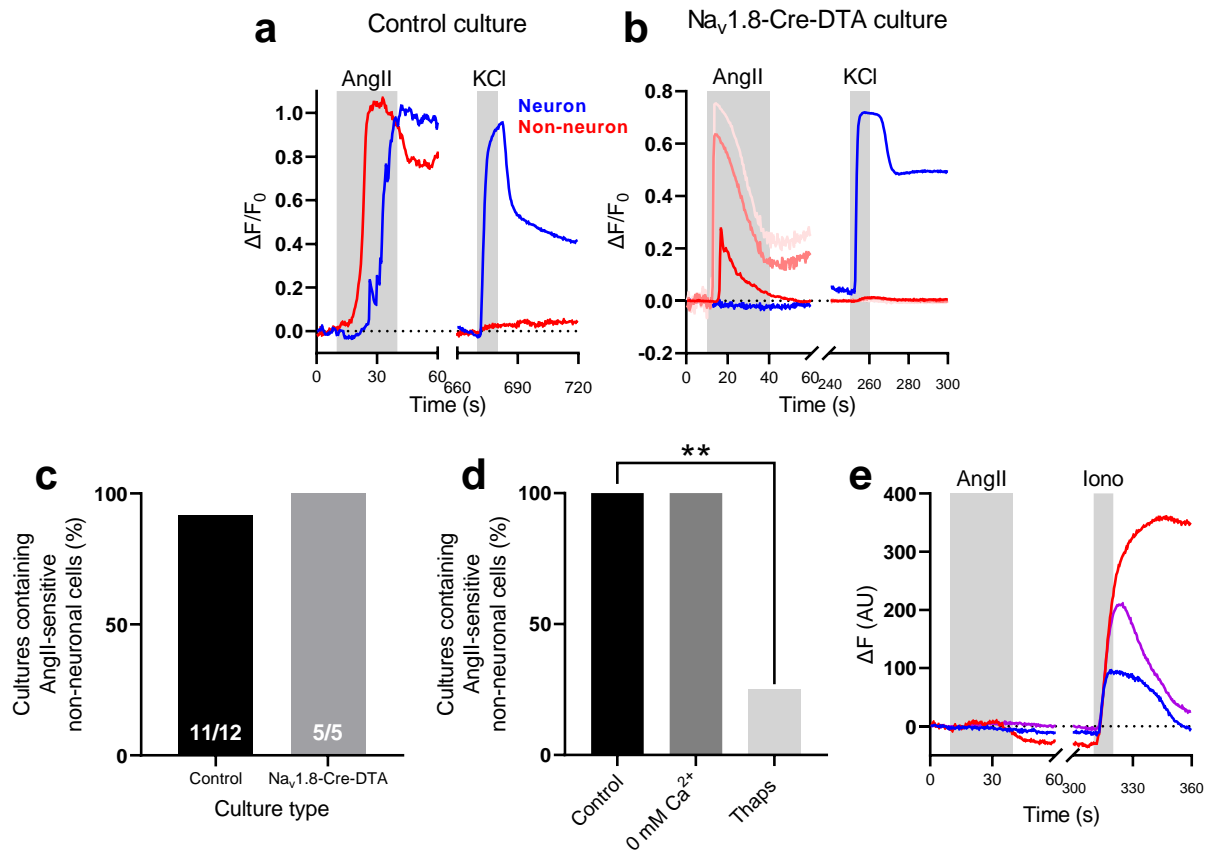


**Figure 3.18 Non-neuronal satellite cells respond to Ang II application**

- Representative Fluo-4 fluorescence traces (fold change in fluorescence relative to baseline) for a randomly selective neuron (blue) and satellite cell (red) from a control culture.
- Representative Fluo-4 fluorescence traces (change in fluorescence relative to baseline) for a randomly selective neuron (blue) and three randomly selected satellite cell (shades of red) from a  $\text{Na}_v1.8\text{-Cre-DTA}$  culture.
- The proportion of control and  $\text{Na}_v1.8\text{-Cre-DTA}$  cultures in which Ang II-sensitive non-neuronal cells were observed. Control:  $n = 12$ ,  $N = 10$ .  $\text{Na}_v1.8\text{-Cre-DTA}$ :  $n = 5$ ,  $N = 2$ . Data analysed using Chi-square test.
- The proportion of cultures in which Ang II-sensitive non-neuronal cells were observed under control conditions, in the absence of extracellular  $\text{Ca}^{2+}$  and following incubation with thapsigargin. Control:  $n = 5$ ,  $N = 5$ . 0 mM  $\text{Ca}^{2+}$ :  $n = 5$ ,  $N = 5$ . Thapsigargin:  $n = 8$ ,  $N = 5$ . Data analysed using Chi-square test.
- Representative Fluo-4 fluorescence traces from single macrophages during Ang II and ionomycin application.

### **3.2.5. Alamandine stimulates sensory neurons independently of AT1R**

The possibility that a metabolite of Ang II could stimulate cultured sensory neurons was tested. Alamandine is formed by the breakdown of Ang II by angiotensin converting enzyme 2 (ACE2), which is highly expressed by sensory neurons, raising the possibility of its formation following Ang II application.

When alamandine (100 nM) was applied to neuronal cultures, a Ca<sup>2+</sup> signal was observed in a subset of neurons (Figure 3.19a). The mean area of alamandine-sensitive soma was 64.7±3.1% of that of insensitive neurons ( $p < 0.0001$ , Figure 3.19b). Neither the magnitude of the response to alamandine (0.19, Figure 3.19c), nor the proportion of responding neurons ( $p = 0.26$ , Figure 3.19d), was affected by pre-incubation with valsartan.

To test whether alamandine contributed to the neuronal response following Ang II application, cultures were pre-incubated with MLN4760 (10 μM) – an ACE2 inhibitor – prior to Ang II (100 nM) application. Inhibition of ACE2 did not appear to affect the magnitude of the response to Ang II (Figure 3.19e). The peak fluorescence signal was 0.33±0.09 under control conditions and 0.42±0.04 following incubation with MLN4760 ( $p = 0.69$ , Figure 3.19f). Moreover, there was no change in the proportion of neurons responding to Ang II (control: 8.0±2.2%, MLN4760: 6.8±1.4%,  $p = 0.89$ , Figure 3.19g). A rise in intracellular Ca<sup>2+</sup> in non-neuronal (K<sup>+</sup>-insensitive) cells during alamandine application was observed in 1 of 9 cultures examined (Figure 3.19h).

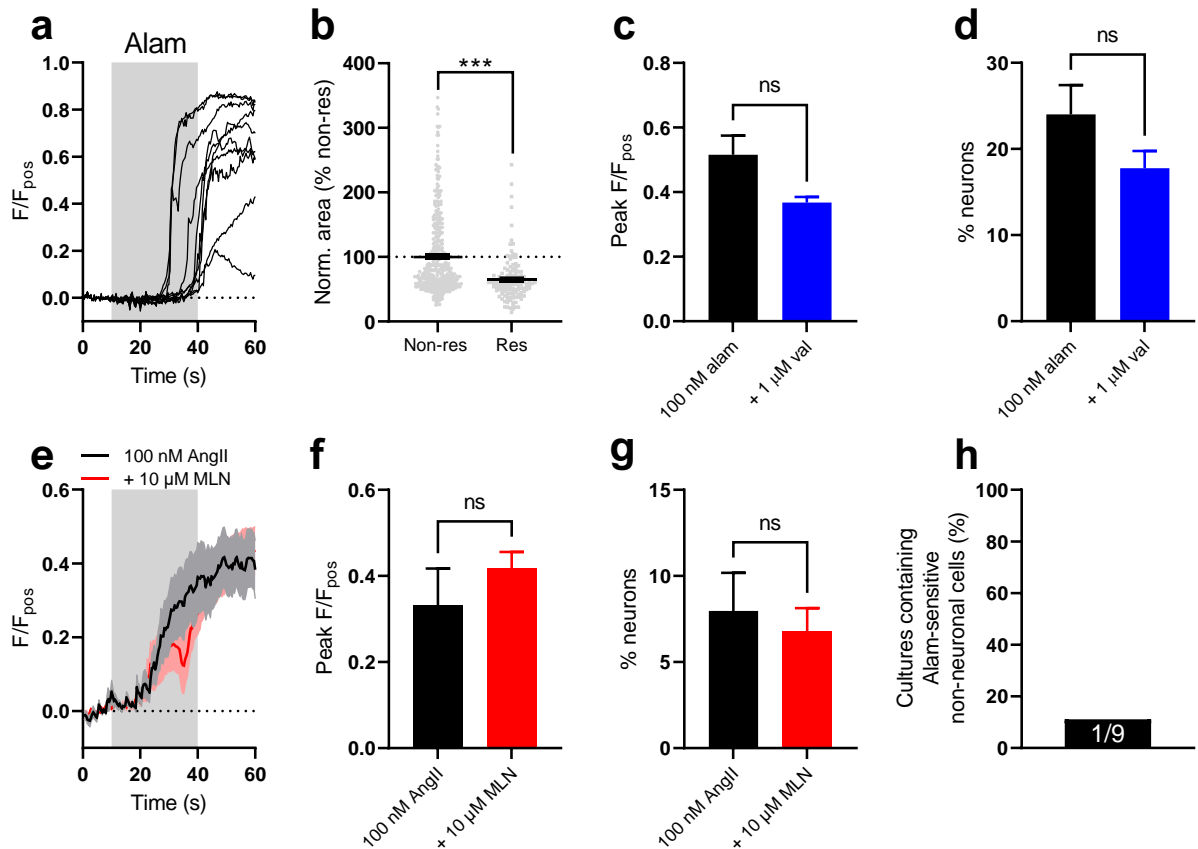


**Figure 3.19 Alamandine stimulates small-sized sensory neurons independently of AT1R**

- Exemplar Fluo-4 fluorescence traces from ten randomly selected alamandine-sensitive neurons during the application of alamandine.
- Grouped data showing normalised soma area for alamandine-sensitive and -insensitive neurons. Data analysed using a two-tailed Mann-Whitney U test.
- Peak magnitude of the response to alamandine with and without pre-incubation with valsartan. Control:  $n = 5$ ,  $N = 5$ . Valsartan:  $n = 4$ ,  $N = 4$ . Data analysed using a two-tailed Mann-Whitney U test.
- Proportion of neurons responding to alamandine application with and without valsartan pre-incubation. Control:  $n = 5$ ,  $N = 5$ . Valsartan:  $n = 4$ ,  $N = 4$ . Data analysed using a two-tailed Mann-Whitney U test.
- Exemplar average Fluo-4 fluorescence traces from all Ang II-responsive neurons in single experiments with and without pre-incubation with MLN4760. Control: 9 responsive neurons. MLN4760: 8 responsive neurons.
- Peak magnitude of the response to Ang II with and without pre-incubation with MLN4760. Control:  $n = 4$ ,  $N = 4$ . MLN4760:  $n = 4$ ,  $N = 4$ . Data analysed using a two-tailed Mann-Whitney U test.
- Proportion of neurons responding to Ang II with and without pre-incubation with MLN4760. Control:  $n = 4$ ,  $N = 4$ . MLN4760:  $n = 4$ ,  $N = 4$ . Data analysed using a two-tailed Mann-Whitney U test.
- Proportion of cultures containing alamandine-sensitive non-neuronal cells;  $n = 9$ ,  $N = 4$ .

### **3.3. Discussion**

This Chapter aimed to resolve the identity of Ang II-sensitive sensory neurons in culture and to begin to elucidate the mechanisms underpinning Ang II-evoked Ca<sup>2+</sup> signals.

#### **3.3.1. Ang II-sensitive neurons exhibit key features of nociceptors**

Nociceptive neurons are a highly heterogeneous population of sensory neurons serving to relay noxious signals to the central nervous system. Despite this heterogeneity, there are salient features which can be used to identify these neurons, or subsets thereof. An important consideration here is that the neurons imaged in this Chapter do not only innervate the gut. In future experiments, colon-innervating neurons will be retrogradely labelled using a tracer – such as FastBlue (Hockley *et al.*, 2019) – injected into the colon such that the properties of Ang II-sensitive colonic neurons can be ascertained.

##### **3.3.1.1. Ang II-sensitive neurons are small-sized**

Analysis of neuronal soma cross-sectional area demonstrated two normally-distributed populations of sensory neuron based on size (see Figures 3.1c and 3.6c). Ang II-sensitive neurons fit into the smaller of these two populations and were absent if this small-sized population was genetically ablated.

While nociceptors may be myelinated (A $\delta$  fibres) or unmyelinated (C fibres), they tend to be of smaller soma size than other sensory neurons, such as proprioceptors or low-threshold mechano-receptors (LTMRs, e.g., A $\alpha$  or A $\beta$  fibres) (Lawson, Fang and Djouhri, 2019). Previous work also identified two normally-distributed populations of sensory neuron based on soma area (Lawson, 1979; Lawson, Fang and Djouhri, 2019). Neurons within the smaller of these populations stain more poorly for neurofilament – a marker of myelination – than their larger counterparts, suggesting many are unmyelinated. Transcriptomic studies have resolved two broad sensory neuron populations based on neurofilament expression (Usoskin *et al.*, 2015). Neurons with high neurofilament expression also express markers of LTMRs and proprioceptors, such as *Cacna1h* and *Trkc*. Conversely, neurons with low expression of neurofilament express markers of nociceptive neurons, such as *Gfra2* and *Scn10a*. What's more, neurons responding to noxious stimuli, such as noxious heat, cold or pressure, tend to be of small soma area (Cesare and Mcnaughton, 1996; Emery *et al.*,

2016) – though some neurons responding to innocuous stimuli, like innocuous cold, are also of small soma area (Dhaka *et al.*, 2008), but this is a relatively small population. Together, these reports strongly suggest that small-sized sensory neurons – a subset of which are stimulated by Ang II – are likely to be nociceptors.

### **3.3.1.2. Ang II stimulates a TRPV1-positive neuronal population**

The non-selective cation channel TRPV1 is expressed in a subset of the small-diameter, neurofilament-lacking sensory neuron population (Usoskin *et al.*, 2015). Ang II stimulated >80% of the TRPV1-expressing (i.e., capsaicin-responsive) population. TRPV1 is expressed by *Mrgpra3*- and *Il31ra*-positive non-peptidergic neurons, as well as unmyelinated peptidergic neurons (Usoskin *et al.*, 2015). These neurons have been implicated in itch in the skin: neuronal IL31R is vital for the generation of immune cell-mediated itch in conditions such as atopic dermatitis and cutaneous T-cell lymphoma (Cevikbas *et al.*, 2014). Importantly, MrgA3, activated by chloroquine, has recently been shown to mediate visceral hypersensitivity – an important mechanism underpinning visceral pain in irritable bowel disease (IBS) and IBD (Castro *et al.*, 2019). This group showed mechanical hypersensitivity of colonic afferent nerves and behavioural hypersensitivity to rectal distension following administration of chloroquine. Ca<sup>2+</sup> imaging indicated that chloroquine, like Ang II, stimulated TRPV1-expressing sensory neurons.

Ang II also stimulated a small population of capsaicin-insensitive neurons. This population is likely to contain *Mrgprd*-expressing neurons, which account for ~20% of all sensory neurons in the DRG (Usoskin *et al.*, 2015; Patil, Hovhannisyan and Akopian, 2018). Of these neurons, ~50%, or ~10% of all DRG neurons, express a receptor for Ang II. This is not dissimilar to the ~7% of DRG neurons making up the Ang II-sensitive, capsaicin-insensitive population. Activation of MrgD with 5-oxo-ete, an endogenous agonist elevated in constipation-predominant IBS, raised intracellular Ca<sup>2+</sup> in a subset of DRG neurons, stimulated colonic afferents and induced hypersensitivity to rectal distention (Bautzova *et al.*, 2018). It appears that Ang II stimulates sensory neuron populations already implicated in nociceptive signalling from the gut; given the elevated presence of Ang II in the inflamed gut, this raises the possibility that Ang II may contribute to visceral nociception.

In addition to Ca<sup>2+</sup> imaging data presented here, it has been found that Ang II stimulates TRPV1-expressing colonic afferent nerves (Charity Bhebe and Rohit Gupta, unpublished observation). Ang II also appears to induce modest mechanical hypersensitivity of colonic afferent fibres (Charity Bhebe, unpublished observation), lending further credence to the notion that Ang II may play a role in visceral nociception and pain in IBD.

### **3.3.1.3. Expression of Nav1.8 in Ang II-sensitive neurons**

Nav1.8 conveys a tetrodotoxin (TTX)-resistant Na<sup>+</sup> current and is only expressed in a subset of sensory neurons, of which more than 85% are nociceptive (Stirling *et al.*, 2005). Nav1.8 itself plays a role in visceral pain; Nav1.8-null mice display blunted nocifensive behaviours following intracolonic administration of capsaicin or mustard oil (Laird *et al.*, 2002). This is unlikely due to a direct role of Nav1.8 in the transduction of these noxious chemical stimuli, but rather a role in action potential generation (Renganathan, Cummins and Waxman, 2001).

The role of Nav1.8-expressing sensory neurons in different sensory modalities has been extensively investigated. Noxious mechanosensation, but not innocuous mechanosensation, is dependent on Nav1.8-expressing sensory neurons (Abrahamsen *et al.*, 2008). The sensation of noxious cold also requires Nav1.8-expressing neurons, while these neurons are dispensable in noxious heat sensation. Finally, hypersensitivity to cold and mechanical stimuli resulting from an inflammatory insult, such as experimental arthritis, is ameliorated if Nav1.8-expressing sensory neurons are destroyed (Abrahamsen *et al.*, 2008). In alignment with this, optogenetic silencing of Nav1.8-positive afferents alleviated mechanical hypersensitivity under inflammatory conditions (Daou *et al.*, 2016). The role of Nav1.8-expressing sensory neurons in mechanical hypersensitivity during inflammation may support a role for these neurons in visceral nociception in IBD, which is largely driven by hypersensitivity to physiological gut distension.

Two methods were used to demonstrate Nav1.8 expression by Ang II-sensitive neurons: labelling of Nav1.8-positive neurons using Cre-dependent tdTomato expression, and ablation of Nav1.8-positive neurons using Cre-dependent DTA expression.

Labelling of Nav1.8-positive neurons with tdTomato was achieved by inserting a tdTomato sequence within the *ROSA26* locus downstream of a synthetic CAG promoter and floxed stop site (J. Zhao *et al.*, 2021); the CAG promoter is frequently used to drive high gene expression in transgenic animals. Excision of the floxed region and subsequent tdTomato expression was driven by Nav1.8-Cre. This revealed Nav1.8 expression in 81% of DRG neurons, a value well in-line with previous reports using immunohistochemistry (Luiz *et al.*, 2019), immunocytochemistry (Thakur *et al.*, 2014) and gene expression (Usoskin *et al.*, 2015). Nav1.8-Cre-positive neurons also accounted for >80% of the Ang II-sensitive population. This provides more evidence indicating that Ang II-sensitive neurons belong to a population of nociceptors. However, a small population of Ang II-sensitive, Nav1.8-Cre-negative neurons was observed, accounting for ~13% of the total Ang II-sensitive population and ~4% of all neurons. Could these neurons be nociceptors too? Indeed, they have a similarly small cross-sectional area compared to tdTomato-positive, Ang II-sensitive neurons. Moreover, while Nav1.8 is enriched in nociceptive sensory neuron populations, it is not necessarily expressed in all nociceptors. For example, a related Na<sup>+</sup> channel, Nav1.9, is also enriched in nociceptor populations. While these two Na<sup>+</sup> channels are frequently co-expressed, there is a distinct subset of neurons which express Nav1.9 but not Nav1.8, suggesting there may be some Nav1.8-lacking nociceptive neurons (Usoskin *et al.*, 2015).

The selective expression of DTA to ablate genetically-identified cell types was first reported almost two decades ago (Brockschneider *et al.*, 2004; Matsumura *et al.*, 2004; Ivanova *et al.*, 2005; Sato and Tanigawa, 2005). In the construct used in the present study, the DTA gene was inserted into the *ROSA26* locus – a ubiquitously expressed gene – and is repressed by an upstream floxed stop cassette (Ivanova *et al.*, 2005; Abrahamsen *et al.*, 2008). Excision of the stop sequence by Nav1.8-driven Cre leads to DTA expression in only Nav1.8-positive cells. The ubiquitous expression of *ROSA26* is of no concern due to the expression of Nav1.8 being limited to the peripheral sensory nervous system. However, it is important to consider Cre expression outside of the target cells to avoid effects of DTA in other tissues. What's more, leaky expression of DTA is a concern in these experiments due to the risk of ablating neurons outside the population of interest, particularly given that as little as a single molecule of DTA is sufficient to kill a cell (Yamaizumi *et al.*, 1978). Leaky

expression from the *ROSA26* locus has not been reported (Ivanova *et al.*, 2005; Abrahamsen *et al.*, 2008). This may be due to the presence of a neomycin resistance cassette within the floxed region which increases the distance between the loxP sites, reducing the likelihood of recombination in the absence – or presence of minute quantities – of Cre (Stifter and Greter, 2020). A final consideration of this experiment is the control group used. Here, wild-type (C57Bl/6) mice were used because only Nav1.8-Cre<sup>-</sup>/DTA<sup>+</sup> animals were available as an alternative control genotype. Neurons from these mice would express GFP as the floxed sequence would remain in situ (see Figure 2.1b); this is not appropriate as the fluorescence from GFP would interfere with that of Fluo-4.

Expression of DTA by Nav1.8-Cre led to the loss of small-diameter neurons (with no effect on larger-diameter neurons) and a near-complete loss of IB4-positive and capsaicin-sensitive neurons. This validates the selective loss of nociceptive neurons (Abrahamsen *et al.*, 2008). Consequently, the marked attenuation of the neuronal response to Ang II distinguishes the Ang II-sensitive population as nociceptive.

### **3.3.2. Unexpected sensitivity of a subpopulation of IB4-negative neurons to Ang II**

Transcriptomic studies have consistently shown selective expression of *Agtr1a* and *Agtr1b* – the genes encoding AT1R receptors – in non-peptidergic sensory neurons (Usoskin *et al.*, 2015; Ray *et al.*, 2018; Zeisel *et al.*, 2018). Consistently, a subset IB4-positive neurons in culture responded to Ang II application. However, ~30% of the IB4-negative population also responded to Ang II application; this was unexpected given the apparent lack of Ang II receptor expression in these neurons. IB4-negative, Ang II-sensitive neurons were of a similar cross-sectional area to IB4-positive, Ang II-sensitive neurons. IB4-negative, Ang II-insensitive neurons were of a larger cross-sectional area, indicating this population contained neurons other than nociceptors. Given the expression of TRPV1 and Nav1.8 in the majority of Ang II-sensitive neurons, it is likely that most of the IB4-negative, Ang II-sensitive population also expresses these nociceptor markers. IB4-negative neurons expressing TRPV1 and Nav1.8 are very likely to fall within the peptidergic class of nociceptors, i.e., those which also express markers such as CGRP and trkA, and which mediate neurogenic inflammation. Further evidence for this could be ascertained using CGRP-Cre to drive

DTA expression in – and subsequently destroy – peptidergic neurons (J. Zhao *et al.*, 2021) and examining if this abolished the response of IB4-negative neurons to Ang II.

### **3.3.2.1. Stimulation of IB4-negative neurons is not dependent on IB4-positive neurons**

The magnitude of Ang II-evoked  $Ca^{2+}$  signals differed between IB4-positive and -negative neurons. This may indicate that different mechanisms underpin these  $Ca^{2+}$  signals. It was first hypothesised that the IB4-positive neurons which responded to Ang II released an unidentified mediator which could subsequently stimulate IB4-negative neurons. If this were true, one might expect a time delay between the  $Ca^{2+}$  signals evoked in IB4-positive and -negative neurons, owed to the time taken for mediator release and for this mediator to reach an IB4-negative neuron. No time delay was observed. Given the close apposition of neurons in culture, any such time delay may be very small – too small, perhaps, to be detected by the experimental set up used here.

To further evaluate the role of IB4-positive neurons in the response of IB4-negative neurons to Ang II, the IB4-positive population was ablated by selective expression of DTA. For these experiments, *Tmem45b-Cre* was used to direct DTA expression as this gene is selectively in the non-peptidergic population of sensory neurons (Usoskin *et al.*, 2015; Zeisel *et al.*, 2018; J. Zhao *et al.*, 2021). Of all neurons which express either *Agtr1a* or *Agtr1b*, ~90% co-express *Tmem45b* (Usoskin *et al.*, 2015). *Tmem45b* is expressed outside of the peripheral sensory nervous system and is known to contribute to the proliferation and invasion of cancer cells (Hu *et al.*, 2016; Shen *et al.*, 2018). Consequently, there is a risk of DTA expression outside of the target cell population. To avoid this, the DTA construct was inserted into the *Advillin* locus – rather than *ROSA26* used in earlier experiments – as this gene is only expressed in peripheral sensory neurons (J. Zhao *et al.*, 2021). The risk of leaky DTA expression was reduced by inserting a tdTomato gene within the floxed region to increase the distance between loxP sites and avoid spontaneous recombination. Cre-negative neurons did not exhibit red fluorescence due to a weak Kozak sequence upstream of tdTomato leading to inefficient translation (Zhao *et al.*, 2021; J Cox, personal communication).

Expression of DTA in *Tmem45b*-positive sensory neurons markedly reduced the IB4-positive population. Despite this, a population of IB4-negative neurons still responded

to Ang II application, meaning that almost all Ang II-sensitive neurons were now IB4-negative. Moreover, the Ang II-sensitive, IB4-negative population was unaffected by the loss of IB4-positive neurons. This observation demonstrated that an interaction between IB4-positive and -negative neurons – be it mediator release or otherwise – was not necessary for the response of IB4-negative neurons to Ang II.

### **3.3.2.2. Non-neuronal satellite cells are required for the response of IB4-negative neurons to Ang II application**

After eliminating a role for IB4-positive neurons, the contribution of non-neuronal satellite cells (NNSCs) to the response to Ang II was investigated. NNSCs accounted for ~80% of cells in dissociated DRG cultures, in agreement with previous experiments (Thakur *et al.*, 2014). To assess the role of NNSCs, they were removed from culture using MACS, a technique frequently used in haematology to separate blood components, but only recently employed in neuroscience to separate neurons from supporting cells (Thakur *et al.*, 2014; Tewari *et al.*, 2020). While MACS successfully removed NNSCs, there was also a loss of some large-diameter neurons as documented by Thakur *et al.* (2014). The loss of these neurons is attenuated if the non-neuronal cell antibody cocktail was omitted during the sorting protocol, suggesting that large diameter neurons are more commonly or more strongly physically associated with NNSCs. The lost neurons tended to be large-diameter, IB4-negative and Ang II-insensitive. The soma size distribution of Ang II-sensitive, IB4-negative neurons in unsorted cultures matched that of IB4-negative neurons remaining after MACS. The soma size distribution of IB4-positive neurons was unaffected by MACS. These data strongly suggest that Ang II-sensitive neurons – both IB4-positive and -negative – remained after MACS, while large-diameter, IB4-negative neurons, which tend to be Ang II-insensitive were lost.

It was found that the same proportion of neurons in unsorted and MACS cultures responded to Ang II. If MACS had no effect on the response to Ang II, one would expect the proportion of Ang II-sensitive neurons to have increased due to the loss of Ang II-insensitive neurons. Therefore, this data implies a modest reduction in the response to Ang II. In agreement, the peak magnitude of the response to Ang II was ameliorated after MACS. Additionally, after MACS the Ang II-sensitive population was made up of ~75% IB4-positive neurons, compared to ~40% in unsorted cultures, suggesting that the response of IB4-negative neurons had been attenuated. Finally,

the proportion of Ang II-sensitive neurons within the IB4-negative population was halved after MACS (though no statistical significance was attributed to this, possibly due to low statistical power). Again, if there had been no effect of MACS on the response to Ang II, one would have expected an increase in the proportion of Ang II-sensitive neurons within the IB4-negative population due to the loss of large-diameter, IB4-negative, Ang II-insensitive neurons. These data indicate that, in the absence of NNSCs, the response of IB4-negative neurons to Ang II was ameliorated. The stimulation of IB4-negative neurons by Ang II appears to be mediated by NNSCs present in culture, while the stimulation of IB4-positive neurons does not depend on NNSCs.

In control cultures, the AT1R antagonist valsartan reduced the proportion of Ang II-responding neurons by ~40%, showing that a component of the response was mediated by AT1R. After MACS, valsartan's inhibitory effect was increased to ~80%, suggesting the almost all of the response depended on AT1R. In MACS cultures, the majority – again ~80% – of neurons responding to Ang II are IB4-positive. The response of IB4-positive neurons to Ang II is very likely, therefore, to be direct – i.e., independent of NNSCs – and mediated by AT1R, in alignment with the expression of this receptor (Zeisel *et al.*, 2018). In contrast to this, the inhibitory effect of valsartan was lost in cultures from *Tmem45b-Cre<sup>+</sup>/DTA<sup>+</sup>* mice. The Ang II-sensitive population in these cultures was made up of ~90% IB4-negative neurons. These data indicate that Ang II-mediated Ca<sup>2+</sup> signals in IB4-negative neurons not only depend on NNSCs but are also independent of AT1R. This goes some way towards resolving the apparently paradoxical stimulation of Ang II receptor-lacking IB4-negative neurons by Ang II.

### **3.3.2.3. Stimulation of NNSCs in vitro**

If NNSCs contribute to Ang II-mediated neuronal stimulation, it was reasoned that they must also respond to Ang II application. Ang II-evoked Ca<sup>2+</sup> signals were observed in NNSCs identified by their insensitivity to high [K<sup>+</sup>] application. It has been shown that NNSCs can be stimulated by nearby neurons through their release of ATP or through gap junctions (Koizumi *et al.*, 2004; Suadicani *et al.*, 2010). Ang II-evoked signals in NNSCs were still observed in the absence of Ang II-sensitive neurons (*Nav1.8-Cre-DTA*), indicating that NNSCs were not stimulated downstream of Ang II-mediated

neuronal stimulation. This demonstrated that Ang II application can evoke a rise in intracellular  $\text{Ca}^{2+}$  in NNSCs present in the DRG.

The identity of the Ang II-sensitive NNSCs was probed with little success. Cultured macrophages did not exhibit  $\text{Ca}^{2+}$  signals in response to Ang II application, so they are unlikely to be the Ang II-sensitive NNSCs in DRG. Glial cells account for ~50% of NNSCs in culture (Thakur *et al.*, 2014), so it seems likely that these cells may be the elusive Ang II-sensitive NNSCs, but this remains unclear.

In addition to the identity of the NNSCs involved, other questions about Ang II-evoked stimulation of IB4-negative neurons remain unanswered. How does Ang II application stimulate NNSCs? Data thus far indicates that it cannot be through AT1R, and data in Chapter 4 rules out a role for AT2R. While it is possible that Ang II could be acting through an unidentified receptor, it can also be broken down into numerous fragments, depending on the enzymes present, which could then activate other receptors. Angiotensin converting enzyme 2 (ACE2) converts Ang II into alamandine and is highly expressed on non-peptidergic sensory neurons (Shiers *et al.*, 2020). Could it be that Ang II stimulates IB4-positive neurons, while alamandine stimulates NNSCs? While alamandine application did result in  $\text{Ca}^{2+}$  signals in small-sized sensory neurons independently of AT1R, inhibition of ACE2 did not attenuate the response to Ang II. This indicates that alamandine production from Ang II via ACE2 *in vitro* did not mediate a component of the response arising from Ang II application. What's more, alamandine application did not appear to evoke  $\text{Ca}^{2+}$  signals in NNSCs in culture – certainly not to the same extent as Ang II application. It seems unlikely, therefore, that alamandine mediates the stimulation of NNSCs and, subsequently, IB4-negative neurons. Another possibility is that AngIV, another Ang II fragment, is produced *in vitro* and goes on to stimulate NNSCs. The AT4 receptor is poorly characterised, although activation of AT4 has previously been shown to raise intracellular  $\text{Ca}^{2+}$  in hippocampal neurons (Davis *et al.*, 2006). What's more, the gene encoding the AT4 receptor – *Lnpep* – is also expressed in satellite glial cells in the DRG (Zeisel *et al.*, 2018), so this fragment may be a promising candidate for future experiments.

Downstream of receptor activation, it appeared that the rise in intracellular  $\text{Ca}^{2+}$  in NNSCs resulted from release from internal stores and not influx from the extracellular milieu. It is assumed that this rise in intracellular  $\text{Ca}^{2+}$  is required for the exocytic event

which releases the unknown mediator which goes on to stimulate IB4-negative neurons. In excitable cells, voltage-gated  $\text{Ca}^{2+}$  channels provide the source of  $\text{Ca}^{2+}$  required for exocytosis, for example, from a pre-synaptic terminal or pancreatic  $\beta$  cell. In these cells,  $\text{Ca}^{2+}$  release from internal stores can modulate exocytosis (Dyachok and Gylfe, 2004; ZhuGe *et al.*, 2006). However, in many non-excitable cells, similar to the NNSCs present in DRG cultures,  $\text{Ca}^{2+}$  release from intracellular stores provides the  $\text{Ca}^{2+}$  required for exocytosis (Tse *et al.*, 1997; Low *et al.*, 2010).

#### **3.3.2.4. How do NNSCs communicate with IB4-negative neurons?**

It is not clear what mediates the interaction between NNSCs and IB4-negative neurons, nor why this interaction appears to be selective for IB4-negative neurons. It has been demonstrated that tumour necrosis factor  $\alpha$  (TNF $\alpha$ ) is expressed in NNSCs and is upregulated and released following the induction of gut inflammation, contributing to visceral hypersensitivity (Song *et al.*, 2014). Ang II application may evoke TNF $\alpha$  release by NNSCs, which then goes on to stimulate IB4-negative neurons. Indeed, Ang II evokes the release of TNF $\alpha$  in the central nervous system (Woods *et al.*, 2021), kidney (Rosa *et al.*, 2012) and heart (Sriramula *et al.*, 2008; Sriramula and Francis, 2015). Preliminary work revealed that knock-out of the neuronally-expressed type 1 TNF $\alpha$  receptor (TNFR1) reduced the proportion of neurons responding to Ang II application (data not shown; see Appendix A1.1, Figure A1). With these observations, one can tentatively suggest that TNF $\alpha$  may be released by NNSCs and go on to stimulate IB4-negative neurons via TNFR1.

The apparently selective interaction between NNSCs and IB4-negative neurons could also be due to a closer association between these cell types *in vitro*. Pilot data suggests that the distance between a neuron and its closest non-neuronal neighbour is smaller for IB4-negative than for IB4-positive neurons (data not shown; see Appendix A1.1.). NNSCs also appear more clustered around IB4-negative neurons. Therefore, over a short period of time, any mediator released by NNSCs has more chance of encountering an IB4-negative neuron. This close association between NNSCs and IB4-negative neurons may also account for the lack of a time delay between  $\text{Ca}^{2+}$  signals evoked in IB4-positive and -negative neurons. Beyond this, if the released mediator really is TNF $\alpha$ , one would expect a bias towards IB4-negative neurons given the expression of TNFR1 in peptidergic neurons (Usoskin *et al.*, 2015; Zeisel *et al.*, 2018). Of 56 neurons found to express *Tnfrsf1a* (the gene encoding

TNFR1), 49 (87.5%) co-expressed *Calca* (the gene encoding CGRP), a marker of peptidergic nociceptors (Usoskin *et al.*, 2015). Figure 3.20 summarises the conclusions drawn from experiments in this Chapter.

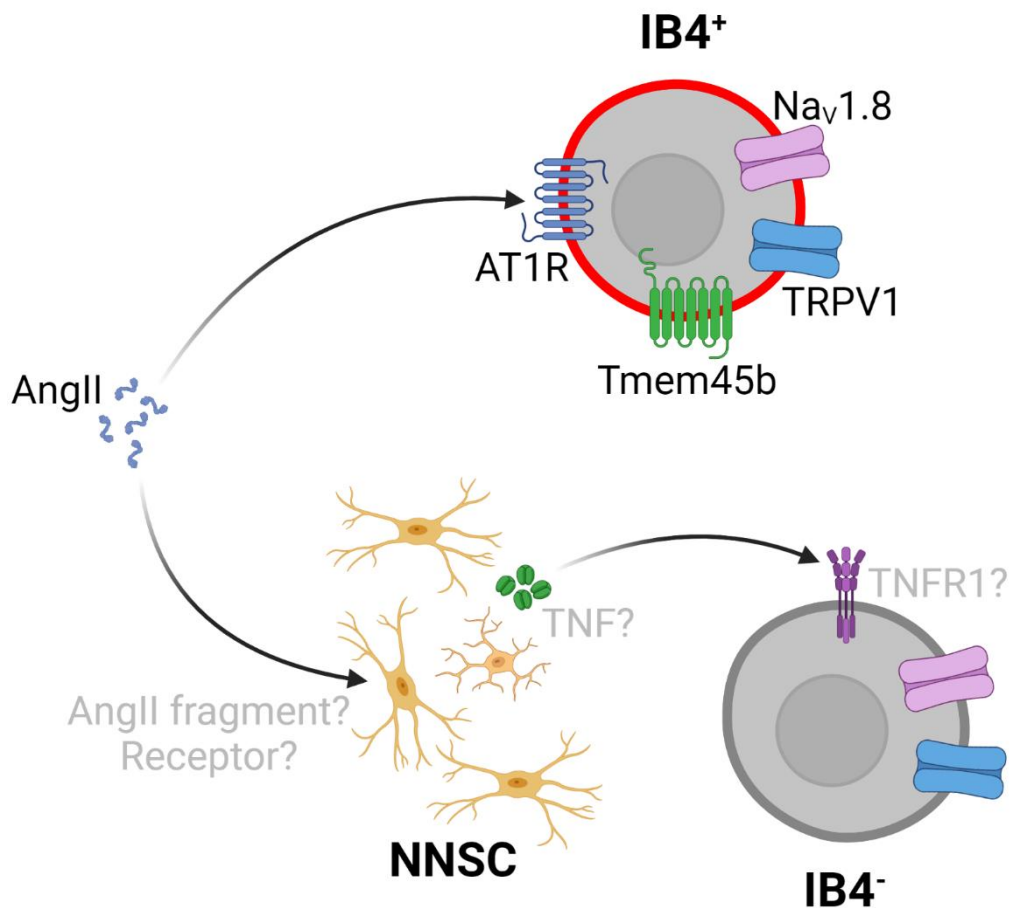


**Figure 3.20 Proposed model for the interaction between Ang II and sensory neurons *in vitro***

Observations made in this Chapter indicate that Ang II directly stimulates IB4-positive neurons via the AT1 receptor. Ang II can also stimulate IB4-negative neurons (which lack Ang II receptors), but this is indirect and is mediated by NNSCs. The mechanism underpinning the stimulation of IB4-negative neurons is not clear. It is proposed that (i) a fragment of Ang II initially stimulates NNSCs to (ii) release TNFα which subsequently evokes a Ca<sup>2+</sup> response in IB4-negative neurons via (iii) TNFR1. Image created using Biorender.

### 3.3.3. What's the (patho)physiological relevance?

It goes without saying that dissociated DRG in culture represent a highly non-physiological system. Sensory neurons *in vitro* are axotomized and maintained in a semi-physiological buffer: it is not unreasonable to assert that the removal, dissociation and maintenance of sensory neurons may alter their properties. Furthermore, it is the sensory afferent terminals that first interact with inflammatory mediators in the tissue *in vivo* – not the neuronal soma in the DRG. We must, therefore, assume that the properties of the terminals and soma are similar.

It is not clear whether this assumption is wholly accurate. *In vivo* Ca<sup>2+</sup> imaging of sensory neurons in the DRG during the application of mechanical, hot and cold stimuli to the hind paw revealed that all mechanically-insensitive, thermosensitive neurons were modality specific (Emery *et al.*, 2016). Mechanically-activated neurons were also largely modality specific, with very few co-sensitive to hot or cold stimuli. This is in stark contrast to experiments carried out using cultured DRG sensory neurons in which ~50% of neurons responded to both hot and cold stimuli (Emery *et al.*, 2016). *In vivo* administration of PGE<sub>2</sub> rapidly increased the proportion of neurons exhibiting polymodality, indicating that this phenomenon may be influenced by inflammation (Emery *et al.*, 2016). At odds with this report, a later study, also utilising *in vivo* Ca<sup>2+</sup> imaging, found that between 50-80% of thermally-activated neurons also responded to noxious mechanical stimulation, in line with observations made *in vitro* (Chisholm *et al.*, 2018). These differences may result from Chisholm and colleagues imaging a much greater sample of neurons, or as a consequence of differing methods of stimulus application. Emery *et al* immersed the hind paw in water at 55°C; this results in the stimulation of a much larger receptive field than mechanical stimulation applied by pinching the plantar surface of the hind paw. The receptive fields of many thermally-responsive neurons may not have overlaid with the site of the mechanical stimulus, resulting in an underestimation of polymodality. In contrast, Chisholm *et al* applied thermal stimuli using a Peltier placed directly on the plantar surface of the hind paw, very similar to the area to which mechanical stimulation was applied. Whether cultured sensory neurons exhibit similar properties to those *in vivo* is still a source of controversy.

It is possible that the invasive procedure used to harvest DRG here caused the release of inflammatory mediators which changed the properties of sensory neurons *in vitro*,

or that sensory neuron terminals and soma exhibit distinct properties. However, electrophysiological recording from colonic afferents has shown that Ang II can evoke afferent firing via AT1R (Charity Bhebhe, unpublished observation), indicating a role for Ang II in the tissue. Ang II-sensitive colonic afferents were also stimulated by noxious pressure and capsaicin (Charity Bhebhe, unpublished observation), identifying them as nociceptors, in agreement with the results presented in this Chapter, indicating broad alignment between findings in the tissue and in cultured neurons. With regard to the work presented here, cultured DRG neurons appear to represent a useful model for investigating the interaction between Ang II and sensory neurons.

Recent work has highlighted a key role for immune cells in the DRG in driving pain. Much of this work has focused on macrophages infiltrating the DRG, which appear to be important in neuropathic pain – due either to chemotherapy (H. Zhang *et al.*, 2016) or nerve injury (Yu *et al.*, 2020) – and inflammatory pain following the induction of experimental osteoarthritis (Raouf *et al.*, 2021). Two models of osteoarthritis resulted in mechanical hypersensitivity and infiltration of macrophages in the DRG (Raouf *et al.*, 2021). Importantly, Diphtheria toxin-mediated ablation of macrophages after the induction of osteoarthritis abolished mechanical hypersensitivity, indicating that these infiltrating immune cells drive pain (Raouf *et al.*, 2021). It appears that M1-like macrophages may be drivers of pain (Raouf *et al.*, 2021), while M2-like macrophages seem to contribute to the resolution of pain after an inflammatory insult (van der Vlist *et al.*, 2022).

It is not known whether macrophage infiltration in the DRG is a consequence of colitis, though this could be ascertained by inducing colitis – using, say, DSS – and subsequently harvesting T12-L2 DRG for immunofluorescent labelling of macrophages. Alternatively, one could use quantitative PCR to identify genetic markers of macrophages, such as *Cd14* and *Cd68*. Expression of both Angiotensinogen and Ang II has been documented in monocytes (Gomez *et al.*, 1993; Kitazono *et al.*, 1995), suggesting that these peptides could be released in the DRG upon infiltration. Ang II could then interact with sensory neuronal soma – and NNSCs in the DRG – in a manner not dissimilar to that described here.

### 3.4. Key points

Experiments outlined in this Chapter have demonstrated that:

- i. Ang II stimulates a subset of small-sized sensory neurons which express TRPV1 and Nav1.8.
- ii. This Ang II-sensitive population can be divided into IB4-positive (Tmem45b-expressing) and IB4-negative (Tmem45b-lacking) neurons.
- iii. The stimulation of IB4-positive neurons by Ang II is direct and is mediated by AT1R.
- iv. The stimulation of IB4-negative neurons by Ang II is indirect – requiring NNSCs – and is not mediated by AT1R.
- v. Ang II application stimulates NNSCs in culture through an AT1R (and AT2R) independent mechanism.

## **Chapter 4**

### **Mechanisms underpinning Ang II-evoked Ca<sup>2+</sup> signals**

## 4.1. Introduction

Neuronal  $\text{Ca}^{2+}$  signals downstream of G-protein-coupled receptors (GPCRs), such as AT1R, often arise through a dynamic interplay between release from intracellular  $\text{Ca}^{2+}$  stores and influx across the plasma membrane.

### 4.1.1. Intracellular $\text{Ca}^{2+}$ stores

Given the numerous roles played by  $\text{Ca}^{2+}$  in the normal physiology of sensory neurons, it is of paramount importance that its cytosolic concentration is tightly controlled. Unlike other second messengers,  $\text{Ca}^{2+}$  cannot be broken down into inactive metabolites, and so its regulation depends on its sequestration away from cellular components with which it could interact. Intracellular membrane-bound organelles comprise machinery required to sequester and store  $\text{Ca}^{2+}$ . This not only provides a buffer for  $\text{Ca}^{2+}$ , maintaining low cytosolic  $\text{Ca}^{2+}$  (~100 nM), but also provides a source of  $\text{Ca}^{2+}$  for signalling. The largest of these stores is the endoplasmic reticulum (ER).  $\text{Ca}^{2+}$  is pumped into the ER by the sarco-endoplasmic reticulum  $\text{Ca}^{2+}$  ATPase (SERCA), where the  $\text{Ca}^{2+}$  concentration can reach ~800  $\mu\text{M}$  (Samtleben *et al.*, 2013). Inhibition of SERCA results in the passive depletion of  $\text{Ca}^{2+}$  from the ER, though the channel(s) responsible for this loss of  $\text{Ca}^{2+}$  are yet to be identified. Members of the transmembrane BAX inhibitor motif-containing (TMBIM) family of proteins have been shown to form pH-sensitive  $\text{Ca}^{2+}$  leak channels (Chang *et al.*, 2014). Proteins in this family have been shown to localise to the ER and reduce  $\text{Ca}^{2+}$  content, indicating a potential role in the passive extrusion of  $\text{Ca}^{2+}$  from the ER (Lisak *et al.*, 2014).

Activation of Gq-coupled GPCRs results in the dissociation of the heterotrimeric G-protein and subsequent activation of phospholipase C (PLC). PLC catalyses the hydrolysis of phosphatidylinositol-4,5-bisphosphate ( $\text{PIP}_2$ ), a phospholipid component of the neuronal membrane, yielding diacylglycerol (DAG) and inositol-1,4,5-triphosphate ( $\text{IP}_3$ ). The signals carried by these second messengers are spatially and temporally controlled by enzymes which catabolise them into inactive metabolites. DAG functions in the downstream activation of various isoforms of protein kinase C (PKC), while  $\text{IP}_3$  stimulates the release of  $\text{Ca}^{2+}$  from the ER through the activation of  $\text{IP}_3$  receptors ( $\text{IP}_3\text{Rs}$ ), which form large-conductance cation channels with modest selectivity for  $\text{Ca}^{2+}$  (Foskett *et al.*, 2007).  $\text{IP}_3\text{Rs}$  are also regulated by both cytosolic and ER  $\text{Ca}^{2+}$ . Binding of  $\text{Ca}^{2+}$  to a stimulatory site on the cytosolic face of the  $\text{IP}_3\text{R}$  (or to an accessory protein) acts as an essential co-agonist with  $\text{IP}_3$  (Finch, Turner and

Goldin, 1991). ER  $\text{Ca}^{2+}$  retunes the sensitivity of  $\text{IP}_3\text{Rs}$  to cytosolic  $\text{IP}_3$  and  $\text{Ca}^{2+}$ , such that depleted stores lose sensitivity to  $\text{IP}_3$  (Berridge, 2007), perhaps enabling more effective refilling.

$\text{Ca}^{2+}$  release from the ER is a vital component of numerous signalling pathways and serves a multitude of functions. Bradykinin evokes action potential discharge in sensory neurons through the inhibition of M-current, a tonically active  $\text{K}^+$  current which contributes to the maintenance of resting membrane potential (Linley *et al.*, 2008; Liu *et al.*, 2010). The depletion of ER  $\text{Ca}^{2+}$  stores prior to bradykinin application blocked the inhibition of M-current (Cruzblanca, Koh and Hille, 1998), indicating a role for ER  $\text{Ca}^{2+}$  release in the acute modulation of ion channel function. Store release also regulates neuronal function over more prolonged durations through the activation of enzymes, such as PKC, which can induce prolonged changes in downstream protein function. Finally, the ER  $\text{Ca}^{2+}$  store can only function if the store is replete; as such, a mechanism for store refilling after depletion is required. This store-operated  $\text{Ca}^{2+}$  entry not only ensures that  $\text{Ca}^{2+}$  stores remain adequately filled, but also provides a prolonged source of  $\text{Ca}^{2+}$  now known to fulfil multiple signalling roles.

#### **4.1.2. Store-operated $\text{Ca}^{2+}$ entry**

Upon activation of  $\text{IP}_3\text{Rs}$ ,  $\text{Ca}^{2+}$  will be released into the cytosol where, after engaging in signalling, it will either be pumped back into the ER or extruded from the cell altogether by plasma membrane  $\text{Ca}^{2+}$  pumps, such as the  $\text{Na}^+/\text{Ca}^{2+}$  exchanger (NCX) and the plasma membrane  $\text{Ca}^{2+}$  ATPase (PMCA). As a consequence, when the cell returns to rest, there will be a net loss of  $\text{Ca}^{2+}$  from the ER. If this continues, the ER store will eventually be depleted entirely, disrupting intracellular signalling and proper cell function. Therefore, a mechanism for refilling the ER  $\text{Ca}^{2+}$  stores is required.

Jim Putney first put forward the notion of capacitive  $\text{Ca}^{2+}$  entry (CCE), whereby plasma membrane  $\text{Ca}^{2+}$  permeability is increased upon depletion of intracellular  $\text{Ca}^{2+}$  stores (Putney, 1986). Two decades passed before the identity of the cellular machinery responsible for CCE – later renamed store-operated  $\text{Ca}^{2+}$  entry (SOCE) – was resolved. Using  $\text{Ca}^{2+}$  signals evoked by store depletion as a readout, RNAi studies identified two families of genes as important mediators of SOCE: *ORAI* and *STIM* (Hogan and Rao, 2015). Three genes encode members of the Orai protein family – *ORAI1*, *ORAI2* and *ORAI3* – while two genes encode the STIM family – *STIM1* and

*STIM2*. All members of both families are expressed to varying degrees in mouse sensory neurons (Zeisel *et al.*, 2018). STIM is localised to the ER, with its luminal (N-terminal) face containing a Ca<sup>2+</sup> binding site, and its cytosolic (C-terminal) face containing a basic region which interacts with plasma membrane channels. Upon store depletion, STIM undergoes a conformational change, forming oligomers at ER-plasma membrane junctions (Liou *et al.*, 2007). Here, the C-terminus of STIM interacts with Orai, promoting channel activity and, hence, Ca<sup>2+</sup> influx (DeHaven *et al.*, 2007; Lis *et al.*, 2007; Gudlur *et al.*, 2014). Orai1, 2 and 3 are gated by STIM, though they do display divergent properties, such as differing ion selectivity and regulation by intracellular Ca<sup>2+</sup> (Lis *et al.*, 2007).

While it is now well-established that Orai channels mediate Ca<sup>2+</sup> influx downstream of store depletion, other store-operated channels (SOCs) also exist. Of particular interest is the canonical subfamily of the transient receptor potential family (TRPC) of ion channels, of which there are seven members (TRPC1-7). TRPC1, 3 and 6 are broadly expressed in mouse sensory neurons, with other members of the TRPC family being absent or poorly expressed (Zeisel *et al.*, 2018). TRPC3 and 6 are highly co-expressed with AT1R (Zeisel *et al.*, 2018). The role of these channels in SOCE is far less clear than that of Orai channels. TRPC1, 3 and 4 have been shown to contribute to SOCE in certain cell types (Zhu *et al.*, 1996; Wang *et al.*, 2004; Séguéla *et al.*, 2014), though not in others (Hofmann *et al.*, 1999; Harper *et al.*, 2013). TRPC5, 6 and 7 channels have been described as store-independent (Hofmann *et al.*, 1999), though TRPC5 functions in SOCE in mast cells (Ramos-nino *et al.*, 2008) and TRPC6 forms store-operated heteromeric channels with TRPC4 in smooth muscle (Zhang *et al.*, 2018). The role of different families of TRPC channels in sensory neuron SOCE is not yet fully understood. In vagal sensory neurons, SOCE is independent of Orai channels (Hooper *et al.*, 2013), while both Orai and TRPC3 channels appear to contribute to SOCE in rat sensory neurons in the DRG (Séguéla *et al.*, 2014).

SOCE is not only vital for maintaining intracellular Ca<sup>2+</sup> stores. In neurons, SOCE is known to regulate gene expression via changes in the activity and localisation of transcription factors (Lalonde, Saia and Gill, 2014; Mitra and Hasan, 2022). Changes in gene expression may lead to prolonged perturbations in neuronal function, so neuronal SOCE provides an important source of Ca<sup>2+</sup> for signalling in addition to store refilling (Majewski and Kuznicki, 2014).

### **4.1.3. Store-independent Ca<sup>2+</sup> entry**

In non-excitable cells, SOCE forms the major route through which Ca<sup>2+</sup> enters the cytosol from the extracellular space. However, neurons express store-independent pathways for Ca<sup>2+</sup> entry, predominantly formed by ligand- and voltage-gated ion channels. Ang II is not known to interact with any ligand-gated ion channels, and so this is not a likely route for Ca<sup>2+</sup> entry in sensory neurons. However, Ang II is known to induce membrane depolarisation in sympathetic neurons, which may lead to the activation of voltage-gated Ca<sup>2+</sup> channels (VGCCs) (Shapiro, Wollmuth and Hille, 1994; Zaika *et al.*, 2006). VGCCs were initially categorised by the waveform of the current they convey. L-type (Ca<sub>v</sub>1.1-1.4) and T-type Ca<sup>2+</sup> (Ca<sub>v</sub>3.1-3.3) channels convey long-lasting and transient currents, respectively, while N-type Ca<sup>2+</sup> (Ca<sub>v</sub>2.2) channels convey an incompletely inactivating current (neither long-lasting, nor transient). R-type Ca<sup>2+</sup> (Ca<sub>v</sub>2.3) channels carry the current remaining after pharmacological blockade of other VGCCs, while P/Q-type Ca<sup>2+</sup> (Ca<sub>v</sub>2.1) channels were first identified in Purkinje cells (Usowicz *et al.*, 1992). Genes encoding Ca<sub>v</sub>1.2 and 1.3, along with Ca<sub>v</sub>2.1 and 2.2, are expressed within the same sensory neuronal population as receptors for Ang II (Usoskin *et al.*, 2015). If Ang II induces membrane depolarisation in sensory neurons, it is likely that these channels will contribute to the observed rise in cytosolic Ca<sup>2+</sup>.

### **4.1.4. Experimental outline**

Experiments in this Chapter sought to resolve the mechanisms underlying Ang II-evoked Ca<sup>2+</sup> signals in sensory neurons, with particular focus on the role of Ca<sup>2+</sup> release from intracellular stores and SOCE. The signalling pathway downstream of AT1R was ascertained, and the role of intracellular Ca<sup>2+</sup> stores was probed by *i*) depleting stores using thapsigargin prior to Ang II application, and *ii*) indirectly measuring Ca<sup>2+</sup> store content using ionomycin. Given the role of TRPC3 in Ca<sup>2+</sup> entry in rat sensory neurons, and the high co-expression of TRPC3 and AT1R, the contribution of this channel to Ang II-evoked Ca<sup>2+</sup> signals and SOCE was investigated using a selective inhibitor.

## 4.2. Results

### 4.2.1. Ang II signals through AT1R to release Ca<sup>2+</sup> from intracellular stores

Data in Chapter 3 indicated that Ang II-evoked Ca<sup>2+</sup> signals rely on AT1R. Here, the signalling downstream of this receptor was investigated. Ang II has previously been shown to release Ca<sup>2+</sup> from intracellular stores; to probe whether this is the case in sensory neurons, intracellular stores were depleted by pre-incubation with thapsigargin (1  $\mu$ M), an inhibitor of SERCA. First, it was validated that thapsigargin did indeed deplete intracellular Ca<sup>2+</sup> stores. In Ca<sup>2+</sup>-free external buffer, the magnitude of ionomycin (5  $\mu$ M) induced Ca<sup>2+</sup> transients was measured with and without thapsigargin pre-incubation. Under these conditions, the rise in cytosolic Ca<sup>2+</sup> must arise from intracellular stores, as there is no Ca<sup>2+</sup> in the extracellular bathing solution, so the magnitude of the transient indicates the Ca<sup>2+</sup> content of the intracellular stores. Figures 4.1a and b show exemplar ionomycin-induced Ca<sup>2+</sup> transients in the absence (Figure 4.1a) and presence (Figure 4.1b) of thapsigargin. Grouping all transients together shows a marked reduction in magnitude after thapsigargin pre-incubation (Figure 4.1c). The magnitude of ionomycin-induced Ca<sup>2+</sup> transients under control conditions was  $0.52 \pm 0.02$ , compared to  $0.11 \pm 0.01$  after thapsigargin incubation ( $p < 0.0001$ , Figure 4.1d). Thapsigargin also prolonged the decay of KCl-induced Ca<sup>2+</sup> transients (Figure 4.1e). The half-time for the decay of these transients was increased by thapsigargin from  $2.9 \pm 0.1$  s to  $3.9 \pm 0.2$  s ( $p = 0.0002$ , Figure 4.1f). See Appendix A1.2. for details of curve fitting of KCl-evoked transients. These data demonstrate that thapsigargin depletes intracellular Ca<sup>2+</sup> stores, and that these stores are important in buffering changes in cytosolic Ca<sup>2+</sup>.

The requirement of AT1R for Ang II-evoked Ca<sup>2+</sup> signals was tested by pre-incubating neuronal cultures with either of two structurally distinct AT1R antagonists, EMD66684 (100 nM) or valsartan (1  $\mu$ M). In control conditions,  $40.9 \pm 2.6\%$  of neurons responded to Ang II application. This was reduced to  $25.7 \pm 4.3\%$  ( $p = 0.008$ ) and  $23.3 \pm 5.2\%$  ( $p = 0.008$ ) by EMD66684 and valsartan, respectively (Figure 4.2a). To probe the coupling of AT1R to G-proteins, G $\alpha_q$  was inhibited by YM254890 (100 nM); this reduced the Ang II-responsive population to  $20.8 \pm 2.8\%$  of all neurons ( $p = 0.002$ , Figure 4.2a). The phospholipase C inhibitor, U73122 (10  $\mu$ M), also ameliorated the response to Ang II ( $24.0 \pm 4.7\%$ ,  $p = 0.008$ , Figure 4.2a). Finally, the source of Ca<sup>2+</sup> was probed:

intracellular stores were depleted with thapsigargin. This reduced the response to Ang II to only  $18.8 \pm 3.4\%$  of neurons ( $p = 0.0003$ , Figure 4.2a). Incubation with Xestospongine C, an  $IP_3$  receptor antagonist, attenuated the response to Ang II to  $10.2 \pm 5.8\%$  of neurons ( $p = 0.0003$ , Figure 4.2a).

The inhibition of the response to Ang II by antagonists of AT1R was not complete, as was shown for unsorted DRG cultures in Chapter 3. The neurons in which the response to Ang II is dependent on AT1R are those which are sensitive to inhibition by EMD66684 or valsartan. These AT1R-antagonist-sensitive neurons account for  $15.2 \pm 4.3\%$  (EMD66684) and  $17.6 \pm 5.2\%$  (valsartan) of all neurons in culture. The size of these populations is very similar to the population of neurons found to express either *Agtr1a* or *Agtr1b* (118/696, 17.0%, Figure 4.2b) (Usoskin *et al.*, 2015). One-sample t-tests comparing the size of the AT1R-antagonist-sensitive populations with the *Agtr1*-expressing population revealed no difference (EMD66684:  $p = 0.69$ , valsartan:  $p = 0.90$ ). The magnitude of inhibition of the response to Ang II is similar for all antagonists used, indicating that the response in the same population of neurons – i.e., the same pathway – is being blocked.

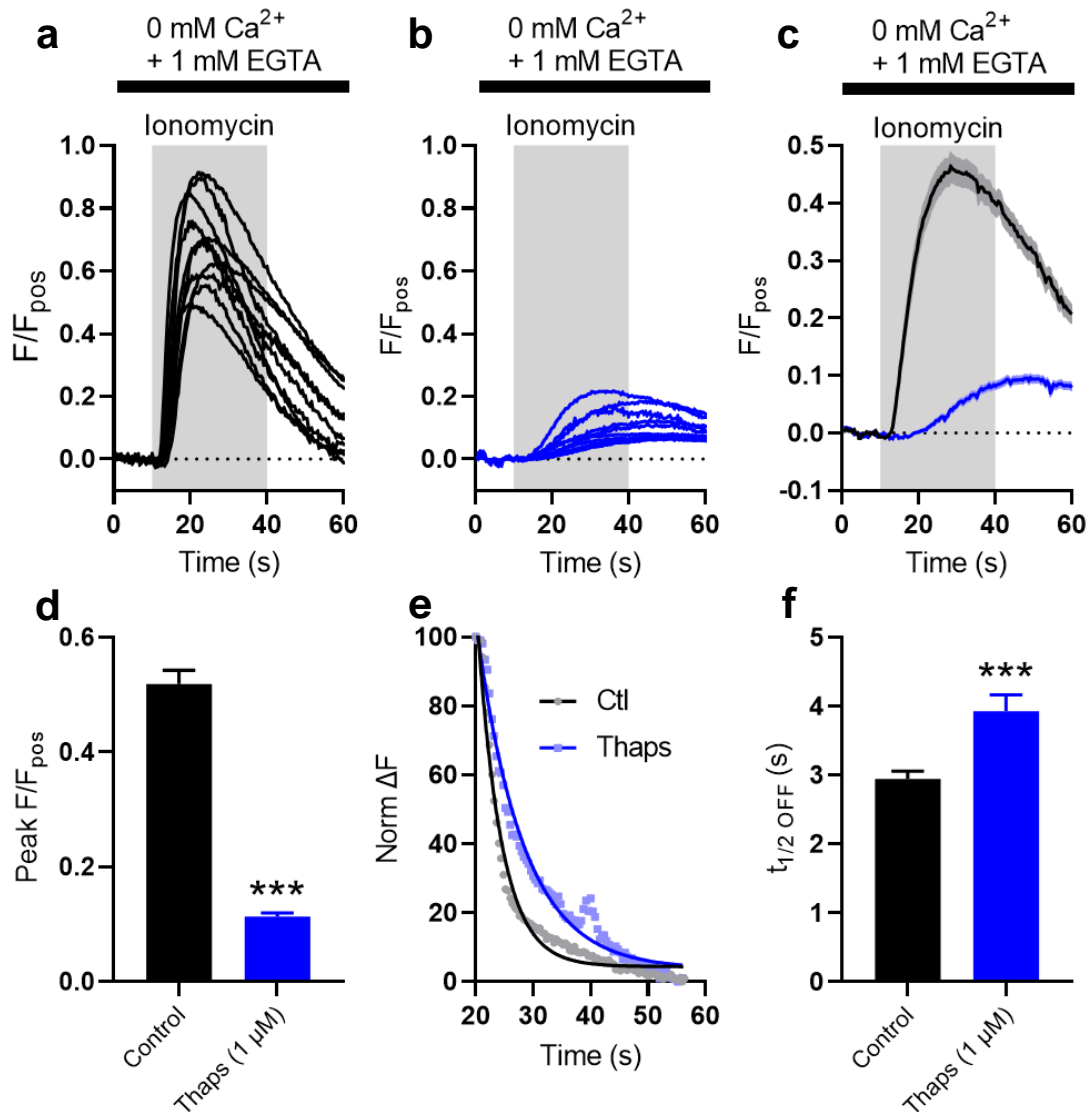


**Figure 4.1 Thapsigargin depletes intracellular  $\text{Ca}^{2+}$  stores**

- Exemplar ionomycin-induced  $\text{Ca}^{2+}$  transients from ten randomly selected neurons under control conditions.
- Exemplar ionomycin-induced  $\text{Ca}^{2+}$  transients from ten randomly selected neurons after incubation with thapsigargin.
- Grouped ionomycin-induced  $\text{Ca}^{2+}$  transients. Black: control conditions, blue: thapsigargin. Solid line shows mean, shaded area shows standard error. Control: 245 neurons,  $n = 3$ ,  $N = 3$ . Thapsigargin: 258 neurons,  $n = 3$ ,  $N = 3$ .
- Grouped data showing the peak magnitude of ionomycin-induced  $\text{Ca}^{2+}$  transients. Control: 245 neurons,  $n = 3$ ,  $N = 3$ . Thapsigargin: 258 neurons,  $n = 3$ ,  $N = 3$ . Data analysed using a two-tailed unpaired t-test with Welch's correction.
- Exemplar time courses of the decay of KCl-induced  $\text{Ca}^{2+}$  transients, shown from the termination of KCl application (20 s). Traces were normalised to their respective peaks and fit with a single exponential decay (solid line).
- Grouped data showing the half-time for the decay of KCl-induced  $\text{Ca}^{2+}$  transients. Control: 177 neurons,  $n = 3$ ,  $N = 3$ . Thapsigargin: 158 neurons,  $n = 3$ ,  $N = 3$ . Data analysed using a two-tailed unpaired t-test with Welch's correction.

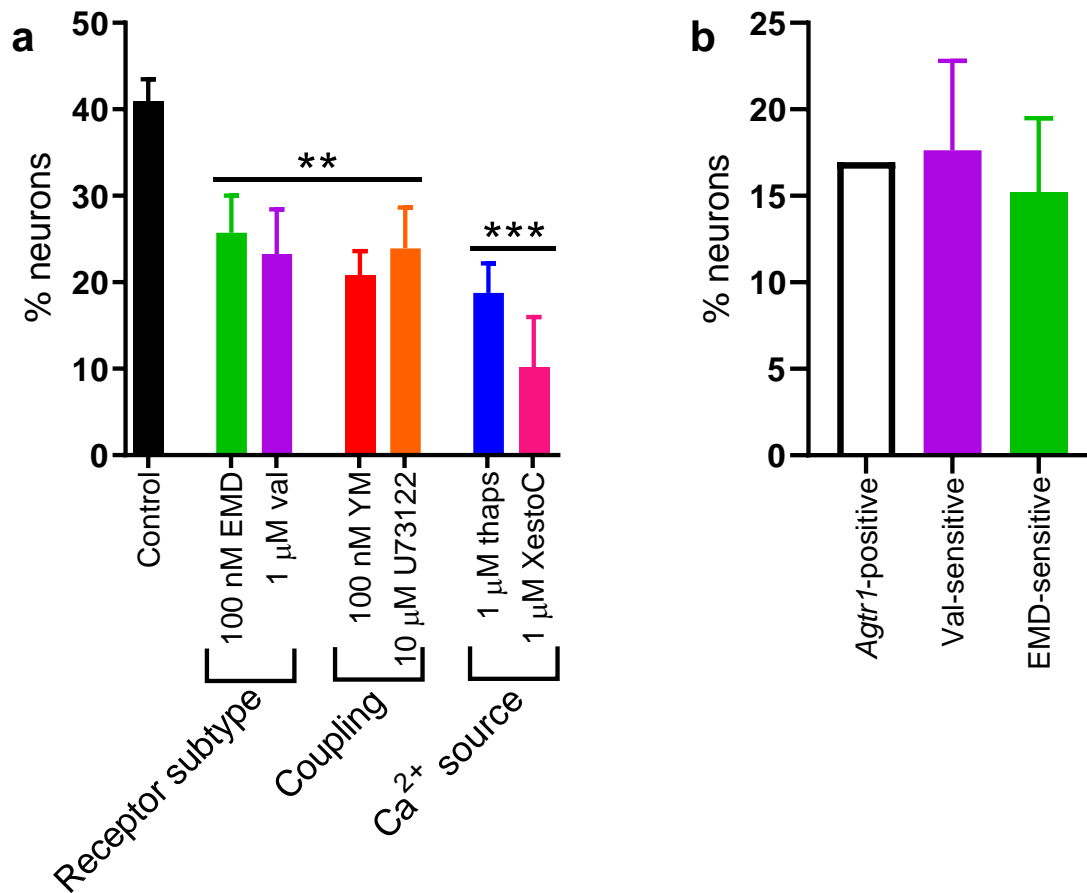


**Figure 4.2 Ang II signals through AT1R to release Ca<sup>2+</sup> from intracellular stores**

- (a) Grouped data showing the proportion of neurons responding to Ang II under control conditions and following pre-incubation with the indicated drugs. Control: n = 9, N = 6; EMD66684: n = 9, N = 5; valsartan: n = 5, N = 5; YM254890: n = 5, N = 4; U73122: n = 4, N = 4; thapsigargin: n = 8, N = 5; Xestospongine C: n = 3, N = 3. Data analysed using a one-way ANOVA with Holm-Sidak post-tests.
- (b) Comparison of the proportion of neurons which express either *Agtr1a* or *Agtr1b* (ascertained from Usoskin *et al.*, 2015) with the proportion of neurons sensitive to valsartan or EMD66684.

#### **4.2.2. Ang II depletes intracellular Ca<sup>2+</sup> stores in small-sized sensory neurons**

Data above provides evidence that Ca<sup>2+</sup> release from intracellular stores is required for the neuronal response to Ang II. Using the same approach as was taken to validate store depletion by thapsigargin, store depletion by Ang II was investigated. Following Ang II incubation in Ca<sup>2+</sup>-free buffer, there was a modest reduction in the magnitude of ionomycin-induced Ca<sup>2+</sup> transients (Figure 4.3a) from  $0.47 \pm 0.02$  to  $0.37 \pm 0.02$  ( $p = 0.0001$ , Figure 4.3b).

Neurons were then parsed by size into quartiles and the effect of Ang II incubation on ionomycin-induced Ca<sup>2+</sup> transients was re-examined. Intracellular Ca<sup>2+</sup> stores in the smallest neurons in culture (i.e., those in the 1<sup>st</sup> quartile) were depleted by Ang II, as indicated by a reduction in the magnitude of ionomycin-induced Ca<sup>2+</sup> transients (Figure 4.3c and e). Ionomycin-induced transients were reduced from  $0.58 \pm 0.03$  to  $0.37 \pm 0.02$  ( $p < 0.0001$ , Figure 4.3e). Larger neurons – those in quartiles 2, 3 and 4 – exhibited no reduction in the magnitude of ionomycin-induced Ca<sup>2+</sup> transients following Ang II application (Figure 4.3d and e; 4.3d shows exemplar traces from 4<sup>th</sup> quartile).

Application of Ang II to sensory neurons in Ca<sup>2+</sup>-free external buffer resulted in a small rise in cytosolic Ca<sup>2+</sup> due to release from intracellular stores (Figure 4.3f). Subsequent re-addition of 2 mM Ca<sup>2+</sup> to the external buffer resulted in a large rise in cytosolic Ca<sup>2+</sup>, resembling store-operated Ca<sup>2+</sup> entry which occurs after depletion of intracellular stores (Figure 4.3f). It also appeared that the response to Ang II was attenuated in Ca<sup>2+</sup>-free buffer, suggesting a component of the Ca<sup>2+</sup> rise was due to influx from the extracellular buffer.

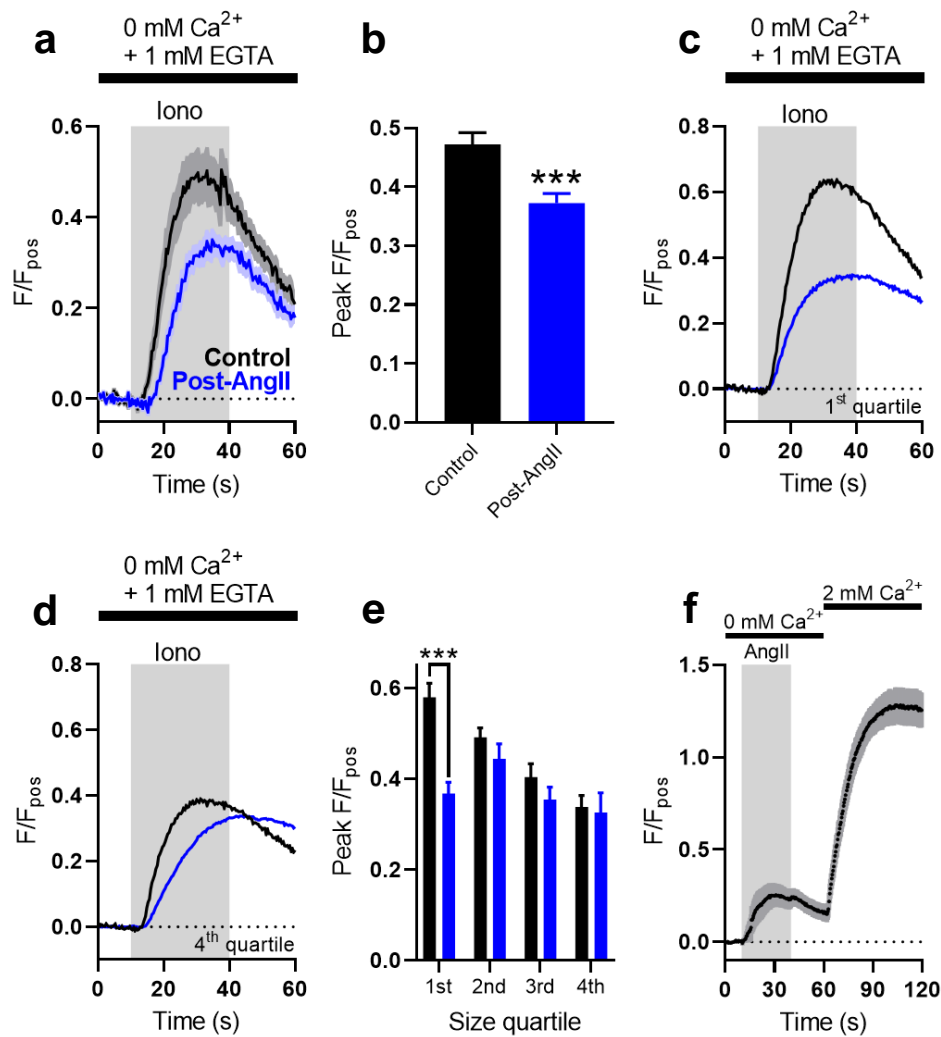


**Figure 4.3 Ang II depletes intracellular  $\text{Ca}^{2+}$  stores**

- Grouped ionomycin-induced  $\text{Ca}^{2+}$  transients. Control (black): 292 neurons,  $n = 3$ ,  $N = 3$ . Post-Ang II (blue), 295 neurons,  $n = 3$ ,  $N = 3$ . Solid line shows mean, shaded area shows standard error.
- Grouped data showing the peak magnitude of ionomycin-induced  $\text{Ca}^{2+}$  transients. Control: 292 neurons,  $n = 3$ ,  $N = 3$ . Post-Ang II, 295 neurons,  $n = 3$ ,  $N = 3$ . Data analysed using a two-tailed unpaired t-test with Welch's correction.
- Exemplar ionomycin-induced  $\text{Ca}^{2+}$  transients from neurons in the 1<sup>st</sup> size quartile with (blue) and without (black) Ang II pre-application.
- Exemplar ionomycin-induced  $\text{Ca}^{2+}$  transients from neurons in the 4<sup>th</sup> size quartile with (blue) and without (black) Ang II pre-application.
- Grouped data showing the peak magnitude of ionomycin-induced  $\text{Ca}^{2+}$  transients across each size quartile. Data analysed using a two-way ANOVA with Sidak post-tests.
- Grouped traces (10 neurons) showing Fluo-4 fluorescence during Ang II application in  $\text{Ca}^{2+}$ -free buffer and the subsequent re-addition of  $2 \text{ mM Ca}^{2+}$ . Solid line shows mean, shaded area shows standard error.

### **4.2.3. Neither activation of AT2R nor action potential firing underlies Ang II-evoked Ca<sup>2+</sup> signals**

Pre-incubation of cultures with PD123319 (1  $\mu$ M), an antagonist of AT2R, did not appear to have any effect on the neuronal response to Ang II (Figure 4.4a). The peak of the Ang II-evoked Ca<sup>2+</sup> signal was  $0.59 \pm 0.11$  in control experiments and  $0.62 \pm 0.18$  after incubation with PD123319 ( $p = 0.89$ , Figure 4.4b). Moreover, the proportion of neurons responding to Ang II application was  $50.6 \pm 8.5\%$  and  $39.5 \pm 4.8\%$  in control and PD123319-incubated cultures, respectively ( $p = 0.27$ , Figure 4.4c).

Inhibition of action potential discharge by pre-incubation with tetrodotoxin (TTX, 1  $\mu$ M), a blocker of voltage-gated Na<sup>+</sup> channels, did not attenuate the neuronal response to Ang II (Figure 4.5a). The peak magnitude of the response to Ang II was unchanged by pre-incubation with TTX ( $0.55 \pm 0.13$  vs  $0.46 \pm 0.01$ ,  $p = 0.57$ , Figure 4.5b). Under control conditions, Ang II-responsive neurons accounted for  $23.9 \pm 4.3\%$  of neurons in culture, compared to  $23.4 \pm 5.3\%$  after TTX incubation ( $p = 0.94$ , Figure 4.5c). Current-clamp recording (injected current = 0 pA) from IB4-positive neurons during the application of Ang II revealed no depolarisation ( $p = 0.35$ ) or action potential firing (0/9 neurons tested displayed action potential discharge, Figure 4.5d).

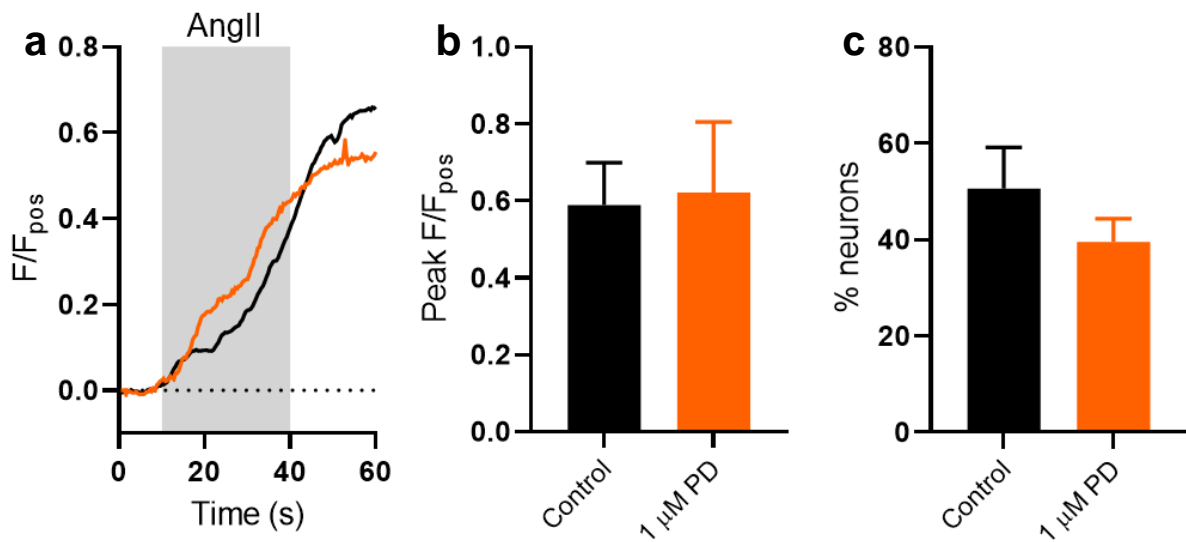


**Figure 4.4 AT2R is not required for the neuronal response to Ang II**

- (a) Example Fluor-4 fluorescence traces during the application of Ang II in control (black) and PD123319-incubated (orange) cultures.
- (b) Grouped data showing the peak magnitude of the response to Ang II. Control: n = 6, N = 5; PD123319: n = 6, N = 5). Data analysed using a two-tailed unpaired t-test.
- (c) Grouped data showing the proportion of neurons responding to Ang II. Control: n = 6, N = 5; PD123319: n = 6, N = 5). Data analysed using a two-tailed unpaired t-test.

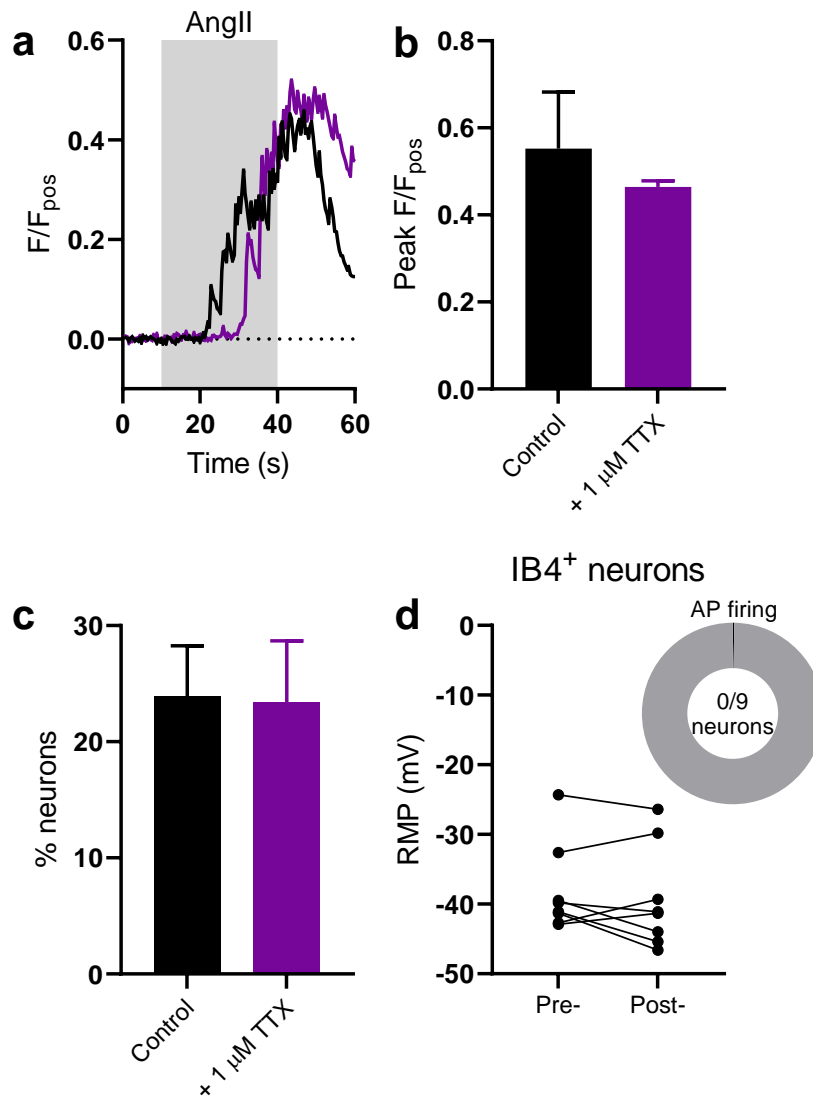


**Figure 4.5 Action potential discharge does not contribute to the Ang II-evoked Ca<sup>2+</sup> rise**

- (a) Example Fluo-4 fluorescence traces during the application of Ang II in control (black) and TTX-incubated (purple) cultures.
- (b) Grouped data showing the peak magnitude of the response to Ang II. Control: n = 5, N = 5; TTX: n = 4, N = 4). Data analysed using a two-tailed unpaired t-test.
- (c) Grouped data showing the proportion of neurons responding to Ang II. Control: n = 5, N = 5; TTX: n = 4, N = 4). Data analysed using a two-tailed unpaired t-test.
- (d) Resting membrane potential of IB4-positive neurons before and after application of Ang II. 9 neurons from 3 mice. Data analysed using a two-tailed paired t-test. *Inset*: pie chart showing the number of neurons which discharge at least one action potential during Ang II application (0 of 9).

#### 4.2.4. Ang II also stimulates Ca<sup>2+</sup> influx through TRPC3 channels

In the above experiments using Ca<sup>2+</sup>-free buffer, it was noticed that the response to Ang II was attenuated, indicating that a component of this response may be underpinned by Ca<sup>2+</sup> influx. The average of all Ang II-evoked Ca<sup>2+</sup> transients in control (2 mM) and Ca<sup>2+</sup>-free conditions verified this earlier observation: transients are smaller in Ca<sup>2+</sup>-free conditions (Figure 4.6a).

The identity of the ion channel responsible for this Ca<sup>2+</sup> influx was investigated. It has been shown that AT1R couples to the non-selective, Ca<sup>2+</sup>-permeable transient receptor potential channel C3 (TRPC3). *Agtr1a* and *Agtr1b* are co-expressed with *Trpc3* in sensory neurons (Usoskin *et al.*, 2015; Kupari *et al.*, 2021). The neuronal response to Ang II was attenuated by pre-incubation with a TRPC3-selective antagonist, Pyrazole-3 (Pyr3 [10 µM], Figure 4.6b). The proportion of neurons responding to Ang II was reduced by Pyr3 from 55.7±5.8% to 24.4±6.1% (p = 0.005, Figure 4.6c). Incubation of neurons with valsartan in Ca<sup>2+</sup>-free external buffer resulted in a greater inhibition of the response to Ang II compared to valsartan alone (p = 0.04, Figure 4.6d).

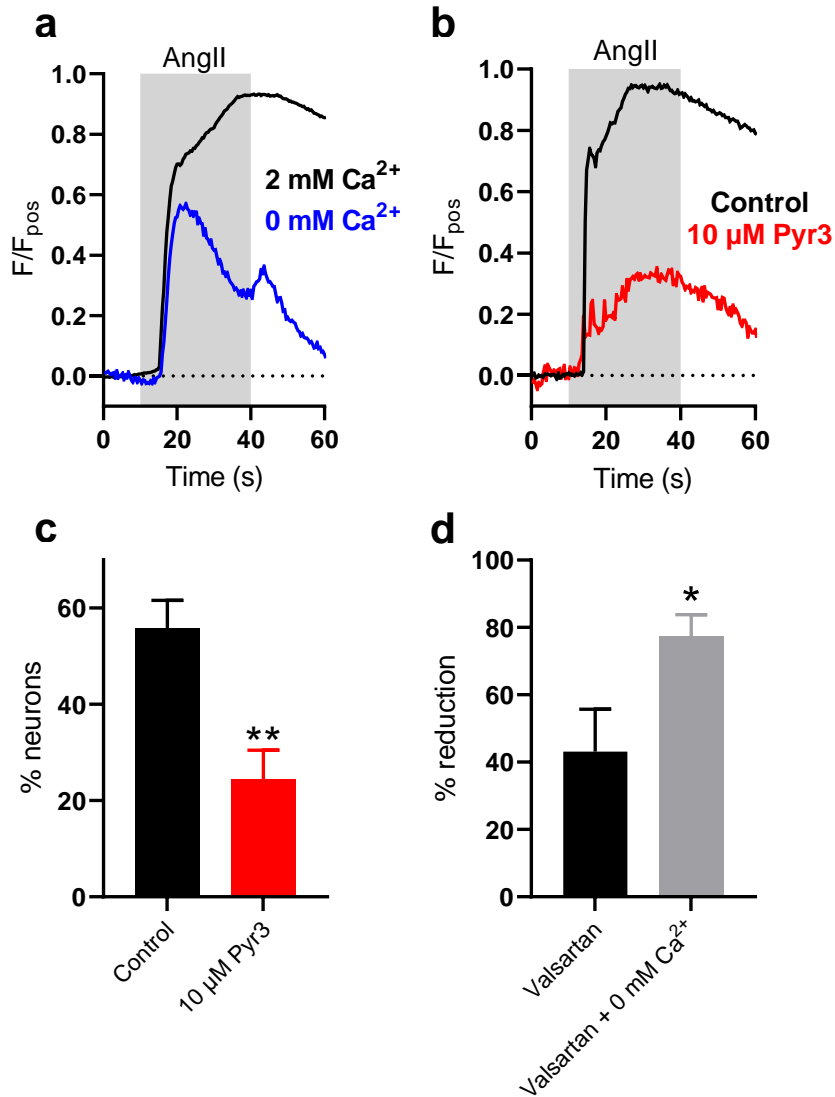


**Figure 4.6 Ang II induces Ca<sup>2+</sup> influx through TRPC3 channels**

- (a) Exemplar Fluo-4 fluorescence traces from neurons bathed in 2 mM or 0 mM external Ca<sup>2+</sup>.
- (b) Example Fluo-4 fluorescence traces from a neuron in control conditions and following Pyr3 incubation.
- (c) Grouped data showing the proportion of neurons responding to Ang II. Control: n = 5, N = 5; Pyr3: n = 6, N = 5. Data analysed using a two-tailed unpaired t-test.
- (d) Grouped data showing the percentage reduction in the proportion of neurons responding to Ang II. Valsartan: n = 5, N = 5; Valsartan + 0 mM Ca<sup>2+</sup>: n = 5, N = 5. Data analysed using a two-tailed unpaired t-test.

#### 4.2.5. Agonist-induced desensitisation of TRPC3 attenuates the neuronal response to Ang II

As is the case for many GPCR agonists, the response to Ang II application undergoes tachyphylaxis – that is, the response to a second application of Ang II is lower than that of the first application (Figure 4.7a and b). The peak magnitude of the response to the first application of Ang II was  $1.2 \pm 0.15$ , compared to  $0.49 \pm 0.08$  for the second application ( $p = 0.003$ , Figure 4.7c). What's more, the proportion of neurons responding to Ang II was reduced ( $44.2 \pm 10.5\%$  to  $16.3 \pm 7.0\%$ ,  $p = 0.003$ , Figure 4.7d). This is a reduction in the proportion of responding neurons of  $69.1 \pm 8.6\%$  (Figure 4.7d *inset*).

The response to a second application of a TRPC3/6 agonist, GSK1702934A (500 nM), was also reduced compared to the first (Figure 4.7e and f). The peak magnitude of the response to GSK1702934A was reduced from  $0.59 \pm 0.05$  to  $0.34 \pm 0.06$  ( $p = 0.006$ , Figure 4.7g). The GSK1702934A-sensitive population accounted for  $41.0 \pm 6.9\%$  of all neurons on the first application, and  $13.4 \pm 1.2\%$  on the second ( $p = 0.02$ , Figure 4.7h). This is a reduction of  $64.5 \pm 6.1\%$  (Figure 4.7h *inset*).

If TRPC3 is required for a component of the response to Ang II – as was suggested by experiments with Pyr3 – then agonist-induced desensitisation of TRPC3 would be expected to reduce the response to Ang II. Pre-application of GSK1702934A prior to Ang II attenuated the response to Ang II (compared to a time-matched control with Ang II applied alone; Figure 4.7i). The peak magnitude of the response to Ang II alone was  $0.91 \pm 0.12$ , whereas after GSK1702934A pre-application, it was  $0.31 \pm 0.03$  ( $p = 0.002$ , Figure 4.7j). The magnitude of the response to high  $[K^+]$  was no different between neurons to which GSK1702934A and Ang II had been applied compared to those to which only Ang II had been applied ( $p = 0.61$ , Figure 4.7k). Finally, the proportion of neurons responding to Ang II was  $37.1 \pm 3.9\%$  under control conditions, and  $17.0 \pm 4.1\%$  after GSK1702934A pre-application ( $p = 0.006$ , Figure 4.7l).

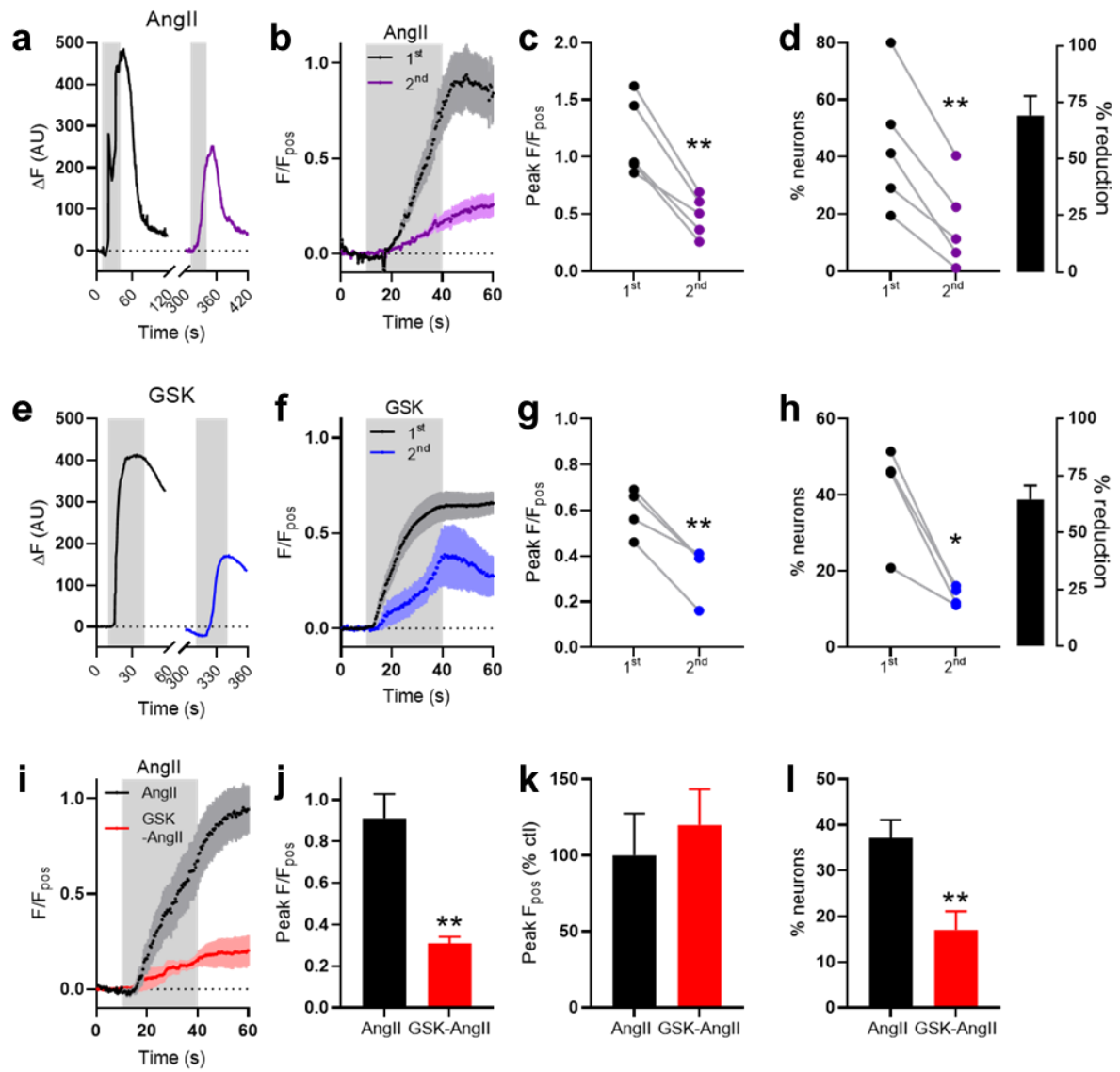


Figure 4.7 Legend on next page

**Figure 4.7 Cross-desensitisation of responses to Ang II and GSK1702934A, a TRPC3 agonist**

- (a) Example Fluo-4 fluorescence trace from a single neuron showing two applications of Ang II.
- (b) Example averaged traces from a single experiment showing the response to the first and second application of Ang II. 1<sup>st</sup> application: 40 responsive neurons, 2<sup>nd</sup> application: 21 responsive neurons.
- (c) Grouped data showing the peak magnitude of the response to Ang II. Data from  $n = 5$ ,  $N = 5$ . Data analysed using a two-tailed paired t-test.
- (d) Grouped data showing the proportion of neurons responding to Ang II. Data from  $n = 5$ ,  $N = 5$ . Data analysed using a two-tailed paired t-test. *Inset*: The percent reduction in the proportion of responsive neurons.
- (e) Example Fluo-4 fluorescence trace from a single neuron showing two applications of GSK1702934A.
- (f) Example averaged traces from a single experiment showing the response to the first and second application of GSK1702934A. 1<sup>st</sup> application: 36 responsive neurons, 2<sup>nd</sup> application: 8 responsive neurons.
- (g) Grouped data showing the peak magnitude of the response to GSK1702934A. Data from  $n = 4$ ,  $N = 3$ . Data analysed using a two-tailed paired t-test.
- (h) Grouped data showing the proportion of neurons responding to GSK1702934A. Data from  $n = 4$ ,  $N = 3$ . Data analysed using a two-tailed paired t-test. *Inset*: The percent reduction in the proportion of responsive neurons.
- (i) Example averaged traces from a single experiment showing the response to Ang II applied alone, and Ang II applied after GSK1702934A. Ang II alone: 21 responsive neurons, GSK1702934A pre-application: 8 responsive neurons.
- (j) Grouped data showing the peak magnitude of the response to Ang II. Ang II alone:  $n = 7$ ,  $N = 4$ . GSK1702934A pre-incubation:  $n = 5$ ,  $N = 3$ . Data analysed using a two-tailed unpaired t-test.
- (k) Grouped normalised (to mean of control) data showing the peak response to KCl application. Ang II alone:  $n = 6$ ,  $N = 4$ . GSK1702934A pre-incubation:  $n = 5$ ,  $N = 3$ . Data analysed using a two-tailed unpaired t-test.
- (l) Grouped data showing the proportion of neurons responding to Ang II. Ang II alone:  $n = 7$ ,  $N = 4$ . GSK1702934A pre-incubation:  $n = 5$ ,  $N = 3$ . Data analysed using a two-tailed unpaired t-test.

#### **4.2.6. TRPC3 functions in TRPV1-expressing neurons**

The functional co-expression of TRPC3 with the nociceptive marker TRPV1 was probed by the sequential application of GSK1702934A and capsaicin to cultured sensory neurons (Figure 4.8a). After the elimination of neurons which responded to neither compound, three populations of varying size were identified. The smallest of these populations, accounting for only  $1.7\pm 1.1\%$  of neurons in culture, responded to GSK1702934A but not capsaicin (Figure 4.8b). A population comprising neurons responsive to capsaicin but not GSK1702934A accounted for  $8.9\pm 2.1\%$  of all neurons (Figure 4.8b). Finally, the largest identified population –  $25.9\pm 5.6\%$  – was sensitive to both GSK1702934A and capsaicin (Figure 4.8b). The total size of the capsaicin-sensitive population was  $34.8\pm 5.2\%$  (Figure 4.8b). This data indicates high co-sensitivity between GSK1702934A and capsaicin:  $94.6\pm 3.1\%$  of GSK1702934A-sensitive neurons also responded to capsaicin (Figure 4.8c). In two of four replicates, co-sensitivity was 100%. A non-parametric one-sample t-test revealed that the observed co-sensitivity is indistinguishable from a hypothetical value of 100% ( $p = 0.50$ ).

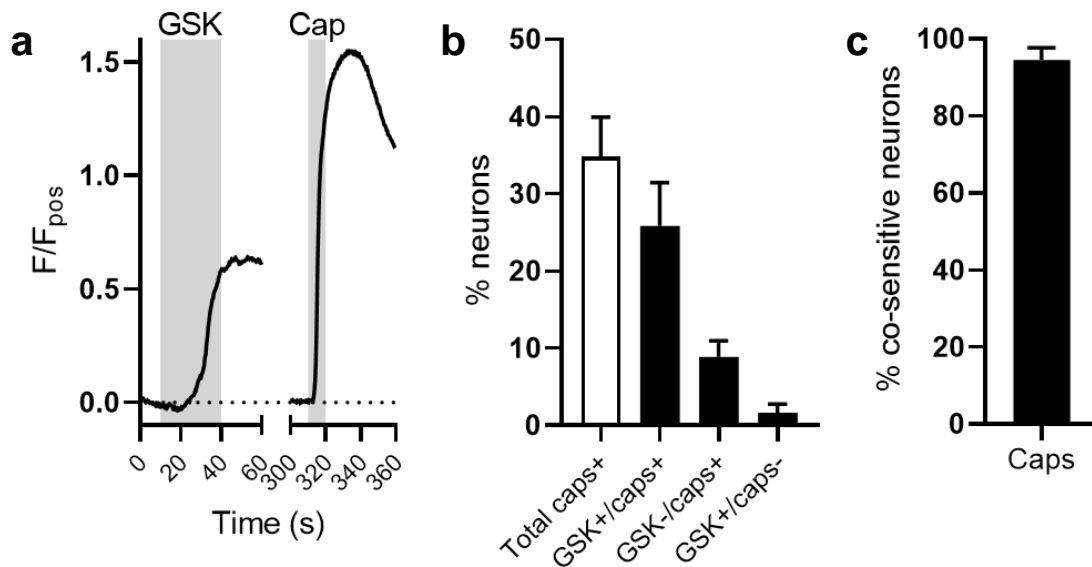


**Figure 4.8 TRPC3 functions in TRPV1-expressing neurons**

- (a) Example Fluo-4 fluorescence trace from a single neuron showing the sequential application of GSK1702934A and capsaicin. This neuron responded to both compounds.
- (b) The proportional size of each of the neuronal populations identified based on sensitivity to GSK1702934A and capsaicin. Data from  $n = 4$ ,  $N = 1$ .
- (c) The proportion of neurons exhibiting co-sensitivity to GSK1702934A and capsaicin. Data from  $n = 4$ ,  $N = 1$ . Data analysed using a one-sample Wilcoxon Signed Rank test.

#### **4.2.7. Ca<sup>2+</sup> influx through TRPC3 drives prolongation of Ang II-evoked Ca<sup>2+</sup> signals**

Store-operated Ca<sup>2+</sup> entry (SOCE), initiated by depletion of intracellular Ca<sup>2+</sup> stores, gives rise to prolonged Ca<sup>2+</sup> signals long outlasting the store-depleting stimulus. TRPC3 has been posited as a store-operated channel (SOC) in the past, but its role in mouse sensory neurons is not clear. While it has become clear that the majority of Ang II-evoked Ca<sup>2+</sup> signals in sensory neurons are prolonged – lasting up to 5 minutes (Figure 4.9a) – it isn't possible to say if TRPC3 contributes to this with protocols used thus far. This is because store release and SOCE initially occur on similar timescales; over longer timescales, the Ca<sup>2+</sup> signal arising from store release will subside, and that arising from SOCE will predominate. To test the role of TRPC3 in SOCE, the channel was blocked by application of Ca<sup>2+</sup>-free buffer or Pyr3 to fully-developed Ang II-evoked Ca<sup>2+</sup> signals (see Figure 4.9a).

Application of either Ca<sup>2+</sup>-free buffer after Ang II can be seen in Figure 4.9a; this resulted in the hastened decay of the Ang II-evoked Ca<sup>2+</sup> signal. Under control conditions, 80% (12 of 15) of neurons displayed persistently raised Ca<sup>2+</sup> up to 300 s after Ang II application (Figure 4.9b). For this sample of neurons as a whole, there was no significant decrease in the Ang II-evoked Ca<sup>2+</sup> rise between the peak (between 10 – 40 s) and 300 s later ( $p = 0.78$ ). If Ca<sup>2+</sup>-free external buffer was applied to the neurons, the Ang II-evoked Ca<sup>2+</sup> signal did decrease ( $p < 0.0001$ ) and re-approached the baseline (Figure 4.9c). Application of Pyr3 after Ang II also resulted in a decrease in the Ang II-evoked Ca<sup>2+</sup> signal after the peak of  $53.0 \pm 11.2\%$  ( $p = 0.006$ , Figure 4.9d). In each of these conditions, the initial peak response to Ang II application was the same ( $p = 0.52$ , Figure 4.9e).

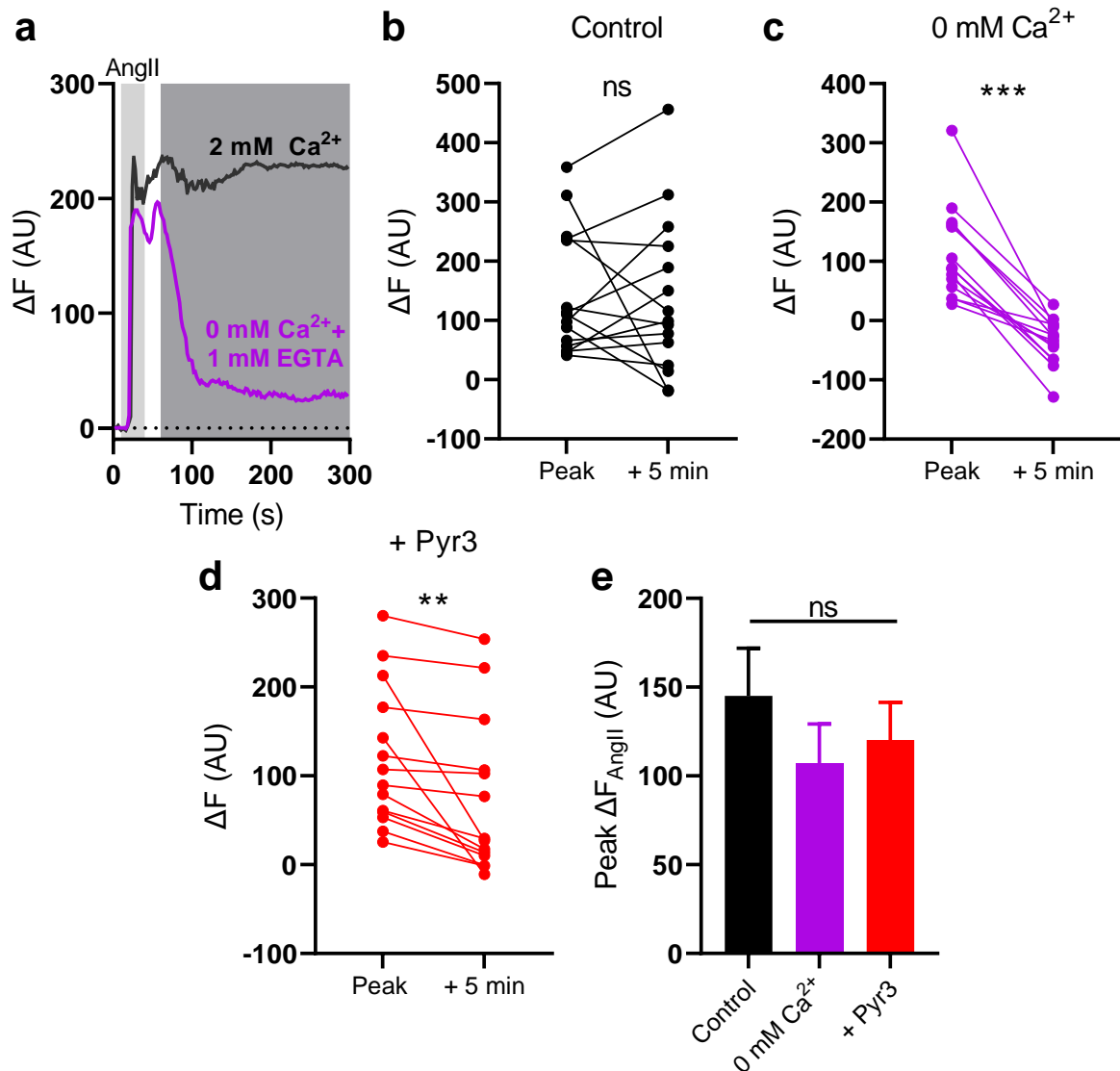


**Figure 4.9 Ang II evokes prolonged Ca<sup>2+</sup> signals which depend on TRPC3**

- (a) Example Fluo-4 fluorescence traces (increase over baseline) showing the application of Ang II and the subsequent application of control buffer (black) or Ca<sup>2+</sup>-free buffer (purple). Solutions were switched at 60 s (dark grey shaded area). Images were acquired at 0.5 fps rather than the standard 2.5 fps.
- (b) Grouped data showing the magnitude of Ang II-evoked Ca<sup>2+</sup> signals at their peak (between 10 – 40 s) and 300 s later in control conditions. 15 neurons from a single experiment. Data analysed using a two-tailed paired t-test.
- (c) Grouped data showing the magnitude of Ang II-evoked Ca<sup>2+</sup> signals at their peak (between 10 – 40 s) and 300 s later in Ca<sup>2+</sup>-free buffer. 13 neurons from a single experiment. Data analysed using a two-tailed paired t-test.
- (d) Grouped data showing the magnitude of Ang II-evoked Ca<sup>2+</sup> signals at their peak (between 10 – 40 s) and 300 s later in Pyr3-containing buffer. 14 neurons from a single experiment. Data analysed using a two-tailed paired t-test.
- (e) Grouped data showing the peak magnitude of the response to Ang II between 10 – 40 s. Data analysed using a one-way ANOVA.

#### **4.2.8. TRPC3 is activated by store depletion in mouse sensory neurons**

While the protocol outlined in 4.2.7. implies a role for TRPC3 in prolonged  $\text{Ca}^{2+}$  entry, it cannot provide adequate evidence for a role for TRPC3 in SOCE. Prolonged  $\text{Ca}^{2+}$  entry is likely store-operated given that Ang II depletes stores, but more data is required to clarify this. SOCE can be initiated in a receptor-independent manner by incubating neurons with thapsigargin in  $\text{Ca}^{2+}$ -free buffer: thapsigargin causes store depletion, activating SOCs, but the absence of extracellular  $\text{Ca}^{2+}$  prevents store refilling. 2 mM  $\text{Ca}^{2+}$  can then be re-instated in the extracellular buffer, permitting  $\text{Ca}^{2+}$  entry through SOCs (Figure 4.10a).

Neurons under control conditions exhibited robust  $\text{Ca}^{2+}$  influx upon re-instatement of 2 mM extracellular  $\text{Ca}^{2+}$  (Figure 4.11a). Incubation with Pyr-3 resulted in a suppression of SOCE: a peak of  $0.53 \pm 0.02$  compared to  $0.84 \pm 0.04$  in control experiments ( $p < 0.0001$ , Figure 4.11a and b). Pre-incubation with Pyr3 did not affect thapsigargin-induced  $\text{Ca}^{2+}$  release from intracellular stores ( $p = 0.91$ ), indicating that the inhibition of SOCE by Pyr3 was not due to attenuated loss of  $\text{Ca}^{2+}$  from intracellular stores.

Orai channels are known to mediate SOCE and are highly expressed across all sensory neuronal populations. These channels are sensitive to block by  $\text{Gd}^{3+}$ . Incubation of neurons with both Pyr-3 and  $\text{Gd}^{3+}$  (10  $\mu\text{M}$ ) brought about a further reduction in SOCE ( $p < 0.0001$ , Figure 4.11a and b), suggesting that both channels – TRPC3 and Orai – contribute to SOCE. It is important to note that  $\text{Gd}^{3+}$  also blocks voltage-gated  $\text{Ca}^{2+}$  channels, which could affect the response to high  $[\text{K}^+]$ . 10  $\mu\text{M}$   $\text{Gd}^{3+}$  did not affect the peak magnitude of the response to KCl application ( $p = 0.07$ , Figure 4.11c and d). Increasing the concentration of  $\text{Gd}^{3+}$  did, however, suppress the response to KCl application ( $p < 0.0001$ , Figure 4.11c and d). Finally, the ER  $\text{Ca}^{2+}$  sensor, STIM, is expressed in sensory neurons and, in other cell types, mediates the opening of SOCs by ER  $\text{Ca}^{2+}$  depletion. Incubation of neurons with ML-9 (10  $\mu\text{M}$ ), an inhibitor of STIM (Jairaman and Prakriya, 2013), almost abolished SOCE ( $p < 0.0001$ , Figure 4.11a and b).

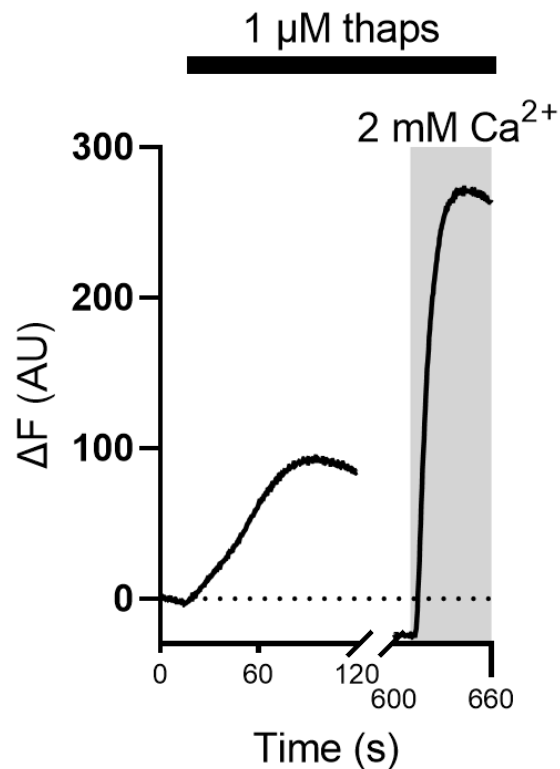


**Figure 4.10 Protocol to evoke SOCE**

Application of thapsigargin (starting at 10 s) in  $\text{Ca}^{2+}$ -free external bathing solution depletes intracellular  $\text{Ca}^{2+}$  stores. The resulting rise in  $\text{Ca}^{2+}$  reflects draining of stores and the loss of  $\text{Ca}^{2+}$  buffering capacity of the neuron. No  $\text{Ca}^{2+}$  entry due to SOCE can be observed, despite the activation of SOCs, because of the absence of extracellular  $\text{Ca}^{2+}$ . After 600 s, stores are fully depleted and 2 mM  $\text{Ca}^{2+}$  is re-added to external bathing solution (grey shaded area).  $\text{Ca}^{2+}$  can now enter the neuron through the activated SOCs, and SOCE is observed.

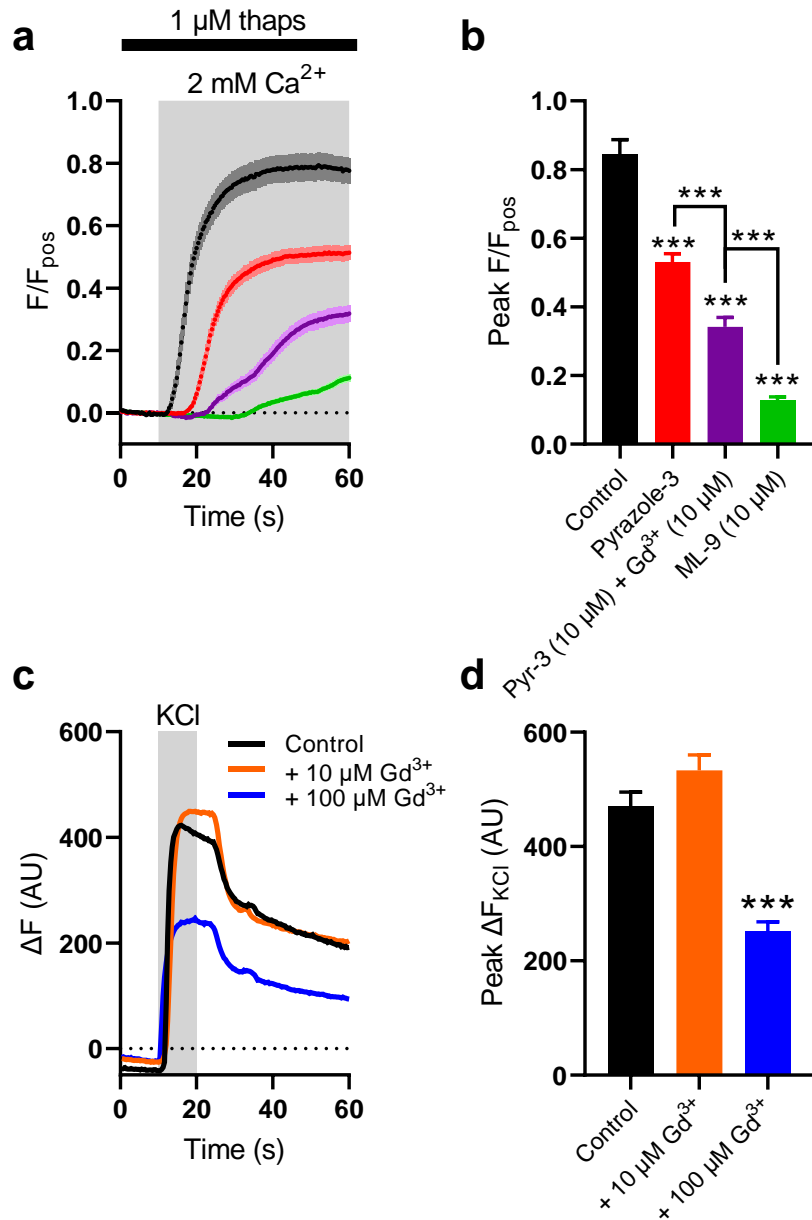


**Figure 4.11 TRPC3 channels mediate a component of SOCE in sensory neurons**

- (a) Grouped Fluo-4 fluorescence traces showing SOCE upon re-instatement of 2 mM external  $\text{Ca}^{2+}$ . Control (black): 139 neurons,  $n = 3$ ,  $N = 3$ . Pyr3 (red): 238 neurons,  $n = 3$ ,  $N = 3$ . Pyr3 +  $\text{Gd}^{3+}$  (purple): 187 neurons,  $n = 3$ ,  $N = 3$ . ML-9 (green): 246 neurons,  $n = 3$ ,  $N = 3$ . Solid line shows mean, shaded area shows standard error.
- (b) Grouped data showing the peak magnitude of SOCE for the traces shown in (a). Data analysed using a one-way ANOVA with Holm-Sidak post-tests.
- (c) Example traces showing the application of 50 mM KCl in control neurons (black) and neurons incubated with either 10  $\mu\text{M}$  (orange) or 100  $\mu\text{M}$  (blue)  $\text{Gd}^{3+}$ .
- (d) Grouped data showing the peak magnitude of the response to KCl. Control: 137 neurons,  $n = 3$ ,  $N = 3$ . 10  $\mu\text{M}$   $\text{Gd}^{3+}$ : 88 neurons,  $n = 2$ ,  $N = 2$ . 100  $\mu\text{M}$   $\text{Gd}^{3+}$ : 143 neurons,  $n = 3$ ,  $N = 3$ .

#### 4.2.9. TRPC3 contributes to SOCE in small-sized sensory neurons

TRPC3 is expressed in non-peptidergic nociceptors (Usoskin *et al.*, 2015) and, as shown above (4.2.6.), functions in TRPV1-expressing neurons. It would, therefore, be expected that TRPC3 would only contribute to SOCE in small-sized neurons. To test this, neurons were again parsed into size quartiles. SOCE was attenuated by pre-incubation with Pyr-3 in neurons within the 1<sup>st</sup> ( $p < 0.0001$ , Figure 4.12a and c) and 2<sup>nd</sup> ( $p < 0.0001$ , Figure 4.12c) quartiles. SOCE in neurons within the 3<sup>rd</sup> ( $p = 0.93$ , Figure 4.12c) and 4<sup>th</sup> ( $p = 0.58$ , Figure 4.12b and c) quartiles was unaffected by Pyr-3.

The addition of Gd<sup>3+</sup> with Pyr-3 inhibited SOCE compared to control conditions ( $p < 0.0002$ ) but did not further attenuate SOCE compared to Pyr-3 alone in neurons in the 1<sup>st</sup> ( $p = 0.99$ , Figure 4.12a and c) or 2<sup>nd</sup> ( $p = 0.99$ , Figure 4.12c) quartiles. However, Gd<sup>3+</sup> robustly inhibited SOCE in neurons within the 3<sup>rd</sup> ( $p < 0.0001$ , Figure 4.12c) and 4<sup>th</sup> ( $p = 0.032$ , Figure 4.12b and c) quartiles, where Pyr-3 was without effect. Pre-incubation with ML-9 almost abolished SOCE in neurons of all sizes ( $p < 0.0001$  for all quartiles, Figure 4.12a, b and c). In neurons in the 1<sup>st</sup> and 2<sup>nd</sup> quartiles, ML-9 suppressed SOCE to a greater than Pyr-3 and Gd<sup>3+</sup> ( $p < 0.0001$ , Figure 4.12c). Conversely, in neurons in the 3<sup>rd</sup> and 4<sup>th</sup> quartiles, there was no difference in the inhibition attained by Gd<sup>3+</sup> and ML-9 ( $p > 0.98$ , Figure 4.12c). Incubation with Gd<sup>3+</sup> alone did not affect SOCE in small-sized neurons (those from the 1<sup>st</sup> size quartile) but did attenuate SOCE in large-diameter neurons (those from the 4<sup>th</sup> size quartile) (Figure 4.12d), in line with the effect of Gd<sup>3+</sup> applied with Pyr3.

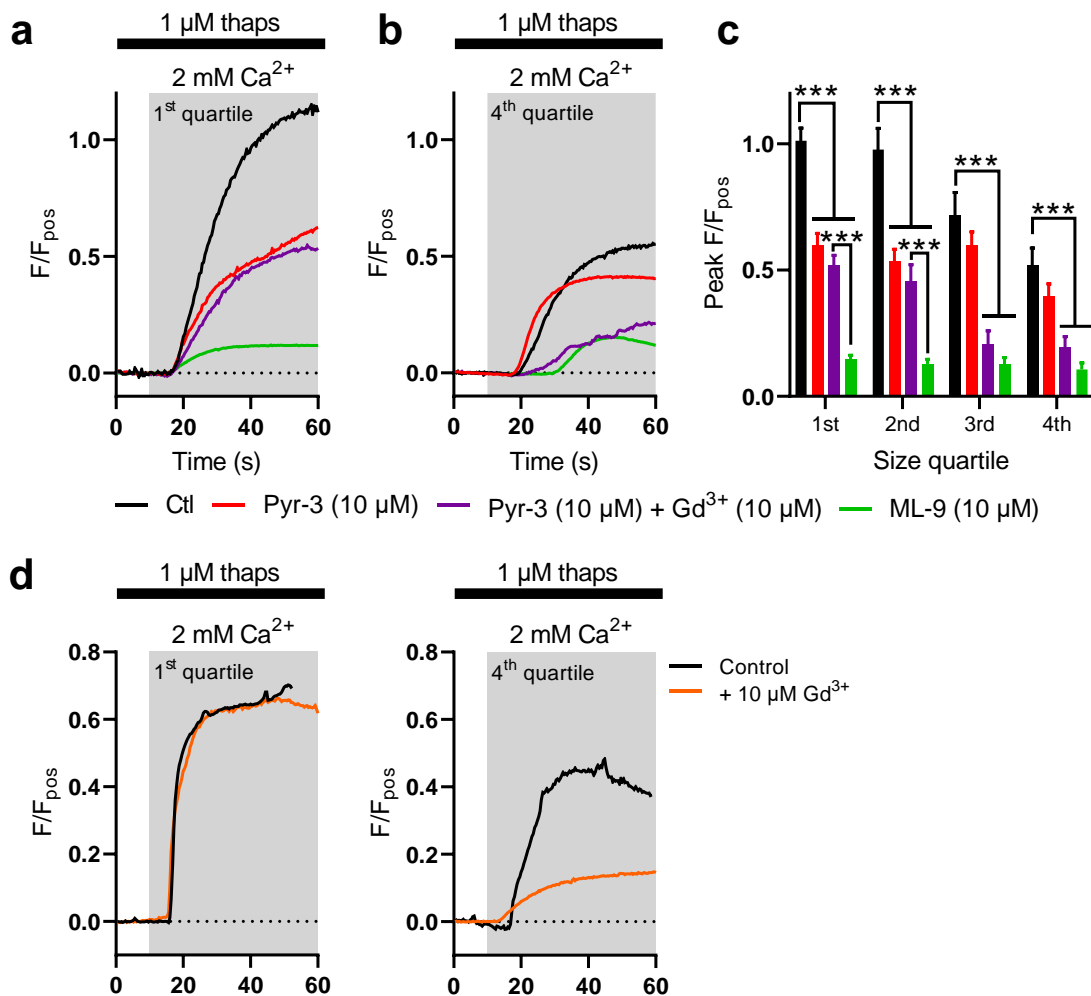


**Figure 4.12 TRPC3 channels contribute to SOCE in small-sized sensory neurons**

- (a) Example Fluo-4 fluorescence traces from neurons within the 1<sup>st</sup> size quartile during the re-addition of 2 mM  $\text{Ca}^{2+}$  to the external buffer.
- (b) Example Fluo-4 fluorescence traces from neurons within the 4<sup>th</sup> size quartile during the re-addition of 2 mM  $\text{Ca}^{2+}$  to the external buffer.
- (c) Grouped data showing the peak magnitude of SOCE in each experimental condition for neurons within each size quartile. Control (black): 139 neurons,  $n = 3$ ,  $N = 3$ . Pyr3 (red): 238 neurons,  $n = 3$ ,  $N = 3$ . Pyr3 +  $\text{Gd}^{3+}$  (purple): 187 neurons,  $n = 3$ ,  $N = 3$ . ML-9 (green): 246 neurons,  $n = 3$ ,  $N = 3$ . Data analysed using a two-way ANOVA with Sidak's post-tests.
- (d) Example Fluo-4 fluorescence traces from neurons within the 1<sup>st</sup> (*left*) and 4<sup>th</sup> (*right*) size quartiles in the absence (black traces) and presence (orange traces) of  $\text{Gd}^{3+}$  during the re-addition of 2 mM  $\text{Ca}^{2+}$  to the external buffer.

#### **4.2.10. Ang II activates TRPC3 via store depletion**

Data presented thus far indicates that Ang II depletes intracellular  $\text{Ca}^{2+}$  stores and stimulates TRPC3; given that TRPC3 is a SOC, is Ang II-evoked TRPC3 activity dependent on store depletion? If store depletion mediates TRPC3 activation, blocking STIM-dependent communication between the store and plasma membrane would be expected to block TRPC3 activation, negating the effect of Pyr3. Neurons were incubated with ML-9 with and without co-incubation with Pyr3, and subsequently stimulated with Ang II. In previous experiments, Pyr3 attenuated the response to Ang II (see 4.2.4.). However, in the presence of ML-9, Pyr-3 had no effect on the neuronal response to Ang II (Figure 4.13a). The peak magnitude of the response to Ang II was  $0.57 \pm 0.10$  in the absence of Pyr-3, and  $0.50 \pm 0.03$  in the presence of Pyr-3 ( $p > 0.99$ , Figure 4.13b). The proportion of neurons exhibiting a rise in intracellular  $\text{Ca}^{2+}$  following Ang II application was also unchanged by Pyr-3 in the presence of ML-9:  $23.2 \pm 2.6\%$  vs  $29.5 \pm 6.2\%$  ( $p = 0.69$ , Figure 4.13c). Quantifying the inhibitory effect of Pyr-3 revealed an inhibition in the absence of ML-9 (control) of  $56.3 \pm 10.9\%$ , compared to  $-26.1 \pm 20.3\%$  in the presence of ML-9 ( $p = 0.005$ , Figure 4.13d). A one-sample t-test revealed that the inhibitory effect of Pyr-3 in the presence of ML-9 was indistinguishable from 0% ( $p = 0.29$ ), showing a loss of effect of Pyr-3.

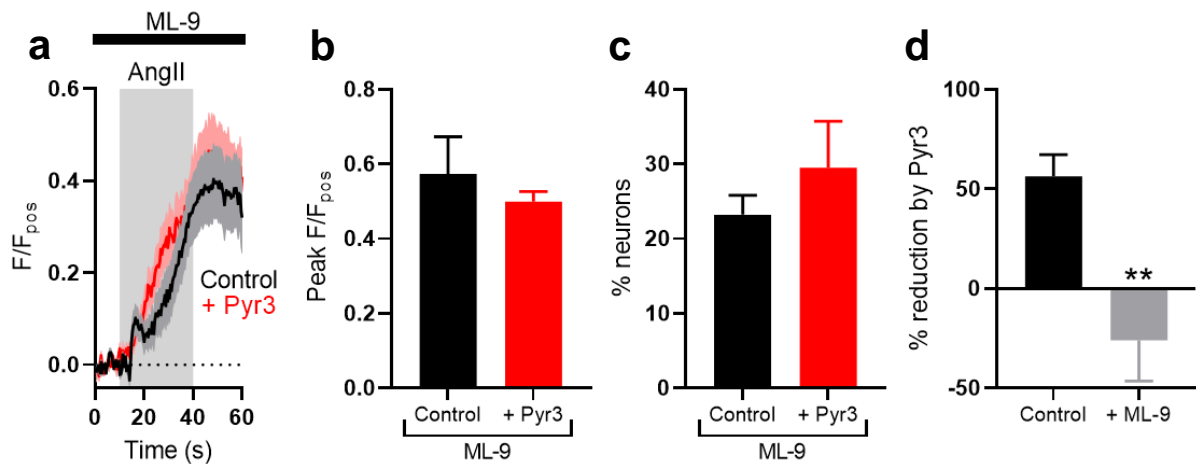


**Figure 4.13 Activation of TRPC3 by Ang II is dependent on STIM**

- (a) Grouped Fluo-4 fluorescence traces from single experiments showing the application of Ang II in the presence of ML-9 with (red, 16 neurons) or without (black, 24 neurons) Pyr3. Solid line shows mean, shaded area shows standard error.
- (b) Grouped data showing the peak magnitude of the response to Ang II. Control: n = 4, N = 4. Pyr-3: n = 4, N = 4. Data analysed using a two-tailed Mann-Whitney U test.
- (c) Grouped data showing the proportion of neurons responding to Ang II. Control: n = 4, N = 4. Pyr-3: n = 4, N = 4. Data analysed using a two-tailed Mann-Whitney U test.
- (d) Grouped data showing the percentage reduction in the proportion of Ang II-responsive neurons by Pyr-3 in the absence or presence of ML-9. Control: n = 6, N = 5. ML-9: n = 4, N = 4. Data analysed using a two-tailed unpaired t-test.

#### 4.2.11. Regulation of SOCE and TRPC3 by protein kinases C and G

Given the myriad roles played by intracellular  $\text{Ca}^{2+}$ , the regulation of  $\text{Ca}^{2+}$  entry pathways is of utmost importance. The effect of protein kinase C (PKC) activation on TRPC3-mediated SOCE was investigated by incubating neurons with the phorbol ester, PDBu (1  $\mu\text{M}$ ), and thapsigargin in  $\text{Ca}^{2+}$ -free external buffer and subsequently re-adding 2 mM external  $\text{Ca}^{2+}$ . PKC activation has been shown to suppress SOCE mediated by Orai channels in recombinant expression systems, so  $\text{Gd}^{3+}$  was present throughout these experiments to block this pathway, isolating the TRPC3-mediated component. PDBu attenuated SOCE compared to control conditions: peak fluorescence upon  $\text{Ca}^{2+}$  re-addition was reduced to  $0.33 \pm 0.04$  from  $0.75 \pm 0.06$  ( $p < 0.0001$ , Figure 4.14a and b). The proportion of neurons responding to GSK1702934A was also reduced from  $39.1 \pm 3.9\%$  to  $13.3 \pm 3.4\%$  by PDBu ( $p = 0.006$ , Figure 4.14c), directly demonstrating an inhibitory effect of PKC activation on TRPC3.

Previous reports have suggested that the inhibitory effect of PKC on TRPC3 channels is in part mediated by protein kinase G (PKG). Addition of the PKG inhibitor, KT5832 (1  $\mu\text{M}$ ), did not reverse PDBu-induced SOCE inhibition (Figure 4.14a). In the presence of KT5832, PDBu reduced SOCE to  $0.36 \pm 0.04$  ( $p < 0.0001$  compared to control, Figure 4.14b). What's more, there was no difference in the magnitude of SOCE in neurons incubated with only PDBu and PDBu with KT5832 ( $p = 0.73$ , Figure 4.14b).

To confirm that PKG does not regulate SOCE in sensory neurons, SOCE was measured after pre-incubation with 100  $\mu\text{M}$  8-Br-cGMP – a membrane-permeable analogue of cGMP which stimulates PKG.  $\text{Gd}^{3+}$  was omitted from these experiments. 8-Br-cGMP had no effect on SOCE (Figure 4.14d). In control cultures, the peak fluorescence attained after  $\text{Ca}^{2+}$  re-addition was  $0.64 \pm 0.05$ , compared to  $0.52 \pm 0.05$  after 8-Br-cGMP incubation ( $p = 0.11$ , Figure 4.14e). Parsing neurons into size quartiles also revealed no effect of 8-Br-cGMP ( $p > 0.60$  for all quartiles, Figure 4.14f).

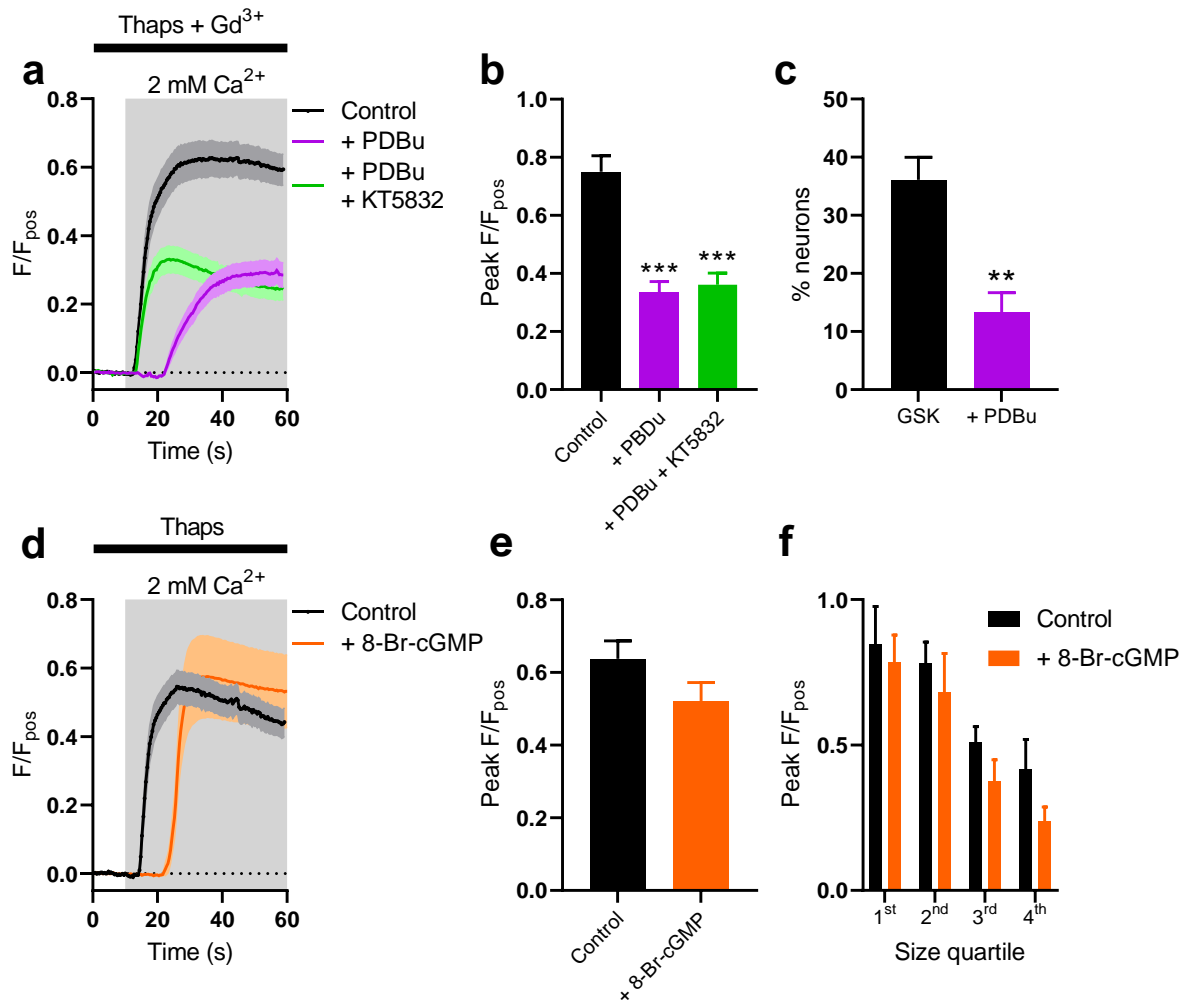


**Figure 4.14 PKC, but not PKG, regulates TRPC3-mediated SOCE**

- (a) Grouped Fluo-4 fluorescence traces showing the re-addition of external Ca<sup>2+</sup> to initiate SOCE in control conditions (black, 155 neurons), in the presence of PDBu (purple, 89 neurons), and in the presence of PDBu and KT5832 (green, 108 neurons). Solid line shows mean, shaded area shows standard error.
- (b) Grouped data showing the peak fluorescence attained during SOCE. Control: 155 neurons, n = 3, N = 3. PDBu: 118 neurons, n = 4, N = 4. PDBu + KT5832: 108 neurons, n = 2, N = 2. Data analysed using a one-way ANOVA with Holm-Sidak post-tests.
- (c) Grouped data showing the proportion of neurons responding to GSK1702934A. Control (GSK): n = 11, N = 5. PDBu: n = 4, N = 4. Data analysed using a two-tailed unpaired t-test.
- (d) Grouped Fluo-4 fluorescence traces from single experiments showing the re-addition of external Ca<sup>2+</sup> to initiate SOCE in control conditions (black, 67 neurons) and in the presence of 8-Br-cGMP (orange, 38 neurons). Solid line shows mean, shaded area shows standard error.
- (e) Grouped data showing the peak fluorescence attained during SOCE. Control: 180 neurons, n = 3, N = 3. 8-Br-cGMP: 123 neurons, n = 3, N = 3. Data analysed using a two-tailed unpaired t-test.
- (f) Grouped data showing the peak magnitude of SOCE for neurons within each size quartile. Data analysed using a two-way ANOVA with Sidak post-tests.

#### **4.2.12. Stimulation of TRPC3 by store-independent pathways**

Whether TRPC3 is a SOC has been the source of considerable debate for over 25 years. Data presented here has indicated that TRPC3 forms a SOC in small-sized sensory neurons. However, it is not clear whether other, store-independent mechanisms are also able to stimulate TRPC3 activity in sensory neurons.

##### **4.2.12.1. Diacylglycerol activates TRPC3 in sensory neurons**

To raise the intracellular concentration of diacylglycerol (DAG), neurons were incubated with RHC80267 (25  $\mu$ M), an inhibitor of DAG lipase, to block DAG breakdown. This resulted in a slow, steady rise in intracellular  $\text{Ca}^{2+}$  (Figure 4.15a and c). The soma area of neurons which exhibited a rise in cytosolic  $\text{Ca}^{2+}$  was  $77.6 \pm 2.4\%$  of that of non-responsive neurons ( $p < 0.0001$ , Figure 4.15d). Pre-incubation with Pyr-3 attenuated the proportion of neurons responding to RHC80267 application (Figure 4.15b) from  $44.2 \pm 8.6\%$  to  $14.0 \pm 4.8\%$  ( $p = 0.02$ , Figure 4.15e). Inhibition of PKC with staurosporine (1  $\mu$ M) did not affect the proportion of neurons responding to RHC80267 ( $63.9 \pm 4.5\%$ ,  $p = 0.10$ , Figure 4.15e). Stimulation of PKC by pre-treatment with PDBu also had no affect the proportion of neurons responding to RHC80267 application ( $41.3 \pm 9.4\%$ ,  $p = 0.80$ , Figure 4.15e). Application of 1-oleoyl-2-acetyl-sn-glycerol (OAG, 100  $\mu$ M), a membrane-permeable analogue of DAG, resulted in a rise in cytosolic  $\text{Ca}^{2+}$  in  $47.8 \pm 14.9\%$  of neurons (Figure 4.15e).

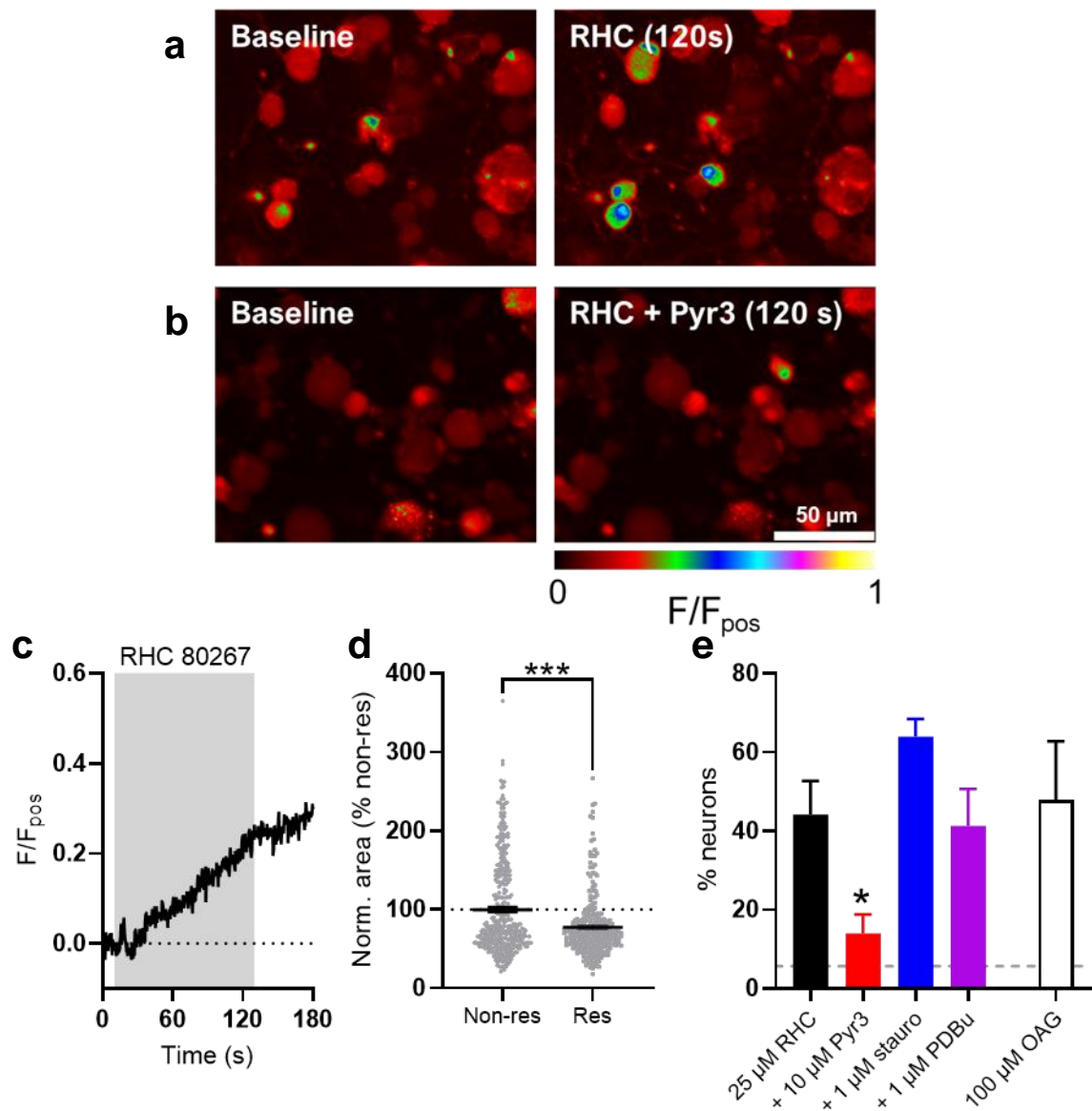


**Figure 4.15 DAG stimulates TRPC3 channels independently of PKC**

- (a) False-coloured images showing Fluo-4 fluorescence before (left) and during (right) RHC80267 application under control conditions.
- (b) False-coloured images showing Fluo-4 fluorescence before (left) and during (right) RHC80267 application in the presence of Pyr-3.
- (c) Example Fluo-4 fluorescence traces from a single neuron during RHC80267 application.
- (d) Grouped data showing the soma area (normalised to the mean of non-responders) of neurons which did and did not respond with a rise in cytosolic  $\text{Ca}^{2+}$  upon RHC80267 application. Non-res: 374 neurons; Res: 271 neurons;  $n = 6$ ,  $N = 5$ .
- (e) Grouped data showing the proportion of neurons responding to RHC80267 (filled bars) or OAG (open bar) application. Control:  $n = 6$ ,  $N = 5$ . Pyr-3:  $n = 4$ ,  $N = 4$ . Staurosporine:  $n = 5$ ,  $N = 5$ . PDBu:  $n = 3$ ,  $N = 3$ . OAG:  $n = 4$ ,  $N = 4$ . Data analysed using a one-way ANOVA with Dunnett's post-tests (excluding the OAG group). Grey dotted line shows the mean response to vehicle (0.1% DMSO;  $5.7 \pm 1.1\%$ ).

#### **4.2.12.2. Ang II-evoked Ca<sup>2+</sup> signals do not require PKC**

Pre-treatment of sensory neurons with staurosporine to inhibit PKC did not appear to affect the neuronal response to Ang II application (Figure 4.16a). Under control conditions, the peak magnitude of the Ca<sup>2+</sup> response to Ang II was  $0.53 \pm 0.07$ , compared to  $0.57 \pm 0.05$  after pre-treatment with staurosporine ( $p = 0.60$ , Figure 4.16b). The proportion of neurons responding to Ang II was also unchanged:  $34.8 \pm 7.5\%$  and  $34.2 \pm 7.1\%$  for control and staurosporine pre-treatment, respectively ( $p = 0.96$ , Figure 4.16c). It is important to note that 1  $\mu\text{M}$  staurosporine is also likely to inhibit the activity of protein kinase A and Ca<sup>2+</sup>-calmodulin-dependent serine-threonine kinase II.

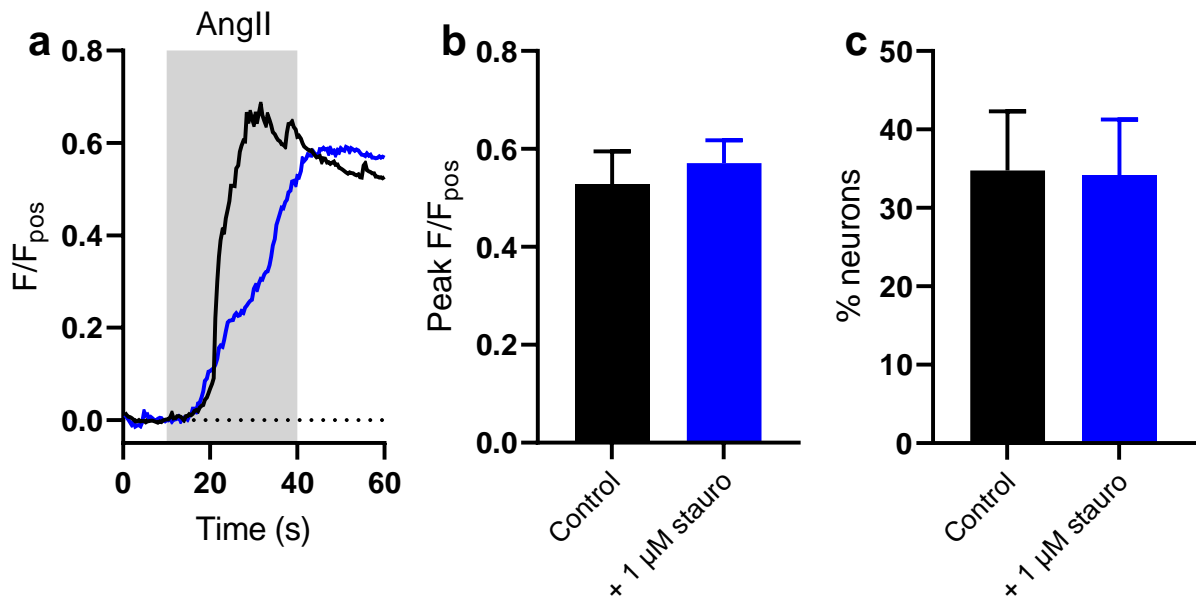


**Figure 4.16 PKC is not required for Ang II-evoked Ca<sup>2+</sup> signals in sensory neurons**

- (a) Example Fluo-4 fluorescence traces showing Ang II application to single neurons under control conditions (black) or after pre-treatment with staurosporine (blue).
- (b) Grouped data showing the peak magnitude of the response to Ang II application. Control: n = 5, N = 3. Stauro: n = 5, N = 3. Data analysed using a two-tailed unpaired t-test.
- (c) Grouped data showing the proportion of neurons responding to Ang II application. Control: n = 5, N = 3. Stauro: n = 5, N = 3. Data analysed using a two-tailed unpaired t-test.

#### **4.2.13. Pre-incubation with vehicles does not affect the response to Ang II**

Many of the drugs used in this Chapter were dissolved either dimethyl sulfoxide (DMSO) or ethanol. To verify that these vehicles did not affect the neuronal response to Ang II, neurons were pre-incubated with the vehicle at its maximal concentration, 0.1% for both DMSO and ethanol. In this set of experiments, under control conditions, Ang II application resulted in a maximal fluorescence of  $0.75 \pm 0.11$ . Neither ethanol ( $0.81 \pm 0.01$ ,  $p = 0.85$ ) nor DMSO ( $0.77 \pm 0.08$ ,  $p = 0.99$ ) pre-incubation had any effect on the magnitude of the response to Ang II (Figure 4.17a and b). The proportion of neurons exhibiting a response to Ang II was  $49.1 \pm 4.1\%$ , compared to  $47.7 \pm 10.7\%$  ( $p = 0.99$ ) and  $37.6 \pm 6.9\%$  ( $p = 0.45$ ) after pre-incubation with ethanol and DMSO, respectively (Figure 4.17c).

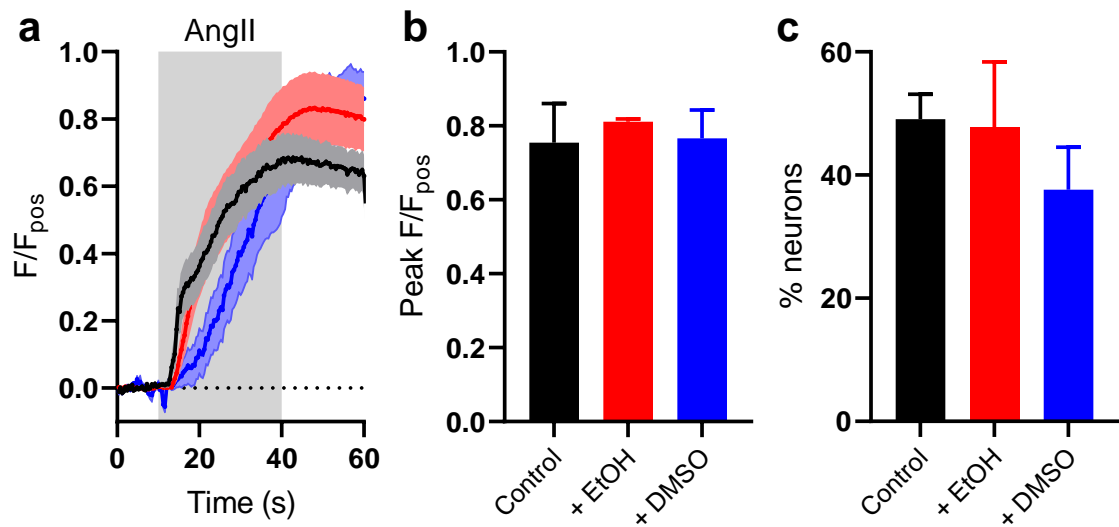


**Figure 4.17 Pre-incubation with ethanol or DMSO had no effect on the response to Ang II**

- (a) Grouped Fluo-4 fluorescence traces from single experiments showing the application of Ang II under control conditions (black), and after ethanol (red) or DMSO (blue) pre-incubation. Control: 33 neurons; ethanol: 36 neurons; DMSO: 15 neurons. Solid line shows mean, shaded area shows standard error.
- (b) Grouped data showing the peak magnitude of the response to Ang II. Control:  $n = 5$ ,  $N = 4$ . Ethanol:  $n = 4$ ,  $N = 4$ . DMSO:  $n = 4$ ,  $N = 4$ . Data analysed using a one-way ANOVA with Dunnett's post-tests.
- (c) Grouped data showing the proportion of neurons responding to Ang II. Control:  $n = 5$ ,  $N = 4$ . Ethanol:  $n = 4$ ,  $N = 4$ . DMSO:  $n = 4$ ,  $N = 4$ . Data analysed using a one-way ANOVA with Dunnett's post-tests.

### 4.3. Discussion

Experiments detailed in this Chapter have resolved a signalling pathway leading to a rise in cytosolic  $[Ca^{2+}]$  in sensory neurons stimulated with Ang II.

#### 4.3.1. Signalling downstream of AT1R

In alignment with data in Chapter 3, two structurally-distinct antagonists of AT1R attenuated the neuronal response to Ang II, while an AT2R antagonist was without effect. This lends further credence to the conclusion that Ang II acts through AT1R and not AT2R, in agreement with transcriptomic studies reporting expression of *Agtr1a* and *Agtr1b*, but not *Agtr2*, in sensory neurons (Usoskin *et al.*, 2015; Zeisel *et al.*, 2018). A component of the response to Ang II remained after blockade of AT1R, presumably representing the response of IB4-negative neurons to Ang II, which is independent of AT1R. In Chapter 3, it was tentatively proposed that TNFR1 may mediate the response of IB4-negative neurons to Ang II. This is in line with the AT1R-independent component of the response to Ang II being dependent on extracellular  $Ca^{2+}$  - indicated by the inhibition of the valsartan-insensitive response by omission of external  $Ca^{2+}$  - as TNFR1 activation stimulates  $Ca^{2+}$  influx through TRP channels (Barker *et al.*, in press, 2022).

Downstream of AT1R,  $Ca^{2+}$  was released from intracellular stores through  $IP_3$  receptor activation, as indicated by the inhibition of Ang II-evoked  $Ca^{2+}$  signals by  $IP_3$  receptor blockade or draining of intracellular  $Ca^{2+}$  stores with thapsigargin. Ang II-evoked  $Ca^{2+}$  signals in rat luteal cells and chemosensory cells from the carotid body were also dependent on AT1R and replete intracellular  $Ca^{2+}$  stores (Pepperell *et al.*, 1993; Murali, Zhang and Nurse, 2014). Direct evidence for  $Ca^{2+}$  store depletion by Ang II was obtained by applying ionomycin to sensory neurons in a  $Ca^{2+}$ -free bathing solution. Under these conditions, the rise in cytosolic  $Ca^{2+}$  is indicative of the content of the intracellular stores (Saraiva *et al.*, 2013; Srivats *et al.*, 2016). Ang II reduced the magnitude of ionomycin-induced  $Ca^{2+}$  transients – and, therefore, depleted  $Ca^{2+}$  stores – in only small-sized neurons, consistent with the conclusions from Chapter 3.

After depletion of intracellular  $Ca^{2+}$  stores by Ang II, addition of 2 mM  $Ca^{2+}$  to the external bathing solution resulted in a substantial rise in cytosolic  $Ca^{2+}$  resembling SOCE. What's more, the removal of  $Ca^{2+}$  from the bathing solution attenuated the response to Ang II; both of these observations indicate that Ang II also evokes  $Ca^{2+}$  influx. The channel conveying this influx of  $Ca^{2+}$  was assumed to belong to the TRP

family because of their high expression in sensory neurons and permeability to  $\text{Ca}^{2+}$ . Voltage-gated  $\text{Ca}^{2+}$  channels were excluded because Ang II-evoked  $\text{Ca}^{2+}$  signals did not depend on membrane depolarisation. That being said, PLC-coupled pathways are exquisitely sensitive to temperature and the components of this pathway are easily dialysed during whole-cell recording. Perhaps different results would be obtained if these experiments were carried out at  $37^\circ\text{C}$  in the perforated patch configuration.

There is an extensive literature showing that Ang II-evoked processes – including  $\text{Ca}^{2+}$  signals – require TRPC3. In cells heterologously expressing AT1R, the application of Ang II evoked a transient rise in cytosolic  $\text{Ca}^{2+}$  which was potentiated and significantly prolonged by the co-expression of TRPC3 (Zitt *et al.*, 1997). What's more, in cells expressing both AT1R and TRPC3, Ang II evoked a transient inward current which was absent in cells lacking TRPC3 (Zitt *et al.*, 1997). In a study of mouse cardiomyocytes, Ang II induced a slowly-developing increase in stretch-evoked  $\text{Ca}^{2+}$  transients (Yamaguchi *et al.*, 2018). This effect of Ang II was abolished by TRPC3 inhibition with Pyr3, or RNAi-mediated knock-down of TRPC3 (Yamaguchi *et al.*, 2018). Over more prolonged durations, Ang II has also been found to induce cardiac hypertrophy. This pathophysiological change also requires  $\text{Ca}^{2+}$  influx through TRPC3 and the closely related channel, TRPC6 (Onohara *et al.*, 2006). Finally, adrenal chromaffin cells exhibited a rise in cytosolic  $\text{Ca}^{2+}$  and catecholamine secretion in response to a  $\beta$ -arrestin-biased AT1R agonist which was abolished by inhibition of TRPC3, and absent in cells from mice lacking TRPC3 (Liu *et al.*, 2017). Together, these observations demonstrate the coupling between AT1R and TRPC3 across diverse cell types, which is also reconstituted in a heterologous expression system. Given the co-expression of AT1R and TRPC3 in non-peptidergic sensory neurons, it was hypothesised that these channels mediate  $\text{Ca}^{2+}$  influx downstream of Ang II application. More evidence to support the hypothesis that TRPC3 lies downstream of AT1R could be ascertained by co-applying valsartan and Pyr3. If these two drugs exhibit a non-additive inhibition of the response to Ang II, it is likely that they are blocking the same pathway; that is, AT1R and TRPC3 are part of the same pathway.

Blockade of TRPC3 channels with Pyr3 ameliorated the neuronal response to Ang II, suggesting that these channels may well convey  $\text{Ca}^{2+}$  influx. Pyr3 is highly selective for TRPC3, showing no inhibitory effect on any other member of the TRPC family up to  $10\ \mu\text{M}$  (Kiyonaka *et al.*, 2009). Agonist-induced tachyphylaxis of TRPC3 channels

also reduced the neuronal response to Ang II, providing further evidence that TRPC3 mediates a component of Ang II-evoked  $\text{Ca}^{2+}$  signals. As seems to be case in many other cell types, it appears that in sensory neurons co-expressing AT1R and TRPC3, Ang II evokes  $\text{Ca}^{2+}$  signals which depend – at least in part – on TRPC3 channels.

#### **4.3.2. Mechanisms underpinning the activation of TRPC3**

Unlike many other TRP channels, TRPC3 is not directly activated by extracellular stimuli, such as heat and acid in the case of TRPV1 (Caterina *et al.*, 1997), or reactive oxygen species in the case of TRPA1 (Bessac *et al.*, 2008; Sullivan *et al.*, 2015). Rather, TRPC3 activity is tightly coupled to the activity of upstream receptors, such as the histamine H1 receptor (Hofmann *et al.*, 1999) or the neurotrophin receptor TrkB (Li, Xu and Montell, 1999). Despite over two decades of work, it remains unclear whether or not TRPC3 forms store-dependent or -independent channels. The application of thapsigargin to cortical neurons in  $\text{Ca}^{2+}$ -containing bathing solution induced a prolonged rise in cytosolic  $\text{Ca}^{2+}$  that could be attenuated by the SOCE inhibitors, YM58483 and 2-ABP (González-Sánchez *et al.*, 2017). This observation demonstrates that – under physiological conditions – store depletion and SOCE occur over similar timescales. Therefore, TRPC3 activation upon Ang II application may well be as a result of SOCE occurring over a similar timescale to store depletion. Consequently, it was necessary to employ different experimental protocols to resolve the mechanism(s) contributing to SOCE and TRPC3 activation.

Rather than pre-incubating neurons with  $\text{Ca}^{2+}$ -free or Pyr3-containing bathing solutions, they were instead applied to fully-developed Ang II-evoked  $\text{Ca}^{2+}$  signals in an attempt to temporally distinguish store release and SOCE. While these two processes initially occur over similar timescales, SOCE is prolonged, outlasting store release (Venkatachalam *et al.*, 2002). As such, the sustained part of the  $\text{Ca}^{2+}$  signal is likely to be largely dependent on SOCE. Indeed, this sustained component appeared to be dependent on continued  $\text{Ca}^{2+}$  entry from the bathing solution, in part through TRPC3 channels.

To more effectively isolate SOCE, intracellular  $\text{Ca}^{2+}$  stores were depleted by incubation with thapsigargin in  $\text{Ca}^{2+}$ -free buffer. This activates the machinery required for SOCE, but no  $\text{Ca}^{2+}$  entry is observed due to the lack of extracellular  $\text{Ca}^{2+}$ . Upon the re-addition of external  $\text{Ca}^{2+}$ , SOCE can be observed (see 4.2.8.). Here, it was

found that SOCE was dependent on Pyr3-sensitive TRPC3 channels (Kiyonaka *et al.*, 2009), as well as Gd<sup>3+</sup>-sensitive Orai channels (Trebak *et al.*, 2003; Azimi *et al.*, 2020). These results are similar to those obtained in rat sensory neurons in which Pyr10 – another TRPC3 blocker – and Gd<sup>3+</sup> were used to resolve the function of TRPC3 and Orai channels, respectively, in neuronal SOCE (Séguéla *et al.*, 2014). Inhibition of STIM function almost abolished SOCE – a greater inhibition than Pyr3 and Gd<sup>3+</sup> applied together. This was not the case in rat sensory neurons, in which Pyr10 and Gd<sup>3+</sup> together abolished SOCE (Séguéla *et al.*, 2014), and may suggest a third channel contributes to SOCE in mouse sensory neurons. Parsing neurons by size revealed that TRPC3 channels only contributed to SOCE in small-sized neurons, while Orai channels only contributed in large-sized neurons. This is in agreement with the expression of TRPC3 in small-diameter non-peptidergic neurons (Usoskin *et al.*, 2015). A component of SOCE in small-sized neurons was insensitive to both Pyr3 and Gd<sup>3+</sup>, but was inhibited by ML-9, suggesting that a third STIM-interacting channel contributes to SOCE in these neurons. TRPC6 is closely related to TRPC3 and the two channels are highly co-expressed in mouse sensory neurons (Usoskin *et al.*, 2015; Zeisel *et al.*, 2018). TRPC6 has been shown to function in SOCE in vascular smooth muscle cells, but only when in a heteromeric channel formation with TRPC4 (Zhang *et al.*, 2018). TRPC4 is poorly co-expressed with TRPC6 in mouse sensory neurons (Zeisel *et al.*, 2018), though perhaps TRPC3 and TRPC6 are able to form heteromeric store-operated channels which lack sensitivity to Pyr3. TRPC3 and TRPC6 subunits co-immunoprecipitate and exhibit high resonance energy transfer (RET) when fluorescently tagged, suggesting that they're able to form heteromeric assemblies, though the pharmacological properties of these assemblies have not been fully resolved (Hofmann *et al.*, 2002).

There is little consensus in the literature on whether or not TRPC3 forms store-operated channels. TRPC3 was first described as a store-operated channel in 1996: expression of *Htrpc3* in COS cells augmented SOCE, while antisense oligonucleotides directed against multiple members of the *Trpc* family attenuated SOCE in a fibroblast cell line (Zhu *et al.*, 1996). However, it was subsequently shown that DAG could directly activate TRPC3 channels expressed in HEK293 cells downstream of the activation of PLC-coupled GPCRs, and that TRPC3-mediated currents were insensitive to store depletion by thapsigargin (Hofmann *et al.*, 1999; Trebak *et al.*,

2003). Similarly conflicting reports on the mechanisms of TRPC3 activation continued to emerge long after the initial cloning of *Trpc3*. In an avian B lymphocyte cell line, for example, TRPC3 expression potentiated SOCE (Vazquez *et al.*, 2001), while in CHO cells, TRPC3 activity was independent of store depletion (Zitt *et al.*, 1997). More recently, SOCE in rat sensory neurons was abrogated by a TRPC3-selective inhibitor (Séguéla *et al.*, 2014), while SOCE in platelets from mice lacking TRPC3 and TRPC6 was comparable to that of wildtype littermates (Harper *et al.*, 2013).

Perhaps the cell type in which TRPC3 is expressed determines the functional properties of the channel. The cell type will determine the binding partners available to TRPC3, as well as the channel's localisation and proximity to other machinery within the cell, all of which can impact channel properties. It also seems that the level of expression of TRPC3 – which may differ between cell types – determines its mode of activation. When expressed at low levels in avian B lymphocytes, TRPC3 forms a store-operated channel, but this property is lost when the channel is expressed at higher levels (Vazquez *et al.*, 2003). Additionally, when more highly expressed, TRPC3 exhibited sensitivity to OAG, an analogue of DAG (Vazquez *et al.*, 2003). The magnitude of SOCE mediated by a TRPC3 homologue from rat brain was inversely correlated with time after transfection, in line with elevated expression of TRPC3 negating its sensitivity to store depletion (Preuß *et al.*, 1997). Many properties of ion channels can be regulated by expression level, but why might a given property – such as sensitivity to store depletion – be lost upon elevated expression? TRPC3 may form complexes with other proteins which confer sensitivity to store depletion. Increasing the expression of TRPC3, such that it is in excess relative to other members of these complexes, increases the probability that incomplete or stoichiometrically unfavourable complexes are formed (Vazquez *et al.*, 2003). Based on these experiments, one would expect TRPC3 expression in sensory neurons to be low enough to permit the proper formation of store-operated complexes – though this is difficult to ascertain – and to be co-expressed with binding partners known to function in SOCE.

The robust inhibition of SOCE by blocking STIM function indicates that both Orai and TRPC3 channel function depends on STIM. It is well-established that STIM-Orai interactions mediate SOCE (Mercer *et al.*, 2006; Soboloff *et al.*, 2006; Hewavitharana *et al.*, 2007), but whether STIM interacts with TRPC3 is less clear. RNAi-mediated

knock-down of STIM1 attenuated endogenous, Gd<sup>3+</sup>-sensitive SOCE in HEK293 cells (Dehaven *et al.*, 2009). Transiently expressed TRPC3 gave rise to Gd<sup>3+</sup>-insensitive SOCE which was unaffected by overexpression of STIM1, suggesting that these proteins do not interact (Dehaven *et al.*, 2009). However, it was not shown that TRPC3-mediated SOCE is reduced by loss or inhibition of STIM1. In a later study, increasing amounts of an RNAi directed against STIM1 was found to progressively inhibit TRPC3-mediated currents, suggesting an interaction between STIM1 and TRPC3 (Lee *et al.*, 2014).

It has been proposed that Orai interacts with TRPC3 to confer sensitivity to STIM. TRPC3-mediated SOCE was inhibited by the expression of the non-functional R91W mutant of Orai1 (Liao *et al.*, 2009), which is associated with severe combined immunodeficiency (Thompson, Mignen and Shuttleworth, 2009), while wild-type Orai1 had no such effect. Co-immunoprecipitation revealed an association between TRPC3 and Orai1 *in vitro*, and a potentiation of SOCE in TRPC3-expressing cells by co-expression of Orai1 has also been reported (Liao *et al.*, 2007). The authors of these studies posited that Orai, through its interaction with STIM, confers sensitivity to store depletion to TRPC3 by forming a multimeric protein complex. Beyond a role for Orai, TRPC1 has been implicated in SOCE – both alone and in tandem with TRPC3. In a cell line derived from human salivary gland tissue, antisense oligonucleotides against *Trpc1* attenuated SOCE, with a similar effect being found with transiently transfected TRPC1 lacking a functional pore domain (Liu, Singh and Ambudkar, 2003). In the inactive state, the N- and C-terminal domains of TRPC3 interact via coiled-coil domains, prohibiting an interaction with STIM; TRPC1 may complex with TRPC3, causing dissociation of its N- and C-terminal domains and permitting an interaction with STIM (Lee *et al.*, 2014). RNAi-mediated knock-down of TRPC1 resulted in a loss of sensitivity of TRPC3 to store depletion (Lee *et al.*, 2014).

While experiments presented here suggest an interaction between TRPC3 and STIM in mouse sensory neurons, the nature of this interaction is not clear. There is little evidence that TRPC3 and STIM are able to directly interact – an intermediate, such as Orai1 or TRPC1, seems to be required to mediate the interaction. In sensory neurons, TRPC3 is highly co-expressed with both Orai1 (as well as Orai2 and Orai3) and TRPC1 (Zeisel *et al.*, 2018), so an interaction amongst these proteins cannot be excluded as a possibility. To further test the interaction between STIM and TRPC3,

one could make use of tissue-specific knock-out of STIM1 or STIM2, both of which are expressed in sensory neurons (Zeisel *et al.*, 2018). Global knock-out of STIM1 or STIM2 results in either perinatal lethality or death shortly after birth – reaffirming the vital role of these proteins (Oh-hora *et al.*, 2008; Varga-Szabo *et al.*, 2008). Even in the case of targeted loss of STIM1/2 in sensory neurons – say, by using Advillin-Cre – it is likely that the mice generated will exhibit some deleterious phenotypes. Instead, neurons from wild-type mice could be transfected with RNAi against STIM1/2 to knock-down expression. A similar approach could be taken with Orai1/2/3 and TRPC1 to examine their role in TRPC3-mediated SOCE.

In mouse sensory neurons, it appears that TRPC3 is sensitive to both store depletion and DAG. The application of OAG, a commonly-used membrane-permeable DAG analogue, raised cytosolic Ca<sup>2+</sup> in a similar proportion of neurons as a TRPC3 agonist. However, it was not shown whether OAG-evoked Ca<sup>2+</sup> signals were sensitive to block by Pyr3. Raising the concentration of endogenous DAG through the inhibition of DAG lipase resulted in a steady rise in cytosolic Ca<sup>2+</sup> which was attenuated by Pyr3. This method of increasing endogenous DAG has been shown to stimulate recombinant TRPC3 channels (Hofmann *et al.*, 1999; Venkatachalam, Zheng and Gill, 2003). Inhibition of PKC by staurosporine had no effect on the response to raised DAG, indicating that DAG stimulation of TRPC3 is PKC-independent and likely direct (Hofmann *et al.*, 1999). Thus, TRPC3 expressed in sensory neurons appears to be sensitive to both store depletion and DAG. This observation has been reported previously. At low expression levels in avian B lymphocytes, TRPC3 is sensitive to both store depletion and DAG (Vazquez *et al.*, 2003). What's more, a non-selective cation channel activated by store depletion – with properties similar to those of heterologously expressed TRPC3 and TRPC6 channels – was also directly activated by OAG (Su *et al.*, 2001). In a prostate smooth muscle cell line, antisense oligonucleotides directed against TRPC3 abrogated Ca<sup>2+</sup> entry evoked by both OAG and thapsigargin (Thebault *et al.*, 2005).

Despite the sensitivity of sensory neuronal TRPC3 channels to DAG, activation of TRPC3 downstream of Ang II application seems to be entirely dependent on STIM function and, hence, store depletion. This conclusion is based on the loss of inhibitory effect of Pyr3 on Ang II-evoked Ca<sup>2+</sup> signals in the presence of ML-9: inhibition of STIM function blocks Ang II-mediated TRPC3 activation. Activation of AT1R liberates DAG

(Forrester *et al.*, 2018); though this was not shown directly here, this conclusion can be inferred from the requirement for PLC and IP<sub>3</sub> receptors for Ang II-evoked Ca<sup>2+</sup> signals. Why does DAG liberated by Ang II application not stimulate TRPC3 channels? It may be that AT1R and TRPC3 reside in different membrane domains held at a distance too great for DAG to traverse before being metabolised. Spatially restricted DAG signalling has been reported downstream of P2Y receptor activation by ATP (Wuttke, Idevall-Hagren and Tengholm, 2013). The C-terminus of AT1R contains a caveolin binding domain, suggesting an association with lipid rafts (Adebiyi *et al.*, 2014). Caveolin is also required for the trafficking of AT1R to the plasma membrane, while RET measurements demonstrated an association between AT1R and markers of lipid rafts in the resting state (Wyse *et al.*, 2003; Balla *et al.*, 2012). These data suggest that AT1R resides within lipid rafts in the plasma membrane, while – in platelets, at least – TRPC3 channels assemble independently of lipid rafts (Brownlow and Sage, 2005), consistent with TRPC3-mediated Ca<sup>2+</sup> entry occurring outside of lipid rafts (Liao *et al.*, 2009). The spatial restriction of the Ang II-evoked DAG signal could be tested by incubating neurons with inhibitors of DAG lipase and kinase to extend the distance over which DAG can diffuse before being metabolised. If the subsequent response to Ang II – in the presence of Xestospongine C or ML-9 to block store depletion-evoked TRPC3 activity – is sensitive to inhibition by Pyr3, then TRPC3 must have been stimulated by DAG.

Data in this Chapter indicates that Ang II, through AT1R coupling to PLC, stimulates the release of Ca<sup>2+</sup> from IP<sub>3</sub>-sensitive intracellular stores. This store depletion leads to the activation of STIM, which, in turn, interacts with TRPC3 to permit Ca<sup>2+</sup> entry from the extracellular milieu (Figure 4.18).

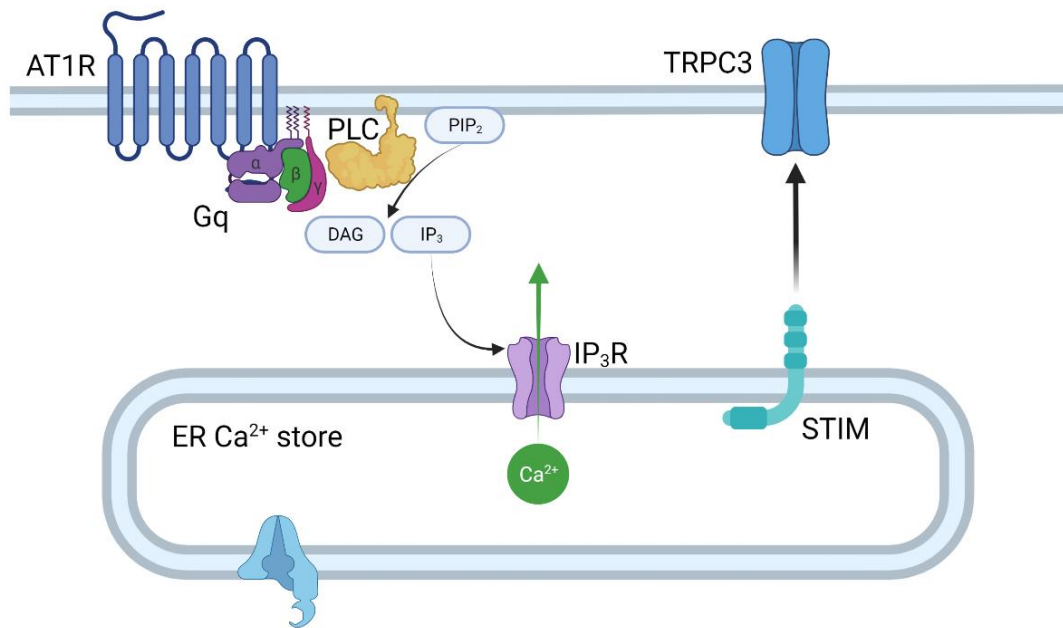


**Figure 4.18 Proposed mechanisms underpinning Ang II-evoked  $\text{Ca}^{2+}$  signals in sensory neurons**

Ang II application stimulates AT1R and, consequently, Gq and PLC. This results in the liberation of  $\text{IP}_3$  which goes on to open  $\text{IP}_3$  receptors, allowing  $\text{Ca}^{2+}$  release from intracellular stores. Depletion of  $\text{Ca}^{2+}$  in the intracellular store stimulates STIM, such that it is now able to interact with plasma membrane TRPC3 channels, permitting  $\text{Ca}^{2+}$  entry in a store-dependent manner.

### 4.3.3. Regulation of TRPC3 channels by PKC

Incubation of cells with phorbol esters, such as PDBu, for brief durations of time – 10-15 minutes – stimulates PKC (Trebak *et al.*, 2003). Here, this stimulation of PKC resulted in a suppression of TRPC3 activity when the channel was activated by either store depletion or a selective agonist. Physiologically, PKC sits downstream of DAG production, requiring this lipid and  $Ca^{2+}$  for its activity. For some novel isoforms of PKC, such as PKC $\delta$ , which is enriched in TRPC3-expressing sensory neurons (Usoskin *et al.*, 2015), DAG binding alone is sufficient for kinase activity (Kikkawa, Matsuzaki and Yamamoto, 2002). It is possible that PKC serves as a negative regulator to temper TRPC3-mediated  $Ca^{2+}$  entry, avoiding the potential cytotoxic effects of prolonged elevations in cytosolic [ $Ca^{2+}$ ].

Previous reports have investigated the regulation of TRPC3 channels and found similar results to those present here. Incubation of HEK293 cells stably expressing TRPC3 with PMA, another phorbol ester, for a short duration abolished OAG-induced  $Ca^{2+}$  signals (Trebak *et al.*, 2003; Venkatachalam, Zheng and Gill, 2003). Conversely, prolonged incubation with PMA downregulates PKC, which was found to have no effect on the cellular response to OAG (Trebak *et al.*, 2003). This parallels experiments in this Chapter showing that PKC inhibition did not affect the response to Ang II – a component of which depends on TRPC3 – or to raised DAG which stimulates TRPC3 directly. PKC phosphorylates Serine 712 on TRPC3, resulting in a suppression of TRPC3-mediated  $Ca^{2+}$  entry (Trebak *et al.*, 2005). Substitution for Serine 712 for Alanine (S712A) yielded a PKC-resistant TRPC3 channel which conveyed greater agonist-induced  $Ca^{2+}$  compared to the wild-type channel, suggesting tonic inhibition of TRPC3 function by PKC in HEK293 cells (Trebak *et al.*, 2005).

In addition to a role for PKC, it has also been put forward that PKG acts as a negative regulator of TRPC3. PKC can directly inhibit TRPC3 via phosphorylation at S712, and indirectly via PKG (Trebak *et al.*, 2005; Kwan, Huang and Yao, 2006). In HEK293 cells transiently transfected with human TRPC3 and PKG, PMA-mediated inhibition of TRPC3 could be partially reversed by inhibition of PKG (Kwan, Huang and Yao, 2006). Sites on TRPC3 containing PKG phosphorylation sequences were identified, and their loss abolished PKC- and PKG-mediated phosphorylation and inhibition of TRPC3 (Kwan, Huang and Yao, 2004, 2006). Consistently, stimulation of PKG activity with 8-Br-cGMP attenuated  $Ca^{2+}$  entry through TRPC3 (Kwan, Huang and Yao, 2004). These

results were not recapitulated in experiments detailed in this Chapter. Inhibition of PKG failed to reverse PKC-mediated suppression of TRPC3-mediated SOCE. Further, activation of PKG by incubation with 8-Br-cGMP had no effect on SOCE. Transfection of PKG in HEK293 cells was required to observe an effect of 8-Br-cGMP on TRPC3-mediated  $\text{Ca}^{2+}$  entry; perhaps PKG expression is lacking in TRPC3-expressing sensory neurons. At the transcript and protein level, PKG is broadly expressed across all sensory neuron populations, and enriched in small-diameter neurons (Qian *et al.*, 1996; Usoskin *et al.*, 2015). Stimulation of PKG potentiated neuronal hyperexcitability after nerve injury (Song *et al.*, 2006). Therefore, PKG appears to be present and functional in sensory neurons.

A further consideration is whether mouse TRPC3 contains PKG phosphorylation sites, given that the studies discussed above pertain to recombinantly expressed human TRPC3. Human TRPC3 can be phosphorylated by PKG at T11 and S263 (Kwan, Huang and Yao, 2004, 2006). Alignment of the amino acid sequences of human and mouse TRPC3 reveals the conservation of sites equivalent to S263 and S712, but a lack of T11 in mouse TRPC3 (Figure 4.19). The conservation of S712 provides a likely mechanism for PKC-mediated inhibition of mouse TRPC3. Human TRPC3 lacking T11 was markedly less sensitive to inhibition by PKG compared to wild-type TRPC3 (Kwan, Huang and Yao, 2004), providing a possible explanation for the lack of PKG-sensitivity of mouse TRPC3.

Suppression of TRPC3-mediated  $\text{Ca}^{2+}$  entry by PKC appears to be dependent on the mechanism by which the channels are activated. TRPC3 stimulated by  $\text{Ca}^{2+}$  store depletion is inhibited by PKC, whereas DAG-stimulated TRPC3 is not. In recombinant expression systems, TRPC3 activated by OAG is suppressed by PKC activation (Trebak *et al.*, 2003, 2005; Venkatachalam, Zheng and Gill, 2003; Kwan, Huang and Yao, 2006). However, endogenous TRPC3 is not always sensitive to inhibition by PKC. For example, in cerebellar Purkinje neurons, mGluR1-mediated currents are carried by TRPC3, but these currents are resistant to inhibition by PKC (Nelson and Glitsch, 2012). However, this study did not resolve whether the mode of activation of TRPC3 determined its regulation by PKC.

This observation may be explained by three potential mechanisms. (1) A single population of TRPC3 (or TRPC3 subunit-containing, defined by their sensitivity to

Pyr3) channels is differentially regulated by PKC. When STIM interacts with TRPC3 downstream of store depletion, the PKC binding/phosphorylation site is accessible, but DAG occludes this site (Figure 4.20a). (2) A single population of channels can dynamically interact with different binding partners, some of which preclude the binding of PKC (Figure 4.20b). (3) Two populations of TRPC3 subunit-containing channels exist in sensory neurons; this may be one population of homomeric TRPC3 channels and one population of heteromeric TRPC3/6 channels, for instance, but this is not known. One population is activated by an interaction with STIM, and is sensitive to PKC, while the other population is activated by DAG, but is insensitive to PKC (Figure 4.20c). Evidence for mechanism (2) comes from a study by Lee *et al* (2014) discussed above. The authors demonstrated that the N- and C-termini of TRPC3 closely interact in the absence of STIM/TRPC1 – i.e., when  $Ca^{2+}$  stores are replete – which may hinder the interaction of PKC with S712, which is close to the channel's C-terminus. DAG is thought to bind closer to the membrane-spanning domains of the channel, with particular focus on transmembrane helix one and the linker between transmembrane helices three and four (Fan *et al.*, 2018). Under these conditions, one may predict that TRPC3 is sensitive to activation by DAG, but insensitive to phosphorylation by PKC. Yet, if  $Ca^{2+}$  stores are depleted, the N- and C-termini of TRPC3 dissociate, providing access for interactions with both STIM and PKC. Whether any of these proposed mechanisms reflect the reality in sensory neurons is not clear from the current data.

```

Mouse 1  -----MRDKGRRQAVRGPAPFMFGARGPSLTAAEEERFLDAAEYGNIPVVRKMLEESRTLNVNCVDYMGQNALQL 68
Human 1  MEGSPSLRRMTVMREKGRQAVRGPAPFMFNDRGTSLTAAEEERFLDAAEYGNIPVVRKMLEESKTLNVNCVDYMGQNALQL 80
          ↑T11
69  AVGNEHLEVTPELLKKENLARIGDALLAISKGYVRIVEAAILGHPGFAASRRLT LSPCEQELRDDDFYAYDEGDGTRFSPD 148
81  AVGNEHLEVTPELLKKENLARIGDALLAISKGYVRIVEAAILNHPGFAASKRLT LSPCEQELQDDDFYAYDEGDGTRFSPD 160

149  IPTIILAAACHKYEVVHLLLLKGARIERPHDYFCRSDCAEKQLDAFSSHRSRINAYKGLASPAYLSLSEDPVLTALE 228
161  IPTIILAAHCQKYEVVHMLLMKGARIERPHDYFCCKGDCMEKQRHDSFSSHRSRINAYKGLASPAYLSLSEDPVLTALE 240

229  LSNELAKLANIEKEFKNDYRKLMSQCKDFVVGVLDCRDSEEEVAILNGDLESAEPLERHGHKASLSRVKLAIKYEVKKF 308
241  LSNELAKLANIEKEFKNDYRKLMSQCKDFVVGVLDCRDSEEEVAILNGDLESAEPLVHRHKASLSRVK----- 310
          ↑S263
309  VAHPNCQQQLLTIWYENLSGLREQTIAIKCLVVLVWALGLPFLAIGYMIAPCSR LGKILRSPFMKFAVAHAASF IIFLGLL 388
311  -----LAIKYEY---KLGKILRSPFMKFAVAHAASF IIFLGLL 345

389  VFNASDRFEGITTLPNITVIDYPKQIFRVKTTQFTWTEMLIMVWVWGMMWSECKELWLEGPREYIVQLWNVLDFGMLSIF 468
346  VFNASDRFEGITTLPNITVTDYPKQIFRVKTTQFTWTEMLIMVWVWGMMWSECKELWLEGPREYIQLWNVLDFGMLSIF 425

469  IAAFTARFLAFLQATKAQQVVDSHVQESDLSEVTLPEEVQYFTYARDKWLPSDPQIISEGLYAIAVVLSFSRIAYILPAN 548
426  IAAFTARFLAFLQATKAQQVVDYVQESDLSEVTLPEEQYFTYARDKWLPSDPQIISEGLYAIAVVLSFSRIAYILPAN 505

549  ESFGPLQISLGRTVKDIFKFMVLFIMVFLAFMIGMFI LYSYLLGAKVNAFTTVEESFKTLFWSIFGLSEVTSVWLKYDH 628
506  ESFGPLQISLGRTVKDIFKFMVLFIMVFAFMIGMFI LYSYLLGAKVNAFTTVEESFKTLFWSIFGLSEVTSVWLKYDH 585

629  KFIENIGYVLYGIYNVTMVVLLNMLIAMINSSYQEI EDDSDVEWKFARSKLWLSYFDDGKTLPPFSLVSPKSFVYFI 708
586  KFIENIGYVLYGIYNVTMVVLLNMLIAMINSSYQEI EDDSDVEWKFARSKLWLSYFDDGKTLPPFSLVSPKSFVYFI 665

709  MRITNFSKCRRRRLQKDELGMGNSKSRLNLFQSN SRFESHFSNLSLNQPTRYQQIMKRLIKRYVLKAQVDKENDEVN 788
666  MRIVNFPKCRRRRLQKDIEMGMGNSKSRLNLFQSN SRFESHFSNLSLNQPTRYQQIMKRLIKRYVLKAQVDKENDEVN 745
          ↑S712
789  EGELKEIKQDISSLRYELLEDKSQATEELAILIHK LSEKLNPSVLRC 836
746  EGELKEIKQDISSLRYELLEDKSQATEELAILIHK LSEKLNPSMLRC 793

```

**Figure 4.19 PKC and PKG phosphorylation sites on mouse and human TRPC3**

Amino acid sequences for mouse and human TRPC3 were compiled and aligned using the BLAST constraint-based multiple alignment tool. Residues highlighted in red are conserved between species, while those in blue differ. Phosphorylation sites for PKC (S712) and PKG (T11 and S263) are highlighted. T11 is not conserved in mouse TRPC3, offering a potential mechanism for PKG-insensitivity of mouse TRPC3.

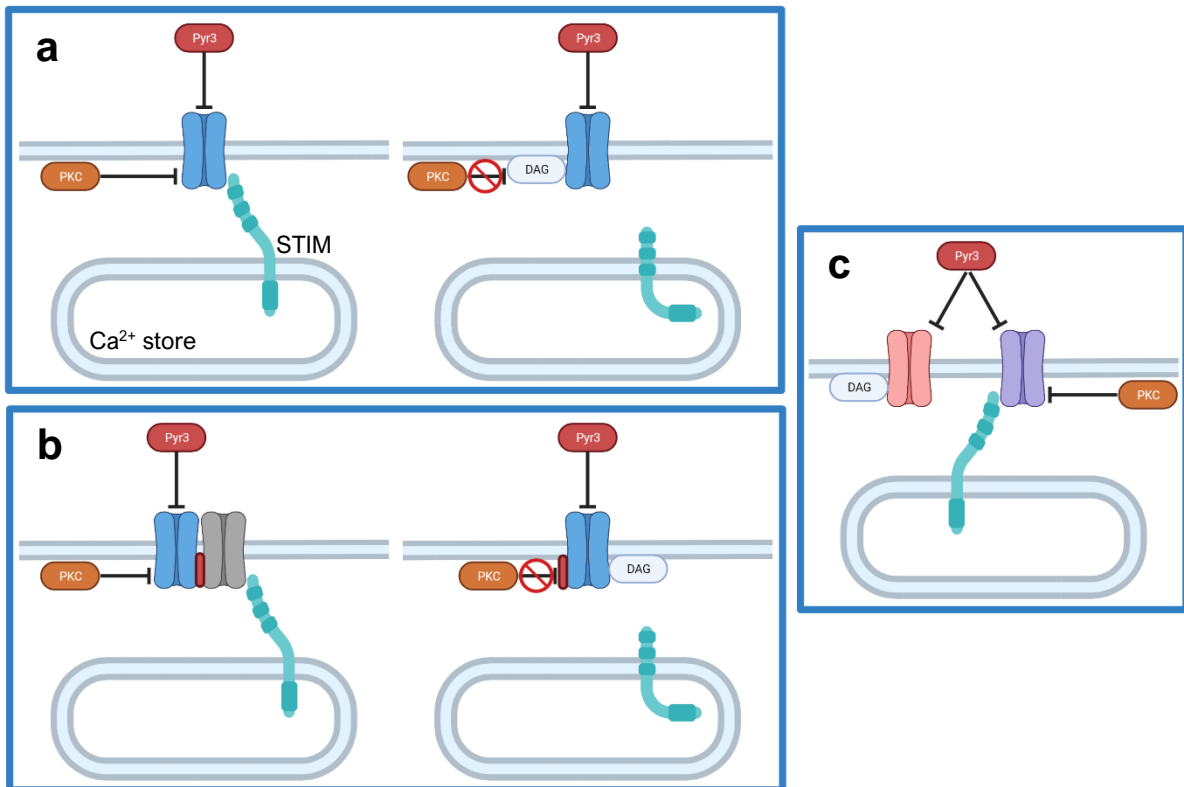


**Figure 4.20 Regulation of TRPC3 channels by PKC**

- (a) A single population of TRPC3 channels (blue channels) is differentially regulated by PKC depending on whether STIM or DAG is bound. STIM binding does affect the interaction with PKC (*left*), but DAG binding precludes an interaction with PKC (*right*).
- (b) A single population of channels interacts with multiple binding partners which determines regulation by PKC, similar to the mechanism proposed by Lee *et al* (2014). When stores are depleted (*left*), TRPC3 interacts with STIM and TRPC1 (grey channel), causing a conformational change permitting an interaction with PKC (see text). When stores are replete (*right*), such a conformational change cannot occur due to a lack of interaction with STIM and TRPC1. The conformation of TRPC3 prohibits an interaction with PKC.
- (c) Two populations of TRPC3 subunit-containing channels are present. Due to other subunits present (e.g., TRPC6), or the structure of the channels, one population is store-dependent and sensitive to inhibition by PKC, while the other population is insensitive to PKC but is stimulated by DAG.

#### **4.4. Key points**

Experiments outlined in this Chapter have demonstrated that:

- i. Ang II signals through AT1R to release  $\text{Ca}^{2+}$  from intracellular stores in sensory neurons.
- ii. TRPC3 is a store-operated channel in small-sized, TRPV1-expressing sensory neurons.
- iii. Ang II stimulates SOCE through TRPC3.
- iv. PKC negatively regulates TRPC3 channel function.

## **Chapter 5**

### **Ang II-evoked Ca<sup>2+</sup> signals drive nuclear translocation of Nuclear Factor of Activated T-cells 5 (NFAT5)**

## 5.1. Introduction

Experiments outlined so far in this Thesis have shed some light on the mechanisms of Ang II-evoked  $\text{Ca}^{2+}$  signals in cultured sensory neurons. The function of these  $\text{Ca}^{2+}$  signals remains to be understood.  $\text{Ca}^{2+}$  is a ubiquitous second messenger which can influence myriad signalling pathways. SOCE is known to provide a sustained source of  $\text{Ca}^{2+}$  associated with changes in neuronal gene expression (Mitra and Hasan, 2022). This is achieved through enzyme-mediated changes in the activity and/or localisation of transcription factors.

### 5.1.1. Nuclear Factor of Activated T-cells

Nuclear Factor of Activated T-cells (NFAT) is a family of transcription factors, initially made up of four members, NFAT1-4, with NFAT5 being attributed to this family later. The family was first identified through its role in the stimulation of IL2 expression in T cells following T-cell receptor activation (Durand *et al.*, 1988; Shaw *et al.*, 2010). In T-cells, and other immune cells, SOCE is of paramount importance in mounting an immune response, as evidenced by loss-of-function mutations in the proteins required for SOCE – such as R91W in Orai1 – resulting in severe combined immunodeficiency (Thompson, Mignen and Shuttleworth, 2009). SOCE provides a source of  $\text{Ca}^{2+}$  needed for immediate secretion of cytokines, as well as for transcriptional changes leading to proliferation and differentiation (Gwack *et al.*, 2007). This function of SOCE is not limited to immune cells, and it is now clear that SOCE does not function solely to replenish  $\text{Ca}^{2+}$  stores, but it an important component of  $\text{Ca}^{2+}$  signalling in neurons (Majewski and Kuznicki, 2014).

The function of NFAT relies on its translocation into the nucleus following raised cytosolic  $\text{Ca}^{2+}$ . At rest, NFAT1-4 reside in the cytosol in a highly phosphorylated state. Raised cytosolic  $\text{Ca}^{2+}$  activates the calcium-binding intermediate messenger, calmodulin, which recruits calcineurin, a neuronally-expressed protein phosphatase. NFAT1-4 contain a calcineurin binding motif, permitting dephosphorylation and subsequent translocation into the nucleus (Crabtree and Olson, 2002). Once within the nucleus, NFAT binds with a nine base pair response element sequence in the promotor of target genes (Feske *et al.*, 2007). Upon the return of cytosolic  $\text{Ca}^{2+}$  to basal levels, kinases, such as glycogen synthase kinase  $3\beta$ , re-phosphorylate NFAT, resulting in translocation back to the cytosol (Hogan *et al.*, 2003). There is some evidence that the duration for which NFAT resides within the nucleus – controlled by

the relative activities of phosphatases and kinases – determines the resultant changes on gene expression (Feske *et al.*, 2007). NFAT5 differs from other members of the NFAT family in that it was first described as a component of the osmotic stress response to immune cells – a process which did not require  $\text{Ca}^{2+}$  or calcineurin (Halterman, Moo Kwon and Wamhoff, 2012). This is corroborated by the lack of a calcineurin binding motif in NFAT5. However, it was later shown that the dependence of NFAT5 on  $\text{Ca}^{2+}$  and calcineurin was determined by the stimulus (Trama *et al.*, 2000; Li *et al.*, 2007). While it appears that, under some circumstances, NFAT5 can respond to raised cytosolic  $\text{Ca}^{2+}$  and subsequent calcineurin activity, it is not yet clear how this response is orchestrated.

Since the initial studies on the immune system, members of the NFAT family have been found to function in numerous disease states. The gene encoding leucine-rich repeat kinase 2, *LRRK2*, contains a susceptibility locus for IBD. *LRRK2* suppresses the activity of NFAT2 in macrophages, so a loss-of-function polymorphism leads to increased NFAT2 activity and subsequent release of inflammatory cytokines, precipitating severe inflammation in the GI tract (Liu *et al.*, 2011). Members of the NFAT family are also found in the nervous system, with NFAT3 and NFAT5 (and NFAT4 to a much lesser extent) expressed in sensory neurons in the DRG (Usoskin *et al.*, 2015; Zeisel *et al.*, 2018). NFAT3 links sustained electrical activity of sensory neurons with changes in gene expression (Kim and Usachev, 2009), and several nociceptive genes – including *COX2* and *BDNF* – are regulated by NFAT signalling (Groth *et al.*, 2007). Inflammatory mediators drive changes in sensory neuron gene expression: a two-minute application of bradykinin induced the translocation of fluorescently labelled NFAT4 to the nucleus in a  $\text{Ca}^{2+}$ -dependent manner (Jackson, Usachev and Thayer, 2007). NFAT4-mediated expression of a luciferase reporter gene was also elevated by bradykinin (Jackson, Usachev and Thayer, 2007). Although NFAT5 is expressed in sensory neurons, its role remains unknown. Ang II has been shown to induce NFAT5, but not NFAT3, activity and translocation in muscle cells (Halterman *et al.*, 2011; Lunde *et al.*, 2011), but it is unclear whether this effect is conserved in sensory neurons.

### **5.1.2. Experimental outline**

Experiments in this Chapter aimed to resolve whether incubation of sensory neurons with Ang II could drive the translocation of NFAT5 to the nucleus, as indicated by immunofluorescent staining. Given the role of SOCE in NFAT translocation – and the previously identified role for TRPC3 in SOCE in sensory neurons – the requirement for TRPC3-mediated  $\text{Ca}^{2+}$  entry was also investigated. Changes in the activity or localisation of transcription factors may indicate prolonged changes in neuronal properties induced by Ang II. To resolve whether Ang II induces such persistent changes in sensory neuronal properties, the electrical excitability of IB4-positive sensory neurons was examined following overnight incubation with Ang II.

## 5.2. Results

### 5.2.1. Neuronal staining for NFAT5

The localisation of NFAT5 was determined by immunocytochemistry after neuronal cultures were stimulated with Ang II for 60 minutes. In the absence of primary antibodies, staining for NFAT5 was markedly reduced (Figure 5.1a), as well as the staining profile being markedly different compared to experiments in which the primary antibody was included (Figure 5.1b). NFAT5 staining – even under basal conditions – was found to be greater in the nucleus compared to the cytosol (Figure 5.1c). Examination of single neurons revealed that staining for NFAT5 and DAPI is highly correlated, emphasising the apparent nuclear localisation of NFAT5 (Figure 5.1d). This is in agreement with previous reports documenting that NFAT5 is constitutively nuclear (López-Rodríguez *et al.*, 1999). The proportion of neurons positively stained for NFAT5 was 48.4% (119 of 246 neurons), roughly in line with the 40.8% of neurons found to express transcripts for NFAT5 (Usoskin *et al.*, 2015).

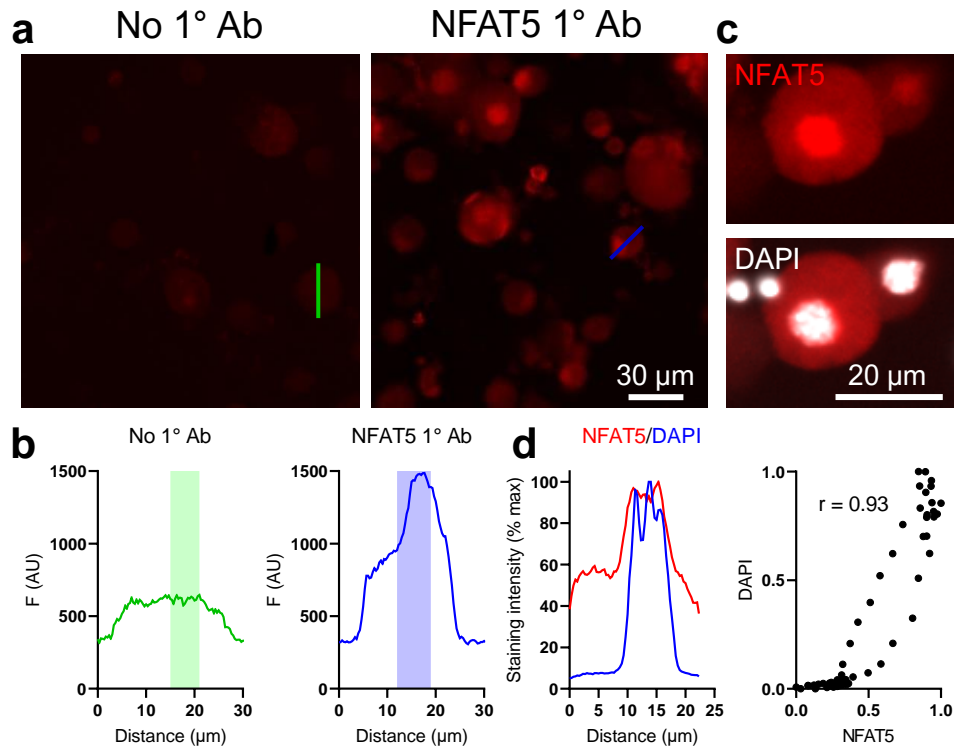


**Figure 5.1 NFAT5 is constitutively nuclear in sensory neurons**

- (a) *Left*: Image showing neuronal staining with AlexaFluor-568 (1:1000) secondary antibodies in the absence of NFAT5 primary antibodies. *Right*: Image showing neuronal staining for NFAT5 under basal (unstimulated) conditions. Scale bar applies to both panels.
- (b) *Left*: Profile plot of the intensity of fluorescent staining of the neuron marked by the green line in (a); primary antibody omitted. The green shaded area shows the location of the nucleus. *Right*: Profile plot of the intensity of fluorescent staining of the neuron marked by the blue line in (a); primary antibody present. The blue shaded area shows the location of the nucleus; note the increase in NFAT5 staining intensity in this area.
- (c) *Top*: Image showing neuronal staining for NFAT5 under basal conditions. *Bottom*: The above image overlaid with DAPI staining to highlight the location of the neuronal nucleus. Scale bar applies to both panels.
- (d) *Left*: Profile plot of the staining intensity for NFAT5 (red) and DAPI (blue) for the neuron in (c); white dashed line. *Right*: Correlation between the staining intensity for NFAT5 and DAPI for the cell shown in the left panel.

### **5.2.2. Nuclear translocation of NFAT5 depends on AT1R and TRPC3**

The criteria for nuclear translocation of NFAT5 was nuclear staining intensity greater than three standard deviations above the mean of the unstimulated condition. Incubation of neuronal cultures with ionomycin resulted in the translocation of NFAT5 to the nucleus in a subset of neurons (Figure 5.2 shows an example experiment). Ionomycin induced NFAT5 translocation in  $52.5 \pm 8.8\%$  of neurons. Given the proportion of neurons expressing NFAT5 was found to be  $\sim 48\%$  (see 5.2.1.), it seems that ionomycin induced translocation in all NFAT5-expressing neurons, demonstrating that a rise in cytosolic  $\text{Ca}^{2+}$  is sufficient to drive translocation.

Under control conditions, no neurons were found to surpass the cut off for translocation (Figure 5.3a). However, after incubation with Ang II, a population of neurons exhibited translocation of NFAT5 to the nucleus (Figure 5.3b). Valsartan attenuated this effect of Ang II, reducing the number of neurons exhibiting NFAT5 translocation (Figure 5.3c). In addition, TRPC3 blockade by Pyr3 also reduced the effect of Ang II on NFAT5 translocation (Figure 5.3d). Figure 5.3a-d are from a single experiment; Figure 5.3e summarises this experiment. Overall, Ang II induced NFAT5 translocation in  $29.0 \pm 2.5\%$  of neurons (Figure 5.3f). Valsartan attenuated the proportion of neurons displaying NFAT5 translocation to  $6.1 \pm 2.9\%$  ( $p < 0.0001$ , Figure 5.3f). Finally, Pyr3 also reduced the proportion of neurons in which NFAT5 translocation was observed ( $12.3 \pm 1.1\%$ ,  $p = 0.0004$ , Figure 5.3f).

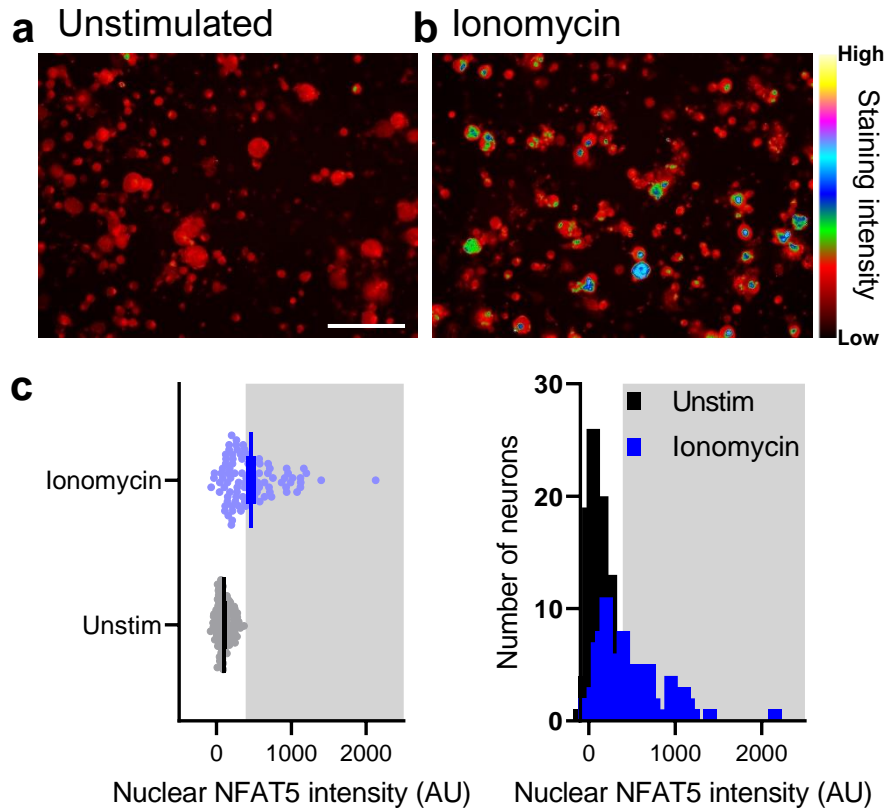


**Figure 5.2 Raised cytosolic  $\text{Ca}^{2+}$  is sufficient to drive NFAT5 translocation**

- (a) False-coloured image showing NFAT5 staining intensity in unstimulated neurons. Scale: 100  $\mu\text{m}$ , applies to panels (a) and (b).
- (b) False-coloured image showing NFAT5 staining intensity after stimulation with Ang II. Increases in fluorescence are usually punctate and overlap with DAPI staining.
- (c) Scatter plot (*left*) and frequency histogram (*right*) showing NFAT5 translocation by Ang II (both depict the same experiment). These results are representative of three replicates. Grey shaded area shows the mean of the unstimulated group plus three standard deviations.

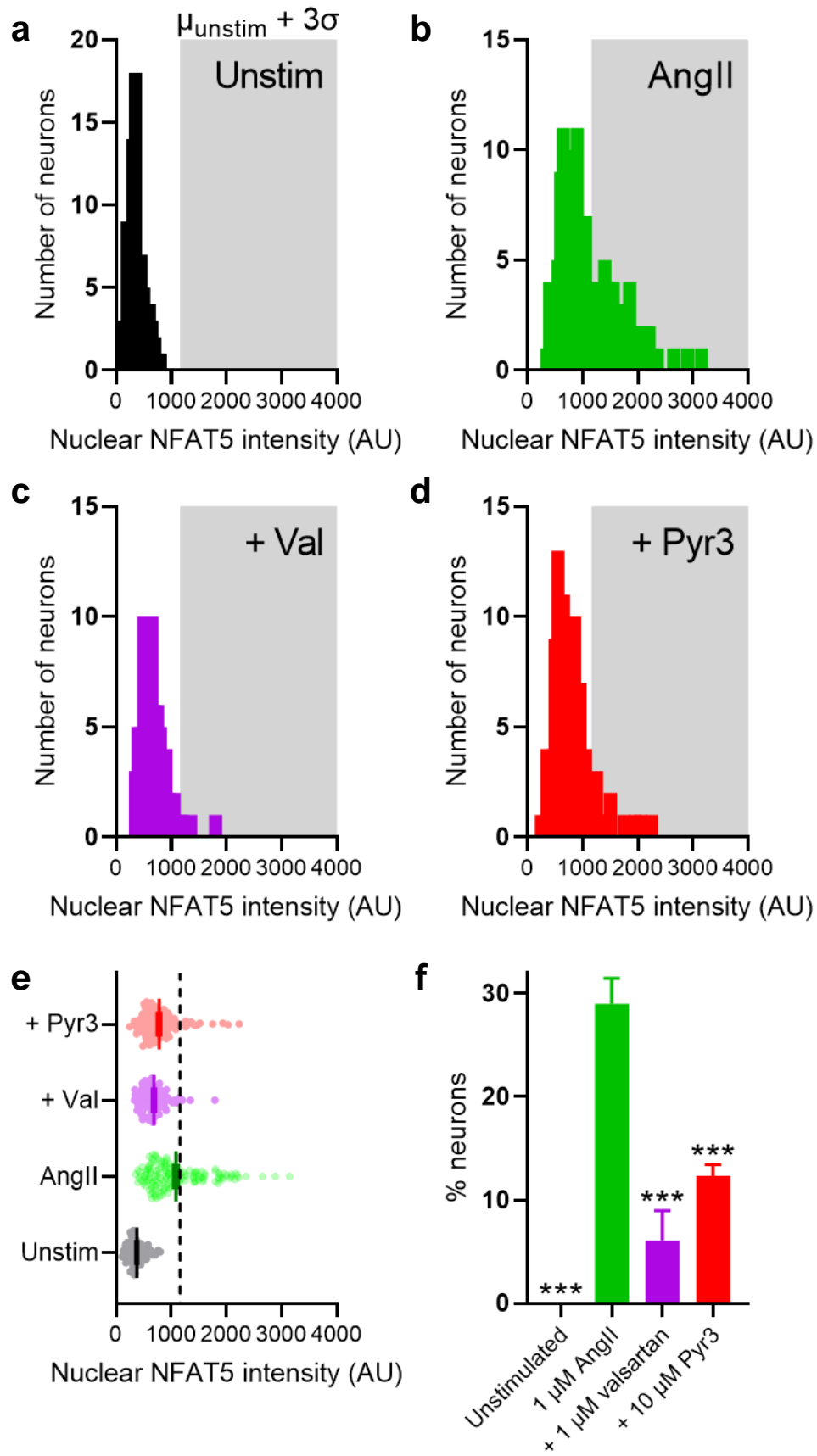


**Figure 5.3 Legend on next page**

### Figure 5.3 Ang II-mediated translocation of NFAT5

- (a) Histogram showing nuclear NFAT5 staining intensity in neurons under control conditions. The grey shaded area shows the mean of this unstimulated group plus three standard deviations ( $\mu_{\text{unstim}} + 3\sigma$ ); applies to (a) – (d).
- (b) Histogram from a single experiment showing nuclear NFAT5 staining intensity in neurons incubated with Ang II.
- (c) Histogram from a single experiment showing nuclear NFAT5 staining intensity in neurons incubated with Ang II and valsartan.
- (d) Histogram from a single experiment showing nuclear NFAT5 staining intensity in neurons incubated with Ang II and Pyr3.
- (e) Scatter plot from a single experiment depicting the data in (a) – (d). The dotted line shows the mean of the unstimulated group plus three standard deviations.
- (f) Grouped data showing the proportion of neurons in which NFAT5 translocation to the nucleus was observed. All groups:  $n = 3$ ,  $N = 3$ . Unstimulated: 214 neurons; Ang II: 237 neurons; valsartan: 331 neurons; Pyr3: 306 neurons. Data analysed with a one-way ANOVA with Holm-Sidak post-tests.

### 5.2.3. Calcineurin mediates nuclear translocation of NFAT5

The experiments above indicate that a rise in cytosolic  $\text{Ca}^{2+}$  drives NFAT5 translocation to the nucleus. TRPC3 channels may provide a source of  $\text{Ca}^{2+}$  to drive NFAT5 translocation downstream of Ang II stimulation. However, NFAT5 – like all members of this family of transcription factors – is insensitive to  $\text{Ca}^{2+}$  *per se*. NFAT1-4 must be dephosphorylated by calcineurin, a  $\text{Ca}^{2+}$ -sensitive phosphatase, before they can enter the nucleus. The case for NFAT5 is less clear (see 5.3.1.), but calcineurin has been implicated in the regulation of NFAT5 localisation (Trama *et al.*, 2000) and may function downstream of Ang II receptor stimulation (Halterman *et al.*, 2011). Calcineurin is highly expressed in sensory neurons (Usoskin *et al.*, 2015), and so this phosphatase's involvement in NFAT5 translocation was investigated by inhibiting calcineurin activity using Cyclosporine A.

In the next set of experiments, it was again observed that unstimulated neurons did not display NFAT5 translocation to the nucleus (Figure 5.4a and d). Incubation with Ang II drove NFAT5 translocation in a subset of neurons (Figure 5.4b and d) – as was observed in earlier experiments. Inhibition of calcineurin with Cyclosporine A (1  $\mu\text{M}$ , CsA) blocked Ang II-induced NFAT5 translocation (Figure 5.4c and d). Ang II induced NFAT5 translocation in  $22.3 \pm 8.3\%$  of neurons under control conditions, compared to  $1.7 \pm 1.1\%$  when calcineurin was inhibited ( $p = 0.04$ , Figure 5.4e). Another way of analysing the data gathered in these experiments is to consider the ratio of – rather than the difference between – nuclear and cytosolic NFAT5 staining intensity. In control conditions, the nuclear/cytosolic ratio was  $1.33 \pm 0.02$ , significantly greater than a hypothetical median of 1 ( $p < 0.0001$ , one sample Wilcoxon test), again showing preferential nuclear localisation. Following incubation with Ang II, the nuclear/cytosolic ratio was increased to  $1.98 \pm 0.12$  ( $p < 0.0001$ , Figure 5.4f). Inhibition of calcineurin with CsA resulted in a nuclear/cytosolic ratio indistinguishable from control ( $1.45 \pm 0.04$ ,  $p = 0.22$ , Figure 5.4f) and significantly reduced from the Ang II-treated group ( $p < 0.0001$ , Figure 5.4f).

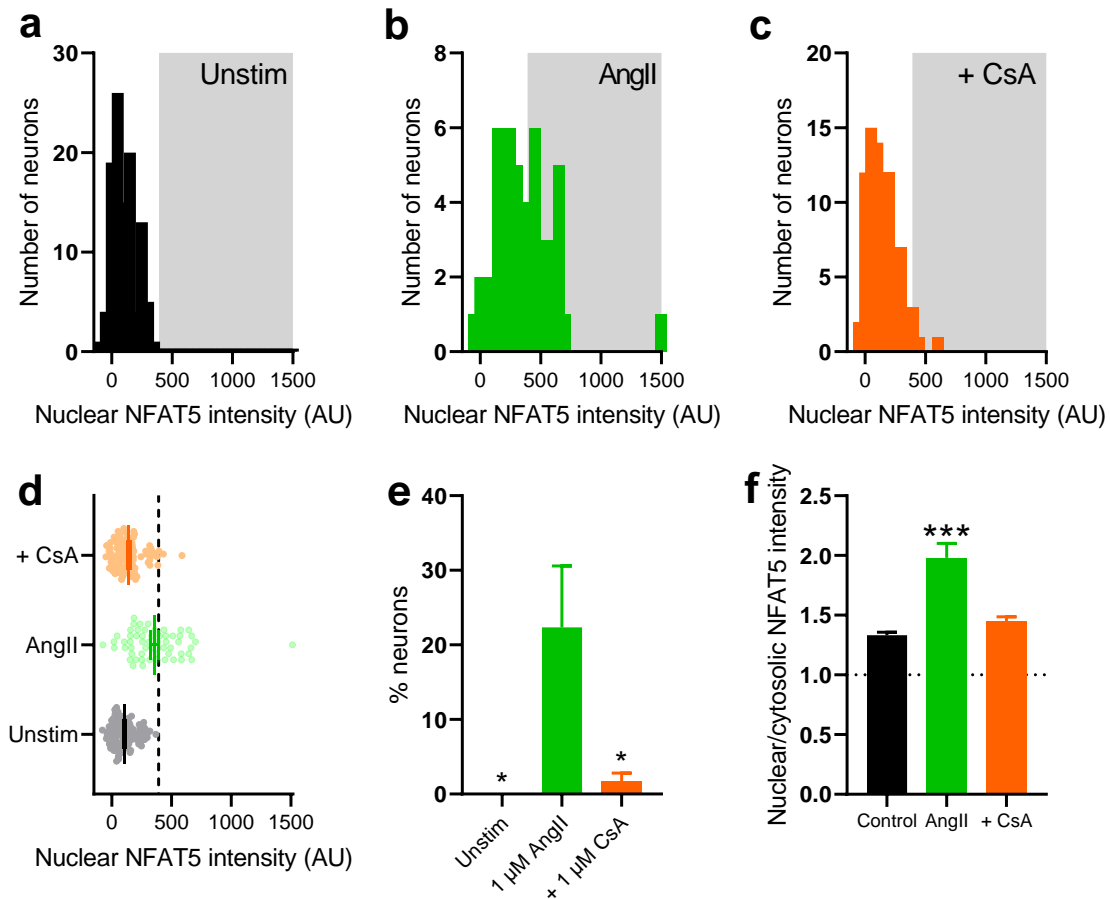


**Figure 5.4 Calcineurin mediates NFAT5 translocation**

- (a) Histogram showing nuclear NFAT5 staining intensity in neurons under control conditions. The grey shaded area shows the mean of this unstimulated group plus three standard deviations; applies to (a) – (c).
- (b) Histogram from a single experiment showing nuclear NFAT5 staining intensity in neurons incubated with Ang II.
- (c) Histogram from a single experiment showing nuclear NFAT5 staining intensity in neurons incubated with Ang II and CsA.
- (d) Scatter plot from a single experiment depicting the data in (a) – (c). The dotted line shows the mean of the unstimulated group plus three standard deviations.
- (e) Grouped data showing the proportion of neurons in which NFAT5 translocation to the nucleus was observed. All groups:  $n = 3$ ,  $N = 3$ . Unstimulated: 242 neurons; Ang II: 225 neurons; CsA: 209 neurons. Data analysed with a one-way ANOVA with Holm-Sidak post-tests.
- (f) Grouped data showing the ratio of nuclear to cytosolic NFAT5 staining intensity for all neurons examined in this experiment. All groups:  $n = 3$ ,  $N = 3$ . Unstimulated (control): 242 neurons; Ang II: 225 neurons; CsA: 209 neurons. Data analysed using a Kruskal-Wallis test with Dunn's post-tests.

#### **5.2.4. Incubation with Ang II causes increased excitability of IB4-positive neurons**

So far, experiments in this Thesis have examined the effects of Ang II on sensory neurons over relatively short time scales, i.e., seconds to minutes. If Ang II induces prolonged changes in sensory neuronal properties, it is more likely that it may play a role in nociception in inflammatory diseases. Sensitisation of sensory neurons is an important driver of pain in IBD. To investigate whether or not Ang II is able to sensitise sensory neurons *in vitro*, neurons were incubated with Ang II (10  $\mu$ M; concentration increased to account for degradation *in vitro*) over night (16-24 hours). Neurons were then stained with IB4, such that IB4-positive neurons could be selected, and used for current-clamp recording.

The neuronal rheobase – the minimum depolarising current required to evoke action potential discharge – was ascertained by applying current pulses to neurons from 0-1050 pA in 50 pA increments. Under control conditions – neurons incubated with 0.1% ddH<sub>2</sub>O – rheobase was found to be  $491.1 \pm 62.9$  pA (Figure 5.5a). However, following incubation with Ang II, rheobase was reduced to  $207.1 \pm 49.4$  pA ( $p = 0.0008$ , Figure 5.5a), indicating an increase in excitability. The histogram in Figure 5.5b highlights the shift in rheobase after incubation with Ang II, as well as the large variance in the data, though this has also been documented in previous studies (Chakrabarti *et al.*, 2018, 2020).

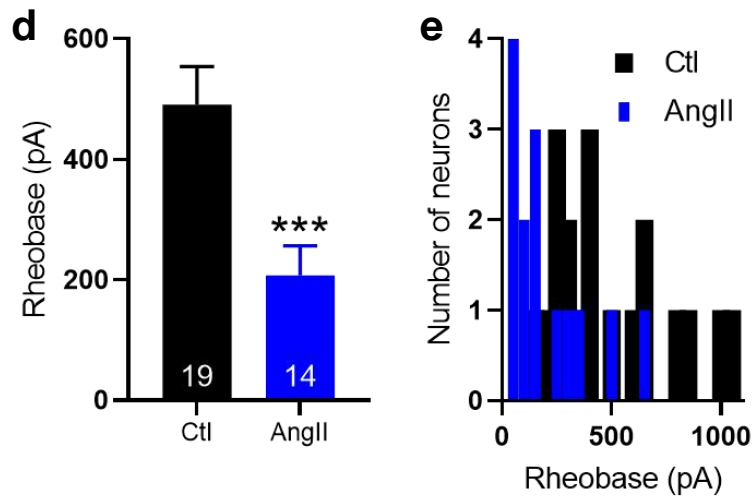
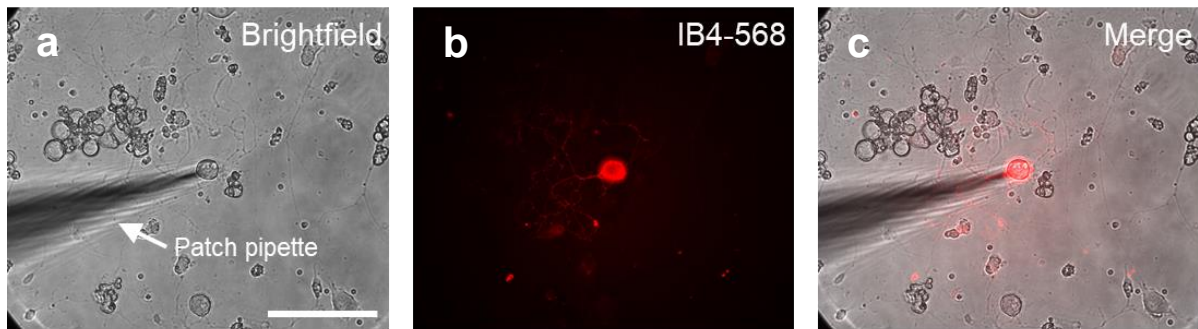


**Figure 5.5 Ang II sensitises IB4-positive sensory neurons**

- (a) Brightfield image showing a patch pipette above a neuron from which a recording was taken. Scale bar: 80  $\mu$ m, applies to panels (a) - (c).
- (b) IB4-AlexaFluor568 fluorescence image showing staining with IB4.
- (c) Merge of (a) and (b): the neuron of interest is IB4-positive.
- (d) Grouped data showing the rheobase of IB4-positive neurons under control conditions and after incubation with Ang II. Control: 19 neurons from 4 mice. Ang II: 14 neurons from 4 mice. Data analysed with a two-tailed Mann-Whitney U-test.
- (e) Histogram showing the rheobase of all neurons within the sampled population.

### 5.3. Discussion

Experiments in this Chapter indicate that incubation of sensory neurons with Ang II induces increased translocation of the transcription factor NFAT5 to the neuronal nucleus. This effect of Ang II seemed to be mediated by AT1R (and it therefore likely to be due to a direct interaction with neurons), with the necessary source of Ca<sup>2+</sup> possibly provided by TRPC3. Finally, the Ca<sup>2+</sup>-sensitive phosphatase, calcineurin, may also function in this pathway to mediate NFAT5 translocation (Figure 5.6).

#### 5.3.1. Ang II-mediated nuclear translocation of NFAT5

Changes in gene expression underpin many of the actions of chemical messengers on neuronal function. Members of the NFAT family are important transcription factors which couple cell stimulation with changes in gene expression. NFAT3 has been shown to undergo nuclear translocation in sensory neurons following prolonged depolarisation, mediated by mitochondrial Ca<sup>2+</sup> cycling (Kim and Usachev, 2009). Here, NFAT3 translocation was not induced by incubation with Ang II (data not shown), indicating that different stimuli may engage distinct signalling pathways and, hence, different transcription factors. In cardiomyocytes, Ang II failed to induce dephosphorylation and activation of NFAT3, further supporting the notion that NFAT isoforms are activated in a tissue-specific or stimulus-specific manner (Lunde *et al.*, 2011).

NFAT5 was found to be preferentially localised to the nucleus under basal conditions, aligning with previous reports in other cell types (López-Rodríguez *et al.*, 1999). The first descriptions of NFAT5 showed that it was a mediator of the cellular response to osmotic stress (Miyakawa *et al.*, 1998). The mechanisms regulating the subcellular localisation of NFAT5 are not entirely clear and appear to depend on the stimulus. During osmotic stress, activation of NFAT5 was found to be independent of Ca<sup>2+</sup> and calcineurin (López-Rodríguez *et al.*, 1999). A later report indicated that NFAT5 induction in T-cells downstream of T-cell receptor activation could be blocked by calcineurin inhibition, and the expression of constitutively active calcineurin drove NFAT5-dependent gene transcription (Trama *et al.*, 2000). The upregulation of *Aqp2* expression in the renal collecting tubules – important for water reabsorption – is also dependent on NFAT5 and can be attenuated by Cyclosporine A-mediated calcineurin inhibition (Li *et al.*, 2007).

While there is compelling evidence supporting a role for calcineurin-mediated dephosphorylation in the regulation of the cellular localisation of NFAT1-4 (Park *et al.*, 2020), the role of (de)phosphorylation in the regulation of NFAT5 is not fully understood. Numerous phosphorylation sites on NFAT5 have been found to control the protein's subcellular localisation. Phosphorylation at Y143 or T135 promotes nuclear localisation, whereas phosphorylation at S155 or S158 attenuates nuclear localisation (Gallazzini *et al.*, 2010; Zhou *et al.*, 2010; Zhou, 2016). Experiments detailed in this Chapter suggest a role for calcineurin in regulating the localisation of NFAT5. Perhaps calcineurin mediates dephosphorylation of NFAT5 at S155 or S158, thereby enhancing translocation to the nucleus. Another possibility could be that calcineurin activates a downstream kinase which phosphorylates NFAT5 at Y143 or T135, again enhancing nuclear translocation. The latter of these hypotheses may be more plausible given that NFAT5 does not contain a known calcineurin binding motif, precluding a direct interaction between the two proteins.

Ang II appears to play an important role in the regulation of NFAT5 activity and localisation in smooth muscle cells. Ang II application to these cells elevated the expression of luciferase under the control of NFAT5, as well as numerous endogenous genes, indicating an increase in NFAT5 activity (Haltermann *et al.*, 2011). There was no change in the level of NFAT5 at the transcript or protein levels, though Ang II induced NFAT5 translocation to the nucleus (Haltermann *et al.*, 2011). The authors did not resolve the signal which prompted NFAT5 translocation, but phosphorylation – presumably at either Y143 or T135 – by p38 or PKC was put forward. Calcineurin has been shown to colocalise with and promote the activity of some isoforms of PKC in cardiomyocytes (De Windt *et al.*, 2000), so it remains possible that PKC functions to phosphorylate NFAT5 downstream of calcineurin in sensory neurons. If this is the case, it would be expected that PKC inhibition – with, for example, staurosporine – would block Ang II-induced translocation of NFAT5. Beyond this, it may also be expected that the stimulation of PKC with PDBu would promote NFAT5 translocation.

The function of NFAT5 in the sensory nervous system is not wholly clear. The suppression of NFAT5 activity has been shown to alleviate inflammation in a model of arthritis (Han *et al.*, 2017), though this may be attributed to the role of NFAT5 in the production of pro-inflammatory cytokines by macrophages (Buxadé *et al.*, 2012; Kim *et al.*, 2014). Nocifensive behaviours between 15-60 minutes following intra-plantar

formalin injection – phase two of this nocifensive response – is attenuated in mice deficient in NFAT5, indicating NFAT5 may be important in the sensitisation of sensory neurons (Gwon *et al.*, 2021).

It has not yet been shown if Ang II application affects the activity or subcellular localisation of other transcription factors, though it does not appear that NFAT3 localisation or CREB phosphorylation at S133 are influenced by Ang II (preliminary data not shown). The end result of the translocation of NFAT5 to the nucleus is presumably increased expression of NFAT5-controlled genes. This could be ascertained by performing RNA sequencing of neurons stimulated with Ang II, Ang II plus Pyr3, Ang II plus an NFAT inhibitor, alongside unstimulated control neurons. This would not only demonstrate if there is a change in sensory neuronal gene expression, but also whether this is dependent on TRPC3 and NFAT signalling.

### **5.3.2. Sensitisation of IB4-positive sensory neurons**

Overnight incubation with Ang II increased the electrical excitability of IB4-binding non-peptidergic neurons. Given the findings in Chapter 1, it is likely that this results from a direct interaction between Ang II and the neurons via AT1R, though this has not been confirmed. The sensitisation of cultured sensory neurons by Ang II has not been reported previously. In fact, it has previously been shown that a five-minute application of Ang II to sensory neurons had no effect on excitability (Shepherd *et al.*, 2018). In line with this, experiments in Chapter 4 showed that the acute application of Ang II (for one minute) did not cause membrane depolarisation or action potential discharge. While Shepherd *et al* concluded that Ang II had no direct effect on sensory neuronal function, it may be that the effects of Ang II on neuronal excitability require a longer period of time to manifest. It is also important to note that Shepherd *et al* used neurons 48-72 hours after dissociation, a time point at which they also demonstrated abrogated expression of AT1R (Wangzhou *et al.*, 2020).

Ang II seems to evoke a range of temporally distinct signals in sensory neurons: Ca<sup>2+</sup> signals occur over seconds to minutes; translocation of transcription factors occurs over minutes to hours; and sensitisation occurs over many hours. It appears that Ang II-evoked Ca<sup>2+</sup> signals drive transcription factor translocation and, presumably, changes in neuronal gene expression. It is not unreasonable to assert that these changes in gene expression may give rise to the observed increase in sensory neuron

excitability. Many other inflammatory mediators, such as TNF $\alpha$ , nerve growth factor (NGF) and prostaglandin E2, have also been shown to induce changes in gene expression and post-translational changes in sensory neurons, leading to sensitisation and persistent pain (Cheng and Ji, 2008). To resolve whether Ang II-mediated sensitisation is dependent on *de novo* gene transcription, overnight incubation with Ang II could be carried out in the presence of actinomycin. This approach has been used before to demonstrate that the NGF-mediated acquisition of mechanosensitivity depends on gene transcription (Prato *et al.*, 2017). In any case, the sensitisation of IB4-positive sensory neurons by Ang II raises the possibility that this peptide contributes to nociception and pain in IBD.

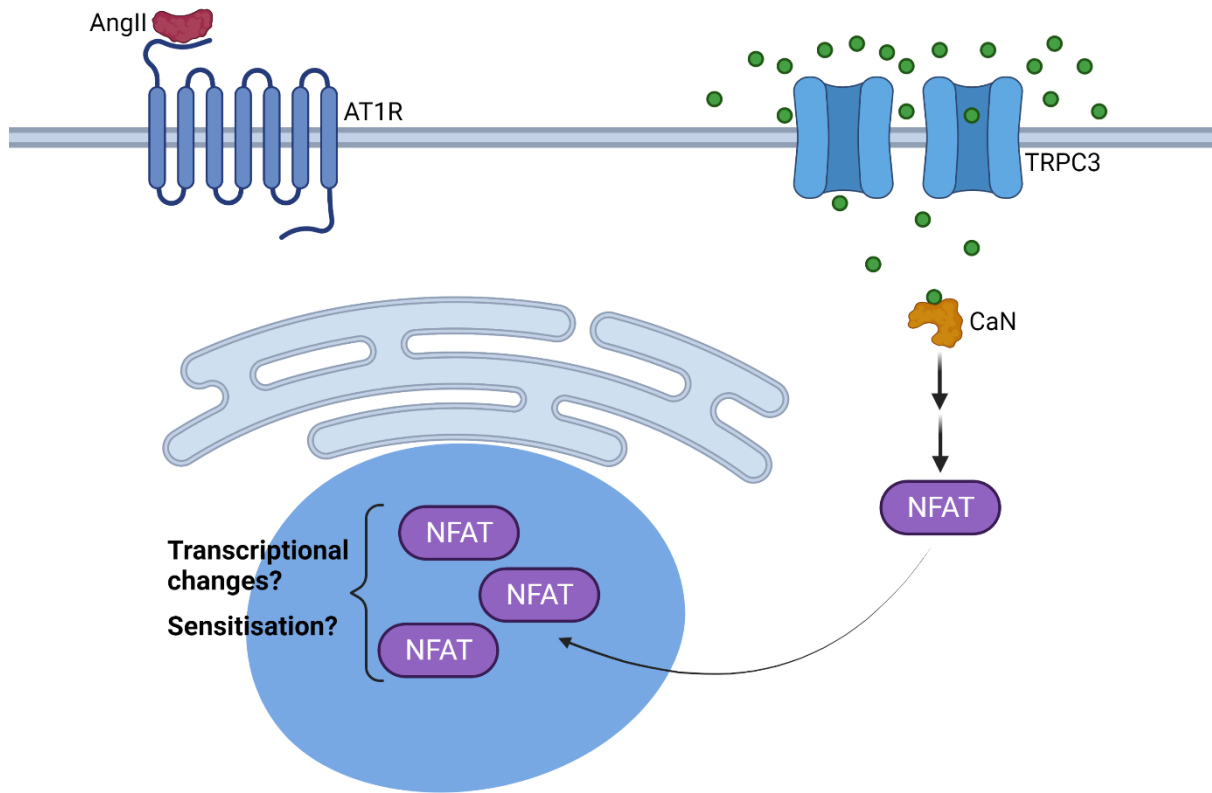


**Figure 5.6 Ang II-evoked NFAT5 translocation**

Diagram depicting the proposed findings from experiments in this Chapter. Incubation of sensory neurons with Ang II drives enhanced translocation of NFAT5 into the nucleus. This requires functional TRPC3 channels – providing a source of Ca<sup>2+</sup> (green circles) - and the Ca<sup>2+</sup>-sensitive phosphatase calcineurin. It is posited that NFAT5 translocation leads to changes in neuronal gene expression which may underlie Ang II-induced sensitisation. CaN: calcineurin. Image created using Biorender.

## 5.4. Key points

Experiments outlined in this Chapter have demonstrated that:

- i. NFAT5 is expressed in a subset of sensory neurons, where it is constitutively nuclear.
- ii. Ang II induces enhanced translocation of NFAT5 to the nucleus; a process requiring AT1R, TRPC3 channels and calcineurin.
- iii. Incubation with Ang II raises the electrical excitability of non-peptidergic sensory neurons.

## **Chapter 6**

### **General discussion**

## 6.1. A potential role for Ang II in nociception

Data presented in this Thesis have revealed a novel interaction between Ang II and peripheral sensory neurons *in vitro*. Coupled with existing data documenting the elevation of Ang II in inflammatory diseases, particularly IBD, this indicates that Ang II may be involved in nociception during inflammation.

The use of genetically-engineered neurons, cell sorting, immunofluorescence and  $Ca^{2+}$  imaging revealed that Ang II stimulates two populations of nociceptive neurons, distinguished by their expression of *Tmem45b* and binding of IB4. *Tmem45b*<sup>-</sup>, IB4-positive neurons were stimulated directly by Ang II via AT1R, while *Tmem45b*<sup>-</sup>, IB4-negative neurons were stimulated indirectly in a manner dependent on NNSCs but independent of AT1R. Given the expression of receptors for Ang II on sensory neurons in the DRG, one would have predicted that Ang II-evoked  $Ca^{2+}$  signals would have been observed in IB4-positive neurons only. The response of IB4-negative neurons to Ang II highlights the need to consider that neuronal responses to a mediator of interest may not arise due to an interaction between the mediator and sensory neurons. Tewari and colleagues (2020) made a similar observation, showing that the neuronal effects of GMCSF are driven by an interaction with macrophages. Magnetic cell sorting provides a simple method for ascertaining whether neurons respond directly to a given mediator, as shown here for Ang II and recently for TNF $\alpha$ , too (Barker *et al.*, 2022, in press).

Ang II-evoked  $Ca^{2+}$  signals were dependent on  $Ca^{2+}$  release from IP<sub>3</sub>-sensitive stores and subsequent SOCE mediated by TRPC3, though pharmacological experiments presented here should be ratified using TRPC3 knock out tissue. This pathway is negatively regulated by PKC. TRPC3-mediated  $Ca^{2+}$  entry, and the  $Ca^{2+}$ -sensitive phosphatase calcineurin, drives the translocation of NFAT5 into the neuronal nucleus. This indicates that Ang II-evoked  $Ca^{2+}$  signals – occurring over seconds to minutes – may drive prolonged changes in neuronal function. This is further evidenced by the sensitisation of IB4-positive neurons following incubation with Ang II.

Future work will be focused on three avenues to address the limitations of the current study:

- 1) Clarify the long-term changes in neuronal function induced by Ang II. The nuclear translocation of NFAT5, and sensitisation of IB4-positive neurons,

evoked by incubation with Ang II indicates the induction of persistence changes in neuronal function. The consequences of NFAT5 translocation on gene expression will be investigated by RNA sequencing of cultured DRG neurons stimulated with Ang II. Inhibition TRPC3 and NFAT function will reveal whether changes in gene expression rely on Ca<sup>2+</sup> influx through TRPC3 and nuclear translocation of NFAT5. Finally, measurements of rheobase will be repeated in the presence of Ang II and an inhibitor of transcription, such as actinomycin, to resolve whether Ang II-mediated sensitisation relies on changes in gene expression.

- 2) Probe the infiltration of immune cells into the DRG during colitis. Models of neuropathic and inflammatory diseases have demonstrated that the infiltration of immune cells, especially macrophages, is important in the induction and maintenance of pain (H. Zhang *et al.*, 2016; Yu *et al.*, 2020; Raouf *et al.*, 2021). Oral DSS will be used to induce colitis in mice, and the presence of macrophages in the DRG will be ascertained using either immunohistochemical or genetic markers, such as F4/80 or CD68. The presence of Ang II will also be measured using an immunosorbent assay, given the expression of this peptide and its precursors by macrophages. If Ang II is raised in DRG during colitis, it may indicate an extra-colonic site of action and an interaction with sensory neuronal soma.
- 3) Investigate behavioural responses to intra-colonic Ang II administration. The injection of Ang II into the hind paw is painful (Shepherd *et al.*, 2018), but it is not yet known whether administration into the colon is painful. The visceromotor response is a widely-used metric of visceral pain, either in response to distention of the colon or intra-colonic drug administration (Bautzova *et al.*, 2018), in which contraction of the abdominal muscles is measured. If Ang II increases the visceromotor response to colon distention, it would ratify the role of Ang II in visceral hypersensitivity, a key symptom of IBD. What's more, it would also indicate a site of action in the colon, as has already been suggested by the stimulation of colonic afferent nerves by Ang II (Charity Bhebhe, unpublished observation). In combination with (2), these experiments will resolve whether Ang II exerts its effects in the tissue, in the DRG, or at both sites.

## **6.2. Conclusion**

In conclusion, this Thesis documents a novel interaction between Ang II and IB4-positive nociceptive sensory neurons via AT1R, and with IB4-negative sensory neurons via non-neuronal cells. Ang II evokes TRPC3-dependent  $\text{Ca}^{2+}$  signals in nociceptors which drive changes in the localisation of the transcription factor, NFAT5. Sensitisation of a subset of nociceptors by Ang II indicates the induction of persistent changes in neuronal properties, though the mechanism underpinning this is not fully resolved. These observations highlight a potential role for Ang II in nociception in IBD, a disease in which levels of Ang II are significantly elevated.

## **Chapter 7**

## **Appendix**

## **Appendix 1: Additional data**

This section contains preliminary data related to data presented in the main body of the Thesis, but which is not necessarily required for the arguments and conclusions made.

### **A1.1. Preliminary data implicating TNF $\alpha$ in Ang II signalling**

*Related to Section 3.3.2.4.*

Previous studies have suggested the Ang II application can evoke the synthesis and release of TNF $\alpha$  (Ruiz-Ortega *et al.*, 2002; Sriramula *et al.*, 2008; Sriramula and Francis, 2015). Data presented so far in this Thesis has failed to resolve the mechanism by which Ang II application leads to a rise in cytosolic Ca<sup>2+</sup> in Ang II receptor-lacking (IB4-negative) sensory neurons. The data indicate that the response of IB4-negative neurons to Ang II is reliant on NNSCs present in DRG cultures, in which TNF $\alpha$  is purportedly expressed.

A receptor for TNF $\alpha$ , TNFR1, is expressed in IB4-negative neurons which align with the properties of IB4-negative Ang II-sensitive neurons, e.g., expression of Na<sub>v</sub>1.8 (Figure A1a). To assess the role of TNFR1 in the response to Ang II, mice lacking the *Tnfrsf1a* gene were obtained (Jackson Laboratory, ME, USA; RRID: IMSR\_JAX:003242). Ang II was applied to cultured sensory neurons from these mice, and the resultant Ca<sup>2+</sup> response was examined. In a neuronal culture from a wild-type mouse, 32.1 $\pm$ 6.6% of neurons exhibited a rise in cytosolic Ca<sup>2+</sup> in response to Ang II application (Figure A1b). In contrast, 10.7 $\pm$ 2.8% of neurons from a TNFR1 knock-out mouse responded to Ang II ( $p = 0.04$ , Figure A1b). The peak magnitude of the response to Ang II was modestly attenuated in TNFR1 knock-out mice (0.40 $\pm$ 0.05 vs. 0.23 $\pm$ 0.07), but this was not labelled statistically significant ( $p = 0.1$ , Figure A1c). For both genotypes, three experimental replicates from a single mouse was used, and so no firm conclusions can be drawn until a greater sample is available. The reduction in the proportion of Ang II-responsive neurons in cultures from TNFR1 knock-out mice may indicate a role for TNF $\alpha$  in the response to Ang II. However, in addition to a greater sample, it is also necessary to test whether Ang II induces TNF $\alpha$  release from NNSCs. This could be achieved by measuring the presence of TNF $\alpha$  in neuronal cultures – using, for example, an immunosorbent assay – in the absence and presence of Ang II. If TNF $\alpha$  release is detected, the experiment could then be re-run in a MACS culture

lacking NNSCs. If TNF $\alpha$  release is lost under these conditions, it must have arisen from NNSCs.

The expression of *Tnfrsf1a* in IB4-negative neurons offers an explanation for the apparent communication between NNSCs and IB4-negative neurons – if TNF $\alpha$  is the mediator of this communication. More than this, there may also be a closer physical association between NNSCs and IB4-negative neurons *on vitro*. Manually measuring the closest approach distance between neurons and their closest non-neuronal neighbour revealed a shorter distance between IB4-negative neurons and NNSCs compared to IB4-positive neurons. Figure A1d shows a histogram of the distances measured for IB4-positive and -negative neurons. The average distance between IB4-positive neurons and their nearest non-neuronal neighbour was  $15.4 \pm 1.0 \mu\text{m}$ , compared to  $9.0 \pm 0.4 \mu\text{m}$  ( $p < 0.0001$ , Figure A1e). This closer association makes it more likely for a NNSC-derived mediator to encounter an IB4-negative neuron.

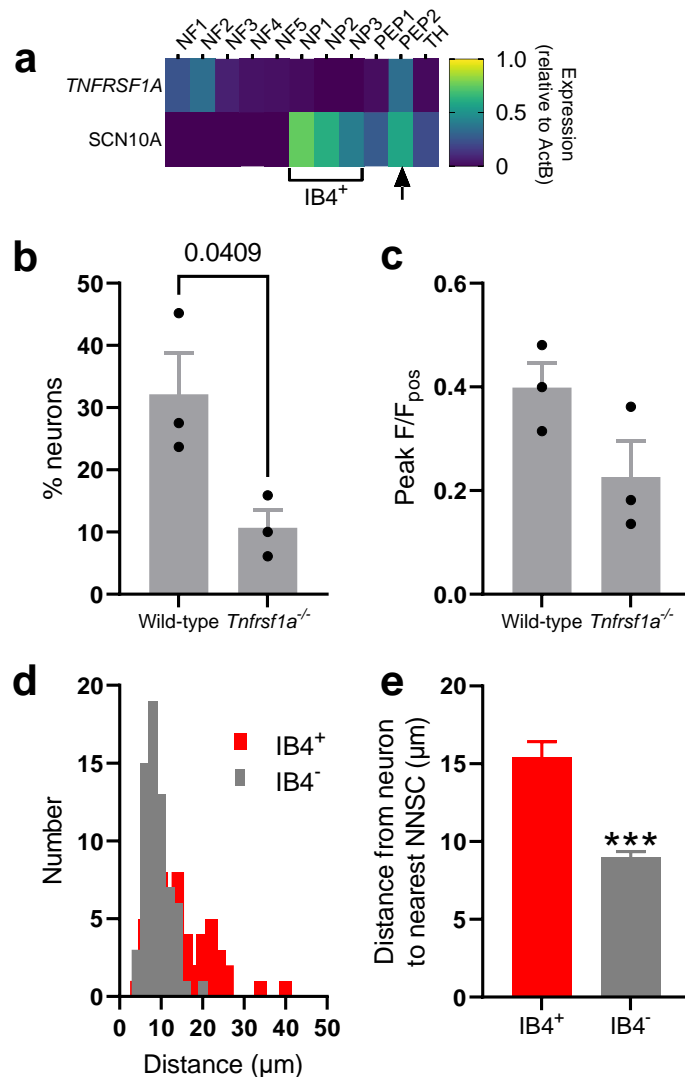


**Figure A1 A potential role for TNF $\alpha$  in the response of IB4-negative neurons to Ang II**

- (a) Expression of transcripts for *Tnfrsf1a* and *SCN10A* across sensory neuron populations (relative to the expression of *ActB*). IB4-positive neurons are highlighted, as is the co-expression of the two transcripts. Data taken and redrawn from Usoskin *et al.*, 2014. Neuronal populations are denoted as in Usoskin *et al.*, such that NF refers to myelinated subpopulations (i.e., low-threshold mechanoreceptors and proprioceptors), NP refers to non-peptidergic neurons, PEP to peptidergic neurons and TH to tyrosine hydroxylase-expressing non-peptidergic neurons.
- (b) Grouped data showing the proportion of Ang II-responsive neurons. Wild-type: n = 3, N = 1; *Tnfrsf1a*: n = 3, N = 1. Data analysed using a Mann-Whitney U test.
- (c) Grouped data showing the peak magnitude of the response to Ang II. Wild-type: n = 3, N = 1; *Tnfrsf1a*: n = 3, N = 1. Data analysed using a Mann-Whitney U test.
- (d) Histogram showing the distance between IB4-positive (red) and IB4-negative (grey) neurons and their closest non-neuronal neighbour.
- (e) Grouped data showing the average distance between IB4-positive (red) and IB4-negative (grey) neurons and their closest non-neuronal neighbour. IB4-positive: 52 neurons from a single mouse; IB4-negative: 65 neurons from a single mouse.

## A1.2. Examining the kinetics of KCl-evoked Ca<sup>2+</sup> transients

*Related to Section 4.2.1.*

In Figure 4.1, it was shown that the decay of KCl-evoked Ca<sup>2+</sup> transients could be slowed by pre-incubation with thapsigargin. The integrity of this observation is reliant on the temporal fidelity of Fluo4 being sufficient to detect such changes in the time course of Ca<sup>2+</sup> transients. To test this, the rate of rise and decay of KCl-evoked Ca<sup>2+</sup> transients was examined for different concentrations of KCl (10, 50 and 100 mM). One would expect the apparent “on-rate”, and hence the rise time, to depend on the KCl concentration, but the “off-rate”, and hence the decay time, to be independent of KCl concentration.

Recordings of cytosolic [Ca<sup>2+</sup>] of 60 s duration were made, with KCl applied between 10 – 20 s. Increasing the concentration of KCl lead to Ca<sup>2+</sup> transients of greater peak magnitude (Figure A2a). To obtain a rise time, the first 20 s of the recording was fit with a plateau (to account for the 10 s baseline) followed by a one-phase association (Figure A2b, black line) of the form

$$F = \begin{cases} F_{min} \forall t < t_0 \\ F_{min} + (F_{max} - F_{min})(1 - e^{-K_{ass}\Delta t}) \forall t > t_0 \end{cases} \dots (1)$$

Where  $F_{min}$  and  $F_{max}$  are the minimal (baseline) and maximal fluorescence values, respectively.  $T$  is time during the experiment,  $t_0$  is the time at which KCl was applied (i.e., where the association phase begins;  $\Delta t$  is  $t-t_0$ ) and  $K_{ass}$  is the rate constant for the association phase. The half time ( $t_{1/2}$ ) is

$$t_{\frac{1}{2}} = \frac{\ln 2}{K} \dots (2)$$

The decay time was ascertained by fitting the later 40 s of the recording with a one-phase decay (Figure A2b, red line) given by

$$F = (F_{max} - F_{min})e^{-K_{dec}t} \dots (3)$$

Where  $K_{dec}$  is the rate constant for the decay phase. Raising the concentration of applied KCl lead to a shortening of the rise time (Figure A2c). 10 mM KCl evoked Ca<sup>2+</sup> transients with a half rise time ( $t_{1/2}$  ON) of  $2.1 \pm 0.2$  s, compared to  $1.4 \pm 0.1$  s and  $0.5 \pm 0.02$  s for 50 mM and 100 mM KCl, respectively (Figure A2d). Conversely, the decay half time ( $t_{1/2}$  OFF) was unaffected by the concentration of KCl applied (Figure

A2e). The decay half time was found to be  $2.9 \pm 0.2$  s,  $3.0 \pm 0.1$  s and  $2.8 \pm 0.1$  s for 10 mM, 50 mM and 100 mM KCl, respectively ( $p = 0.49$ , Figure A2f). The decay of KCl-evoked  $\text{Ca}^{2+}$  transients was best-fit by a single exponential decay, indicating the lack of multiple  $\text{Ca}^{2+}$  extrusion processes distinguishable by rate. These data indicate that Fluo4 is able to detect expected changes in the kinetics of KCl-evoked  $\text{Ca}^{2+}$  transients.

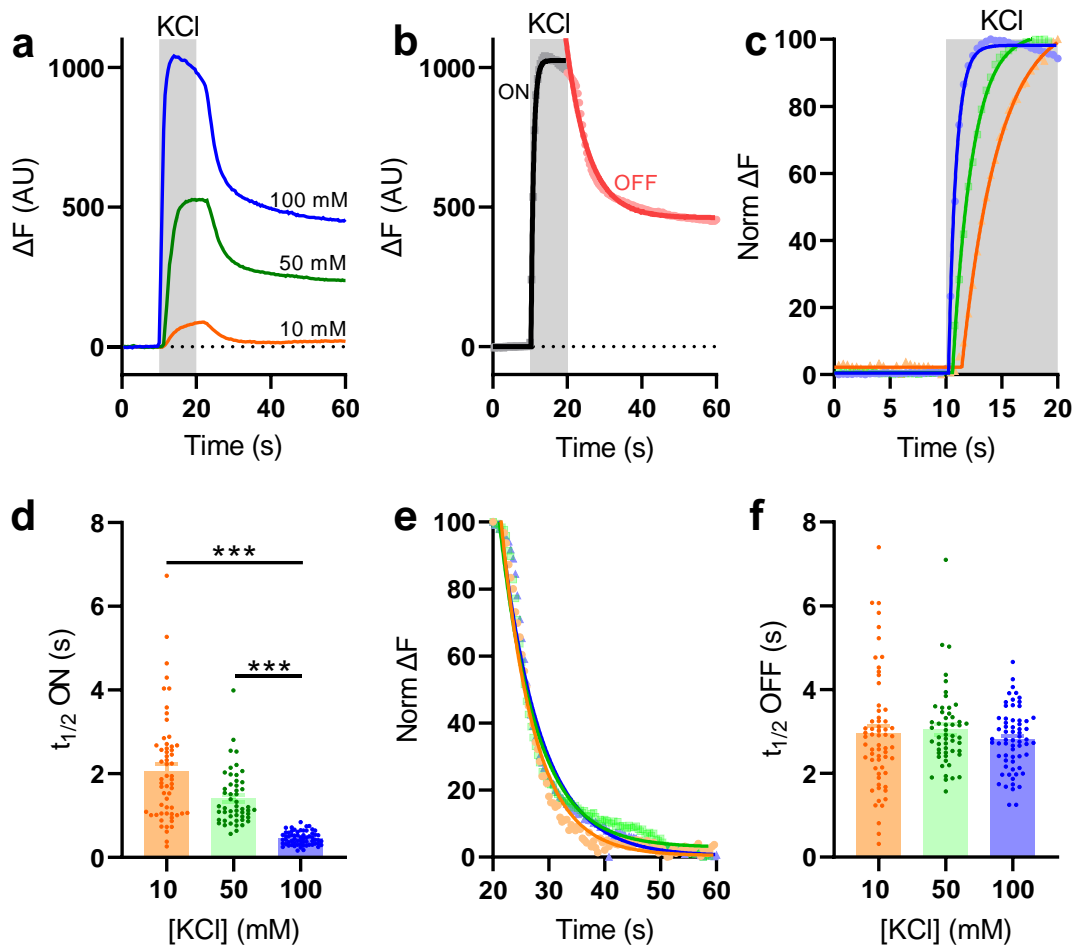


**Figure A2 Kinetics of KCl-evoked Ca<sup>2+</sup> transients**

- (a) Example traces from three neurons to which 10 mM (orange), 50 mM (green) or 100 mM (blue) KCl was applied.
- (b) Example curve fitting to the blue trace in (a). The first 20 s were fit with a plateau followed by a one-phase association (ON), and the latter 40 s were fit with a one-phase decay (OFF).
- (c) Example traces showing the first 20 s of randomly selected recordings in which 10 mM (orange), 50 mM (green) or 100 mM (blue) KCl was applied. Fluorescence is normalised to the minimum and maximum for each condition.
- (d) Grouped data showing the  $t_{1/2}$  ON for each concentration of KCl. 10 mM: 58 neurons from one mouse; 50 mM: 51 neurons from one mouse; 100 mM: 63 neurons from one mouse. Data analysed using a Kruskal-Wallis test with Dunn's post-tests.
- (e) Example traces showing the latter 40 s of randomly selected recordings in which 10 mM (orange), 50 mM (green) or 100 mM (blue) KCl was applied. Fluorescence is normalised to the minimum and maximum for each condition.
- (f) Grouped data showing the  $t_{1/2}$  OFF for each concentration of KCl. 10 mM: 62 neurons from one mouse; 50 mM: 52 neurons from one mouse; 100 mM: 64 neurons from one mouse. Data analysed using a Kruskal-Wallis test with Dunn's post-tests.

### A1.3. Measuring absolute [Ca<sup>2+</sup>] using Fluo4

*Relevant to Section 1.4.1.*

Fluo4 is a single wavelength indicator most commonly used to measure changes in [Ca<sup>2+</sup>], which is appropriate for work in this Thesis wherein changes in [Ca<sup>2+</sup>] in sensory neurons have been used to identify neuronal populations and the mechanisms underpinning the actions of Ang II. As Fluo4 is not a ratiometric indicator, its absolute fluorescence will depend on its concentration and the intensity of illumination. While absolute [Ca<sup>2+</sup>] is often measured using ratiometric Ca<sup>2+</sup> indicators, such as Fura2, it is also possible with a single wavelength indicator.

It has been shown that

$$\frac{F - F_{min}}{F_{max} - F} = \frac{[Fluo4Ca]}{[Fluo4]} \dots (4)$$

where F is the measured Fluo4 fluorescence, F<sub>min</sub> is the minimum Fluo4 fluorescence, F<sub>max</sub> is the maximal Fluo4 fluorescence, [Fluo4Ca] is the concentration of Fluo4 bound to Ca<sup>2+</sup> and [Fluo4] is the concentration of free Fluo4. F<sub>min</sub> is found by applying 0.1% Triton-X to neurons in the presence of 0 mM Ca<sup>2+</sup> and 10 mM EGTA (Figure A3a), and F<sub>max</sub> is found by applying 0.1% Triton-X to neurons in the presence of a saturating concentration (20 mM) of Ca<sup>2+</sup> (Figure A3a). Based on the equilibrium between Fluo4 and Ca<sup>2+</sup>, the concentration of Ca<sup>2+</sup> is

$$[Ca^{2+}] = K_D \frac{[Fluo4Ca]}{[Fluo4]} = K_D \frac{F - F_{min}}{F_{max} - F} \dots (5)$$

where K<sub>D</sub> is the dissociation constant for the binding of Ca<sup>2+</sup> to Fluo4 – 325 nM. It is now possible to relate optically measurable properties of Fluo4 with [Ca<sup>2+</sup>]. It is important to note that as F approaches F<sub>max</sub>, the estimate of [Ca<sup>2+</sup>] will become unreliable as the relationship between F/F<sub>max</sub> and [Ca<sup>2+</sup>]/K<sub>D</sub> becomes non-linear (Figure A3b). Using the above equation, one can now convert measured properties of Fluo4 to the average [Ca<sup>2+</sup>] for the neuron of interest. Ang II was applied to cultured sensory neurons, yielding an increase in Fluo4 fluorescence in a subset of neurons (Figure A3c). This increase in fluorescence was still well within the linear range of the indicator and did not approach the “unreliable zone” highlighted in Figure A3b, i.e., [Ca<sup>2+</sup>] was below K<sub>D</sub> (Figure A3d). The absolute [Ca<sup>2+</sup>] in the basal state was found to

be ~65 nM (Figure A3e), well in line with previous estimates. Ang II application resulted in an increase in  $[Ca^{2+}]$  to ~165 nM (Figure A3e).

While the above equation clearly has utility in ascertaining absolute  $[Ca^{2+}]$ , estimating  $F_{min}$  is not cell-specific because it must be done in a separate parallel experiment. So, not only does this waste a dish of neurons, the estimate is also not specific to the cells being imaged. One can overcome this by considering the dynamic range of the indicator (R)

$$R = \frac{F_{max}}{F_{min}} \dots (6)$$

Substituting equation (6) into (5) yields

$$[Ca^{2+}] = K_D \frac{\frac{F}{F_{max}} - \frac{1}{R}}{1 - \frac{F}{F_{max}}} \dots (7)$$

If R is sufficiently large,  $1/R$  becomes negligible compared to  $F/F_{max}$  and can be ignored from equation (7). For Fluo4, R is ~100 and  $1/R$  can thus be omitted from equation (7) (Maravall *et al.*, 2000). Consequently, equation (7) represents a method for calculating  $[Ca^{2+}]$  without the need for an estimate of  $F_{min}$ . The dependence of  $[Ca^{2+}]$  on absolute fluorescence, F, is eliminated by finding its ratio with  $F_{max}$ , thereby avoiding the effects of indicator concentration, illumination intensity and detector efficiency (Maravall *et al.*, 2000). The blue trace in Figure A3e shows an estimate of  $[Ca^{2+}]$  using equation (5), whereas the dotted pink trace shows  $[Ca^{2+}]$  estimated using equation (7). The greatest discrepancy between the two traces is 384 pM  $Ca^{2+}$ , or 0.59% of baseline  $[Ca^{2+}]$ , so the two methods appear to estimate  $[Ca^{2+}]$  equally well.

The application of Ang II yields a change in fluorescence well within the linear range of Fluo4, but what about the application of 50 mM KCl? Figure A3f shows that the application of KCl yielded a peak  $F/F_{max}$  of ~60%, equivalent to ~1.3 times  $K_D$ . This is still within the linear range of the indicator, and KCl does not increase  $[Ca^{2+}]$  much beyond  $K_D$ , showing that KCl application is unlikely to saturate Fluo4. In this experiment, baseline  $[Ca^{2+}]$  was found to be ~75 nM, raised to ~430 nM during KCl application (Figure A3g). Plotting basal  $[Ca^{2+}]$  against neuronal soma area revealed a negative correlation between these two variables ( $r = -0.25$ ,  $p < 0.0001$ , Figure A3h). The largest neurons (Q4) in this sample were found to have a lower basal  $[Ca^{2+}]$

compared to neurons in all other size quartiles ( $p < 0.02$ , Figure A3i), while neurons in Q1, 2 and 3 had similar basal  $[Ca^{2+}]$  ( $p > 0.40$ , Figure A3i).

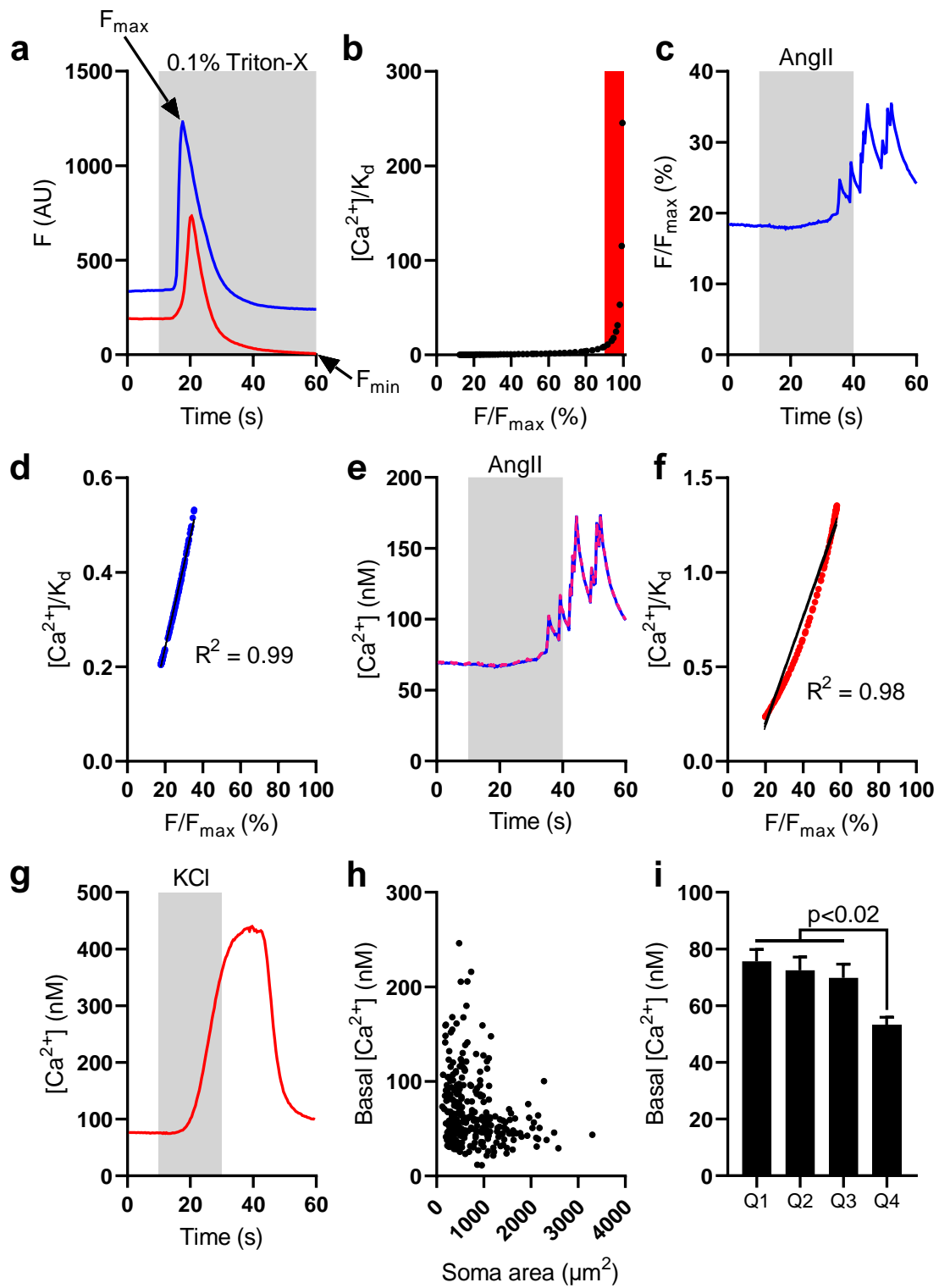


Figure A3 Legend on next page

### Figure A3 Measurements of absolute $[Ca^{2+}]$ using Fluo4

- (a) Example traces from two neurons showing the application of 0.1% Triton-X in the presence of 20 mM  $Ca^{2+}$  (blue) or 0 mM  $Ca^{2+}$  and 10 mM EGTA (red). The peak of the blue trace is taken as  $F_{max}$ , and the minimum of the red trace is taken as  $F_{min}$ . Note the peak of the red trace preceding  $F_{min}$ : this reflects the liberation of  $Ca^{2+}$  from intracellular  $Ca^{2+}$  stores.
- (b) The relationship between  $F/F_{max}$  and  $[Ca^{2+}]/K_D$ . The red shaded area highlights the “unreliable zone” where estimates of  $[Ca^{2+}]$  become unreasonably large.
- (c) Example trace showing the application of Ang II to a single neuron. The vertical axis shows fluorescence relative to the peak attained during Triton-X application.
- (d) The relationship between  $F/F_{max}$  and  $[Ca^{2+}]/K_D$  for the trace shown in (c). The data is well within the linear range (compare to (b)) and is fit with a linear regression.
- (e) Traces showing cytosolic  $[Ca^{2+}]$  during Ang II application. The blue solid trace is an estimate of  $[Ca^{2+}]$  based on equation (5); the pink dotted trace is based on equation (7).
- (f) The relationship between  $F/F_{max}$  and  $[Ca^{2+}]/K_D$  for the application of KCl (raw traces not shown). The data is well within the linear range (compare to (b)) and is fit with a linear regression.
- (g) Example trace showing cytosolic  $[Ca^{2+}]$  during KCl application.
- (h) Scatter plot showing basal  $[Ca^{2+}]$  against neuronal soma area (293 neurons from 3 independent cultures). Data analysed using Pearson’s correlation.
- (i) Basal  $[Ca^{2+}]$  in neurons grouped into size quartiles. Q1 vs Q4:  $p < 0.0001$ , Q2 vs Q4:  $p = 0.0015$ , Q3 vs Q4:  $p = 0.018$ . Data analysed using Kruskal-Wallis test with Dunn’s post-tests.

#### **A1.4. Response of cultured sensory neurons to cold**

*This Section is not referenced in the main text as it details an experiment which is not relevant to the main body of the Thesis. However, it is interesting – at least to the author.*

Sensing of environmental cold is underpinned by the activation of thermosensitive ion channels expressed on sensory neurons. TRPM8 channels, which also serve as menthol receptors, are activated by temperatures between 26 - 8°C (Bautista *et al.*, 2007), indicating that TRPM8 may function in the detection of cooling and acute noxious cold (Peier *et al.*, 2002). In line with this, TRPM8 is expressed in a population of Nav1.8-negative neurons which respond to acute cooling down to 1°C (Luiz *et al.*, 2019). However, the response to prolonged noxious cold was mediated by Nav1.8-expressing sensory neurons, which lack TRPM8 (Luiz *et al.*, 2019).

In cultured sensory neurons from the DRG, a prominent response to the application of 2°C external buffer was observed (starting temperature, 24°C; Figure A4a). 36.6% (34 of 93) neurons exhibited a rise in cytosolic Ca<sup>2+</sup> during cooling to 2°C (Figure A4b), and this response was abolished in the absence of extracellular Ca<sup>2+</sup> (1 of 88 neurons responded; Figure A4c). Figure A4d shows the response of 10 randomly selected neurons in 2 mM Ca<sup>2+</sup> (blue traces and 10 randomly selected neurons in 0 mM Ca<sup>2+</sup> (grey traces). Menthol (100 µM) stimulated 9.1±1.7% of sensory neurons (Figure A4e), in agreement with a previous report in which experiments were carried out at a similar bath temperature (Sarria and Gu, 2010). Menthol-evoked currents decrease in magnitude with increasing temperature, so the responses to menthol observed here may represent a combinatorial effect of menthol and temperature (Peier *et al.*, 2002). A response to capsaicin (1 µM) was observed in 42.8±2.3% of neurons (Figure A4e), in line with other studies (Sarria and Gu, 2010; Chakrabarti *et al.*, 2018). Some neurons exhibited co-sensitivity to menthol and capsaicin (Figure A4e, red trace), in agreement with the modest overlap in TRPM8 and TRPV1 expression identified by immunohistochemistry (Bautista *et al.*, 2007). Capsaicin-sensitive and -insensitive neurons were of similarly small cross-sectional area, though those sensitive to capsaicin were also found to respond to ATP and extracellular acid, and possess TTX-resistant Na<sup>+</sup> currents, identifying them as potential nociceptors (Xing *et al.*, 2006).

The disparity in the proportion of neurons responding to cold and to menthol supports the hypothesis that an unidentified cold sensor must be present in a subset of sensory

neurons (Babes, Zorzon and Reid, 2004; Luiz *et al.*, 2019). A recent transcriptomic study showed poor expression of Nav1.8 in TRPM8-expressing neurons (Figure A4f and g) (Usoskin *et al.*, 2015). The cyclic nucleotide-gated channel  $\alpha 3$  (CNGA3) has been posited as a cold sensory in hypothalamic neurons (Feketa *et al.*, 2020), though its expression in peripheral sensory neurons does not necessarily align with the unidentified cold sensor. Usoskin and colleagues found little to no expression in dissociated DRG neurons (Figure A4f), while Luiz and colleagues noted enriched expression in Nav1.8-negative, TRPM8-positive neurons (Usoskin *et al.*, 2015; Luiz *et al.*, 2019). TRPA1 has been suggested as a sensor for environmental cold. However, physiological and behavioural experiments have thus far failed to resolve the role of TRPA1 in cold thermosensation (Buijs and McNaughton, 2020). TRPA1 is highly expressed in Nav1.8-positive neurons (Figure A4f) (Usoskin *et al.*, 2015; Zeisel *et al.*, 2018). Does pharmacological inhibition of TRPA1 attenuate the neuronal response to cold in our set up? If so, TRPA1 may act as a cold sensor *in vitro*, though its role *in vivo* would require further probing. If not, this *in vitro* platform provides a simple and quick method for ascertaining the properties of the sensory neurons which respond to a 2°C cold stimulus – such as soma size, IB4 reactivity, or expression of neuronal markers. This information will highlight potential cold sensors expressed in the identified neuronal population. One such potential cold sensor beyond TRPA1 is Kv1.1, a voltage-gated K<sup>+</sup> channel which is inhibited by cooling, leading to membrane depolarisation and action potential discharge (Viana, De la Peña and Belmonte, 2002). This channel is highly expressed in Nav1.8-positive neurons (Zeisel *et al.*, 2018; Luiz *et al.*, 2019) and mediates cold allodynia in mechanically- and chemically-induced neuropathic pain (MacDonald *et al.*, 2021).

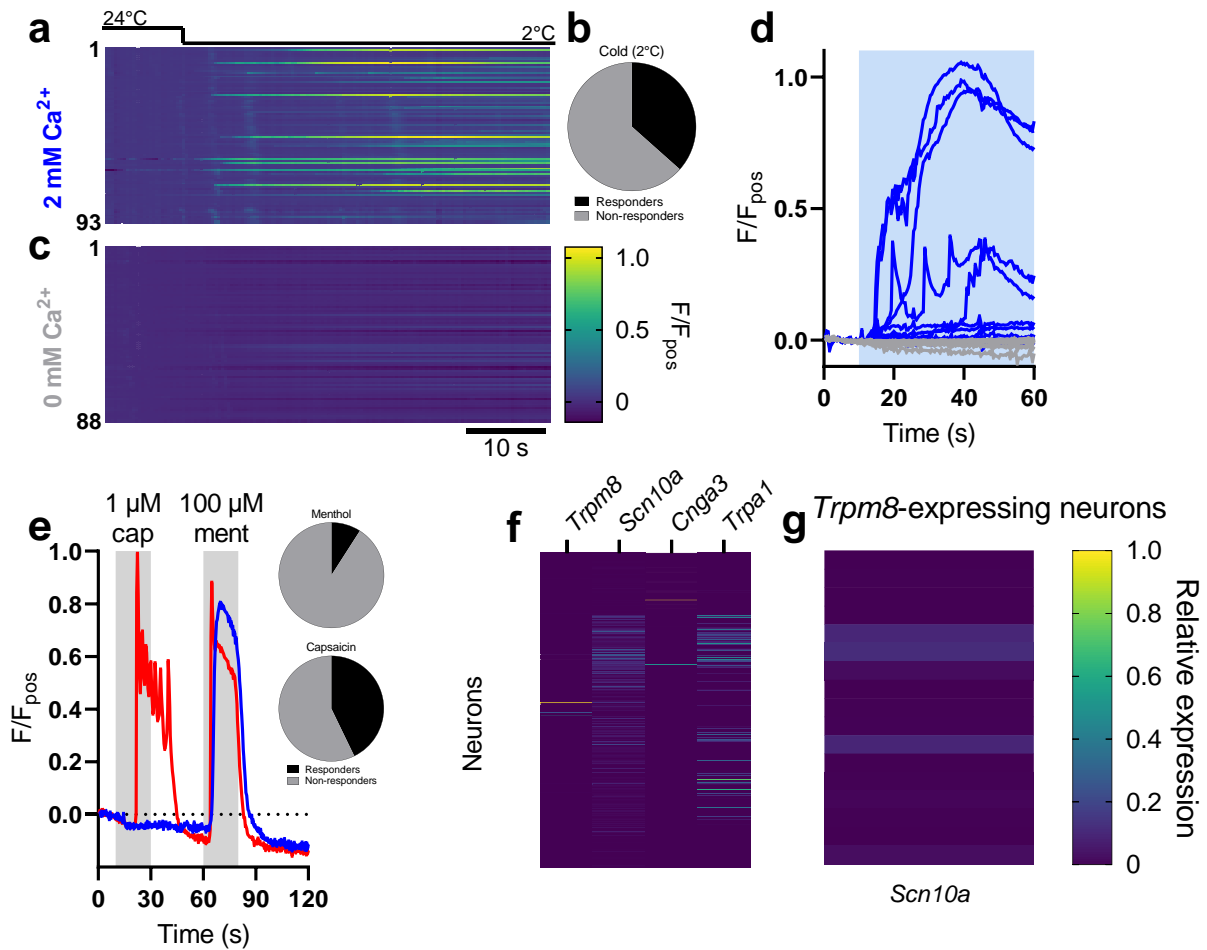


**Figure A1.4 Neuronal responses to cold and menthol**

- (a) Heatmap showing changes in Fluo4 fluorescence in 93 neurons during the application of external buffer at 2°C. Experiments carried out with 2 mM external  $\text{Ca}^{2+}$ .
- (b) Proportion of neurons responding to cold stimulus – 34 of 93.
- (c) Heatmap showing changes in Fluo4 fluorescence in 88 neurons during the application of external buffer at 2°C. Experiments carried out with 0 mM external  $\text{Ca}^{2+}$ .
- (d) Fluo4 fluorescence traces showing the response to a cold stimulus in 10 neurons 2 mM  $\text{Ca}^{2+}$  (blue traces) and 10 neurons in 0 mM  $\text{Ca}^{2+}$  (grey traces).
- (e) Fluo4 fluorescence traces showing the response of two exemplar neurons to capsaicin and menthol application. *Inset*: proportion of neurons responding to menthol (*top*) and capsaicin (*bottom*).
- (f) Heatmap showing the relative expression (normalised to maximum expression per transcript) of *Trpm8*, *Scn10a*, *Cnga3* and *Trpa1* from Usoskin *et al* (2015).
- (g) Heatmap showing the relative expression (normalised to maximum expression) of *Scn10a* within the *Trpm8*-expressing neuronal population.

## **Chapter 8**

### **Bibliography**

## 8.1. References

- Abrahamsen, B. *et al.* (2008) 'The cell and molecular basis of mechanical, cold, and inflammatory pain', *Science*, 321(5889). doi: 10.1126/science.1156916.
- Achuthan, A. *et al.* (2016) 'Granulocyte macrophage colony-stimulating factor induces CCL17 production via IRF4 to mediate inflammation', *Journal of Clinical Investigation*, 126(9). doi: 10.1172/JCI87828.
- Adebiyi, A. *et al.* (2014) 'Lipid rafts are required for signal transduction by angiotensin II receptor type 1 in neonatal glomerular mesangial cells', *Experimental Cell Research*, 324(1). doi: 10.1016/j.yexcr.2014.03.011.
- Adenis, A. *et al.* (1993) 'Increased pulmonary and intestinal permeability in Crohn's disease', *Gut*, 33(5). doi: 10.1136/gut.33.5.678.
- Aguilera, M., Cerdà-Cuellar, M. and Martínez, V. (2015) 'Antibiotic-induced dysbiosis alters host-bacterial interactions and leads to colonic sensory and motor changes in mice', *Gut Microbes*, 6(1). doi: 10.4161/19490976.2014.990790.
- Al-Mofarreh, M. and Al-Mofleh, I. (2013) 'Emerging inflammatory bowel disease in saudi outpatients: A report of 693 cases', *Saudi Journal of Gastroenterology*, 19(1). doi: 10.4103/1319-3767.105915.
- Alatab, S. *et al.* (2020) 'The global, regional, and national burden of inflammatory bowel disease in 195 countries and territories, 1990–2017: a systematic analysis for the Global Burden of Disease Study 2017', *The Lancet Gastroenterology and Hepatology*, 5(1). doi: 10.1016/S2468-1253(19)30333-4.
- Ambort, D. *et al.* (2012) 'Calcium and pH-dependent packing and release of the gel-forming MUC2 mucin', *Proceedings of the National Academy of Sciences of the United States of America*, 109(15). doi: 10.1073/pnas.1120269109.
- Anand, U. *et al.* (2015) 'Mechanisms underlying clinical efficacy of Angiotensin II type 2 receptor (AT2R) antagonist EMA401 in neuropathic pain: Clinical tissue and in vitro studies', *Molecular Pain*, 11(1). doi: 10.1186/s12990-015-0038-x.
- Ananthkrishnan, A. N. *et al.* (2012) 'Aspirin, nonsteroidal anti-inflammatory drug use, and risk for crohn disease and ulcerative colitis', *Annals of Internal Medicine*, 156(5). doi: 10.7326/0003-4819-156-5-201203060-00007.
- Ananthkrishnan, A. N. *et al.* (2013) 'A prospective study of long-term intake of dietary fiber and risk of Crohn's disease and ulcerative colitis', *Gastroenterology*, 145(5). doi:

10.1053/j.gastro.2013.07.050.

Ananthakrishnan, A. N. (2015) 'Epidemiology and risk factors for IBD', *Nature Reviews Gastroenterology and Hepatology*. doi: 10.1038/nrgastro.2015.34.

Azimi, I. *et al.* (2020) 'A New Selective Pharmacological Enhancer of the Orai1 Ca<sup>2+</sup> Channel Reveals Roles for Orai1 in Smooth and Skeletal Muscle Functions', *ACS Pharmacology and Translational Science*, 3(1). doi: 10.1021/acsptsci.9b00081.

Babes, A., Zorzon, D. and Reid, G. (2004) 'Two populations of cold-sensitive neurons in rat dorsal root ganglia and their modulation by nerve growth factor', *European Journal of Neuroscience*, 20(9). doi: 10.1111/j.1460-9568.2004.03695.x.

Bakshi, N. *et al.* (2021) 'Chronic pain in patients with inflammatory bowel disease', *Pain*, 162(10). doi: 10.1097/j.pain.0000000000002304.

Balla, A. *et al.* (2012) 'Mapping of the localization of type 1 angiotensin receptor in membrane microdomains using bioluminescence resonance energy transfer-based sensors', *Journal of Biological Chemistry*, 287(12). doi: 10.1074/jbc.M111.293944.

Bautista, D. M. *et al.* (2007) 'The menthol receptor TRPM8 is the principal detector of environmental cold', *Nature*, 448(7150). doi: 10.1038/nature05910.

Bautzova, T. *et al.* (2018) '5-oxoETE triggers nociception in constipation-predominant irritable bowel syndrome through MAS-related G protein-coupled receptor D', *Science Signaling*, 11(561). doi: 10.1126/scisignal.aal2171.

Bel, S. *et al.* (2017) 'Paneth cells secrete lysozyme via secretory autophagy during bacterial infection of the intestine', *Science*, 357(6355). doi: 10.1126/science.aal4677.

Benchimol, E. I. *et al.* (2015) 'Inflammatory bowel disease in immigrants to Canada and their children: A population-based cohort study', *American Journal of Gastroenterology*, 110(4). doi: 10.1038/ajg.2015.52.

Benigni, A., Cassis, P. and Remuzzi, G. (2010) 'Angiotensin II revisited: New roles in inflammation, immunology and aging', *EMBO Molecular Medicine*. doi: 10.1002/emmm.201000080.

Bennett, R. A., Rubin, P. H. and Present, D. H. (1991) 'Frequency of inflammatory bowel disease in offspring of couples both presenting with inflammatory bowel disease', *Gastroenterology*, 100(6). doi: 10.1016/0016-5085(91)90663-6.

Berndt, B. E. *et al.* (2007) 'The Role of Dendritic Cells in the Development of Acute Dextran Sulfate Sodium Colitis', *The Journal of Immunology*, 179(9). doi:

10.4049/jimmunol.179.9.6255.

Bernstein, C. N. *et al.* (2001) 'The prevalence of extraintestinal diseases in inflammatory bowel disease: A population-based study', *American Journal of Gastroenterology*, 96(4). doi: 10.1016/S0002-9270(01)02319-X.

Berridge, M. J. (2007) 'Inositol trisphosphate and calcium oscillations', *Biochemical Society Symposium*, 74. doi: 10.1042/BSS0740001.

Bessac, B. F. *et al.* (2008) 'TRPA1 is a major oxidant sensor in murine airway sensory neurons', *Journal of Clinical Investigation*, 118(5). doi: 10.1172/JCI34192.

Brockschneider, D. *et al.* (2004) 'Cell Depletion Due to Diphtheria Toxin Fragment A after Cre-Mediated Recombination', *Molecular and Cellular Biology*, 24(17). doi: 10.1128/mcb.24.17.7636-7642.2004.

Brownlow, S. L. and Sage, S. O. (2005) 'Transient receptor potential protein subunit assembly and membrane distribution in human platelets', *Thrombosis and Haemostasis*, 94(4). doi: 10.1160/TH05-06-0391.

Brunner, J., Ragupathy, S. and Borchard, G. (2021) 'Target specific tight junction modulators', *Advanced Drug Delivery Reviews*. doi: 10.1016/j.addr.2021.02.008.

Buijs, T. J. and McNaughton, P. A. (2020) 'The Role of Cold-Sensitive Ion Channels in Peripheral Thermosensation', *Frontiers in Cellular Neuroscience*. doi: 10.3389/fncel.2020.00262.

Buxadé, M. *et al.* (2012) 'Gene expression induced by Toll-like receptors in macrophages requires the transcription factor NFAT5', *Journal of Experimental Medicine*, 209(2). doi: 10.1084/jem.20111569.

Castro, J. *et al.* (2019) 'Activation of pruritogenic TGR5, MRGPRA3, and MRGPRC11 on colon-innervating afferents induces visceral hypersensitivity', *JCI Insight*, 4(20). doi: 10.1172/jci.insight.131712.

Caterina, M. J. *et al.* (1997) 'The capsaicin receptor: A heat-activated ion channel in the pain pathway', *Nature*, 389(6653). doi: 10.1038/39807.

Cesare, P. and Mcnaughton, P. (1996) 'A novel heat-activated current in nociceptive neurons and its sensitization by bradykinin', *Proceedings of the National Academy of Sciences of the United States of America*, 93(26). doi: 10.1073/pnas.93.26.15435.

Ceuleers, H. *et al.* (2016) 'Visceral hypersensitivity in inflammatory bowel diseases and irritable bowel syndrome: The role of proteases', *World Journal of Gastroenterology*. doi:

10.3748/wjg.v22.i47.10275.

Cevikbas, F. *et al.* (2014) 'A sensory neuron-expressed IL-31 receptor mediates T helper cell-dependent itch: Involvement of TRPV1 and TRPA1', *Journal of Allergy and Clinical Immunology*, 133(2). doi: 10.1016/j.jaci.2013.10.048.

Chakrabarti, S. *et al.* (2018) 'Acute inflammation sensitizes knee-innervating sensory neurons and decreases mouse digging behavior in a TRPV1-dependent manner', *Neuropharmacology*, 143. doi: 10.1016/j.neuropharm.2018.09.014.

Chakrabarti, S. *et al.* (2020) 'Human osteoarthritic synovial fluid increases excitability of mouse dorsal root ganglion sensory neurons: An in-vitro translational model to study arthritic pain', *Rheumatology (United Kingdom)*, 59(3). doi: 10.1093/rheumatology/kez331.

Chang, Y. *et al.* (2014) 'Structural basis for a pH-sensitive calcium leak across membranes', *Science*, 344(6188). doi: 10.1126/science.1252043.

Chang, Y. and Wei, W. (2015) 'Angiotensin II in inflammation, immunity and rheumatoid arthritis', *Clinical and Experimental Immunology*. doi: 10.1111/cei.12467.

Cheng, J. K. and Ji, R. R. (2008) 'Intracellular signaling in primary sensory neurons and persistent pain', *Neurochemical Research*. doi: 10.1007/s11064-008-9711-z.

Chisholm, K. I. *et al.* (2018) 'Large scale in vivo recording of sensory neuron activity with GCaMP6', *eNeuro*, 5(1). doi: 10.1523/ENEURO.0417-17.2018.

Collins, C. B. *et al.* (2011) 'Retinoic acid attenuates ileitis by restoring the balance between T-helper 17 and t regulatory cells', *Gastroenterology*, 141(5). doi: 10.1053/j.gastro.2011.05.049.

Conforti, A. *et al.* (2021) 'Beyond the joints, the extra-articular manifestations in rheumatoid arthritis', *Autoimmunity Reviews*. doi: 10.1016/j.autrev.2020.102735.

Cook, A. D. *et al.* (2013) 'Granulocyte-macrophage colony-stimulating factor is a key mediator in inflammatory and arthritic pain', *Annals of the Rheumatic Diseases*, 72(2). doi: 10.1136/annrheumdis-2012-201703.

Crabtree, G. R. and Olson, E. N. (2002) 'NFAT signaling: Choreographing the social lives of cells', *Cell*. doi: 10.1016/S0092-8674(02)00699-2.

Cregger, M., Berger, A. J. and Rimm, D. L. (2006) 'Immunohistochemistry and quantitative analysis of protein expression', *Archives of Pathology and Laboratory Medicine*. doi: 10.5858/2006-130-1026-iaqaop.

Cruzblanca, H., Koh, D. S. and Hille, B. (1998) 'Bradykinin inhibits M current via phospholipase C and Ca<sup>2+</sup> release from IP<sub>3</sub>-sensitive Ca<sup>2+</sup> stores in rat sympathetic neurons', *Proceedings of the National Academy of Sciences of the United States of America*, 95(12). doi: 10.1073/pnas.95.12.7151.

Dabek, M. *et al.* (2009) 'Luminal cathepsin G and protease-activated receptor 4: A duet involved in alterations of the colonic epithelial barrier in ulcerative colitis', *American Journal of Pathology*, 175(1). doi: 10.2353/ajpath.2009.080986.

Danese, S. *et al.* (2019) 'Randomised trial and open-label extension study of an anti-interleukin-6 antibody in Crohn's disease (ANDANTE I and II)', *Gut*, 68(1). doi: 10.1136/gutjnl-2017-314562.

Daou, I. *et al.* (2016) 'Optogenetic silencing of Nav1.8-positive afferents alleviates inflammatory and neuropathic pain', *eNeuro*, 3(1). doi: 10.1523/ENEURO.0140-15.2016.

Davis, C. J. *et al.* (2006) 'AT<sub>4</sub> receptor activation increases intracellular calcium influx and induces a non-N-methyl-D-aspartate dependent form of long-term potentiation', *Neuroscience*, 137(4). doi: 10.1016/j.neuroscience.2005.10.051.

Dehaven, W. I. *et al.* (2009) 'TRPC channels function independently of STIM1 and Orai1', *Journal of Physiology*, 587(10). doi: 10.1113/jphysiol.2009.170431.

DeHaven, W. I. *et al.* (2007) 'Calcium inhibition and calcium potentiation of Orai1, Orai2, and Orai3 calcium release-activated calcium channels', *Journal of Biological Chemistry*, 282(24). doi: 10.1074/jbc.M611374200.

Desormeaux, C. *et al.* (2018) 'Protease-activated receptor 1 is implicated in irritable bowel syndrome mediators-induced signaling to thoracic human sensory neurons', *Pain*, 159(7). doi: 10.1097/j.pain.0000000000001208.

Dhaka, A. *et al.* (2008) 'Visualizing cold spots: TRPM8-expressing sensory neurons and their projections', *Journal of Neuroscience*, 28(3). doi: 10.1523/JNEUROSCI.3976-07.2008.

Díaz-Coránguez, M., Liu, X. and Antonetti, D. A. (2019) 'Tight junctions in cell proliferation', *International Journal of Molecular Sciences*. doi: 10.3390/ijms20235972.

Durand, D. B. *et al.* (1988) 'Characterization of antigen receptor response elements within the interleukin-2 enhancer', *Molecular and Cellular Biology*, 8(4). doi: 10.1128/mcb.8.4.1715-1724.1988.

Dyachok, O. and Gylfe, E. (2004) 'Ca<sup>2+</sup>-induced Ca<sup>2+</sup> release via inositol 1,4,5-trisphosphate receptors is amplified by protein kinase A and triggers exocytosis in pancreatic

- $\beta$ -cells', *Journal of Biological Chemistry*, 279(44). doi: 10.1074/jbc.M407673200.
- Eftychi, C. *et al.* (2019) 'Temporally Distinct Functions of the Cytokines IL-12 and IL-23 Drive Chronic Colon Inflammation in Response to Intestinal Barrier Impairment', *Immunity*, 51(2). doi: 10.1016/j.immuni.2019.06.008.
- Ellinghaus, D. *et al.* (2012) 'Combined analysis of genome-wide association studies for Crohn disease and psoriasis identifies seven shared susceptibility loci', *American Journal of Human Genetics*, 90(4). doi: 10.1016/j.ajhg.2012.02.020.
- Elliott, T. R. *et al.* (2013) 'Quantification and characterization of mucosa-associated and intracellular escherichia coli in inflammatory bowel disease', *Inflammatory Bowel Diseases*, 19(11). doi: 10.1097/MIB.0b013e3182a38a92.
- Emery, E. C. *et al.* (2016) 'In vivo characterization of distinct modality-specific subsets of somatosensory neurons using GCaMP', *Science Advances*, 2(11). doi: 10.1126/sciadv.1600990.
- Epstein, F. H. and Harris, E. D. (1990) 'Rheumatoid arthritis: Pathophysiology and Implications for Therapy', *New England Journal of Medicine*.
- Fairbrass, K. M. *et al.* (2021) 'Effect of ACE inhibitors and angiotensin II receptor blockers on disease outcomes in inflammatory bowel disease', *Gut*. doi: 10.1136/gutjnl-2020-321186.
- Fan, C. *et al.* (2018) 'Structure of the human lipid-gated cation channel TRPC3', *eLife*, 7. doi: 10.7554/eLife.36852.
- Feketa, V. V. *et al.* (2020) 'Cnga3 acts as a cold sensor in hypothalamic neurons', *eLife*, 9. doi: 10.7554/eLife.55370.
- Feske, S. *et al.* (2007) 'The duration of nuclear residence of NFAT determines the pattern of cytokine expression in human SCID T cells', *The Journal of Immunology*, 179(12). doi: 10.4049/jimmunol.179.12.8568.
- Finch, E. A., Turner, T. J. and Goldin, S. M. (1991) 'Calcium as a coagonist of inositol 1,4,5-trisphosphate-induced calcium release', *Science*, 252(5004). doi: 10.1126/science.2017683.
- Forrester, S. J. *et al.* (2018) 'Angiotensin II signal transduction: An update on mechanisms of physiology and pathophysiology', *Physiological Reviews*. doi: 10.1152/physrev.00038.2017.
- Foskett, J. K. *et al.* (2007) 'Inositol trisphosphate receptor Ca<sup>2+</sup> release channels', *Physiological Reviews*. doi: 10.1152/physrev.00035.2006.
- Fullmer, J. M. *et al.* (2004) 'Identification of some lectin IB4 binding proteins in rat dorsal root

ganglia', *NeuroReport*, 15(11). doi: 10.1097/01.wnr.0000136037.54095.64.

Gallazzini, M. *et al.* (2010) 'c-Abl mediates high NaCl-induced phosphorylation and activation of the transcription factor TonEBP/OREBP', *The FASEB Journal*, 24(11). doi: 10.1096/fj.10-157362.

Galvez, J., Rodríguez-Cabezas, M. E. and Zarzuelo, A. (2005) 'Effects of dietary fiber on inflammatory bowel disease', *Molecular Nutrition and Food Research*. doi: 10.1002/mnfr.200500013.

Garg, M. *et al.* (2015) 'Upregulation of circulating components of the alternative renin-angiotensin system in inflammatory bowel disease: A pilot study', *JRAAS - Journal of the Renin-Angiotensin-Aldosterone System*, 16(3). doi: 10.1177/1470320314521086.

Garg, M. *et al.* (2020) 'Imbalance of the renin-angiotensin system may contribute to inflammation and fibrosis in IBD: A novel therapeutic target?', *Gut*, 69(5). doi: 10.1136/gutjnl-2019-318512.

Garrod, D. and Chidgey, M. (2008) 'Desmosome structure, composition and function', *Biochimica et Biophysica Acta - Biomembranes*. doi: 10.1016/j.bbamem.2007.07.014.

Gee, K. R. *et al.* (2000) 'Chemical and physiological characterization of fluo-4 Ca<sup>2+</sup>-indicator dyes', *Cell Calcium*, 27(2). doi: 10.1054/ceca.1999.0095.

Gisbert, J. P. and Chaparro, M. (2021) 'Primary failure to an anti-tnf agent in inflammatory bowel disease: Switch (to a second anti-tnf agent) or swap (for another mechanism of action)?', *Journal of Clinical Medicine*, 10(22). doi: 10.3390/jcm10225318.

Gitter, A. H. *et al.* (2001) 'Epithelial barrier defects in ulcerative colitis: Characterization and quantification by electrophysiological imaging', *Gastroenterology*, 121(6). doi: 10.1053/gast.2001.29694.

Glasser, A. L. *et al.* (2001) 'Adherent invasive Escherichia coli strains from patients with Crohn's disease survive and replicate within macrophages without inducing host cell death', *Infection and Immunity*, 69(9). doi: 10.1128/IAI.69.9.5529-5537.2001.

Gold, M. S. *et al.* (1996) 'Hyperalgesic agents increase a tetrodotoxin-resistant Na<sup>+</sup> current in nociceptors', *Proceedings of the National Academy of Sciences of the United States of America*, 93(3). doi: 10.1073/pnas.93.3.1108.

Gomez, R. A. *et al.* (1993) 'Leukocytes synthesize angiotensinogen', *Hypertension*, 21(4). doi: 10.1161/01.HYP.21.4.470.

González-Sánchez, P. *et al.* (2017) 'Store-operated calcium entry is required for mGluR-

dependent long term depression in cortical neurons', *Frontiers in Cellular Neuroscience*, 11. doi: 10.3389/fncel.2017.00363.

Gross, V. *et al.* (1992) 'Evidence for continuous stimulation of interleukin-6 production in Crohn's disease', *Gastroenterology*, 102(2). doi: 10.1016/0016-5085(92)90098-J.

Groth, R. D. *et al.* (2007) 'Neurotrophin activation of NFAT-dependent transcription contributes to the regulation of pro-nociceptive genes', *Journal of Neurochemistry*, 102(4). doi: 10.1111/j.1471-4159.2007.04632.x.

Gudes, S. *et al.* (2015) 'The role of slow and persistent ttx-resistant sodium currents in acute tumor necrosis factor- $\alpha$ -mediated increase in nociceptors excitability', *Journal of Neurophysiology*, 113(2). doi: 10.1152/jn.00652.2014.

Gudlur, A. *et al.* (2014) 'STIM1 triggers a gating rearrangement at the extracellular mouth of the ORAI1 channel', *Nature Communications*, 5. doi: 10.1038/ncomms6164.

Gwack, Y. *et al.* (2007) 'Signalling to transcription: Store-operated Ca<sup>2+</sup> entry and NFAT activation in lymphocytes', *Cell Calcium*, 42(2). doi: 10.1016/j.ceca.2007.03.007.

Gwon, D. H. *et al.* (2021) 'Nfat5 deficiency alleviates formalin-induced inflammatory pain through mtor', *International Journal of Molecular Sciences*, 22(5). doi: 10.3390/ijms22052587.

Hachiya, K. *et al.* (2021) 'Irbesartan, an angiotensin II type 1 receptor blocker, inhibits colitis-associated tumorigenesis by blocking the MCP-1/CCR2 pathway', *Scientific Reports*, 11(1). doi: 10.1038/s41598-021-99412-8.

Hall, J. E. (1991) 'Control of blood pressure by the renin-angiotensin-aldosterone system', *Clinical Cardiology*, 14(4 S). doi: 10.1002/clc.4960141802.

Halterman, J. A. *et al.* (2011) 'Nuclear factor of activated T cells 5 regulates vascular smooth muscle cell phenotypic modulation', *Arteriosclerosis, Thrombosis, and Vascular Biology*, 31(10). doi: 10.1161/ATVBAHA.111.232165.

Halterman, J. A., Moo Kwon, H. and Wamhoff, B. R. (2012) 'Tonicity-independent regulation of the osmosensitive transcription factor tonebp (NFAT5)', *American Journal of Physiology - Cell Physiology*. doi: 10.1152/ajpcell.00327.2011.

Han, E. J. *et al.* (2017) 'Suppression of NFAT5-mediated Inflammation and Chronic Arthritis by Novel  $\kappa$ B-binding Inhibitors', *EBioMedicine*, 18. doi: 10.1016/j.ebiom.2017.03.039.

Hanauer, S. B. *et al.* (2002) 'Maintenance infliximab for Crohn's disease: The ACCENT I randomised trial', *Lancet*, 359(9317). doi: 10.1016/S0140-6736(02)08512-4.

- Harper, M. T. *et al.* (2013) 'Transient receptor potential channels function as a coincidence signal detector mediating phosphatidylserine exposure', *Science Signaling*, 6(281). doi: 10.1126/scisignal.2003701.
- Hart, A. L. *et al.* (2005) 'Characteristics of intestinal dendritic cells in inflammatory bowel diseases', *Gastroenterology*, 129(1). doi: 10.1053/j.gastro.2005.05.013.
- Hartsock, A. and Nelson, W. J. (2008) 'Adherens and tight junctions: Structure, function and connections to the actin cytoskeleton', *Biochimica et Biophysica Acta - Biomembranes*. doi: 10.1016/j.bbamem.2007.07.012.
- Helyes, Z. *et al.* (1997) 'Inhibition by nociceptin of neurogenic inflammation and the release of SP and CGRP from sensory nerve terminals', *British Journal of Pharmacology*, 121(4). doi: 10.1038/sj.bjp.0701209.
- De Hertogh, G. *et al.* (2008) 'Evidence for the involvement of infectious agents in the pathogenesis of Crohn's disease', *World Journal of Gastroenterology*. doi: 10.3748/wjg.14.845.
- Hewavitharana, T. *et al.* (2007) 'Role of STIM and Orai proteins in the store-operated calcium signaling pathway', *Cell Calcium*, 42(2). doi: 10.1016/j.ceca.2007.03.009.
- Hockley, J. R. F. *et al.* (2016) 'P2Y receptors sensitize mouse and human colonic nociceptors', *Journal of Neuroscience*, 36(8). doi: 10.1523/JNEUROSCI.3369-15.2016.
- Hockley, J. R. F. *et al.* (2019) 'Single-cell RNAseq reveals seven classes of colonic sensory neuron', *Gut*, 68(4). doi: 10.1136/gutjnl-2017-315631.
- Hofmann, T. *et al.* (1999) 'Direct activation of human TRPC6 and TRPC3 channels by diacylglycerol', *Nature*, 397(6716). doi: 10.1038/16711.
- Hofmann, T. *et al.* (2002) 'Subunit composition of mammalian transient receptor potential channels in living cells', *Proceedings of the National Academy of Sciences of the United States of America*, 99(11). doi: 10.1073/pnas.102596199.
- Hogan, P. G. *et al.* (2003) 'Transcriptional regulation by calcium, calcineurin, and NFAT', *Genes and Development*. doi: 10.1101/gad.1102703.
- Hogan, P. G. and Rao, A. (2015) 'Store-operated calcium entry: Mechanisms and modulation', *Biochemical and Biophysical Research Communications*. doi: 10.1016/j.bbrc.2015.02.110.
- Holtmann, M. H. *et al.* (2002) 'Tumor necrosis factor-receptor 2 is up-regulated on lamina propria T cells in Crohn's disease and promotes experimental colitis in vivo', *European*

*Journal of Immunology*. doi: 10.1002/1521-4141(200211)32:11<3142::AID-IMMU3142>3.0.CO;2-4.

Hooper, J. S. *et al.* (2013) 'Store-operated calcium entry in vagal sensory nerves is independent of Orai channels', *Brain Research*, 1503. doi: 10.1016/j.brainres.2013.02.002.

Hu, R. *et al.* (2016) 'TMEM45B, up-regulated in human lung cancer, enhances tumorigenicity of lung cancer cells', *Tumor Biology*, 37(9). doi: 10.1007/s13277-016-5063-5.

Huang, G., Wang, Y. and Chi, H. (2013) 'Control of T Cell Fates and Immune Tolerance by p38 $\alpha$  Signaling in Mucosal CD103 + Dendritic Cells', *The Journal of Immunology*, 191(2). doi: 10.4049/jimmunol.1300398.

Hue, S. *et al.* (2006) 'Interleukin-23 drives innate and T cell-mediated intestinal inflammation', *Journal of Experimental Medicine*, 203(11). doi: 10.1084/jem.20061099.

Hughes, P. A. *et al.* (2013) 'Sensory neuro-immune interactions differ between Irritable Bowel Syndrome subtypes', *Gut*, 62(10). doi: 10.1136/gutjnl-2011-301856.

Iliev, I. D. *et al.* (2009) 'Human intestinal epithelial cells promote the differentiation of tolerogenic dendritic cells', *Gut*, 58(11). doi: 10.1136/gut.2008.175166.

van Itallie, C. M. *et al.* (2008) 'The density of small tight junction pores varies among cell types and is increased by expression of claudin-2', *Journal of Cell Science*, 121(3). doi: 10.1242/jcs.021485.

Ito, H. (2005) 'Treatment of Crohn's disease with anti-IL-6 receptor antibody.', *Journal of gastroenterology*, 40 Suppl 16. doi: 10.1007/BF02990576.

Ivanova, A. *et al.* (2005) 'In vivo genetic ablation by Cre-mediated expression of diphtheria toxin fragment A', *Genesis*, 43(3). doi: 10.1002/gene.20162.

Jablaoui, A. *et al.* (2020) 'Fecal Serine Protease Profiling in Inflammatory Bowel Diseases', *Frontiers in Cellular and Infection Microbiology*, 10. doi: 10.3389/fcimb.2020.00021.

Jackson, J. G., Usachev, Y. M. and Thayer, S. A. (2007) 'Bradykinin-induced nuclear factor of activated T-cells-dependent transcription in rat dorsal root ganglion neurons', *Molecular Pharmacology*, 72(2). doi: 10.1124/mol.107.035048.

Jacobs, J. D. *et al.* (2019) 'Impact of Angiotensin II Signaling Blockade on Clinical Outcomes in Patients with Inflammatory Bowel Disease', *Digestive Diseases and Sciences*, 64(7). doi: 10.1007/s10620-019-5474-4.

Jairaman, A. and Prakriya, M. (2013) 'Molecular pharmacology of store-operated CRAC

channels', *Channels*, 7(5). doi: 10.4161/chan.25292.

Jairath, V. and Feagan, B. G. (2020) 'Global burden of inflammatory bowel disease', *The Lancet Gastroenterology and Hepatology*. doi: 10.1016/S2468-1253(19)30358-9.

Jaszewski, R. *et al.* (1990) 'Increased colonic mucosal angiotensin I and II concentrations in Crohn's colitis', *Gastroenterology*, 98(6). doi: 10.1016/0016-5085(90)91088-N.

Johansson, M. E. V. *et al.* (2008) 'The inner of the two Muc2 mucin-dependent mucus layers in colon is devoid of bacteria', *Proceedings of the National Academy of Sciences of the United States of America*, 105(39). doi: 10.1073/pnas.0803124105.

Johansson, M. E. V. *et al.* (2014) 'Bacteria penetrate the normally impenetrable inner colon mucus layer in both murine colitis models and patients with ulcerative colitis', *Gut*, 63(2). doi: 10.1136/gutjnl-2012-303207.

Johansson, M. E. V. (2014) 'Mucus layers in inflammatory bowel disease', *Inflammatory Bowel Diseases*, 20(11). doi: 10.1097/MIB.000000000000117.

Jongsma, M. M. E. *et al.* (2022) 'First-line treatment with infliximab versus conventional treatment in children with newly diagnosed moderate-to-severe Crohn's disease: An open-label multicentre randomised controlled trial', *Gut*, 71(1). doi: 10.1136/gutjnl-2020-322339.

Joossens, M. *et al.* (2011) 'Dysbiosis of the faecal microbiota in patients with Crohn's disease and their unaffected relatives', *Gut*, 60(5). doi: 10.1136/gut.2010.223263.

Jostins, L. *et al.* (2012) 'Host-microbe interactions have shaped the genetic architecture of inflammatory bowel disease', *Nature*, 491(7422). doi: 10.1038/nature11582.

Katada, K. *et al.* (2008) 'Dextran sulfate sodium-induced acute colonic inflammation in angiotensin II type 1a receptor deficient mice', *Inflammation Research*, 57(2). doi: 10.1007/s00011-007-7098-y.

Kayssi, A. *et al.* (2007) 'Mechanisms of protease-activated receptor 2-evoked hyperexcitability of nociceptive neurons innervating the mouse colon', *Journal of Physiology*, 580(3). doi: 10.1113/jphysiol.2006.126599.

Van Kemseke, C., Belaiche, J. and Louis, E. (2000) 'Frequently relapsing Crohn's disease is characterized by persistent elevation in interleukin-6 and soluble interleukin-2 receptor serum levels during remission', *International Journal of Colorectal Disease*, 15(4). doi: 10.1007/s003840000226.

Khalili, H. *et al.* (2013) 'Oral contraceptives, reproductive factors and risk of inflammatory bowel disease', *Gut*, 62(8). doi: 10.1136/gutjnl-2012-302362.

- Kikkawa, U., Matsuzaki, H. and Yamamoto, T. (2002) 'Protein kinase C $\delta$  (PKC $\delta$ ): Activation mechanisms and functions', *Journal of Biochemistry*, 132(6). doi: 10.1093/oxfordjournals.jbchem.a003294.
- Kim, M. S. and Usachev, Y. M. (2009) 'Mitochondrial Ca<sup>2+</sup> cycling facilitates activation of the transcription factor NFAT in sensory neurons', *Journal of Neuroscience*, 29(39). doi: 10.1523/JNEUROSCI.3384-09.2009.
- Kim, N. H. *et al.* (2014) 'The xanthine oxidase-NFAT5 pathway regulates macrophage activation and TLR-induced inflammatory arthritis', *European Journal of Immunology*, 44(9). doi: 10.1002/eji.201343669.
- Kitazono, T. *et al.* (1995) 'Evidence that angiotensin II is present in human monocytes', *Circulation*, 91(4). doi: 10.1161/01.CIR.91.4.1129.
- Kiyonaka, S. *et al.* (2009) 'Selective and direct inhibition of TRPC3 channels underlies biological activities of a pyrazole compound', *Proceedings of the National Academy of Sciences of the United States of America*, 106(13). doi: 10.1073/pnas.0808793106.
- Kleessen, B. *et al.* (2002) 'Mucosal and invading bacteria in patients with inflammatory bowel disease compared with controls', *Scandinavian Journal of Gastroenterology*, 37(9). doi: 10.1080/003655202320378220.
- Kobayashi, T. *et al.* (2020) 'Ulcerative colitis', *Nature Reviews Disease Primers*, 6(1). doi: 10.1038/s41572-020-0205-x.
- Koizumi, S. *et al.* (2004) 'Ca<sup>2+</sup> waves in keratinocytes are transmitted to sensory neurons: The involvement of extracellular ATP and P2Y<sub>2</sub> receptor activation', *Biochemical Journal*, 380(2). doi: 10.1042/BJ20031089.
- Koleva, P. T. *et al.* (2012) 'Inulin and fructo-oligosaccharides have divergent effects on colitis and commensal microbiota in HLA-B27 transgenic rats', *British Journal of Nutrition*, 108(9). doi: 10.1017/S0007114511007203.
- Kontoyiannis, D. *et al.* (1999) 'Impaired on/off regulation of TNF biosynthesis in mice lacking TNF AU- rich elements: Implications for joint and gut-associated immunopathologies', *Immunity*, 10(3). doi: 10.1016/S1074-7613(00)80038-2.
- Kronman, M. P. *et al.* (2012) 'Antibiotic exposure and IBD development among children: A population-based cohort study', *Pediatrics*, 130(4). doi: 10.1542/peds.2011-3886.
- Kupari, J. *et al.* (2021) 'Single cell transcriptomics of primate sensory neurons identifies cell types associated with chronic pain', *Nature Communications*, 12(1). doi: 10.1038/s41467-

021-21725-z.

Kusugami, K. *et al.* (1995) 'Elevation of interleukin-6 in inflammatory bowel disease is macrophage- and epithelial cell-dependent', *Digestive Diseases and Sciences*, 40(5). doi: 10.1007/BF02064182.

Kwan, H. Y., Huang, Y. and Yao, X. (2004) 'Regulation of canonical transient receptor potential isoform 3 (TRPC3) channel by protein kinase G', *Proceedings of the National Academy of Sciences of the United States of America*, 101(8). doi: 10.1073/pnas.0304471101.

Kwan, H. Y., Huang, Y. and Yao, X. (2006) 'Protein kinase C can inhibit TRPC3 channels indirectly via stimulating protein kinase G', *Journal of Cellular Physiology*, 207(2). doi: 10.1002/jcp.20567.

Laharie, D. *et al.* (2001) 'Inflammatory bowel disease in spouses and their offspring', *Gastroenterology*, 120(4). doi: 10.1053/gast.2001.22574.

Laird, J. M. A. *et al.* (2002) 'Deficits in visceral pain and referred hyperalgesia in Nav1.8 (SNS/PN3)-null mice', *Journal of Neuroscience*, 22(19). doi: 10.1523/jneurosci.22-19-08352.2002.

Lakatos, L. *et al.* (2003) 'Association of extraintestinal manifestations of inflammatory bowel disease in a province of western Hungary with disease phenotype: Results of a 25-year follow-up study', *World Journal of Gastroenterology*, 9(10). doi: 10.3748/wjg.v9.i10.2300.

Lalonde, J., Saia, G. and Gill, G. (2014) 'Store-operated calcium entry promotes the degradation of the transcription factor sp4 in resting neurons', *Science Signaling*, 7(328). doi: 10.1126/scisignal.2005242.

Landy, J. *et al.* (2016) 'Tight junctions in inflammatory bowel diseases and inflammatory bowel disease associated colorectal cancer', *World Journal of Gastroenterology*. doi: 10.3748/wjg.v22.i11.3117.

De Lange, K. M. *et al.* (2017) 'Genome-wide association study implicates immune activation of multiple integrin genes in inflammatory bowel disease', *Nature Genetics*, 49(2). doi: 10.1038/ng.3760.

Lawson, S. N. (1979) 'The postnatal development of large light and small dark neurons in mouse dorsal root ganglia: a statistical analysis of cell numbers and size', *Journal of Neurocytology*, 8(3). doi: 10.1007/BF01236123.

Lawson, S. N., Fang, X. and Djouhri, L. (2019) 'Nociceptor subtypes and their incidence in

rat lumbar dorsal root ganglia (DRGs): focussing on C-polymodal nociceptors, A $\beta$ -nociceptors, moderate pressure receptors and their receptive field depths', *Current Opinion in Physiology*. doi: 10.1016/j.cophys.2019.10.005.

Lawson, S. N. and Waddell, P. J. (1991) 'Soma neurofilament immunoreactivity is related to cell size and fibre conduction velocity in rat primary sensory neurons.', *The Journal of Physiology*, 435(1). doi: 10.1113/jphysiol.1991.sp018497.

Lee, K. P. *et al.* (2014) 'Molecular determinants mediating gating of transient receptor potential canonical (TRPC) channels by stromal interaction molecule 1 (STIM1)', *Journal of Biological Chemistry*, 289(10). doi: 10.1074/jbc.M113.546556.

Li, H. S., Xu, X. Z. S. and Montell, C. (1999) 'Activation of a trpc3-dependent cation current through the neurotrophin bdnf', *Neuron*, 24(1). doi: 10.1016/S0896-6273(00)80838-7.

Li, S. Z. *et al.* (2007) 'Calcineurin-NFATc signaling pathway regulates AQP2 expression in response to calcium signals and osmotic stress', *American Journal of Physiology - Cell Physiology*, 292(5). doi: 10.1152/ajpcell.00588.2005.

Li, X. *et al.* (2011) 'Risk of inflammatory bowel disease in first- and second-generation immigrants in Sweden: A nationwide follow-up study', *Inflammatory Bowel Diseases*, 17(8). doi: 10.1002/ibd.21535.

Liao, Y. *et al.* (2007) 'Orai proteins interact with TRPC channels and confer responsiveness to store depletion', *Proceedings of the National Academy of Sciences of the United States of America*, 104(11). doi: 10.1073/pnas.0611692104.

Liao, Y. *et al.* (2009) 'A role for Orai in TRPC-mediated Ca<sup>2+</sup> entry suggests that a TRPC:Orai complex may mediate store and receptor operated Ca<sup>2+</sup> entry', *Proceedings of the National Academy of Sciences of the United States of America*, 106(9). doi: 10.1073/pnas.0813346106.

Linley, J. E. *et al.* (2008) 'Inhibition of M current in sensory neurons by exogenous proteases: A signaling pathway mediating inflammatory nociception', *Journal of Neuroscience*, 28(44). doi: 10.1523/JNEUROSCI.2297-08.2008.

Liou, J. *et al.* (2007) 'Live-cell imaging reveals sequential oligomerization and local plasma membrane targeting of stromal interaction molecule 1 after Ca<sup>2+</sup> store depletion', *Proceedings of the National Academy of Sciences of the United States of America*, 104(22). doi: 10.1073/pnas.0702866104.

Lis, A. *et al.* (2007) 'CRACM1, CRACM2, and CRACM3 Are Store-Operated Ca<sup>2+</sup> Channels

- with Distinct Functional Properties', *Current Biology*, 17(9). doi: 10.1016/j.cub.2007.03.065.
- Lisak, D. A. *et al.* (2014) 'The transmembrane Bax inhibitor motif (TMBIM) containing protein family: Tissue expression, intracellular localization and effects on the ER  $Ca^{2+}$ -filling state', *Biochimica et Biophysica Acta - Molecular Cell Research*, 1853(9). doi: 10.1016/j.bbamcr.2015.03.002.
- Liu, B. *et al.* (2010) 'The acute nociceptive signals induced by bradykinin in rat sensory neurons are mediated by inhibition of M-type  $K^+$  channels and activation of  $Ca^{2+}$ -activated  $Cl^-$  channels', *Journal of Clinical Investigation*, 120(4). doi: 10.1172/JCI41084.
- Liu, C. H. *et al.* (2017) 'Arrestin-biased AT1R agonism induces acute catecholamine secretion through TRPC3 coupling', *Nature Communications*, 8. doi: 10.1038/ncomms14335.
- Liu, X., Singh, B. B. and Ambudkar, I. S. (2003) 'TRPC1 Is Required for Functional Store-operated  $Ca^{2+}$  Channels', *Journal of Biological Chemistry*, 278(13). doi: 10.1074/jbc.m213271200.
- Liu, Z. *et al.* (2001) 'Role of interleukin-12 in the induction of mucosal inflammation and abrogation of regulatory T cell function in chronic experimental colitis', *European Journal of Immunology*, 31(5). doi: 10.1002/1521-4141(200105)31:5<1550::AID-IMMU1550>3.0.CO;2-3.
- Liu, Z. *et al.* (2011) 'Leucine-rich repeat kinase 2 (LRRK2) regulates inflammatory bowel disease through the Nuclear Factor of Activated T cells (NFAT)', *Nature immunology*, 12(11).
- López-Rodríguez, C. *et al.* (1999) 'NFAT5, a constitutively nuclear NFAT protein that does not cooperate with Fos and Jun', *Proceedings of the National Academy of Sciences of the United States of America*, 96(13). doi: 10.1073/pnas.96.13.7214.
- Low, J. T. *et al.* (2010) 'Exocytosis, dependent on  $Ca^{2+}$  release from  $Ca^{2+}$  stores, is regulated by  $Ca^{2+}$  microdomains', *Journal of Cell Science*, 123(18). doi: 10.1242/jcs.071225.
- Luiz, A. P. *et al.* (2019) 'Cold sensing by Na V 1.8-positive and Na V 1.8-negative sensory neurons', *Proceedings of the National Academy of Sciences of the United States of America*, 116(9). doi: 10.1073/pnas.1814545116.
- Lunde, I. G. *et al.* (2011) 'Angiotensin II and norepinephrine activate specific calcineurin-dependent NFAT transcription factor isoforms in cardiomyocytes', *Journal of Applied Physiology*, 111(5). doi: 10.1152/jappphysiol.01383.2010.

- MacDonald, D. I. *et al.* (2021) 'Silent cold-sensing neurons contribute to cold allodynia in neuropathic pain', *Brain : a journal of neurology*, 144(6). doi: 10.1093/brain/awab086.
- Majewski, L. and Kuznicki, J. (2014) 'SOCE in neurons: Signaling or just refilling?', *Biochimica et Biophysica Acta - Molecular Cell Research*. doi: 10.1016/j.bbamcr.2015.01.019.
- Mantaka, A. *et al.* (2021) 'Is there any role of renin-angiotensin system inhibitors in modulating inflammatory bowel disease outcome?', *European Journal of Gastroenterology and Hepatology*. doi: 10.1097/MEG.0000000000001912.
- Maravall, M. *et al.* (2000) 'Estimating intracellular calcium concentrations and buffering without wavelength ratioing', *Biophysical Journal*, 78(5). doi: 10.1016/S0006-3495(00)76809-3.
- Matsumura, H. *et al.* (2004) 'Lineage-specific cell disruption in living mice by Cre-mediated expression of diphtheria toxin A chain', *Biochemical and Biophysical Research Communications*, 321(2). doi: 10.1016/j.bbrc.2004.06.139.
- Matsuno, H. *et al.* (2017) 'CD103+ Dendritic Cell Function Is Altered in the Colons of Patients with Ulcerative Colitis', *Inflammatory Bowel Diseases*, 23(9). doi: 10.1097/MIB.0000000000001204.
- McGovern, D. and Powrie, F. (2007) 'The IL23 axis plays a key role in the pathogenesis of IBD', *Gut*. doi: 10.1136/gut.2006.115402.
- Mercer, J. C. *et al.* (2006) 'Large store-operated calcium selective currents due to co-expression of Orai1 or Orai2 with the intracellular calcium sensor, Stim1', *Journal of Biological Chemistry*, 281(34). doi: 10.1074/jbc.M604589200.
- Mitra, R. and Hasan, G. (2022) 'Store-operated Ca<sup>2+</sup> entry regulates neuronal gene expression and function', *Current Opinion in Neurobiology*. doi: 10.1016/j.conb.2022.01.005.
- Mitsuyama, K. *et al.* (1995) 'Soluble interleukin-6 receptors in inflammatory bowel disease: Relation to circulating interleukin-6', *Gut*, 36(1). doi: 10.1136/gut.36.1.45.
- Miyakawa, H. *et al.* (1998) 'Cis- and trans-acting factors regulating transcription of the BGT1 gene in response to hypertonicity', *American Journal of Physiology - Renal Physiology*, 274(4 43-4). doi: 10.1152/ajprenal.1998.274.4.f753.
- Mokry, M. *et al.* (2014) 'Many inflammatory bowel disease risk loci include regions that regulate gene expression in immune cells and the intestinal epithelium', *Gastroenterology*, 146(4). doi: 10.1053/j.gastro.2013.12.003.

- Mora, J. R. and von Andrian, U. H. (2006) 'T-cell homing specificity and plasticity: new concepts and future challenges', *Trends in Immunology*. doi: 10.1016/j.it.2006.03.007.
- Murali, S., Zhang, M. and Nurse, C. A. (2014) 'Angiotensin II mobilizes intracellular calcium and activates pannexin-1 channels in rat carotid body type II cells via AT1 receptors', *Journal of Physiology*, 592(21). doi: 10.1113/jphysiol.2014.279299.
- Neher, E. and Sakmann, B. (1976) 'Single-channel currents recorded from membrane of denervated frog muscle fibres', *Nature*, 260(5554). doi: 10.1038/260799a0.
- Nelson, C. and Glitsch, M. D. (2012) 'Lack of kinase regulation of canonical transient receptor potential 3 (TRPC3) channel-dependent currents in cerebellar Purkinje cells', *Journal of Biological Chemistry*, 287(9). doi: 10.1074/jbc.M111.246553.
- Neurath, M. F. *et al.* (1995) 'Antibodies to interleukin 12 abrogate established experimental colitis in mice', *Journal of Experimental Medicine*, 182(5). doi: 10.1084/jem.182.5.1281.
- Neurath, M. F. (2014) 'Cytokines in inflammatory bowel disease', *Nature Reviews Immunology*. doi: 10.1038/nri3661.
- Ng, S. C. *et al.* (2010) 'Intestinal dendritic cells: Their role in bacterial recognition, lymphocyte homing, and intestinal inflammation', *Inflammatory Bowel Diseases*. doi: 10.1002/ibd.21247.
- Ng, S. C. *et al.* (2011) 'Relationship between human intestinal dendritic cells, gut microbiota, and disease activity in Crohn's disease', *Inflammatory Bowel Diseases*, 17(10). doi: 10.1002/ibd.21590.
- Norton, C. *et al.* (2017) 'Systematic review: interventions for abdominal pain management in inflammatory bowel disease', *Alimentary Pharmacology and Therapeutics*. doi: 10.1111/apt.14108.
- O'Mahony, S. M. *et al.* (2014) 'Disturbance of the gut microbiota in early-life selectively affects visceral pain in adulthood without impacting cognitive or anxiety-related behaviors in male rats', *Neuroscience*, 277. doi: 10.1016/j.neuroscience.2014.07.054.
- Oh-hora, M. *et al.* (2008) 'Dual functions for the endoplasmic reticulum calcium sensors STIM1 and STIM2 in T cell activation and tolerance', *Nature Immunology*, 9(4). doi: 10.1038/ni1574.
- Onohara, N. *et al.* (2006) 'TRPC3 and TRPC6 are essential for angiotensin II-induced cardiac hypertrophy', *EMBO Journal*, 25(22). doi: 10.1038/sj.emboj.7601417.
- Oppmann, B. *et al.* (2000) 'Novel p19 protein engages IL-12p40 to form a cytokine, IL-23,

- with biological activities similar as well as distinct from IL-12', *Immunity*, 13(5). doi: 10.1016/S1074-7613(00)00070-4.
- Orholm, M. *et al.* (2000) 'Concordance of inflammatory bowel disease among Danish twins: Results of a nationwide study', *Scandinavian Journal of Gastroenterology*, 35(10). doi: 10.1080/003655200451207.
- Oshima, T., Miwa, H. and Joh, T. (2008) 'Changes in the expression of claudins in active ulcerative colitis', in *Journal of Gastroenterology and Hepatology (Australia)*. doi: 10.1111/j.1440-1746.2008.05405.x.
- Owen, C. A. and Campbell, E. J. (1998) 'Angiotensin II generation at the cell surface of activated neutrophils: novel cathepsin G-mediated catalytic activity that is resistant to inhibition.', *Journal of immunology (Baltimore, Md. : 1950)*, 160(3).
- Ozkul, C. *et al.* (2020) 'A single early-in-life antibiotic course increases susceptibility to DSS-induced colitis', *Genome Medicine*, 12(1). doi: 10.1186/s13073-020-00764-z.
- Palmela, C. *et al.* (2018) 'Adherent-invasive Escherichia coli in inflammatory bowel disease', *Gut*. doi: 10.1136/gutjnl-2017-314903.
- Park, Y. J. *et al.* (2020) 'The Role of Calcium–Calcineurin–NFAT Signaling Pathway in Health and Autoimmune Diseases', *Frontiers in Immunology*. doi: 10.3389/fimmu.2020.00195.
- Patel, K. K. *et al.* (2013) 'Autophagy proteins control goblet cell function by potentiating reactive oxygen species production', *EMBO Journal*, 32(24). doi: 10.1038/emboj.2013.233.
- Patil, M. J., Hovhannisyan, A. H. and Akopian, A. N. (2018) 'Characteristics of sensory neuronal groups in CGRP-cre-ER reporter mice: Comparison to Nav1.8-cre, TRPV1-cre and TRPV1-GFP mouse lines', *PLoS ONE*, 13(6). doi: 10.1371/journal.pone.0198601.
- Peier, A. M. *et al.* (2002) 'A TRP channel that senses cold stimuli and menthol', *Cell*, 108(5). doi: 10.1016/S0092-8674(02)00652-9.
- Pelaseyed, T. *et al.* (2014) 'The mucus and mucins of the goblet cells and enterocytes provide the first defense line of the gastrointestinal tract and interact with the immune system', *Immunological Reviews*. doi: 10.1111/imr.12182.
- Pepperell, J. R. *et al.* (1993) 'The type 1 angiotensin-II receptor mediates intracellular calcium mobilization in rat luteal cells', *Endocrinology*, 133(4). doi: 10.1210/endo.133.4.8404609.
- Perler, B. *et al.* (2019) 'Presenting symptoms in inflammatory bowel disease: Descriptive

- analysis of a community-based inception cohort', *BMC Gastroenterology*, 19(1). doi: 10.1186/s12876-019-0963-7.
- Perrier, C. *et al.* (2013) 'Neutralization of membrane TNF, but not soluble TNF, is crucial for the treatment of experimental colitis', *Inflammatory Bowel Diseases*, 19(2). doi: 10.1002/ibd.23023.
- Pituch-Zdanowska, A., Banaszkiwicz, A. and Albrecht, P. (2015) 'The role of dietary fibre in inflammatory bowel disease', *Przegląd Gastroenterologiczny*. doi: 10.5114/pg.2015.52753.
- Van Der Post, S. *et al.* (2019) 'Structural weakening of the colonic mucus barrier is an early event in ulcerative colitis pathogenesis', *Gut*, 68(12). doi: 10.1136/gutjnl-2018-317571.
- Prato, V. *et al.* (2017) "'Genetic} identification of mechanoinensitive 'silent' nociceptors'", *Cell reports*, 21(11).
- Preuß, K. D. *et al.* (1997) 'Expression and characterization of a trpl homolog from rat', *Biochemical and Biophysical Research Communications*, 240(1). doi: 10.1006/bbrc.1997.7528.
- Priest, B. T. *et al.* (2005) 'Contribution of the tetrodotoxin-resistant voltage-gated sodium channel Nav1.9 to sensory transmission and nociceptive behavior', *Proceedings of the National Academy of Sciences of the United States of America*, 102(26). doi: 10.1073/pnas.0501549102.
- Probert, C. S. J. *et al.* (1992) 'Epidemiological study of ulcerative proctocolitis in Indian migrants and the indigenous population of Leicestershire', *Gut*, 33(5). doi: 10.1136/gut.33.5.687.
- Pullan, R. D. *et al.* (1994) 'Thickness of adherent mucus gel on colonic mucosa in humans and its relevance to colitis', *Gut*, 35(3). doi: 10.1136/gut.35.3.353.
- Putney, J. W. (1986) 'A model for receptor-regulated calcium entry', *Cell Calcium*, 7(1). doi: 10.1016/0143-4160(86)90026-6.
- Qian, Y. *et al.* (1996) 'cGMP-dependent protein kinase in dorsal root ganglion: Relationship with nitric oxide synthase and nociceptive neurons', *Journal of Neuroscience*, 16(10). doi: 10.1523/jneurosci.16-10-03130.1996.
- Quévrain, E. *et al.* (2016) 'Identification of an anti-inflammatory protein from *Faecalibacterium prausnitzii*, a commensal bacterium deficient in Crohn's disease', *Gut*, 65(3). doi: 10.1136/gutjnl-2014-307649.
- Ramos-nino, M. E. *et al.* (2008) 'TRPC5/Orai1/STIM1-dependent Store-operated Entry of

Ca<sup>2+</sup> Is Linked to Degranulation in a Rat Mast Cell Line', *J Immunol*, 180(4).

Ranade, S. S. *et al.* (2014) 'Piezo2 is the major transducer of mechanical forces for touch sensation in mice', *Nature*, 516(729). doi: 10.1038/nature13980.

Rankin, G. B. *et al.* (1979) 'National Cooperative Crohn's Disease Study: Extraintestinal manifestations and perianal complications', *Gastroenterology*, 77(4 PART 2). doi: 10.1016/0016-5085(79)90391-3.

Raouf, R. *et al.* (2021) 'Dorsal root ganglia macrophages maintain osteoarthritis pain', *Journal of Neuroscience*, 41(39). doi: 10.1523/JNEUROSCI.1787-20.2021.

Ray, P. *et al.* (2018) 'Comparative transcriptome profiling of the human and mouse dorsal root ganglia', *PAIN*, 159(7).

Reinisch, W. (1999) 'Clinical relevance of serum interleukin-6 in Crohn's disease: Single point measurements, therapy monitoring, and prediction of clinical relapse', *American Journal of Gastroenterology*, 94(8). doi: 10.1111/j.1572-0241.1999.01288.x.

Renganathan, M., Cummins, T. R. and Waxman, S. G. (2001) 'Contribution of Nav 1.8 sodium channels to action potential electrogenesis in DRG neurons', *Journal of Neurophysiology*, 86(2). doi: 10.1152/jn.2001.86.2.629.

Rescigno, M. *et al.* (2001) 'Dendritic cells shuttle microbes across gut epithelial monolayers', *Immunobiology*, 204(5). doi: 10.1078/0171-2985-00094.

Rice, A. S. C. *et al.* (2014) 'EMA401, an orally administered highly selective angiotensin II type 2 receptor antagonist, as a novel treatment for postherpetic neuralgia: A randomised, double-blind, placebo-controlled phase 2 clinical trial', *The Lancet*, 383(9929). doi: 10.1016/S0140-6736(13)62337-5.

Roda, G. *et al.* (2020) 'Crohn's disease', *Nature Reviews Disease Primers*, 6(1). doi: 10.1038/s41572-020-0156-2.

Rodríguez-Cabezas, M. E. *et al.* (2002) 'Dietary fiber down-regulates colonic tumor necrosis factor  $\alpha$  and nitric oxide production in trinitrobenzenesulfonic acid-induced colitic rats', *Journal of Nutrition*, 132(11). doi: 10.1093/jn/132.11.3263.

Rosa, A. C. *et al.* (2012) 'Angiotensin II induces tumor necrosis factor- $\alpha$  expression and release from cultured human podocytes', *Inflammation Research*, 61(4). doi: 10.1007/s00011-011-0412-8.

Ru, F. *et al.* (2017) 'Mechanisms of pruritogen-induced activation of itch nerves in isolated mouse skin', *Journal of Physiology*, 595(11). doi: 10.1113/JP273795.

- Ruiz-Ortega, M. *et al.* (2002) 'Angiotensin II regulates the synthesis of proinflammatory cytokines and chemokines in the kidney', *Kidney International, Supplement*, 62(82). doi: 10.1046/j.1523-1755.62.s82.4.x.
- Salama, N. N., Eddington, N. D. and Fasano, A. (2006) 'Tight junction modulation and its relationship to drug delivery', *Advanced Drug Delivery Reviews*. doi: 10.1016/j.addr.2006.01.003.
- Samtleben, S. *et al.* (2013) 'Direct imaging of ER calcium with targeted-esterase induced dye loading (TED)', *Journal of Visualized Experiments*, (75). doi: 10.3791/50317.
- Sands, B. E. *et al.* (2017) 'Efficacy and Safety of MEDI2070, an Antibody Against Interleukin 23, in Patients With Moderate to Severe Crohn's Disease: A Phase 2a Study', *Gastroenterology*, 153(1). doi: 10.1053/j.gastro.2017.03.049.
- Santiago, O. I. *et al.* (2008) 'An angiotensin II receptor antagonist reduces inflammatory parameters in two models of colitis', *Regulatory Peptides*, 146(1–3). doi: 10.1016/j.regpep.2007.10.004.
- Saraiva, N. *et al.* (2013) 'HGAAP promotes cell adhesion and migration via the stimulation of store-operated  $Ca^{2+}$  entry and calpain 2', *Journal of Cell Biology*, 202(4). doi: 10.1083/jcb.201301016.
- Sarria, I. and Gu, J. (2010) 'Menthol response and adaptation in nociceptive-like and nonnociceptive-like neurons: Role of protein kinases', *Molecular Pain*, 6. doi: 10.1186/1744-8069-6-47.
- Sato, M. and Tanigawa, M. (2005) 'Production of CETD transgenic mouse line allowing ablation of any type of specific cell population', *Molecular Reproduction and Development*, 72(1). doi: 10.1002/mrd.20323.
- Schirbel, A. *et al.* (2010) 'Impact of pain on health-related quality of life in patients with inflammatory bowel disease', *World Journal of Gastroenterology*. doi: 10.3748/wjg.v16.i25.3168.
- Schmidt-Ott, K. M., Kagiya, S. and Phillips, M. I. (2000) 'The multiple actions of angiotensin II in atherosclerosis', *Regulatory Peptides*. doi: 10.1016/S0167-0115(00)00178-6.
- Schmitz, H. *et al.* (1999) 'Altered tight junction structure contributes to the impaired epithelial barrier function in ulcerative colitis', *Gastroenterology*, 116(2). doi: 10.1016/S0016-5085(99)70126-5.

- Séguéla, P. *et al.* (2014) 'Contribution of TRPC3 to store-operated calcium entry and inflammatory transductions in primary nociceptors', *Molecular pain*, 10. doi: 10.1186/1744-8069-10-43.
- Shan, M. *et al.* (2013) 'Mucus enhances gut homeostasis and oral tolerance by delivering immunoregulatory signals', *Science*, 342(6157). doi: 10.1126/science.1237910.
- Shapiro, M. S., Wollmuth, L. P. and Hille, B. (1994) 'Angiotensin II inhibits calcium and M current channels in rat sympathetic neurons via G proteins', *Neuron*, 12(6). doi: 10.1016/0896-6273(94)90447-2.
- Shaw, J. P. *et al.* (2010) 'Identification of a putative regulator of early T cell activation genes', *Journal of Immunology*, 185(9). doi: 10.1126/science.3260404.
- Shaw, S. Y., Blanchard, J. F. and Bernstein, C. N. (2010) 'Association between the use of antibiotics in the first year of life and pediatric inflammatory bowel disease', *American Journal of Gastroenterology*, 105(12). doi: 10.1038/ajg.2010.398.
- Shen, K. *et al.* (2018) 'Knockdown of TMEM45B inhibits cell proliferation and invasion in gastric cancer', *Biomedicine and Pharmacotherapy*, 104. doi: 10.1016/j.biopha.2018.05.016.
- Shepherd, A. J. *et al.* (2018) 'Angiotensin II triggers peripheral macrophage-to-sensory neuron redox crosstalk to elicit pain', *Journal of Neuroscience*, 38(32). doi: 10.1523/JNEUROSCI.3542-17.2018.
- Shi, Y. *et al.* (2016) 'Activation of the Renin-Angiotensin System Promotes Colitis Development', *Scientific Reports*, 6. doi: 10.1038/srep27552.
- Shiers, S. *et al.* (2020) 'ACE2 and SCARF expression in human dorsal root ganglion nociceptors: implications for SARS-CoV-2 virus neurological effects', *Pain*, 161(11). doi: 10.1097/j.pain.0000000000002051.
- Shinoda, M., Feng, B. and Gebhart, G. F. (2009) 'Peripheral and Central P2X3 Receptor Contributions to Colon Mechanosensitivity and Hypersensitivity in the Mouse', *Gastroenterology*, 137(6). doi: 10.1053/j.gastro.2009.06.048.
- Sipe, W. E. B. *et al.* (2008) 'Transient receptor potential vanilloid 4 mediates protease activated receptor 2-induced sensitization of colonic afferent nerves and visceral hyperalgesia', *American Journal of Physiology - Gastrointestinal and Liver Physiology*, 294(5). doi: 10.1152/ajpgi.00002.2008.
- Smith, M. T. *et al.* (2013) 'A Small Molecule Angiotensin II Type 2 Receptor (AT2R) Antagonist Produces Analgesia in a Rat Model of Neuropathic Pain by Inhibition of p38

Mitogen-Activated Protein Kinase (MAPK) and p44/p42 MAPK Activation in the Dorsal Root Ganglia', *Pain Medicine (United States)*, 14(10). doi: 10.1111/pme.12157.

Soboloff, J. *et al.* (2006) 'Orai1 and STIM reconstitute store-operated calcium channel function', *Journal of Biological Chemistry*, 281(30). doi: 10.1074/jbc.C600126200.

Sokol, H. *et al.* (2008) 'Faecalibacterium prausnitzii is an anti-inflammatory commensal bacterium identified by gut microbiota analysis of Crohn disease patients', *Proceedings of the National Academy of Sciences of the United States of America*, 105(43). doi: 10.1073/pnas.0804812105.

Song, D. D. *et al.* (2014) 'Neuron-glia communication mediated by TNF- $\alpha$  and glial activation in dorsal root ganglia in visceral inflammatory hypersensitivity', *American Journal of Physiology - Gastrointestinal and Liver Physiology*, 306(9). doi: 10.1152/ajpgi.00318.2013.

Song, X. J. *et al.* (2006) 'cAMP and cGMP contribute to sensory neuron hyperexcitability and hyperalgesia in rats with dorsal root ganglia compression', *Journal of Neurophysiology*, 95(1). doi: 10.1152/jn.00503.2005.

Sood, A. and Midha, V. (2007) 'Epidemiology of inflammatory bowel disease in Asia', *Indian Journal of Gastroenterology*. doi: 10.1007/978-1-4020-9353-1\_4.

Spencer, A. U. *et al.* (2007) 'Reduced severity of a mouse colitis model with angiotensin converting enzyme inhibition', *Digestive Diseases and Sciences*, 52(4). doi: 10.1007/s10620-006-9124-2.

Sriramula, S. *et al.* (2008) 'Involvement of tumor necrosis factor- $\alpha$  in angiotensin II-mediated effects on salt appetite, hypertension, and cardiac hypertrophy', *Hypertension*, 51(5). doi: 10.1161/HYPERTENSIONAHA.107.102152.

Sriramula, S. and Francis, J. (2015) 'Tumor necrosis factor - Alpha is essential for angiotensin II-induced ventricular remodeling: Role for oxidative stress', *PLoS ONE*, 10(9). doi: 10.1371/journal.pone.0138372.

Srivats, S. *et al.* (2016) 'Sigma1 receptors inhibit store-operated Ca<sup>2+</sup> entry by attenuating coupling of STIM1 to Orai1', *Journal of Cell Biology*, 213(1). doi: 10.1083/jcb.201506022.

Stagg, A. J. (2018) 'Intestinal Dendritic Cells in Health and Gut Inflammation', *Frontiers in Immunology*. doi: 10.3389/fimmu.2018.02883.

Stevens, C. *et al.* (2013) 'The intermediate filament protein, vimentin, is a regulator of NOD2 activity', *Gut*, 62(5). doi: 10.1136/gutjnl-2011-301775.

Stifter, S. A. and Greter, M. (2020) 'STOP floxing around: Specificity and leakiness of

inducible Cre/loxP systems', *European Journal of Immunology*. doi: 10.1002/eji.202048546.

Stirling, L. C. *et al.* (2005) 'Nociceptor-specific gene deletion using heterozygous Na V1.8-Cre recombinase mice', *Pain*, 113(1–2). doi: 10.1016/j.pain.2004.08.015.

Strober, W., Fuss, I. J. and Blumberg, R. S. (2002) 'The immunology of mucosal models of inflammation', *Annual Review of Immunology*. doi: 10.1146/annurev.immunol.20.100301.064816.

Strugala, V., Dettmar, P. W. and Pearson, J. P. (2008) 'Thickness and continuity of the adherent colonic mucus barrier in active and quiescent ulcerative colitis and Crohn's disease', *International Journal of Clinical Practice*, 62(5). doi: 10.1111/j.1742-1241.2007.01665.x.

Su, Z. *et al.* (2001) 'A store-operated nonselective cation channel in lymphocytes is activated directly by  $Ca^{2+}$  influx factor and diacylglycerol', *American Journal of Physiology - Cell Physiology*, 280(5 49-5). doi: 10.1152/ajpcell.2001.280.5.c1284.

Suadicani, S. O. *et al.* (2010) 'Bidirectional calcium signaling between satellite glial cells and neurons in cultured mouse trigeminal ganglia', *Neuron Glia Biology*, 6(1). doi: 10.1017/S1740925X09990408.

Sullivan, M. N. *et al.* (2015) 'Vascular biology: Localized TRPA1 channel  $Ca^{2+}$  signals stimulated by reactive oxygen species promote cerebral artery dilation', *Science Signaling*, 8(358). doi: 10.1126/scisignal.2005659.

Takahashi, K. *et al.* (2021) 'Post-inflammatory Abdominal Pain in Patients with Inflammatory Bowel Disease during Remission: A Comprehensive Review', *Crohn's and Colitis 360*. doi: 10.1093/crocol/otab073.

Teichert, R. W. *et al.* (2012) 'Functional profiling of neurons through cellular neuropharmacology', *Proceedings of the National Academy of Sciences of the United States of America*, 109(5). doi: 10.1073/pnas.1118833109.

Teshima, C. W., Dieleman, L. A. and Meddings, J. B. (2012) 'Abnormal intestinal permeability in Crohn's disease pathogenesis', *Annals of the New York Academy of Sciences*, 1258(1). doi: 10.1111/j.1749-6632.2012.06612.x.

Tewari, D. *et al.* (2020) 'Granulocyte-macrophage colony stimulating factor as an indirect mediator of nociceptor activation and pain', *Journal of Neuroscience*, 40(10). doi: 10.1523/JNEUROSCI.2268-19.2020.

Thakur, M. *et al.* (2014) 'Defining the nociceptor transcriptome', *Frontiers in Molecular*

*Neuroscience*, 7(November). doi: 10.3389/fnmol.2014.00087.

Thebault, S. *et al.* (2005) 'Receptor-operated Ca<sup>2+</sup> entry mediated by TRPC3/TRPC6 proteins in rat prostate smooth muscle (PS1) cell line', *Journal of Cellular Physiology*, 204(1). doi: 10.1002/jcp.20301.

Thia, K. T. *et al.* (2008) 'An update on the epidemiology of inflammatory bowel disease in Asia', *American Journal of Gastroenterology*. doi: 10.1111/j.1572-0241.2008.02158.x.

Thompson, J. L., Mignen, O. and Shuttleworth, T. J. (2009) 'The Orai1 severe combined immune deficiency mutation and calcium release-activated Ca<sup>2+</sup> channel function in the heterozygous condition', *Journal of Biological Chemistry*, 284(11). doi: 10.1074/jbc.M808346200.

Trama, J. *et al.* (2000) 'The NFAT-Related Protein NFATL1 (TonEBP/NFAT5) Is Induced Upon T Cell Activation in a Calcineurin-Dependent Manner', *The Journal of Immunology*, 165(9). doi: 10.4049/jimmunol.165.9.4884.

Trebak, M. *et al.* (2003) 'Signaling mechanism for receptor-activated canonical transient receptor potential 3 (TRPC3) channels', *Journal of Biological Chemistry*, 278(18). doi: 10.1074/jbc.M300544200.

Trebak, M. *et al.* (2005) 'Negative regulation of TRPC3 channels by protein kinase C-mediated phosphorylation of serine 712', *Molecular Pharmacology*, 67(2). doi: 10.1124/mol.104.007252.

Tse, F. W. *et al.* (1997) 'Local Ca<sup>2+</sup> release from internal stores controls exocytosis in pituitary gonadotrophs', *Neuron*, 18(1). doi: 10.1016/S0896-6273(01)80051-9.

Tsien, R. Y. (1980) 'New Calcium Indicators and Buffers with High Selectivity Against Magnesium and Protons: Design, Synthesis, and Properties of Prototype Structures', *Biochemistry*, 19(11). doi: 10.1021/bi00552a018.

Usoskin, D. *et al.* (2015) 'Unbiased classification of sensory neuron types by large-scale single-cell RNA sequencing', *Nature Neuroscience*, 18(1). doi: 10.1038/nn.3881.

Usovich, M. M. *et al.* (1992) 'P-type calcium channels in the somata and dendrites of adult cerebellar purkinje cells', *Neuron*, 9(6). doi: 10.1016/0896-6273(92)90076-P.

Varga-Szabo, D. *et al.* (2008) 'The calcium sensor STIM1 is an essential mediator of arterial thrombosis and ischemic brain infarction', *Journal of Experimental Medicine*, 205(7). doi: 10.1084/jem.20080302.

Vavricka, S. R. *et al.* (2011) 'Frequency and risk factors for extraintestinal manifestations in

the swiss inflammatory bowel disease cohort', *American Journal of Gastroenterology*, 106(1). doi: 10.1038/ajg.2010.343.

Vazquez, G. *et al.* (2001) 'Human Trp3 forms both inositol trisphosphate receptor-dependent and receptor-independent store-operated cation channels in DT40 avian B lymphocytes', *Proceedings of the National Academy of Sciences of the United States of America*, 98(20). doi: 10.1073/pnas.201238198.

Vazquez, G. *et al.* (2003) 'Expression level of the canonical transient receptor potential 3 (TRPC3) channel determines its mechanism of activation', *Journal of Biological Chemistry*, 278(24). doi: 10.1074/jbc.M302162200.

Veloso, F. T., Carvalho, J. and Magro, F. (1996) 'Immune-related systemic manifestations of inflammatory bowel disease: A prospective study of 792 patients', *Journal of Clinical Gastroenterology*, 23(1). doi: 10.1097/00004836-199607000-00009.

Venkatachalam, K. *et al.* (2002) 'The cellular and molecular basis of store-operated calcium entry', *Nature Cell Biology*. doi: 10.1038/ncb1102-e263.

Venkatachalam, K., Zheng, F. and Gill, D. L. (2003) 'Regulation of canonical transient receptor potential (TRPC) channel function by diacylglycerol and protein kinase C', *Journal of Biological Chemistry*, 278(31). doi: 10.1074/jbc.M302751200.

Viana, F., De la Peña, E. and Belmonte, C. (2002) 'Specificity of cold thermotransduction is determined by differential ionic channel expression', *Nature Neuroscience*, 5(3). doi: 10.1038/nn809.

van der Vlist, M. *et al.* (2022) 'Macrophages transfer mitochondria to sensory neurons to resolve inflammatory pain', *Neuron*, 110(4). doi: 10.1016/j.neuron.2021.11.020.

Wallez, Y. and Huber, P. (2008) 'Endothelial adherens and tight junctions in vascular homeostasis, inflammation and angiogenesis', *Biochimica et Biophysica Acta - Biomembranes*. doi: 10.1016/j.bbamem.2007.09.003.

Walmsley, R. S. *et al.* (1998) 'A simple clinical colitis activity index', *Gut*, 43(1). doi: 10.1136/gut.43.1.29.

Walsh, D. A., Catravas, J. and Wharton, J. (2000) 'Angiotensin converting enzyme in human synovium: Increased stromal [125I]351A binding in rheumatoid arthritis', *Annals of the Rheumatic Diseases*, 59(2). doi: 10.1136/ard.59.2.125.

Wang, X. *et al.* (2004) 'TRPC4 forms store-operated Ca<sup>2+</sup> channels in mouse mesangial cells', *American Journal of Physiology - Cell Physiology*, 287(2 56-2). doi:

10.1152/ajpcell.00068.2004.

Wangzhou, A. *et al.* (2020) 'Pharmacological target-focused transcriptomic analysis of native vs cultured human and mouse dorsal root ganglia', *Pain*, 161(7). doi:

10.1097/j.pain.0000000000001866.

Wehkamp, J. *et al.* (2004) 'NOD2 (CARD15) mutations in Crohn's disease are associated with diminished mucosal  $\alpha$ -defensin expression', *Gut*, 53(11). doi: 10.1136/gut.2003.032805.

Wehkamp, J. *et al.* (2005) 'Reduced Paneth cell  $\alpha$ -defensins in ileal Crohn's disease', *Proceedings of the National Academy of Sciences of the United States of America*, 102(50).

doi: 10.1073/pnas.0505256102.

Wehkamp, J. and Stange, E. F. (2020) 'An Update Review on the Paneth Cell as Key to Ileal Crohn's Disease', *Frontiers in Immunology*. doi: 10.3389/fimmu.2020.00646.

Wichterle, H., Gifford, D. and Mazzone, E. (2013) 'Mapping neuronal diversity one cell at a time', *Science*. doi: 10.1126/science.1235884.

De Windt, L. J. *et al.* (2000) 'Calcineurin Promotes Protein Kinase C and c-Jun NH2-terminal Kinase Activation in the Heart', *Journal of Biological Chemistry*, 275(18). doi:

10.1074/jbc.275.18.13571.

Woods, C. *et al.* (2021) 'Tumor necrosis factor  $\alpha$  receptor type 1 activation in the hypothalamic paraventricular nucleus contributes to glutamate signaling and angiotensin ii-dependent hypertension', *Journal of Neuroscience*, 41(6). doi: 10.1523/JNEUROSCI.2360-19.2020.

Wuttke, A., Idevall-Hagren, O. and Tengholm, A. (2013) 'P2Y1 receptor-dependent diacylglycerol signaling microdomains in  $\beta$  cells promote insulin secretion', *FASEB Journal*, 27(4). doi: 10.1096/fj.12-221499.

Wyatt, J. *et al.* (1997) 'Increased gastric and intestinal permeability in patients with Crohn's disease', *American Journal of Gastroenterology*, 92(10).

Wyse, B. D. *et al.* (2003) 'Caveolin interacts with the angiotensin II type I receptor during exocytic transport but not at the plasma membrane', *Journal of Biological Chemistry*, 278(26). doi: 10.1074/jbc.M212892200.

Xing, H. *et al.* (2006) 'Chemical and cold sensitivity of two distinct populations of TRPM8-expressing somatosensory neurons', *Journal of Neurophysiology*, 95(2). doi:

10.1152/jn.01035.2005.

Xu, G. Y. *et al.* (2008) 'P2X receptor-mediated visceral hyperalgesia in a rat model of chronic

visceral hypersensitivity', *Gut*, 57(9). doi: 10.1136/gut.2007.134221.

Xu, X. *et al.* (2021) 'Endoplasmic reticulum stress/XBP1 promotes airway mucin secretion under the influence of neutrophil elastase', *International Journal of Molecular Medicine*, 47(5). doi: 10.3892/ijmm.2021.4914.

Yamaguchi, Y. *et al.* (2018) 'TRPC3 participates in angiotensin II type 1 receptor-dependent stress-induced slow increase in intracellular Ca<sup>2+</sup> concentration in mouse cardiomyocytes', *Journal of Physiological Sciences*, 68(2). doi: 10.1007/s12576-016-0519-3.

Yamaizumi, M. *et al.* (1978) 'One molecule of diphtheria toxin fragment a introduced into a cell can kill the cell', *Cell*, 15(1). doi: 10.1016/0092-8674(78)90099-5.

Yao, C. K. and Staudacher, H. M. (2019) 'The low-fibre diet: contender in IBD, or has it had its time?', *The Lancet Gastroenterology and Hepatology*. doi: 10.1016/S2468-1253(19)30096-2.

Yen, D. *et al.* (2006) 'IL-23 is essential for T cell-mediated colitis and promotes inflammation via IL-17 and IL-6', *Journal of Clinical Investigation*, 116(5). doi: 10.1172/JCI21404.

Yu, X. *et al.* (2020) 'Dorsal root ganglion macrophages contribute to both the initiation and persistence of neuropathic pain', *Nature Communications*, 11(1). doi: 10.1038/s41467-019-13839-2.

Zaika, O. *et al.* (2006) 'Angiotensin II regulates neuronal excitability via phosphatidylinositol 4,5-bisphosphate-dependent modulation of Kv7 (M-type) K<sup>+</sup> channels', *Journal of Physiology*, 575(1). doi: 10.1113/jphysiol.2006.114074.

Zeisel, A. *et al.* (2018) 'Molecular Architecture of the Mouse Nervous System', *Cell*, 174(4). doi: 10.1016/j.cell.2018.06.021.

Zeissig, S. *et al.* (2007) 'Changes in expression and distribution of claudin 2, 5 and 8 lead to discontinuous tight junctions and barrier dysfunction in active Crohn's disease', *Gut*, 56(1). doi: 10.1136/gut.2006.094375.

Zhang, B. *et al.* (2018) 'TRPC6 and TRPC4 Heteromultimerization Mediates Store Depletion-Activated NCX1 Reversal in Proliferative Vascular Smooth Muscle Cells', *Channels (Austin, Tex.)*, 12(1). doi: 10.1080/19336950.2018.1451696.

Zhang, H. *et al.* (2016) 'Dorsal Root Ganglion Infiltration by Macrophages Contributes to Paclitaxel Chemotherapy-Induced Peripheral Neuropathy', *Journal of Pain*, 17(7). doi: 10.1016/j.jpain.2016.02.011.

Zhang, M. *et al.* (2016) 'Butyrate inhibits interleukin-17 and generates Tregs to ameliorate

colorectal colitis in rats', *BMC Gastroenterology*, 16(1). doi: 10.1186/s12876-016-0500-x.

Zhao, J. *et al.* (2021) 'Tools for analysis and conditional deletion of subsets of sensory neurons', *Wellcome Open Research*, 6. doi: 10.12688/wellcomeopenres.17090.1.

Zhao, M. *et al.* (2021) 'The Burden of Inflammatory Bowel Disease in Europe in 2020', *Journal of Crohn's and Colitis*. doi: 10.1093/ecco-jcc/jjab029.

Zheng, Y. *et al.* (2019) 'Deep Sequencing of Somatosensory Neurons Reveals Molecular Determinants of Intrinsic Physiological Properties', *Neuron*, 103(4). doi: 10.1016/j.neuron.2019.05.039.

Zhou, X. *et al.* (2010) 'Contribution of SHP-1 protein tyrosine phosphatase to osmotic regulation of the transcription factor TonEBP/OREBP', *Proceedings of the National Academy of Sciences of the United States of America*, 107(15). doi: 10.1073/pnas.1002795107.

Zhou, X. (2016) 'How do kinases contribute to tonicity-dependent regulation of the transcription factor NFAT5?', *World Journal of Nephrology*, 5(1). doi: 10.5527/wjn.v5.i1.20.

Zhou, X., Belavek, K. J. and Miller, E. W. (2021) 'Origins of Ca<sup>2+</sup> Imaging with Fluorescent Indicators', *Biochemistry*, 60(46). doi: 10.1021/acs.biochem.1c00350.

Zhu, X. *et al.* (1996) 'trp, a novel mammalian gene family essential for agonist-activated capacitative Ca<sup>2+</sup> entry', *Cell*, 85(5). doi: 10.1016/S0092-8674(00)81233-7.

ZhuGe, R. *et al.* (2006) 'Syntillas release Ca<sup>2+</sup> at a site different from the microdomain where exocytosis occurs in mouse chromaffin cells', *Biophysical Journal*, 90(6). doi: 10.1529/biophysj.105.071654.

Zitt, C. *et al.* (1997) 'Expression of TRPC3 in Chinese hamster ovary cells results in calcium-activated cation currents not related to store depletion', *Journal of Cell Biology*, 138(6). doi: 10.1083/jcb.138.6.1333.